INTERSOLID PYROTECHNIC REACTIONS OF SILICON

THESIS

Submitted in fulfilment of the requirements

for the degree of

Doctor of Philosophy
of Rhodes University

by

RAJAN ANIL RUGUNANAN

December 1991

...for my Parents, Rajesh, Sunil

and for Pragna

ABSTRACT

A study of the role of different oxidants with silicon as the fuel in simple binary pyrotechnic compositions is reported. Several oxidants were examined, but only three (Sb_2O_3, Fe_2O_3 and SnO_2) satisfied the restrictions that the combustion temperatures should be below the melting point of platinum/rhodium thermocouples (1760°C), that burning rates should not exceed the response of the thermocouples, and that burning should occur without significant mass-transport. A fourth oxidant, KNO_3, was selected on account of its low melting point and general importance as a pyrotechnic oxidant.

The oxidation of silicon in the presence of either Sb_2O_3 or KNO_3 could be identified from thermal analysis curves. No thermal events were noted when Si/SnO_2 and Si/Fe_2O_3 compositions were heated under similar conditions. The oxidation of Si powder in oxygen was also studied.

All four binary systems sustained burning over a reasonably wide range of compositions. The range of burning rates measured (2 to 35 mm s^{-1}) depended on the oxidant used. Fe_2O_3 and Sb_2O_3 gave slow burning mixtures compared to SnO_2 and to KNO_3 compositions with a high Si content. Burning rates generally increased with increasing specific surface area of silicon, but decreased in the presence of inert diluents and moisture. The burning rates of the Si/Fe_2O_3 and Si/SnO_2 systems increased with increasing compaction of the samples.

Kinetic parameters derived from the temperature profiles recorded during combustion were generally low (6 to 37 kJ mol^{-1}). This is in keeping with proposals that burning is diffusion controlled. The values of kinetic parameters derived from thermal analysis curves were considerably greater (> 250 kJ mol^{-1}).

Two other fuels, $FeSi_7$ and $CaSi_2$, gave similar thermal analysis curves when used instead of silicon. There were considerable differences in the burning rates for binary mixtures of these fuels compared to silicon.

Ternary systems with two fuels or two oxidants showed that only limited interaction occurs during thermal analysis. The use of a second fuel or oxidant did, however, modify the burning behaviour considerably.

Other techniques used in this study to probe the details of the reaction processes included bomb calorimetry, measurement of thermal conductivities, infrared spectroscopy, X-ray diffraction and scanning electron micoscropy.

ACKNOWLEDGEMENTS

I would like to express my most sincere gratitude to Professor M.E. Brown for his outstanding support and supervision throughout this work. His patience and enthusiasm are an important part of this thesis.

I would also like to thank:

Dr. R.L. Drennan for his friendship and moral support,

Mr. F. Ranftelshöfer for his technical assistance,

Mr. J. Lucas, Mr. D. Williams and the late Mr. B.K. Guthrie for assistance with electronic equipment and software,

Dr. M.W. Taylor of AECI Ltd. for his assistance,

AECI Ltd. for use of scientific equipment,

Mr. M.S. Rugunanan for his invaluable help with the preparation of the final draft of this thesis and

Mr. S. Rugunanan and Miss. P. Vallabh for their help,

Members of staff and colleagues of the Chemistry Department, Rhodes University, for the many years of fond memories, and

My parents and family for their encouragement and loving support.

The financial assistance of the Foundation for Research and Development is gratefully acknowledged.

CONTENTS

LIST OF SYMBOLS

A	constant, Arrhenius pre-exponential factor
B	constant
D	thermal diffusivity ($m^2\ s^{-1}$), or diffusion coefficient
G	Leeds power function
H	reaction enthalpy ($kJ\ g^{-1}$)
I	thermal conductivity integral
L	thickness of oxide layer (μm)
Q	rate of heat supply (power), or molar heat of reaction ($kJ\ mol^{-1}$)
R	universal gas constant ($8.314\ J\ K^{-1}\ mol^{-1}$)
S	Hill factor = 1/rise time, t_r (seconds)
T	temperature
U	excess temperature
V	thermocouple output
X	distance

a	effective radius
c	concentration per unit volume of oxygen, or specific heat capacity
d	thermocouple wire-diameter
h	lateral heat-loss coefficient
f	function describing the integral form of g
g	kinetic function in the rate equations
k	rate constant
m	mass burning rate ($g\ s^{-1}$), or order of reaction
n	order of reaction
q	heat of reaction ($kJ\ g^{-1}$)
r	correlation coefficient
t	time
u	radial distance in the medium from the thermal conductivity probe
v	linear burning rate ($mm\ s^{-1}$)
w	rate of heat evolution ($J\ s^{-1}$)

α	fractional extent of reaction
ε	porosity factor
Φ	rate of change of temperature (dT/dt)
Ω	parameter containing the physical factors which affect reaction
θ	dimensionless temperature
k	thermal conductivity probe constant
z	distance
ω	volume of oxide per molecule of oxygen
ρ	sample density (g cm^{-3})
λ	thermal conductivity (W K^{-1} m^{-1})

Subscripts

a	ambient
d	decay
ign	ignition
p	constant pressure
r	rise
ad	adiabatic
th	thermal relaxation
max	maximum
exp	experimental
calc	calculated

Abbreviations

SSA	specific surface area (cm^{-2} cm^{-3})
c_p	specific heat capacity at constant pressure
M_p	mass of probe
t^*	D/v^2
ρ_c	density of bulk solid (g cm^{-3})
λ_e	effective thermal conductivity
λ_g	thermal conductivity of the gas
E_a	activation energy (kJ mol^{-1})
ΔH_f	enthalpy of formation (kJ mol^{-1})

LIST OF FIGURES

Section 3

Section 4

Section 6

Section 7

Section 8

Section 9

Section 12

Section 13

Section 14

LIST OF PLATES

LIST OF TABLES

Section 1

Section 2

Section 3

Section 5

Section 6

Section 7

Section 12

Section 13

Section 14

1. INTRODUCTION

1.1 Pyrotechnic systems

Pyrotechnic systems, which are often equated with fireworks, are chemical mixtures consisting of an initially solid fuel and an initially solid oxidant. More complex mixtures of several fuels and/or several oxidants and various other additives are also possible. On ignition, these mixtures are capable of undergoing highly exothermic redox reactions. The burning of pyrotechnic mixtures may produce light, heat, motion, noise or smoke and their applications are diverse (1,2). Until relatively recently, the manufacture of pyrotechnics had largely been considered to be an art rather than a science and most compositions were closely guarded secrets. The two World Wars provided much impetus for the further development of pyrotechnic devices for use in sophisticated applications (1). These included the use in precision delay devices, flares, thunderflashes and even in self-heating food cans.

An important use of pyrotechnic mixtures today, other than in the military field, is in mining and in excavation. The blasting of a rock-face is achieved by the careful timing of a series of explosive charges using pyrotechnic delays. These devices are usually a combination of fuses, such as safety fuses and ignitercord, and electric detonators in which the burning of a column of pyrotechnic mixture provides a delay between receiving an ignition stimulus and detonation of the main blasting charge. Several factors affect the burning of these pyrotechnic systems:

(i) the actual chemicals used in the composition, their physical form (e.g. specific surface area and surface oxides) and history of preparation (impurities and grinding);

(ii) the blending and relative composition of the ingredients;

(iii) the deliberate addition of diluents and additives, such as binders, to modify the burning rate;

(iv) the density and degree of confinement during burning and

(v) the formation of gaseous products and participation of condensed phase reactions.

Other factors such as the conditions and duration of storage, humidity and ambient temperatures and pressures during burning also affect the burning of pyrotechnic delay trains. Recently (3), electronic delay detonators, in which the desired delay-time may be programmed into a microchip timing circuit within the detonator, have also been tested. These detonators offer more accurate and more precise delays, but are considerably more expensive than the conventional chemical delay detonator.

1.2 Silicon as a pyrotechnic fuel

The fuel in many pyrotechnic systems is a metal powder and the oxidant is often an oxide (e.g. BaO_2) or an oxysalt (e.g. $K_2Cr_2O_7$), although fluorides and sulphides have also been used in some systems (2). Some of the most common fuels and oxidants are listed in Table 1.1. The heats of reaction for complete oxidation of some fuels to the oxides shown are given in Table 1.2.

TABLE 1.1

Fuels and oxidants used in pyrotechnic mixtures

Fuels	Oxidants
Metals:	
Aluminium	Chlorates
Chromium	Chromates
Iron	Dichromates
Magnesium	Iodates
Manganese	Nitrates
Molybdenum	Oxides
Titanium	Perchlorates
Tungsten	Peroxides
Zirconium	Permanganates
	Sulphides
Non-metals:	
Boron	
Phosphorus	
Carbon	
Selenium	
Silicon	
Sulphur	

One of the most widely-used fuels in industry for pyrotechnic compositions is silicon. Silicon is a stable and chemically abundant material and is readily obtained by chemical reduction of silane or by electrolytic decomposition of molten mixtures of K_2SiF_6-LiF-KF or SiO_2-Na_3AlF_6 (4). Silicon, when

mixed with a suitable oxidant and ignited, provides relatively high heat outputs and such pyrotechnic compositions are used in ignition and in delay compositions (1,5). Some of the silicon-based mixes used as delay compositions in detonators are listed in Table 1.3.

TABLE 1.2

Heats of combustion of a few pyrotechnic fuels

Fuel	Product oxide	$-\Delta H$ kJ (g of fuel)$^{-1}$
B	B_2O_3	57.8
C	CO_2	32.7
Si	SiO_2	32.5
Al	Al_2O_3	31.3
Mg	MgO	24.8
Zr	ZrO_2	12.1
Mn	Mn_3O_4	8.8
Fe	Fe_3O_4	7.5
W	WO_3	4.6
Sb	Sb_2O_3	2.4

TABLE 1.3

Silicon based mixtures used as chemical delays[1] in detonators

Millisecond (0 to 400 ms) series	Long period (0.6 to 12 s) series
Si/PbO_2	Si/MnO_2
Si/PbO	
Si/Pb_3O_4	$Si/KMnO_4$
$Si/B/K_2Cr_2O_7$*	
$Si/Sb_2S_3/Pb_2O_3$	
$Si/Fe/MnO_2$	
$Si/NaF/Pb_3O_4$	

* Gassy mixture

[1] Delay times depend on length of delay elements

Several silicon containing mixtures such $Si/Ti/Pb_3O_4$, $Si/Cu_2O/PbO_2$, and $Si/Al/C/KNO_3/Fe_2O_3$ are used as "first fire" compositions (3). Other formulations include a variation on blackpowder, Si/KNO_3/charcoal, and also $Si/Cu/PbO_2$. A detailed review of silicon-based systems is given in Section 2.

1.3 **Aims of this study**

Despite the widespread use of pyrotechnics, information on the fundamental physical and chemical processes which occur during combustion is available for only a few systems. The aim of this research is to extend the information available on the reactions of, specifically, silicon with various other initially solid oxidants. An attempt will therefore be made to understand the role of the oxidant in binary pyrotechnic mixtures with silicon as the fuel in common.

Other alloys of silicon, for example, ferrosilicon ($FeSi_x$) and calcium silicide ($CaSi_2$), have been found to be of increasing use in pyrotechnic systems. These alloys are generally cheaper than silicon. The behaviour of both $FeSi_7$ and $CaSi_2$, in relation to silicon, is also examined in this study.

Two main experimental techniques have been used to obtain thermochemical and kinetic information on the pyrotechnic systems. These are thermal analysis (6,7) and measurement of temperature profiles during combustion (8,9).

Thermal analysis has been used quite successfully to determine the reaction mechanisms involved during reaction between pyrotechnic ingredients (7). The reactions which occur during a typical thermal analysis experiment, where heating rates are linear and sample masses usually small, are not necessarily the same as those which occur during combustion, where sample masses are large and the temperature rise of the sample is complicated. Thermal analysis does, however, provide useful quantitative as well as qualitative information which may be used to unravel the complex process which occur during burning. The measurement of temperature profiles, using fine thermocouples embedded in the pyrotechnic mixture, can be made to yield further useful kinetic and thermodynamic data for the burning process (9,10,11).

1.4 **References**

1. J.H. Mclain, "*Pyrotechnics: From the Viewpoint of Solid State Chemistry*", Franklin Institute Press, Philadelphia, Pennsylvania, 1980.
2. J.A. Conkling. "*Pyrotechnics*", Marcel Dekker, New York, 1985.
3. ICI Explosives International Ltd., "Downline", 7 (1988).
4. J.C. Bailar, H.J. Emeleus, R. Nyholm and A.F. Trotman-Dickerson, (Eds.), "*Comprehensive Inorganic Chemistry*", Pergamon Press, New York, 1973.
5. A. Bailey and S.G. Murray, "*Explosives, Propellants and Pyrotechnics*", Vol 2, Brassey's, London, 1989.

6. M.E. Brown, "*Introduction to Thermal Analysis: Techniques and Applications*", Chapman and Hall, London, 1988.

7. P.G. Laye and E.L. Charsley, Thermochim. Acta, **120** (1987) 325.

8. R.A.W. Hill, L.E. Sutton, R.B. Temple and A. White, Research, 3 (1950) 569.

9. T. Boddington, P.G. Laye, J.R.G. Pude and J. Tipping, Comb. Flame, **47** (1982) 235.

10. R.A.W. Hill and T.L. Cottrell, 4th Symp. on Combustion, (1953) 349.

11. T. Boddington, P.G. Laye, J. Tipping and D. Whalley, Comb. Flame, **63** (1986) 359.

2. PREVIOUS WORK

2.1 Silicon-based pyrotechnic systems

Silicon is one of the more extensively used fuels in pyrotechnic mixtures in the blasting industry. Some of the silicon-based compositions which have been studied are listed in Table 2.1.

TABLE 2.1

Some silicon-based pyrotechnic mixtures reported in the literature

System studied	Reference
Si/Fe_2O_3	1
$Si/Fe_2O_3/Pb_3O_4$	2
$Si/B/K_2Cr_2O_7$	3
Si/KNO_3	4,5,6
Si/PbO	7,8,9
Si/PbO_2	10
Si/Pb_3O_4	8,11,12,13
$Si/Pb_3O_4/KClO_4$	14
Si/SnO_2	15,16
$FeSi/Pb_3O_4$	17,18
$FeSi/MnO_2$	19
$Si/BaSO_4$	20,21
$Si/S/KNO_3$	10
$CaSi_3/C_2Cl_6/ZnO$	22

Despite the importance of silicon as a fuel, there is, however a lack of kinetic and thermodynamic information on the processes which occur during the burning of silicon-based pyrotechnics.

As in most pyrotechnic systems, one of the important aspects which has to be examined is the relative contributions made by solid-solid reactions, solid-liquid reactions and solid-gas reactions, where the gas is formed by the thermal decomposition of the oxidant.

2.2 Oxidation of silicon by gaseous oxygen

The oxidation of silicon by gaseous oxygen occurs in the temperature range 990 to 1200°C and an amorphous silicon dioxide (SiO_2) is usually formed (23). Studies have shown (23) that the rate of oxidation in atmospheres of wet oxygen is faster than that in dry oxygen. The rate of oxidation in dry atmospheres depends on the partial pressure of O_2, but in wet oxygen the rate depended on the partial pressure of H_2O, and the formation of Si-O-H bonds was reported (24).

Oxidation occurs primarily at the Si/SiO_2 interface and O_2 therefore has to diffuse through the oxide layer for reaction to occur (25). According to Deal and Grove (25), the rate of oxidation depends on the thickness of the oxide-layer and is controlled by the diffusion of the oxidant through the oxide. For thin films (~2 nm), the rate of oxide growth is given by

$$AL = Bt$$

where L is the thickness of the oxide layer, A and B are constants and t is the reaction time. The ratio A/B is proportional to the square-root of the partial pressure of O_2. For greater film thicknesses, the rate of oxidation becomes parabolic

$$dL/dt = (c/L)\ D\ \omega$$

D is the diffusion coefficient, and ω is the volume of oxide per molecule of oxygen and c is the concentration per unit volume of oxygen at the Si/SiO_2 interface. The rate of oxidation at this stage is slow enough for every molecule of O_2 to react with Si. This gives rise to a concentration gradient (c/X). This parabolic term arises from the fact that the SiO_2 film, formed initially, protects the silicon surface from further oxidation. The rate thus becomes independent of the pressure of oxygen.

For intermediate thicknesses, the linear and parabolic aspects of oxidation have been combined to give the rate law

$$AL^2 + BL = t + \text{constant}$$

where $A = 1/k_p$ and $B = 1/k_l$ and k_p and k_l are the rate coefficients for the parabolic and linear processes, respectively. Values of E_a for the parabolic law oxidation are 116 to 125 kJ mol^{-1}.

A recent study, of the reaction over a range of temperatures, claimed that the linear-parabolic (L-P) model is not adequate to account for the actual oxidation (26), but the evidence in support of this claim is not convincing. This L-P rate law has, however, been adopted as a basis from which to describe the oxidation of silicon (27,28,29).

Radioactive labelling experiments have shown (29) that $^{18}O_2$, introduced after some oxide has been formed, concentrates at the Si/SiO_2 interface. This shows that the exchange of oxygen between SiO_2 and O_2 does not occur. Further evidence in support of O_2 as the migrating species was obtained in isotopic studies involving Ar. The O_2 molecule and the Ar atom are about the same size (0.18 nm). Activation energies for the movement of O_2 and Ar through SiO_2 were similar (130 to 135 kJ mol^{-1}). These activation energies are also close to the values of between 116 and 125 kJ mol^{-1} obtained for high-temperature thick film oxidation (25,30).

Phillips (31) suggested that clusters of cristobalite (crystalline SiO_2) were formed initially and that the oxidising species diffused along the boundaries between these clusters. Tiller (32) confirmed the initial formation of α-cristobalite and found that this crystalline structure contained four interstitial Si atoms per unit cell of SiO_2. Subsequent oxidation of the interstitial silicon atoms caused a distortion of the SiO_2 crystal structure to form amorphous or vitreous SiO_2. The process of oxidation (33) was shown to depend on both electric-field effects and on crystal orientation effects, so the oxidation mechanism is thought to involve the formation of both neutral and charged species (33,34,35).

Recently, special emphasis has been placed on studying the initial stages of oxidation on SiO_2-free silicon surfaces (36,37,38). The oxidation of these clean silicon surfaces proceeds initially, at low temperatures (100 K), with the formation of sub-oxides from molecular oxygen. At higher temperatures, oxidation is thought to proceed through the formation of atomic oxygen and, finally, after a few atomic layers, stoichiometric SiO_2 is formed. The process of oxidation between the formation of this initial layer and the formation of a layer sufficiently thick to be considered as stoichiometric SiO_2, is thought to proceed via the L-P mechanism (39). Further studies on the oxidation of the initial layer showed that there is a definite orientation dependence, with the dense 110 plane being preferred at low pressures and the 111 plane being preferred at high temperatures. The existence of stress in the initial oxide film leads to the formation of microchannels. These are believed to provide short-cuts to the Si/SiO_2 interface for the diffusion of oxygen and may thus account for the linear kinetics observed for the oxidation of silicon surfaces coated with protective oxide (40). When these surfaces were irradiated with ultraviolet light or chemical lasers, oxidation was enhanced. Wavelengths with energies greater than 3 eV, further enhanced oxidation (41).

The oxidation of silicides was reported to occur at a faster rate then that of pure silicon (42). Generally, all transition-metal silicides were oxidised at a faster rate than refractory-metal silicides, probably owing to differences in electron mobility. During slow oxidation, SiO_2 is formed predominantly. Under carefully controlled conditions, oxidation of a silicide on a silicon substrate can be made to yield, exclusively, SiO_2 (43). In the oxidation of a thin film of a silicide on a layer of silicon, SiO_2 is formed preferentially and the metal species migrate to the silicon surface where the silicide is reformed.

A reaction between silicon and nitrogen occurs at higher temperatures ($\sim$1400°C) than that with oxygen (44). The reaction proposed is

$$3Si(s) + 2N_2(g) \rightarrow Si_3N_4(s)$$

TG curves showed that the reaction is slow between 1200 and 1300°C but becomes more rapid at temperatures above 1350°C. The reaction order varied between 0.2 and 2 for samples of silicon from different sources, and activation energies of between 825 and 8150 kJ mol^{-1} were measured.

In the presence of antimony and bismuth chlorides (45), the oxidation of Si in oxygen was sensitive to the presence of trace amounts of H_2O. $SbCl_5$ and $BiCl_5$ formed metal oxychlorides through reaction with water, and these intermediates decomposed to the corresponding metal oxides. The following

reactions occurred between the metal oxides and silicon

$$2Sb_2O_3 + 3Si \rightarrow 3SiO_2 + 4Sb$$

and

$$2Bi_2O_3 + 3Si \rightarrow 3SiO_2 + 4Bi$$

2.3 **Silicon/lead oxide systems**

2.3.1 *Thermal analysis*

Silicon/lead oxide mixtures are among the more extensively studied pyrotechnic systems. DTA curves of a 30% Si/PbO mixture in air (7) showed three exotherms at 540, 610 and 710°C. The second exotherm showed an initial gradual rise which became very rapid at 665°C and was followed almost immediately by a rapid return to baseline. In an inert atmosphere, DTA also showed three exothermic processes but these occurred at lower temperatures than those observed in air, and were generally less exothermic, particularly the second exotherm (7). The first reaction step for the reaction in air is the conversion of PbO to Pb_3O_4 (red lead) at temperatures above 350°C

$$6PbO(s) + O_2(g) \overset{350°C}{\underset{540°C}{\leftrightarrow}} 2Pb_3O_4(s) \qquad ...2.1$$

Decomposition of the red lead occurs above 540°C. Then,

$$2Pb_3O_4(s) + Si(s) \overset{590°C}{\rightarrow} SiO_2(s) + 6PbO(s)$$

and,

$$PbO(s) + Si(s) + 0.5O_2\ (g)(\text{from air}) \overset{665°C}{\rightarrow} Pb(l) + SiO_2(s)$$

The reaction between Si and PbO occurred at the onset (540°C) of the decomposition of the intermediate oxidant (Pb_3O_4). In support of this claim, it was shown that silicon in a Si/Pb mixture was oxidised only after the oxidation of elemental Pb to Pb_3O_4. The greater exothermicity of the second exotherm, in air, is due to the formation of Pb_3O_4 from reaction of PbO with atmospheric oxygen.

DTA curves of lead dioxide (PbO_2) showed five endotherms (46). The first four endotherms are due to the decomposition of PbO_2 according to the following reaction steps:

$$PbO_2 \overset{435°C}{\rightarrow} PbO_{1.56} \overset{465°C}{\rightarrow} PbO_{1.43} \overset{495°C}{\rightarrow} Pb_3O_4 \overset{573°C}{\rightarrow} PbO$$

The melting endotherm of PbO at 876°C was also observed. DSC curves of Si/PbO_2 in N_2, showed a sharp exotherm at 500°C which became even sharper at high oxidant contents. TG curves showed that mass loss begins at ~250°C, possibly due to the low-temperature decomposition of the oxidant, and becomes more rapid during the oxidation of silicon.

Al-Kazraji and Rees (47) reported two exotherms in the DTA trace of Si/Pb_3O_4 in an inert atmosphere. The first exotherm formed a shoulder (onset ~540°C) to the second exotherm (onset at 560°C) which peaked at ~590°C. The peak coincided with the endothermic decomposition of Pb_3O_4, so the oxidation of silicon and the decomposition of red lead thus occurs simultaneously. In an oxidising atmosphere, three exotherms were observed. The first two occurred over temperature ranges similar to those in N_2. The second exotherm (onset 620°C) rose sharply at ~660°C and was more exothermic than the corresponding exotherm in nitrogen. For this exotherm, XRD and infrared spectroscopy showed that the elemental lead, previously formed, reacts with atmospheric O_2 to form PbO which, in turn, reacts with silicon and raises the temperature sufficiently for silicon to react with oxygen. The third exotherm (755 to 788°C) was more pronounced for silicon-rich compositions. During this exotherm, reaction occurs between PbO and $PbSiO_2$ (lead silicate) through the migration of PbO into the silicate lattice at its melting point. DSC and TG traces confirmed the above observations.

In a later study (8), in which Si/PbO and Si/Pb_3O_4 compositions were compared (see also ref. 46), the DTA trace of Si/PbO showed two exotherms (640 and 710°C). The first exotherm was due to an irreversible surface reaction between Si and PbO. The SiO_2 layer on the surface of the silicon particles then acted as a barrier which inhibited any further oxidation. During the second exotherm, the temperature of the system was sufficiently high to permit a further reaction between the bulk of the silicon particles and PbO. It was suggested (8) that the solid-solid reaction becomes increasingly significant due to an increase in the mobility of Si within the PbO crystal lattice as the temperature increases. Hot-stage micoscropy (HSM) showed that the mixture usually ignited in the temperature range of this exotherm (715 to 760°C).

Although the DTA curves of the Si/PbO and Si/Pb_3O_4 mixtures were similar, the reactions of Si/PbO were more exothermic (8,46). TG curves, showed that PbO and O_2 were formed on decomposition of Pb_3O_4 (see reaction 2.1). No reaction was observed between this evolved oxygen and the silicon. The increased exothermicity was thus attributed to the formation of a highly reactive PbO with a larger specific surface area (SSA) (8).

Similar observations were reported by Yoganarasimhan for Si/Pb_3O_4 compositions (2). The first exotherm, due mainly to surface effects such as sintering, depended on the surface area of the silicon particles, and the exothermicity decreased with a decrease in the surface area. The second exotherm was regarded as the main oxidation reaction. A critical mass, above which ignition invariably occurs, was observed and was found to vary with composition (2).

The ternary system of Si/Pb_3O_4/$KClO_4$ was examined to determine the effect of gas-phase mass transport in the Si/Pb_3O_4 system (14). The DTA and DSC curves in air, showed a series of overlapping exotherms between 390 and 630°C. At large sample masses (~20 mg), the size of the exotherm at 470°C

increased considerably and was accompanied by a flash and sound. The presence of $KClO_4$ decreased the critical mass required for reproducible ignition to occur. In an inert atmosphere, DSC curves showed five exotherms, which occurred at higher temperatures than those observed (14) in air, but at lower temperatures than the exotherms observed for the Si/Pb_3O_4 mixture alone. Therefore, O_2 in the presence of $KClO_4$ also contributes to the oxidation of silicon.

In the presence of Fe_2O_3 as an additive, a third exotherm, probably due to a reaction of unreacted Si with Fe_2O_3, was observed (2) at a higher temperature than the first two exotherms attributed to the reaction between Si and Pb_3O_4 (14,47). Fe_2O_3, which also acted as a burning retardant, increased the critical mass required for ignition to occur.

2.3.2 *Burning studies*

The silicon/red lead mixture is a fast-burning composition, and is used to provide millisecond delays in detonators. Plot of the linear burning-rate versus composition was a concave-down type curve, i.e. it had a single maximum (48). Compositions containing more than 50% silicon failed to burn. The burning rate depended on the particle-size of the silicon used. A maximum burning rate was observed at approximately 30% Si for coarse silicon (mean particle-diameter 5 μm) and at 15% Si for fine silicon (mean particle-diameter 1.9 μm). A plot of the heat of reaction per mole of oxidant (Q) versus % Si showed an initial increase to a maximum of 10% Si, and flattened out at ~15% Si so that Q remained approximately constant with further increases in % Si. According to Spice and Staveley (49), this behaviour indicates a single controlling reaction and 15% Si represents the stoichiometric amount of silicon used by the oxidant. The composition at which the maximum burning rate occurred (30%) did not correspond to the composition of maximum enthalpy (approximately 10% Si). According to Al-Kazraji and Rees (48), this difference is a result of a decrease in the amount of oxidisable silicon, for a given composition, resulting from the initial formation of a layer of SiO_2 over the surface of the Si particles. The reaction steps proposed were

$$Pb_3O_4(s) \rightarrow 3PbO(s) + 0.5O_2(g)$$

$$Si(s) + O_2(g) \rightarrow SiO_2(s)$$

$$2PbO(s) + Si(s) \rightarrow 2Pb(l) + SiO_2(s)$$

Although a maximum burning rate was observed at ~30% silicon, the maximum shifted to a higher silicon content as the consolidation pressure was increased. Because the thermal conductivity of the mixtures remained relatively unchanged with consolidation pressure, it was suggested (48) that it was the improved surface contact between fuel and oxidant which increased the burning rate. The activation energy, obtained from the analysis of temperature-time profiles of several compositions, was 31 kJ mol^{-1}

(50) and calculated burning rates (from temperature profiles) compared fairly well with experimental values (39 to 129 mm s^{-1}). From an estimation of the physical properties of the mixture (specific heat capacity, thermal diffusivity and thermal conductivity) a diffusion-controlled combustion reaction was suggested (51).

Hedger also measured (13) a maximum burning rate at 30% Si for the Si/Pb_3O_4 system and there was an increase (from 16 to 300 mm s^{-1}) in the burning rate when the specific surface area of the Si was increased from 0.08 to 5.36 $m^2 g^{-1}$. A discontinuity in the plot of burning rate versus specific surface area was suggested to be the result of a change in the mechanism of reaction (13). The burning rate of Si/Pb_3O_4 mixtures increased with pressure, reached a maximum and then decreased with a further increase in pressure (10). This decrease is thought to be due to a decrease in the volatilisation of PbO as the mixture is compacted (10).

The suggested mechanism for the reaction of silicon and red lead involved the formation of a eutectic consisting of SiO_2 and PbO (at 714 to 720°C in the DTA)(13). The PbO is formed from the decomposition of Pb_3O_4 and has a melting point of 886°C and SiO_2 melts at approximately 1610°C. Formation of this eutectic exposes unreacted Si, allowing the reaction to continue. The delay time thus also depends on the rate at which formation of the SiO_2/PbO eutectic progresses along the pyrotechnic column. When the surface area is low, heat conduction effects are mainly responsible for propagation from layer to layer.

For Si/PbO_2 mixtures (51), burning could be sustained for up to 60% silicon and the maximum burning rate occurred at 35% Si. The burning rate also decreased with increasing particle size. From a plot of the enthalpy of reaction per mole of oxidiser (Q) versus % fuel for the Si/PbO_2 mixture, McLain estimated (10) that the stoichiometric point corresponded to approximately 10% silicon and proposed the following reaction

$$Si(s) + PbO_2(s) \rightarrow SiO_2(s) + Pb(l)$$

He noted that probably more than one reaction occurred over the whole burning range, but between 3 and 30% silicon there was one reaction operating and this occurs optimally at ~15% silicon (10). In an earlier study (51), it was shown that the burning rates of Si/PbO_2 mixtures depended on the source of the oxide, its particle-size, density and the density of the pyrotechnic column. Mixtures of 20% Si/PbO_2, containing inert materials to regulate the burning, were found to be easy to ignite but were relatively insensitive to friction.

Goodfield and Rees (16) measured the maximum reaction temperature of Si/Pb_3O_4 mixtures packed in delay elements, using a specially-adapted infrared pyrometer. The reaction temperatures, corrected for the emittance of the sample, were compared to calculated values (52,53). Although the trends were found to be similar, the actual reaction temperatures were lower than the calculated temperatures, possibly due to an excessive heat loss through the walls of the container. The maximum reaction temperature could, however, be located to within 100°C when an approximate value for the emittance was used. Problems due to radiation scatter and inconsistent properties of the optics of the pyrometer were reported.

2.4 The silicon/potassium nitrate system

2.4.1 *Thermal analysis*

The DTA curves of Si/KNO_3 mixtures in a nitrogen atmosphere, showed a range of overlapping exotherms between 500 and 900°C (4). The shape of these exotherms depended on the composition of the mixture. Maximum enthalpy of reaction, from DTA curves, occurred at ~30% silicon. For mixtures consisting of 10% Si/KNO_3, the activation energy and the pre-exponential factor, from DTA curves, were 134 kJ mol^{-1} and 10^9 s^{-1} respectively (54). For KNO_3-rich mixtures, TG curves in N_2 showed an increase in the mass loss with an increase in the KNO_3 content, due to the decomposition of excess oxidant. However, for mixtures containing less than 50% KNO_3 by mass, a slight increase in mass was observed in the same temperature range.

DTA curves also showed that for Si-rich compositions, the reaction between Si and KNO_3 occurred at ~500°C which is below the decomposition temperature of the nitrate, but for KNO_3-rich compositions reaction occurred at ~640°C which is the temperature at which the oxidant decomposes. The authors claimed that there is a reaction between silicon and the nitrogen oxides formed when KNO_3 decomposes. Ignition was observed under a hot-stage microscope (HSM) at temperatures which were found to vary between 500 and 900°C (6) depending on the heating rate of the instrument.

2.4.2 *Burning studies*

Burning rate studies (5) on Si/KNO_3, with nitrocellulose as a binder, loaded in copper tubes, showed that the burning rate increased with an increase in silicon content up to a maximum at 90% Si. At low Si contents, only a marginal increase in the burning rate with increasing consolidation pressure was observed, but the increase was more pronounced for silicon-rich compositions. The high burning-rate in silicon-rich mixtures is possibly due to the high thermal conductivity of Si, while in KNO_3-rich mixtures the burning rate is sustained by the large volume of gas formed during the decomposition of the oxide. The following reaction was suggested

$$2KNO_3(l) + 3Si(s) \rightarrow 3SiO_2(s) + 2K(l) + N_2(g)$$

with ΔH = -1589 kJ mol^{-1}.

Results of measurements in delay elements made from aluminium showed a maximum burning rate at 80% Si (5). The burning behaviour of samples under the confines of a detonator assembly were significantly different from the burning of unconfined samples; burning rates under unconfined conditions increased with increasing consolidation pressures, but no trends were observed for confined systems. The composition at which maximum enthalpy of reaction was observed (~30% Si) did not correspond to the composition at which maximum burning rate occurred (~90% Si) (5).

2.5 Silicon/tin(IV) oxide system - burning studies

Compositions containing 20 to 45% Si and SnO_2 (specific surface area (SSA) between 0.9 and 3.5 $m^2\ g^{-1}$) burnt in drawn lead tubes (15) with burning rates of 12.7 mm s^{-1} for 45% Si (SSA 1.4 m^2g^{-1}), to 33.1 mm s^{-1} for 30% Si (SSA 1.4 to 10.1 m^2g^{-1}). Mixtures containing 20 to 40 % silicon were reported to be essentially gasless.

In a study in which the reactions of Si and B with PbO and SnO_2 were compared (16), the silicon-containing compositions showed a concave-down burning rate versus composition curve. Maximum burning rates were at 30% Si/SnO_2 and 20% Si/PbO. The burning rate, however, decreased with increasing consolidation pressure. To explain the differences between the B and Si-containing compositions, the authors suggested that, at high oxidant levels in the Si systems, volatile intermediates dominate the heat transfer mechanism as a result of the high reaction temperatures (1760°C). At low oxidant levels, where the reaction temperature is about 1250°C, conduction is the main form of heat transfer.

2.6 The silicon/barium sulphate system - burning studies

$Si/BaSO_4$ compositions containing 30 to 45% silicon gave burning rates between 5.7 and 7.5 mm s^{-1} in drawn-lead delay elements (20). The 42% Si composition gave a minimum burning rate of 4.3 mm s^{-1} and Pb_3O_4, as an additive, was found to increase the burning rate considerably.

The viability of a $Si/BaSO_4$ pyrotechnic mixture for use in long-period delay detonators, with a required burning rate of 4.2 mm s^{-1}, was evaluated by Kelly (21). Burn-time data were obtained for compositions containing 33.5 to 50% silicon with specific surface areas (SSA) of between 6.6 and 13 m^2 (g silicon)$^{-1}$ and 0.45 and 2.36 m^2 (g $BaSO_4$)$^{-1}$. A mixture containing 45.5% silicon provided the required burning-time. The minimum burning rate (3.8 mm s^{-1}) was observed at 40% silicon. For a given composition, the burning rate generally increased with increasing SSA of silicon (SSA of $BaSO_4$ kept constant). For a given SSA of silicon, a plot of the burning rate versus percentage silicon showed a minimum at ~40% silicon. Similar observations were made when the SSA of $BaSO_4$ was varied while the SSA of silicon was kept constant. The measured burning rates of the mixtures were very dependent on the source of the ingredients.

2.7 The silicon/boron/potassium dichromate system - thermal analysis

DSC curves of the ternary Si/B/$K_2Cr_2O_7$ mixture in an oxidising atmosphere (3) showed two exothermic processes. The first exotherm (onset at 250°C) is a reaction between molten oxidant and solid boron. This is followed at a higher temperature (>500°C) by the oxidation of silicon. The reaction with boron is more exothermic than with silicon. The rate determining step is suggested (3) to be the formation of a liquid phase which then progresses through the burning composition as a molten front. The Si-$K_2Cr_2O_7$ reaction is thus a back-up reaction and, since the rate at which heat is evolved is lower than that observed for the B-$K_2Cr_2O_7$ reaction, the reaction with silicon only occurs after all the boron has been oxidised.

Charsley *et al* reported (55) that the exothermicity of the B/$K_2Cr_2O_7$ reaction is not affected by the presence of Si, but the exotherm corresponding to the oxidation of Si increases with increasing silicon. The onset temperature of the second exotherm is lowered by the presence of >4% B in the mixture. They suggested that unreacted B participates in the second exotherm which is thought to occur between Si and $KCrO_4$. Maximum enthalpy of reaction occurred on addition of 6% (by mass) of silicon to a binary 5% B/$K_2Cr_2O_7$ mixture. Fine thermocouples were used (55) to measure the temperature profiles of the binary 5% B/$K_2Cr_2O_7$ mixture. The addition of silicon increased the maximum reaction temperature and the slope of the rise region of the temperature profiles (see Section 4.1). The power functions (see Section 4.4), calculated from the temperature profiles mixtures showed two partially resolved exotherms which were taken as confirmation for the two-stage reaction (55).

2.8 Ferrosilicon/oxidant systems

DTA curves of the ingredients of a FeSi/MnO_2 mixture, in air (19), showed that the oxidation of FeSi begins at ~400°C and is rapid at ~700°C. The decomposition of MnO_2 occurs in two stages: the first stage, in which Mn_2O_3 is formed, occurred between 600 and 800°C (mass-loss 9.1%) and the second stage between 800 and 1000°C, in which Mn_3O_4 is formed (mass loss 3.4%). The DTA curves of FeSi/MnO_2 mixtures showed a well-defined exotherm at ~600°C, but the shape of the DTA curves depends on the composition of the mixture. TG curves in nitrogen in the temperature range of the exotherm showed an initial mass-loss followed by a mass-gain, so a quantity of O_2 released on decomposition of the oxide escaped without reacting with the fuel, but reaction occurred only after FeSi became reactive (800°C). The maximum decomposition rate is independent of the composition. At high fuel contents (50 to 70% FeSi), oxidation of the fuel (by MnO_2) occurred rapidly, followed by a slower oxidation (reaction with air) at temperatures above 850°C. Products of these reactions included Fe_2O_3 and SiO_2.

For $FeSi/Pb_3O_4$ mixtures, reaction began at 400°C (17). The gas pressure-wave generated during combustion was shown to precede the burning front (18) and an increase in gas pressure with a decrease in FeSi particle size was observed. Maximum gas pressure was observed at 10% FeSi and maximum burning rate was observed at 30% FeSi.

2.9 $CaSi_3$/oxidant system

A pyrotechnic system consisting of $CaSi_3$ and C_2Cl_6 as fuels and ZnO as an oxidant, used mainly as a smoke generating composition, was studied using thermal analysis as the main technique (22). Sample crucibles were sealed to prevent the vaporisation of hexachloroethane. An endotherm at 266°C followed by four further exotherms were observed. The first endotherm was due to the vaporisation of C_2Cl_6. The first exotherm was due to the reactions

$$CaSi_3 + 3C_2Cl_6 \rightarrow CaCl_2 + 2CCl_4 + 2C_2Cl_4 + 3Si$$

$$6ZnO + 2CCl_4 \rightarrow 2(2ZnO \cdot \beta ZnCl_2) + 2COCl_2$$

$$6ZnO + 2COCl_2 \rightarrow 2(2ZnO \cdot \beta ZnCl_2) + 2CO_2(g)$$

The three remaining exotherms were due to the reactions

$$CaSi_3 + 3C_2Cl_4 \rightarrow 3CaCl_2 + C_6Cl_6 + 9Si$$

$$2ZnO \cdot \beta ZnCl_2 + C_2C_4 \rightarrow 3ZnCl_2 + 2CO$$

$$3CaSi_3 + C_6Cl_6 \rightarrow 3CaCl_2 + 6C + 9Si$$

2.10 Comments

Reactions between solid silicon and gaseous oxygen occur at temperatures generally greater than those for exothermic reaction between Si and the common initially solid oxidants. Some solid oxidants undergo thermal decomposition at temperatures below those required for any reaction with silicon. Oxygen may thus be lost without reacting, depending on the confinement of the composition.

SiO_2 forms a protective layer on silicon particles, markedly decreasing the rate of further oxidation. SiO_2 may react further with the oxidant to give silicates, or with molten oxidant to give eutectic mixtures. The formation of eutectics may result in the dissolution of the SiO_2 layer, thus allowing further oxidation to occur.

Burning rates vary with composition and with particle-size of the fuel and oxidant. Burning rates also generally increase with compression of the mixture, indicating that Si/solid oxidant contact is important, but this does not exclude a role for trapped oxygen gas in the oxidation.

There is a marked difference in the burning rates measured for systems with different oxidants. The lead oxides form fast-burning (100 to 250 mm s^{-1}) compositions and the oxy-salts, KNO_3 and $BaSO_4$, form slow-burning (<10 mm s^{-1}) systems.

There is, as yet, insufficient quantitative information on Si/oxidant systems to reach general conclusions. Information on combustion temperatures, including detailed analyses of temperature profiles to give kinetic parameters, is required.

2.11 References

1. H. Goldschmidt, US Patent No. 906009, 1908.
2. S.R. Yoganarasimhan and O.S. Josyulu, Def. Sci. J., **37** (1987) 73.
3. S.L. Howlett and F.G.J. May, Thermochim. Acta, **9** (1974) 213.
4. G. Krishnamohan, E.M. Kurian and K.R.K. Rao, 8th Int. Pyro. Sem., (1982) 404.
5. T.T.L. Leeuw, Report No. RN 0861/A, Technical Dept., AECI Ltd., 1988.
6. T.T.L. Leeuw, Report No. RN 0839/A, Technical Dept., AECI Ltd., 1988.
7. S.S. Al-Kazraji and G.J. Rees, J. Thermal Anal., **16** (1979) 35.
8. A.Z. Moghaddam and G.J. Rees, Fuel, **60** (1981) 629.
9. J.A.C. Goodfield and G.J. Rees, Fuel, **64** (1985) 1627.
10. J.H. Mclain, "*Pyrotechnics: From the Viewpoint of Solid State Chemistry*",Franklin Institute Press, Philadelphia, Pennsylvania, 1980.
11. S.S. Al-Kazraji, M.S. Doulah and G.J. Rees, Fuel, **60** (1950) 598.
12. S. Nakahara and T. Hikita, J. Ind. Explos. Soc. Japan, **21** (1960) 9.
13. T.J. Hedger, Propellants Explos. Pyrotech., **8** (1983) 95.
14. S.R. Yoganarasimhan, J. Thermal Anal., **34** (1985) 937.
15. UK Patent No. GB 2 084 984 A,1980.
16. J.A.C. Goodfield and G.J. Rees, Fuel, **60** (1981) 151.
17. S. Nakahara, J. Ind. Explos. Soc. Japan, **22** (1961) 259.
18. S. Nakahara, J. Ind. Explos. Soc. Japan, **20** (1959) 356.
19. L. Sulacsik, J. Thermal Anal., **5** (1973) 33.
20. A.L. Davitt and K.A. Yuili, UK Patent No. GB 2 089 336, 1980.
21. G. Kelly, CXA Technical Report No. IR-99-003, CXA Canada, 1984.
22. A.Jarvis, Comb. Flame, **14** (1970) 313.
23. N. Mott, "Conduction in Non-Crystalline Materials", Oxford University Press, 1987.
24. S. Rigo, F. Rochet, B. Agius and A. Straboni, J. Electrochem. Soc., **129** (1982) 867.
25. B.E. Deal and A.S. Grove, J. App. Phys., 36 (1965) 3770.

26. E.A. Irene, CRC Critical Reviews in Solid State and Materials Sciences, **14** (1988) 175.
27 A.G. Revesz and R.J. Evans, J. Phys. Chem. Solids, **30** (1969) 551.
28. W.A. Pliskin, IBM Res. Dev., **10** (1966) 198.
29. E. Rosencher, A. Straboni, S. Rigo and G. Amsel, App. Phys. Lett., **34** (1979) 254.
30. E.A. Irene and D. Dong, J. Electrochem. Soc., **125** (1978) 1146.
31. J.C. Phillips, J. Non-cryst. Solids, **34** (1979) 153.
32. W.A. Tiller, J. Electrochem. Soc., **127** (1980) 619.
33. W.A. Tiller, J. Electrochem. Soc., **127** (1980) 625.
34. W.A. Tiller, J. Electrochem. Soc., **128** (1981) 689.
35. N.T. Cabrera and N.T Mott, Rep. Prog. Phys., **12** (1948) 163.
36. J. Derrien and M. Commandre, Surf. Sci., **118** (1982) 32.
37. H. Ibach, H.D. Bruchmann and H. Wagner, Appl. Phys., **29** (1982) 113.
38. P.Chiaradia and Nannarone, Surf. Sci., **54** (1976) 547.
39. M.A. Hopper, R.A. Clarke and L. Young, J. Electrochem. Soc., **122** (1975) 1216.
40. E.A. Irene, J. Appl. Phys., **54** (1983) 5416.
41. S.A. Schafer and S.A. Lyon, J. Vac. Sci. Technol., **21** (1982) 422.
42. F.M. d'Heurle, A. Cross, R.D. Frampton and E.A. Irene, Philos. Mag., **B55** (1987) 291.
43. S.P. Murarka, "*Silicides for VLSI Applications*", Academic Press, New York, 1983.
44. G Braun, G. Bowden, K. Henkel and H. Rossbach, J. Thermal Anal., 33 (1988) 479.
45. Ya A. Ugai, V.Z. Anokin, Ya Mittova, S.M. Myachin and N.I. Ponomareva, Russ. J. Phys. Chem., **55** (1981) 532.
46. S.S. Al-Kazraji, PhD Thesis, Polytechnic of Wales, 1982.
47. S.S. Al-Kazraji and G.J. Rees, Comb. Flame, **31** (1978) 105.
48. S.S. Al-Kazraji and G.J. Rees, Fuel, **58** (1979) 138.
49. J.E. Spice and L.A.K. Staveley, J. Soc. Chem. Ind., **68** (1949) 313.
50. S.S. Al-Kazraji, M.S. Doulah and G.J. Rees, Fuel, **59** (1980) 598.
51. W. Ripely, 1st Int.Pyro. Sem., (1968) 225.
52. B.T. Fedoroff, O.E. Sheffield, E.F. Reese and G.D. Clift, "Encyclopaedia of Explosives", Vol 2, Picatinny Arsenal, Dover, New Jersey, 1962.
53. R.C. Harris, Proc. 2nd Symp. Chem. Prob. Connected Stab. Explos., (1970) 356.
54. E.M. Kurian and R.V. Tamamnkar, Trans. IIM, (1978) 62.
55. E.L. Charsley and Chieh-Hua Chen, Thermochim. Acta, **35** (1980) 141.

3. EXPERIMENTAL

3.1 Materials

Powdered samples of silicon (Si Dust) were obtained from AECI Ltd. The oxidants used were Fe_2O_3 (Baker Analysis), Sb_2O_3 (Merck), SiO_2 (BDH) and KNO_3 (AECI Ltd). Additional fuels such as ferrosilicon and calcium silicide were obtained from AECI Ltd. and Swartklip Products Ltd. All the constituents were sieved through a 53 μm screen before use.

Thorough mixing of the samples was accomplished by passing the binary mixtures several times through a <75 μm screen with the aid of a soft brush. The mixed samples were then stored in air-tight containers until required.

The physical characteristics of the materials used are listed in Tables 3.1 to 3.4. The measurement of particle-sizes and surface area is described in Section 3.7.

TABLE 3.1

Physical characteristics of the constituents

Sample	Mean particle diameter (μm)	Purity* (%)	Main impurity*
Si	3.4	97.0	1% Fe
$FeSi_7$	6.0	95.0	2% Al
$CaSi_2$	25.8	97.0	Various
Sb_2O_3	0.6	99.0	Various
Fe_2O_3	0.4	99.8	0.2% HCl
SnO_2	0.4	99.8	0.005% Pb
KNO_3	9.7	99.0	HCl

* Manufactures' specifications

TABLE 3.2

Comparison of the specific surface areas of the constituents using BET and obscuration methods

Sample	Surface area	
	BET m^2 (g of sample)$^{-1}$	Obscuration m^2 (cm^3 of sample)$^{-1}$
Silicon	10.0	2.0
$FeSi_7$	3.2	9.3
$CaSi_2$	-	0.3
Sb_2O_3	5.8	10.2
Fe_2O_3	1.2	15.2
SnO_2	8.7	15.4
KNO_3	3.0	-

TABLE 3.3

Particle-size analysis of the constituents

Sample	Mean diameter (μm)	Median diameter (μm)	Cumulative distribution 10%	90%	Overall distribution (skewness)
Silicon	3.41	4.57	1.45	20.07	positive
$FeSi_7$	6.01	6.81	0.24	11.28	positive
$CaSi_2$	25.78	60.0	13.75	130.41	negative
Sb_2O_3	0.64	1.81	0.22	4.87	bimodal
Fe_2O_3	0.41	0.46	0.22	1.00	symmetrical
SnO_2	0.42	0.46	0.20	1.98	positive
KNO_3	9.70	18.35	8.00	30.2	positive

TABLE 3.4

Physical characteristics of silicon of various particle-size ranges

Silicon type	Particle diameter range (μm)	Mean particle diameter (μm)	Specific surface area (m^2 cm^{-3})
0 to 53 μm	0 to 53	3.41	2.04
Dust	0 to 80	3.99	2.81
Type I	0 to 120	8.37	1.03
Type II	0 to 100	1.61	5.40

Substances other than the main fuel and oxidant are often added to pyrotechnic mixtures to modify the burning rate (1,2). These additives may either be reactive or chemically inert. The additives modify the burning rate by participating directly in the reaction, or by altering the heat transfer characteristics, or by decreasing the contact between fuel and oxidant. The additives may act as additional fuels or oxidants and give rise to additional reactions. Various quantities of two presumably inert diluents, silica (SiO_2 m.pt. 1430°C) and alumina (Al_2O_3 m.pt. 2015°C), have been used to examine their effect on the burning rates of the silicon systems. The diluents were added to selected binary mixtures without altering the fuel to oxidant ratios.

Several studies have shown that the oxidation of silicon is enhanced in the presence of water vapour (see Section 2.2). Various quantities of water were added to silicon/oxidant mixtures. These samples were hermetically sealed and left to equilibriate for two days before burning.

3.2 Apparatus for temperature-profile measurement

The apparatus used for temperature-profile measurement consists of a temperature sensing device embedded in a column of a pyrotechnic composition (3). The extreme conditions associated with the burning of pyrotechnic mixtures require that the temperature sensors should be stable and responsive up to high temperatures and be resistant to chemical attack.

Thermocouples of platinum/10% rhodium, platinum (constructed from wires 0.1 mm in diameter for rapid response) were used in this study. The maximum temperature measurable with these thermocouples is~1700°C. Infrared pyrometry is a possible option for the measurement of higher

temperatures, but problems associated with the changes in the emittance of the sample during combustion and possible interference from product vapours, still have to be overcome (4). Thermocouple junctions were made by welding the crossed wires in an oxygen/LP gas flame. The size of the bead of the thermocouple junction was difficult to control.

Samples were burnt in a channel made from 1 mm thick stainless steel and 30 x 6 x 6 mm in internal dimensions. Slits were cut in the channel (Figure 3.1) to accommodate the thermocouple (electrically insulated with asbestos paper) and to allow simultaneous measurement of the burning time through the use of two infrared detectors positioned opposite the slits. These detectors started and stopped a timing device (resolution 1 millisecond). A manually operated RACAL Computing Counter clock was also used as a back-up timing device.

The channel was inserted into a metal block and the sample was loaded in layers. When the channel was full, a lid and a spacer were positioned over the sample (Figure 3.1) and the whole assembly was hydraulically pressed for one minute under a load of approximately 1 ton (55 MPa) in a Research and Development Press. The density of the pressed composition was estimated from the mass of the material and the volume occupied by the mixture.

Burning of the column was initiated using a starter increment of a 50% $Mn/KMnO_4$, or a 20% Si/Pb_3O_4 composition, ignited with the flare of a match-head (see Figure 3.1). An angular brass hood was used to shield the infrared detectors from the flare of the match head. All results reported are the mean of three to five runs.

The apparatus for temperature profile measurement is shown schematically in Figure 3.2.

3.3 Data capture and processing

The thermocouple output was referenced to 0°C, electronically, by a cold junction compensator. The signal was then fed via a low-noise D.C. amplifier to a CW-16 Exel (IBM-compatible) microcomputer operating at 8 MHz. The gain of the amplifier was set at 254X for all the results reported. Amplified thermocouple outputs were fed to a fast (25 μs conversion time) analog-to-digital converter with 12 bit resolution. The entire system was calibrated against the melting points of Pb (327°C) and Zn (420°C) and derived temperatures were within 3% of literature values.

A software system written in PASCAL (see Appendix) was used to monitor the thermocouple output via a PC-26 A/D card on the microcomputer. The system commenced the capture of data when the thermocouple potential rose above a threshold set to ~70°C. Data could be sampled at intervals from 0.1 ms to 60 seconds and the maximum number of data points that could be collected during the recording of one profile was 30 000. Only approximately 5000 point segments could be saved to either BASIC or LOTUS compatible files for later processing.

Figure 3.1 Sample container assembly

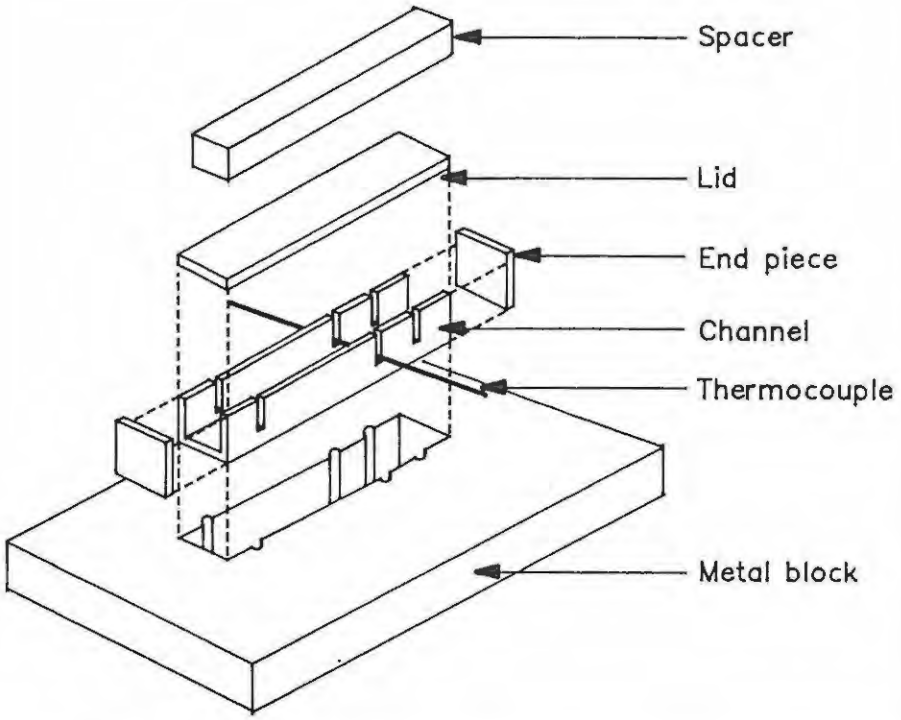

Figure 3.2 Apparatus for measuring temperature profiles and burning rates

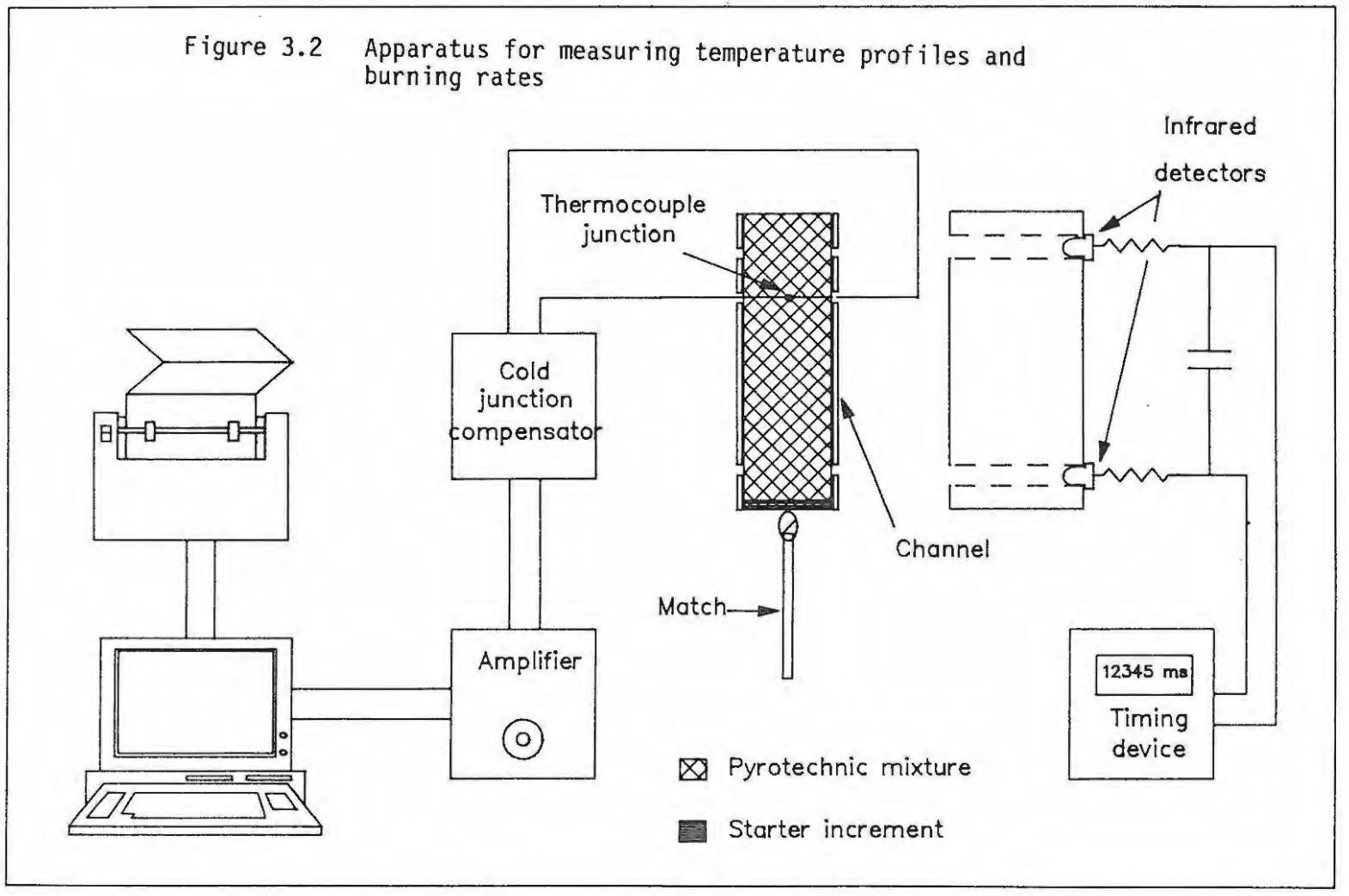

The data capture software was subsequently modified to collect 257 "pre-trigger" points. Prior to triggering, the data capture routine monitored the response of the thermocouples continuously in a buffer. When the response threshold was exceeded, the 257 points prior to triggering were collected and saved together with the rest of the thermocouple response. The capture of pre-trigger points allowed for better resolution of the rise region of the temperature profile.

The thermocouple emf against time data were stored temporarily before conversion into temperature versus time data using a LOTUS 123 spreadsheet and a polynomial expression of the form

$$T = a + bV + cV^2 + dV^3 + eV^4$$

where T is the temperature in °C, V is the thermocouple emf in millivolts and the coefficients: a = 30.1108, b = 120.17982, c = -2.4578, d = 0.041 and e = 6.368×10^{-4}. Further BASIC software was available for the smoothing of the temperature-time data. Numerical integration and differentiation were carried out on spreadsheets. The determinations of the kinetic parameters from temperature profiles according to the procedures developed by Hill *et al* (5,6) and Boddington and Laye *et al* (7,8) were also carried out using menu-driven macros on a LOTUS 123 spreadsheet. (See section 4)

3.4 **Thermal analysis**

A Perkin-Elmer TGA-7 thermogravimetric analyser linked to a Sprint 286 AT microcomputer with a mathematical coprocessor, was used for this study. The upper temperature limit of the TG furnace is 1000°C. The furnace temperature was calibrated against the Curie points of nickel, perkalloy and iron. Sample masses from 0.5 to 10 mg, in standard platinum pans without lids, were heated at rates of 20°C min^{-1} (unless otherwise stated) in nitrogen or in air (flow rate 4 ml min^{-1}, inlet pressure 20 kPa).

DSC studies were carried out under similar conditions in a Perkin-Elmer DSC-7 in platinum pans with lids. The DSC was calibrated against the melting points of indium and zinc (measured in aluminium pans). The upper temperature limit of the DSC was 730°C. All thermal analysis results shown are the mean of three to five runs and errors are calculated from range estimates (9) of the results.

3.5 **Infrared and X-ray diffraction**

Infrared spectra of samples of constituents or mixtures before or after thermal analysis or combustion were recorded using a Perkin-Elmer 180 infrared spectrometer. X-ray diffraction (XRD) studies were carried out on a Philips PW1349-30 diffractometer coupled to a Philips PW1140 X-ray generator. The residues were ground in a mortar to a fine powder before being analysed.

For infrared analysis, the samples were incorporated into KBr disks. The KBr was previously dried by heating over a bunsen flame for two hours. All samples were examined over the wavelength range 2000 to 400 cm^{-1} unless otherwise stated.

The d-values were calculated (10,11) in angstrom (Å) units and literature (10-16) values for a given compound were compared with the experimentally obtained values.

3.6 **Bomb calorimetry**

A Parr 1341 Plain Jacket Bomb Calorimeter was calibrated with benzoic acid using standard procedures. Samples of the pyrotechnic material could not be ignited using fuse wire alone, so a starter increment consisting of 20% Si/Pb_3O_4 (in a solution of 50% acetone in water and 3% carboxymethyl cellulose (CMC)) was fixed to a concentric loop on the fuse wire. The fuse was then air-dried for 1 day and further dried for 1 to 2 hours before use. Samples of the test material (approximately 4 to 6 grams to achieve a 1°C rise in temperature) were placed in a stainless-steel crucible. The pyrotechnic fuse was embedded in the mixture which was then slightly compacted manually. The sealed bomb with sample was charged with helium (3 atmospheres). Argon was found to be unsuitable because of its lower thermal conductivity. The temperature of the system was monitored using a Hewlett Packard 2804 A Quartz Thermometer (in low-resolution mode) and a Bailey Instruments ThermaZip Model TZC digital thermometer.

All results reported are the mean value of three runs.

3.7 **Particle-sizes and surface areas**

For the analysis of the particle-size distributions of the constituents (Tables 3,2 and 3,3), a Malvern Mastersizer Laser Particle-size Analyser and a Coulter Counter Model T_A were used. The laser particle-size analyser method of analysis is based on an obscuration technique in which the particles previously suspended in a liquid medium, are passed through the optical path of a laser. The particle-size distribution is then computed from the amount and direction of scattered light, and the result is obtained as a frequency-distribution. All references to particle-size refer to the mean diameters of the particles in the sample.

The laser obscuration technique also measures the specific surface area (SSA) of a sample but assumes that the particles are perfect spheres. Additional surface area due to surface phenomena such as pore structures and surface fractures, is therefore not taken into account. The SSA of the constituents

were also determined by BET analysis. Sample masses of approximately 1 g were used and nitrogen was used as the adsorbent. The SSA of the ingredients used in this study using obscuration and BET techniques are summarised in Table 3.2. The results obtained from the obscuration technique were, apparently, more reproducible.

Scanning electron micoscropy was carried out on a JOEL JSM 80 scanning electron microscope.

3.8 References

1. J.H. Mclain, "*Pyrotechnics: From the Viewpoint of Solid State Chemistry*", Franklin Institute Press, Philadelphia. Pennsylvania, 1980.
2. A. Bailey and S.G. Murray, "*Explosives, Propellants and Pyrotechnics*", Vol. 2, Brassey's, London, 1989.
3. R. Klein, M.M. Ensler, G. von Elbe and B. Lewis, J. Phys. Colloid Chem., **54** (1950) 877.
4. R.A. Rugunanan and M.E. Brown, J. Thermal Analysis, (1992), in press.
5. R.A.W. Hill, L.E. Sutton, R.B. Temple and A. White, Research, **3** (1950) 569.
6. R.A.W. Hill, L.E. Sutton, R.B. Temple and A. White, 4th Symposium on Combustion, (1958) 349.
7. T. Boddington, P.G. Laye, J.R.G. Pude and J. Tipping, Comb. Flame., **47** (1982) 235.
8. T. Boddington, P.G. Laye, J.R.G. Pude and J. Tipping, Comb. Flame., **63** (1986) 235.
9. A.J. Lyon, "*Dealing with Data*", Pergamon, Oxford,1970, p20.
10. A.R. West, "*Solid State Chemistry and it's Applications*", John Wiley, 1984.
11. E.P Bertin, "*Introduction to X-ray Spectrometric Analysis*", Plenum Press, New York, 1978, Ch. 2, p. 71.
12. L.G. Berry (Ed.), "*Powder Diffraction File: Search Manual, Alphabetical listing of Inorganic Compounds*", Joint Committee on Powder Diffraction Standards, Pennsylvania, 1973.
13. J.V. Smith (Ed.), "*Powder Diffraction File*", American Society for Testing and Minerals, Philadelphia, 1967.
14. J.V. Smith (Ed.), "*Kwic guide to the Powder Diffraction File, 1966*", American Society for Testing and Minerals, Philadelphia, 1966.
15. J.V. Smith (Ed.), "*Fink Inorganic Index to the Powder Diffraction File, 1966*", American Society for Testing and Minerals, Philadelphia, 1966.
16. W.F McClune (Ed.), "*Selected Powder Diffraction Data for Minerals*", Joint Committee on Powder Diffraction Standards, Pennsylvania, 1973

4. EXTRACTION OF KINETIC AND THERMODYNAMIC INFORMATION FROM TEMPERATURE PROFILES

4.1 Introduction

The shapes of temperature profiles can yield valuable information about the structure of the burning front (1,2). Temperature profiles can have complicated structures, but they may be grouped generally into four elementary types (see Figure 4.2) (see also ref. 2). Type I is a classical combustion wave consisting of a heated layer and a narrow reaction zone. For wide reaction zones, the corresponding temperature profiles have a typical Type II shape. The reaction zone itself may be divided into two further sub-zones called the propagation and post-combustion zones (3,4). Only the propagation sub-zone is thought to be responsible for the propagation of burning. Type III profiles show a clear point of inflection and indicate the presence of two zones of active chemical reaction. Usually, only the first zone is responsible for the propagation of burning. Profiles belonging to Type IV characteristically have an isothermal region. This region results from simultaneous chemical reaction and phase transition. The velocity of the combustion front for Type I systems is determined by the complete conversion of reactants to products at maximum temperature. For the other types, the velocity of the burning front is determined by the partial conversion of reactants at a lower temperature than the maximum temperature.

The interpretation of temperature profiles (recorded as described in Section 3) is largely based on the Mallard-Le Chatelier theory (5) in which combustion in gaseous mixtures is propagated mainly by the forward conduction of heat. A similar theoretical basis has been used for describing the propagation of exothermic layer-to-layer reactions between solids. The model used (6) consists of a cylindrical rod of a uniformly packed powder (see Figure 4.1). On application of an ignition stimulus to the end *A*, the reaction front (*O*) moves at a uniform speed, v, along the length of the cylinder. This burning front then effectively divides the cylinder into an unreacted zone (*U*) at temperature T_1 and a reacted zone (*R*) at temperature T_2. It is assumed that reaction is maintained by the conduction of heat from *U* to *R* (see Figure 4.1) and that radiation of heat and the effect of mass transport are negligible. The thermal conductivity, specific heat capacity and density of the powder are also usually assumed to remain unchanged over T_1 and T_2.

Provided that mass transport is absent, the rate at which the temperature increases, within a small volume element of a burning pyrotechnic material, may be determined from the Mallard-Le Chatelier equation (6).

Figure 4.1 Model of a combustion wave

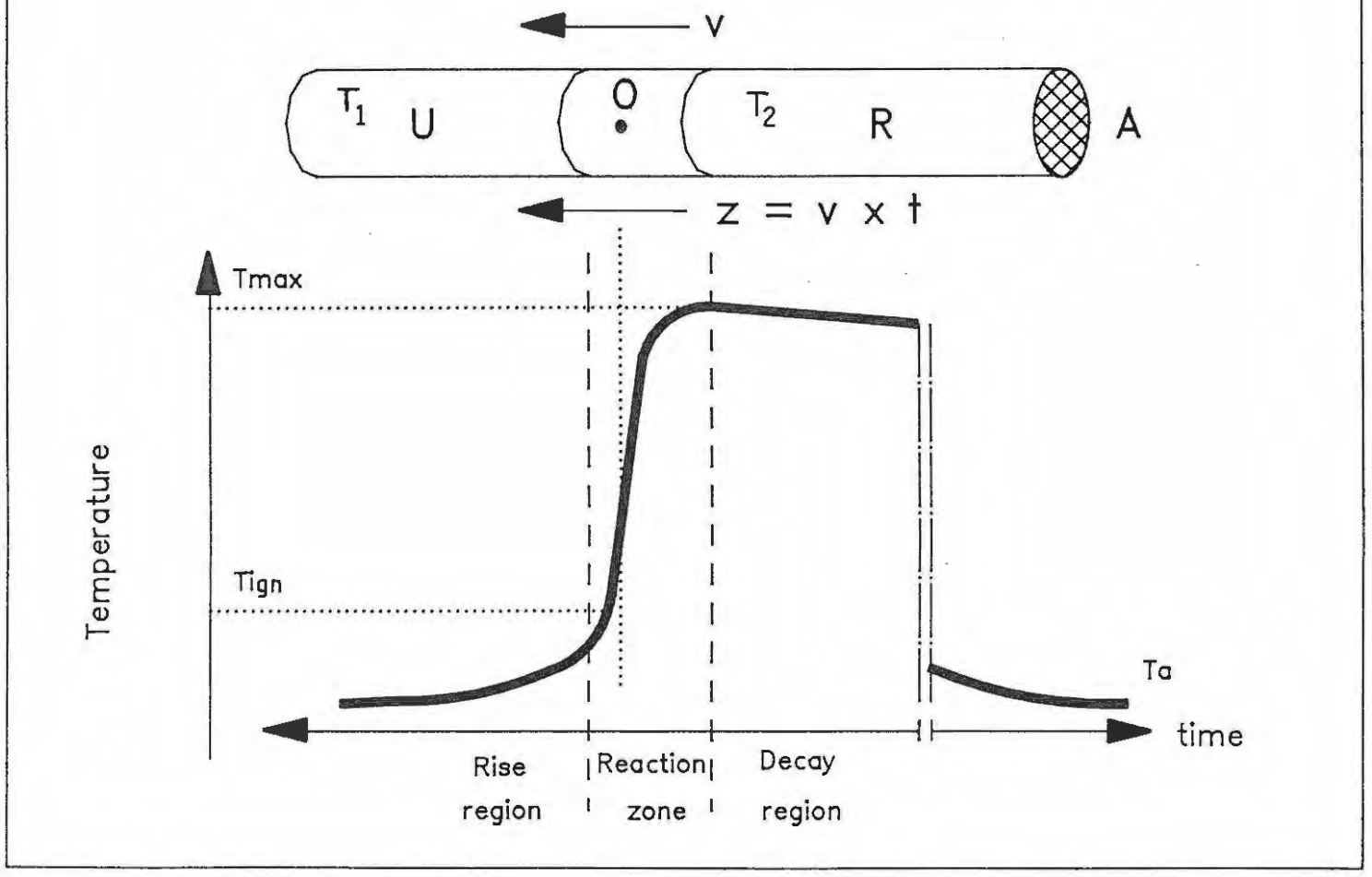

Figure 4.2 Elementary shapes of temperature profiles (Ref. 4)

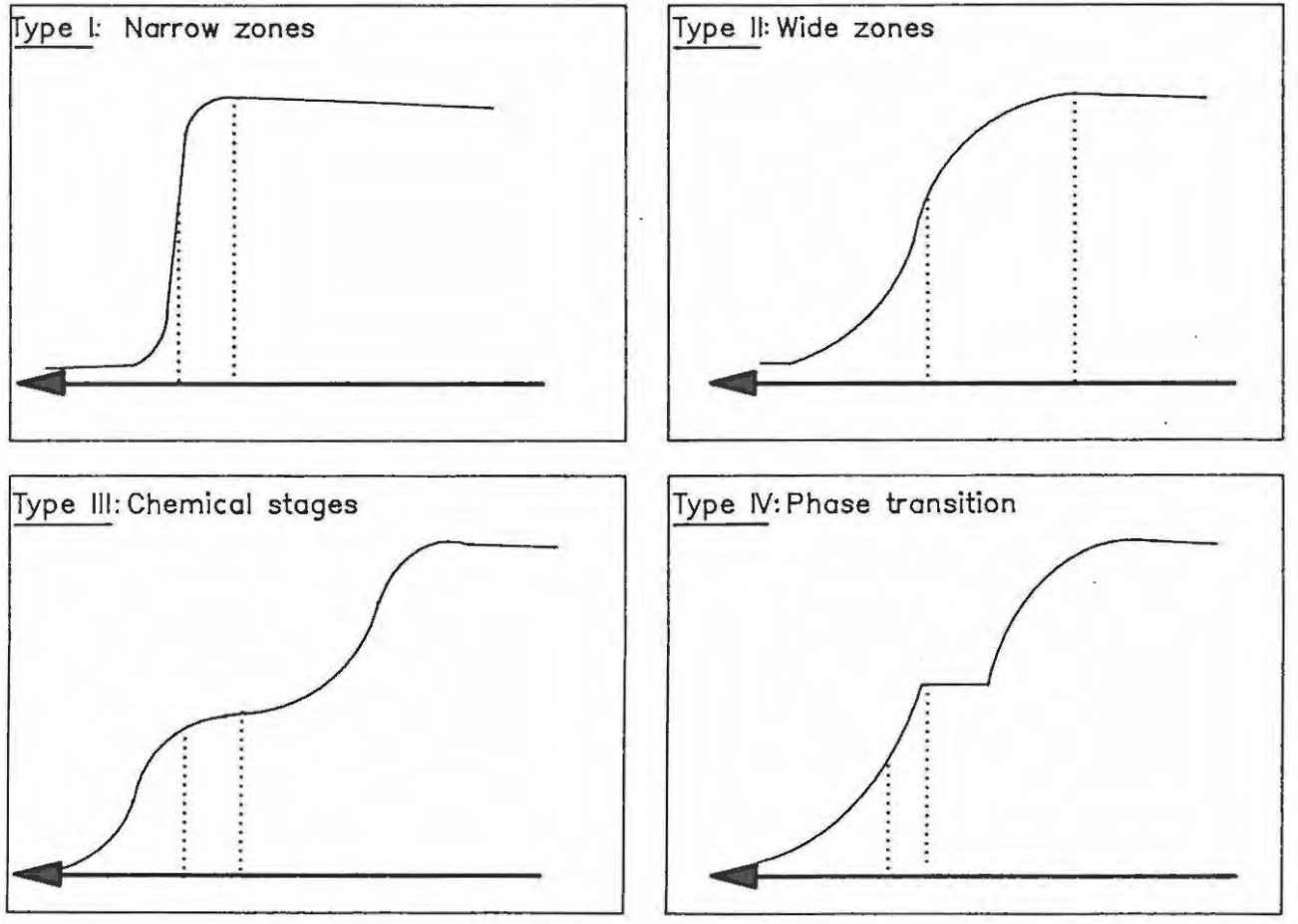

Rate of energy increase	=	Rate of energy generation by reaction	+	Rate of gain of energy by conduction	-	Rate of energy loss through walls

or

$$\rho c \frac{dT}{dt} = \rho q \frac{d\alpha}{dt} + \frac{\lambda}{v^2} \frac{d^2T}{dt^2} - h(T-T_a) \qquad ...(4.1)$$

where ρ is the density, q is the enthalpy change per unit mass, α is the fractional extent of reaction, λ is the thermal conductivity, v is the burning rate, c is the specific heat capacity, h is the lateral heat-loss coefficient and T_a is the ambient temperature.

The kinetics of the reaction were assumed to be of the form

$$d\alpha/dt = f(\Omega, f, T)$$

where α is a measure of the extent of reaction, Ω is a parameter which contains the various physical factors which influence the reaction, and T is the local temperature.

4.2 Kinetic aspects

The general rate equation for reaction at constant temperature can be written as

$$\frac{d\alpha}{dt} = k\, g(\alpha)$$

where α is the fractional extent of reaction, $g(\alpha)$ is some function of α which has to be found by experiment and k is the rate coefficient. Integration between limits (0,0) and (t,α) gives

$$f(\alpha) = kt$$

where

$$f(\alpha) = \int_0^{\alpha} \frac{1}{g(\alpha)}\, d\alpha$$

The influence of temperature is introduced through the Arrhenius equation

$$k = A \exp(-E_a/RT)$$

which is usually assumed to be applicable to heterogeneous reactions. The rate equation may thus be written as

$$d\alpha/dt = A \exp(-E_a/RT)\, g(\alpha)$$

In thermal analysis experiments, the temperature is generally programmed to increase linearly with time so that

$$dT/dt = \Phi = \text{constant}$$

In spite of controversy, the two equations are usually combined

$$\frac{d\alpha}{dt} = \frac{d\alpha}{dT} \cdot \frac{dT}{dt} = \frac{d\alpha}{dT}\Phi$$

Then,

$$\int_0^\alpha \frac{d\alpha}{g(\alpha)} = f(\alpha) = \frac{A}{\Phi}\int_{T_o}^{T} \exp\left[-\frac{E_a}{RT}\right] dT \qquad \ldots(4.2)$$

This equation may be used in various ways to find A and E_a.

Many methods based on equation (4.2) have been developed for determining A and Ea from programmed temperature experiments. The extraction of kinetic information from the temperature profiles of burning pyrotechnic compositions is more complicated since.

(i) α cannot be measured directly, and

(ii) T increases in a non-linear manner through self-heating and therefore depends on α.

4.3 **The Hill approach**

Hill's treatment (7,8) starts with equation (4.1). By assuming that lateral heat loss is negligible, that ρ, q, λ, and c are constants and by integrating between T and T_a in the burning front (using $\alpha = 0$),

$$\frac{\lambda}{v^2}\frac{d^2T}{dt^2} = 0 \quad \text{at } T = T_a$$

then

$$\rho q\alpha + \frac{\lambda}{v^2}\frac{d^2T}{dt^2} = \rho c(T-T_a)$$

By rearranging and letting $q = c(T_{max}-T_a)$, where T_{max} is the maximum temperature of the temperature profile

$$\alpha = \frac{(T-T_a)\ (\lambda/c\rho v^2)\ dT/dt}{(T_{max}-T_a)}$$

If the temperature is converted to a dimensionless temperature, i.e.

$$\theta = \frac{(T-T_a)}{(T_{max}-T_a)} \qquad ...(4.3)$$

then

$$\frac{d\theta}{dt} = \frac{1}{(T_{max}-T_a)}\frac{dT}{dt}$$

so

$$\alpha = \theta - \frac{\lambda}{c\rho v^2}\frac{d\theta}{dt}$$

then

$$\alpha = \theta - (1/S)\ dT/dt \qquad ...(4.4)$$

where $S = c\rho v^2/\lambda = v^2/D$. Where $D = \lambda/(\rho c)$ is the thermal diffusivity.

In practice, the T,t profile is converted to a θ,t profile and dθ/dt is obtained by numerical differentiation. Equation (4.4) is used to calculate a set of values for α at various T values. The original T,t data are used to produce a set of α,t data which can be differentiated numerically to give dα/dt against t, or dα/dt against T data.

Hill made the common assumption of a simple "order-of-reaction" model:

$$g(\alpha) = (1-\alpha)^n \qquad ...(4.5)$$

so

$$d\alpha/dt = A \exp(-E_a/RT)\ (1-\alpha)^n$$

hence

$$\ln (d\alpha/dt) = \ln A - E_a/RT + n \ln(1- \alpha)$$

or

$$h(\alpha) = \ln(d\alpha/dt) - n \ln(1-\alpha)$$

$$= - E_a/RT + \ln A \qquad ...(4.6)$$

Plots of $h(\alpha)$ vs 1/T, at various trial values of n should then lead to straight lines from which E_a and A can be calculated.

From equation (4.4), it can also be seen that

$$\lim_{\theta \to 0} \frac{d\theta/dt}{\theta} = S \qquad ...(4.7)$$

So a plot of $(d\theta/dt)/\theta$ vs θ, when extrapolated to zero, gives S. The burning rate can then be calculated

$$v_{calc} = (SD)^{1/2} \qquad ...(4.8)$$

and compared with values measured independently.

4.4 The Leeds approach

The method for obtaining kinetic information from temperature profiles developed at Leeds University (1,9) is also based on equation (4.1). In the Leeds approach, equation (4.1) is simplified by setting $U = T - T_a$ and by dividing by ρc

$$\frac{c}{\lambda \rho v^2} \frac{d^2U}{dt^2} - \frac{dU}{dt} + \frac{w}{c} - \frac{U}{t_{th}} = 0 \qquad ...(4.9)$$

where w is the rate at which heat is evolved ($d\alpha/dt$) and the thermal relaxation time due to lateral heat conduction alone, t_{th}, is equal to $\rho c/h$. The equation may be further simplified by setting $D = \lambda/\rho c$ and letting $t^* = D/v^2$ and by introducing G which is the rate at which the temperature increases in an adiabatic system.

$$t^* \frac{d^2U}{dt^2} - \frac{dU}{dt} + G - \frac{U}{t_{th}} = 0 \qquad \ldots(4.10)$$

t^* is the rise time of the inert forewave in systems where there is no lateral heat loss, G is the thermal power due to reaction (w/c) and v, c, λ, ρ and h are assumed to be constant for a given combustion wave.

From equation (4.10) there are three contributors to the total thermal power dU/dt:

$t^* \frac{d^2U}{dt^2}$ axial conduction ...(A)

$\frac{U}{t_{th}}$ lateral heat loss ...(B)

$\frac{dU}{t}$ Overall rise ...(C)

and the thermal power due to reaction, G, which may be rewritten as

$$G = \frac{U}{t_{th}} + \frac{dU}{t} - t^* \frac{d^2U}{dt^2} \qquad \ldots(4.11)$$

For a given combustion wave, plots of each of the above component thermal powers as functions of time, give information on the relative importance of each contribution during burning.

Values of the fractional extent of reaction, α, can be obtained from the local thermal power due to reaction, G. G may be written in the form

$$G = \frac{1}{c}\frac{dq}{dt} = U_{ad}\frac{d\alpha}{dt}$$

where U_{ad} is the adiabatic temperature rise (see below).

For nth order kinetics

$$\frac{d\alpha}{dt} = A(1-\alpha)^n \exp(-E_a/RT)$$

and since

$$G = (d\alpha/dt)\, U_{ad}$$

$$G = U_{ad} A (1-\alpha)^n \exp(-E_a/RT) \quad ...(4.12)$$

with three unknown constants, A, E_a and n.

The temperature profile should be corrected for finite thermocouple size (see ref. 9) and then used to calculate G_{exp}. Boddington and Laye (3,9) then used an iterative routine to minimise the sum

$$\Sigma \{(G_{exp}) - (G_{calc})\}^2$$

where G_{calc} is obtained from equation (4.12), by adjustment of the values of A, E_a and n. Values for the kinetic parameters are thus obtained.

A number of additional rate laws, e.g.

$$f(\alpha) = (1 - \alpha)^n$$

$$= (1 - \alpha)^n (1 + \alpha)^m$$

$$= (1 - \alpha)^n \alpha^m$$

were considered (1,9), but did not give significantly improved fits.

4.5 **Thermochemical aspects**

The heat evolved in a given time interval, t_1 to t_2, for unit mass of reactant mixture, is

$$\Delta\Phi = 1/c \int_{t_1}^{t_2} w dt$$

$$= 1/c \int_{t_1}^{t_2} G dt$$

The total heat of reaction, q (in kJ (g mixture)$^{-1}$)), including any contributions from accompanying phase changes, is given as

$$q = U_{ad}\, c \qquad \ldots(4.13)$$

So,

$$q = \int_{-\infty}^{\infty} w\,dt$$

Substituting in equation (4.9), rearranging and integrating between the limits ∞ and $-\infty$

$$\frac{q}{c} = \frac{1}{t_{th}} \int_{-\infty}^{\infty} U\,dt + (U_{\infty} - U_{-\infty}) - t^* \frac{d(U_{\infty} - U_{-\infty})}{dt}$$

After infinite cooling-time, the temperature of the system will be T_a. So $U_{\infty} = U_{-\infty} = 0$. Then

$$U_{ad} = \frac{1}{t_{th}} \int_{-\infty}^{\infty} U\,dt$$

U_{ad} can be measured from the area under a temperature-time plot. If times t_1 and t_2 are arbitarily chosen to lie within the remote rise and decay regions of a temperature profile, then

$$U_{ad} = \frac{1}{t_{th}} \int_{-\infty}^{t_1} U\,dt + \frac{1}{t_{th}} \int_{t_1}^{t_2} U\,dt + \frac{1}{t_{th}} \int_{t_2}^{\infty} U\,dt$$

The first (rise zone) and third (decay zone) integrals have solutions $t_r U(t_1)$ and $t_d U(t_2)$ respectively, where t_r is the rise time and t_d the decay time and $t_{th} = t_d - t_r$. Then,

$$U_{ad} = \frac{t_r}{t_d - t_r} U(t_1) + \frac{t_r}{t_d - t_r} \int_{t_1}^{t_2} U\,dt + \frac{t_d}{t_d - t_r} U(t_2)$$

If it is assumed that $t_d >> t_r$ and if $t_1 = 0$ and $U(t_1) = 0$, then

$$U_{ad} = U(t_2) + \frac{1}{t_d} \int_{0}^{t_2} U\,dt \qquad \ldots(4.14)$$

By choosing arbitary values for t_2 and by integrating a plot of U versus t, U_{ad} and $1/t_d$ can be obtained from the y-intercept and slope, respectively, from a plot of $U(t_2)$ and the integral $\int U dt$ between the limits 0 and t_2.

4.6 Burning rates

If the value of the thermal conductivity of a pyrotechnic mixture is known, the burning rate of the mixture can be calculated. In zones where the internal power is zero, i.e. where chemical reactions occur at negligible rates and phase transitions are absent, equation (4.10) becomes

$$t^* \frac{d^2U}{dt^2} - \frac{dU}{dt} - \frac{U}{t_{th}} = 0$$

If the lateral heat loss is zero then

$$t^* \frac{d^2U}{dt^2} = \frac{dU}{dt}$$

which upon integration gives

$$t^* \frac{dU}{dt} - U + P = 0$$

The value for P is zero since in the case of the rise zone of the profile, $dU/dt \rightarrow 0$ as $U \rightarrow 0$. Then

$$U = t^* \, dU/dt$$

which on integration gives

$$\ln U = t/t^* + \text{constant}$$

After a long time, $T \rightarrow T_a$ as $t \rightarrow \infty$ so

$$\frac{1}{t^*} = \frac{d\ln U}{dt} \qquad \ldots(4.15)$$

Now

$$t^* = D/v^2$$

so

$$v = (D/t^*)^{1/2} \qquad \ldots(4.16)$$

but

$$t^* = 1/(t_r^{-1} - t_d^{-1})$$

Since $t_d >> t_r$

$$1/t^* \equiv 1/t_r$$

t_r can thus be be obtained from the slope in the rise zone of a plot of ln U versus t (i.e. $t_r = (d\ln U/dt)^{-1}$). A plot of ln U against t in the remote region will have a slope of $1/t_d$.

4.7 Other kinetic considerations

Both the Leeds and Hill approaches assume that the kinetic behaviour of pyrotechnic compositions follow simple Arrhenius kinetics

$$k_{AR} = A \exp(-E_a/RT)$$

The low activation energies of pyrotechnic reactions generally imply reactions which are controlled by a diffusion mechanism. Boddington *et al* (10) found that the best fit kinetic parameters obtained from Arrhenius kinetics predicted too great a reaction rate at low temperatures. A more complex relationship was then suggested

$$k^{-1} = [A_{AR} \exp(-E_a/RT)]^{-1} + (BT^m)^{-1}$$

so

$$k^{-1} = k_{AR}^{-1} + (BT^m)^{-1} \qquad ...(4.17)$$

where B is a diffusion coefficient. The above equation combines the Arrhenius behaviour at low temperatures, which predicts a rapid rise in temperature, with diffusion controlled behaviour at high temperature, where the rate becomes less dependent on temperature. On the assumption that the rate of a pyrotechnic reaction is negligible at temperatures below the ignition temperature, and that the high temperature kinetic behaviour is adequately described by the kinetic parameters determined from the analysis of temperature profiles, equation (4.17) may be rewritten as

$$k_{tp}^{-1} = k_{AR}^{-1} + (BT^m)^{-1}$$

(k_{tp} is the rate constant derived from the analysis of temperature profiles). Hence

$$B^{-1} = T^m(k_{tp}^{-1} - k_{AR}^{-1}) \qquad ...(4.18)$$

4.8 Comments

A kinetic study of $W/K_2Cr_2O_7$ mixtures (9,11,12) showed that E_a values were, typically, of the order of 9 to 15 kJ mol^{-1} for mixtures containing various proportions of W and $K_2Cr_2O_7$. Experiments with ternary mixtures which contained Cr_2O_3 as a diluent gave similar activation energies to those observed in binary systems. The activation energies under non-ignition conditions were ~150 kJ mol^{-1}. These differences indicate that there may be different rate controlling process in the reactions under ignition and non-ignition conditions.

Activation energies of the order of 22 kJ mol^{-1} were obtained (Hill method) for the $Sb/KMnO_4$ system (13,14). In a study of binary systems of Mn and Mo as fuels and BaO_2 and SrO_2 as oxidants (15,16), activation energies of the order of 10 kJ mol^{-1} (Hill approach) and ~20 kJ mol^{-1} (Leeds approach) were obtained under ignition conditions. Values obtained from thermal analysis were 235 kJ mol^{-1} (40% Mn/BaO_2), 84 kJ mol^{-1} (40% Mo/BaO_2) and ~430 kJ mol^{-1} (40% Mn/SrO_2).

It is highly unlikely that a simple "order-of-reaction" model (for example, equation (4.5)) will realistically describe the complexity of pyrotechnic reactions. It is, however, often found for heterogeneous reactions that the Arrhenius parameters, A and E_a, are not very dependent on the kinetic model, $g(\alpha)$, used in their derivation. Hence, although the exact kinetic relationship for the pyrotechnic mixture may not be able to be established, the values of E_a may still provide a valuable indication of the rate-controlling processes (i.e. diffusion, conduction) during burning.

4.9 Data processing

4.9.1 *Introduction*

Details of the numerical methods for the analysis of the temperature profiles, using the Hill approach and the Leeds approach, are described. Schematic diagrams of the steps in the analysis are shown in Schemes 4.1 (Hill) and 4.2 (Leeds). An example of a typical temperature (T,t) profile is shown in Figure 4.3.

Figure 4.3 Effect of smoothing on a typical temperature profile

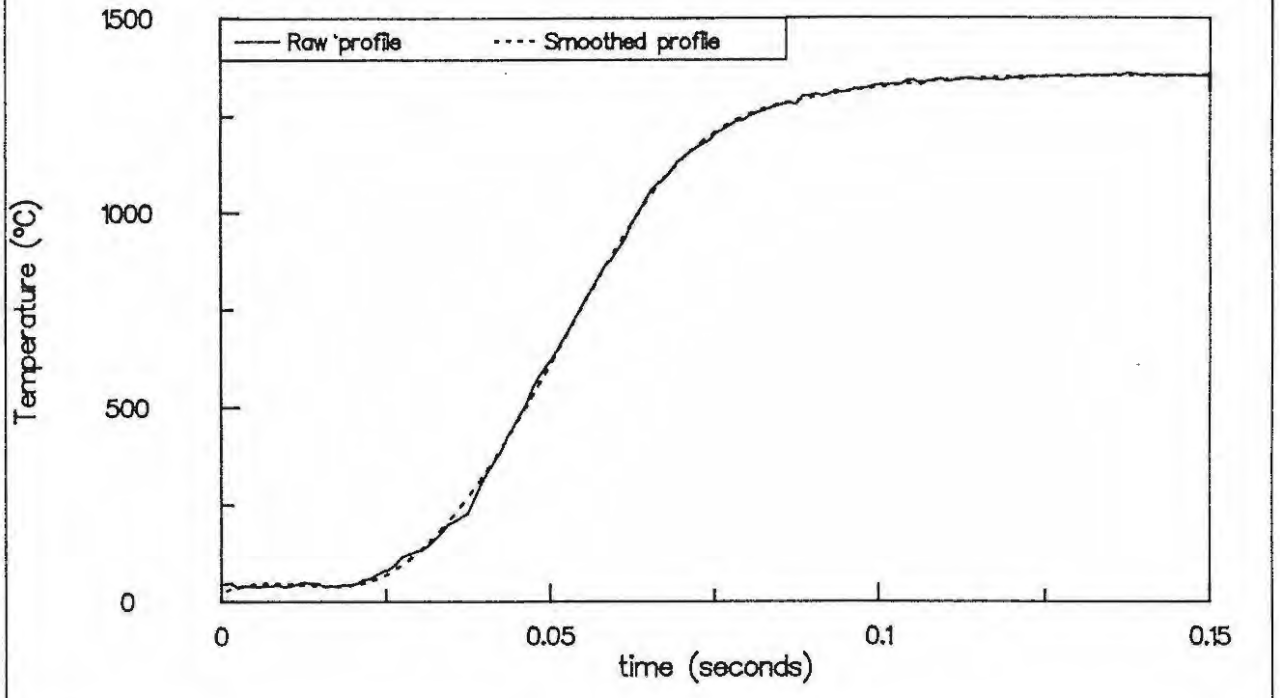

Figure 4.4 U and ln U against time

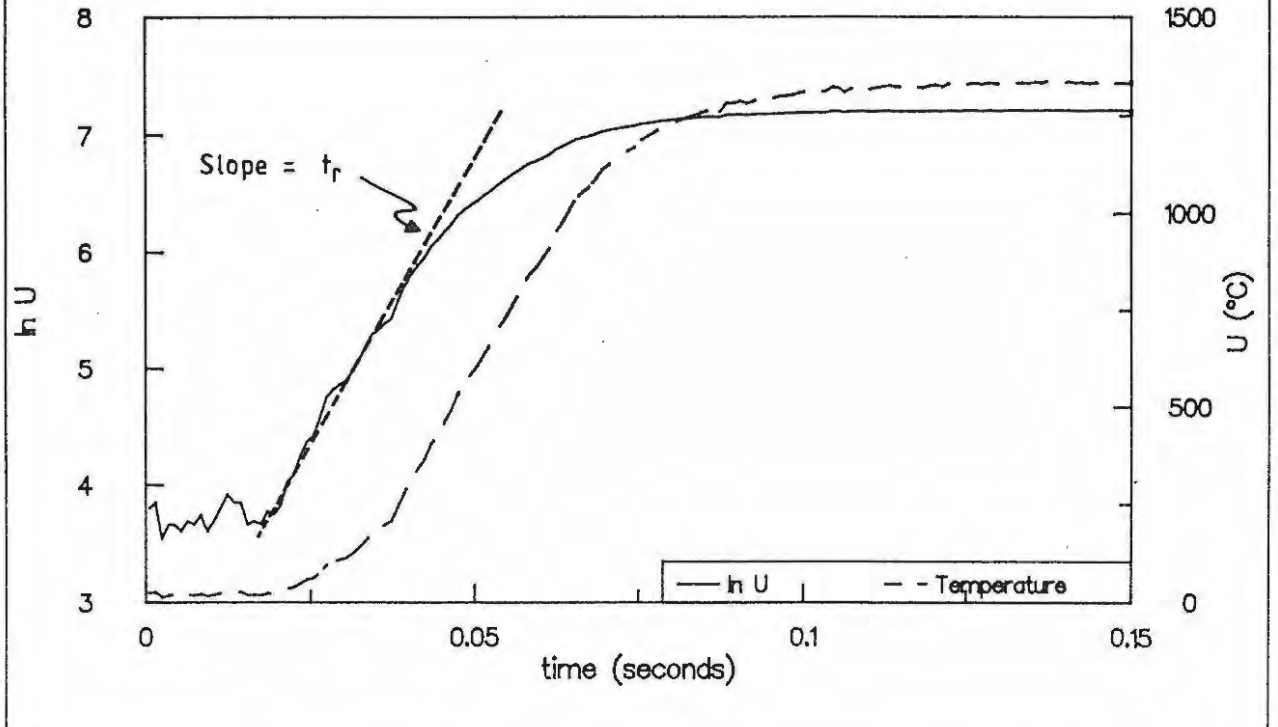

4.9.2 *Numerical methods*

The analyses of temperature profiles were carried out on LOTUS 123 spreadsheets using menu-driven macros. Because the raw temperature profiles contained a considerable amount of noise which may be greatly amplified by subsequent numerical differentiation, profiles were numerically smoothed, where necessary, using a routine (17) written in BASIC (see Appendix). The effect of smoothing on a temperature profile is shown in Figure 4.3. Smoothed profiles were converted from T values to excess temperature values $U = T - T_a$. A Savitsky-Golay 5-point relationship was used for numerical differentiation (see Appendix).

4.9.3 *Rise and decay times*

Hill obtained the rise time from the y-intercept of a plot of $(d\theta/dt)/\theta$ against θ (see equation (4.7) in Section 4.3). In the Leeds analysis, the rise time is obtained from the slope in the initial rise part of a plot of ln U against time (see Figure 4.4). The decay time may be obtained by two methods:

(i) from the slope of a plot of ln U against t for the decay region of the temperature profile. The y-intercept of this plot yields the adiabatic temperature rise, U_{ad};

(ii) from the slope of a plot of $\int U(t)\,dt$ against U(t) (see equation (4.14), in Section 4.5) and the value of U_{ad} can be obtained from the y-intercept of this plot (see Figure 4.5).

If the heat capacity, c, of the mixture is known, then the total heat output of the composition can be calculated from (equation 4.13)

$$q = U_{ad}\, c$$

4.9.4 *Kinetic parameters*

Hill approach

A full theoretical account of the Hill approach to obtaining kinetic parameters from temperature profiles is given in Section 4.3. The region of interest (rise zone) of the actual profile is selected. Hill converted temperature profiles into dimensionless temperature-time values, θ (see Figure 4.6) from which α could be calculated. Figure 4.6 is a plot of $d\theta/dt$ which was calculated using a 5-point Savitsky-Golay differential equation. From the y-intercept of a plot of $(d\theta/dt)/\theta$ against θ (see equation 4.7), the value of S (thermal diffusivity term) was determined (see Figure 4.7).

Figure 4.5 U(t) against $\int_0^{t_2} U\,dt$

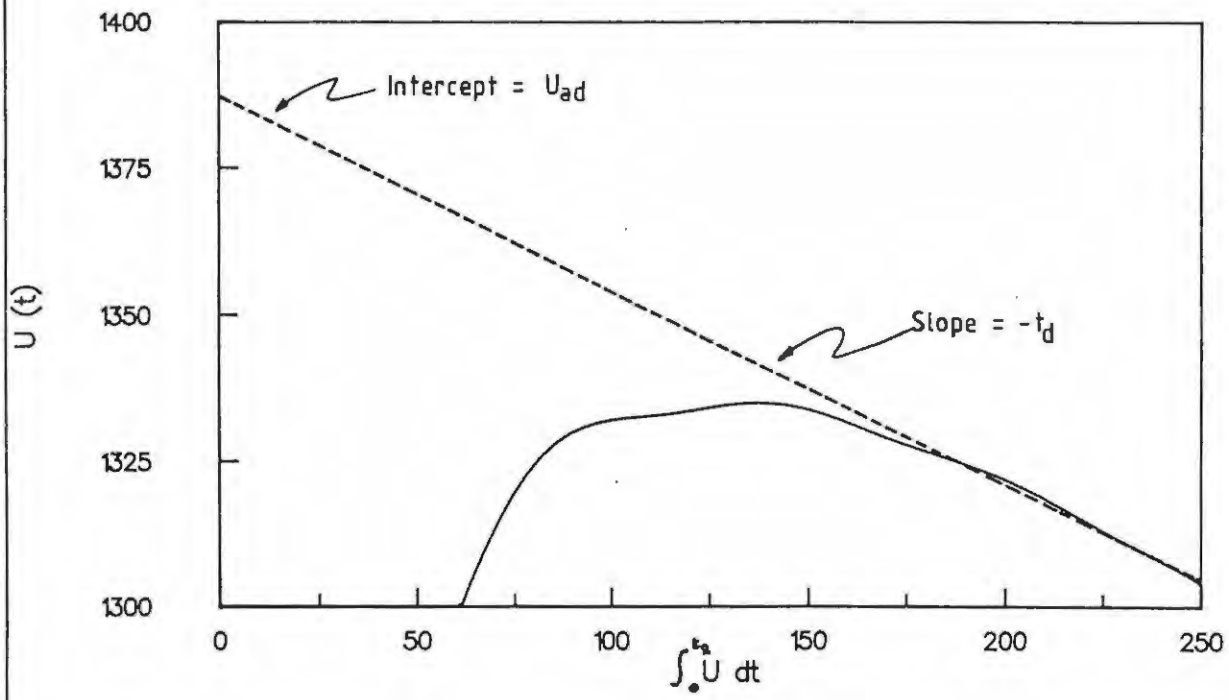

Figure 4.6 dθ/dt against time

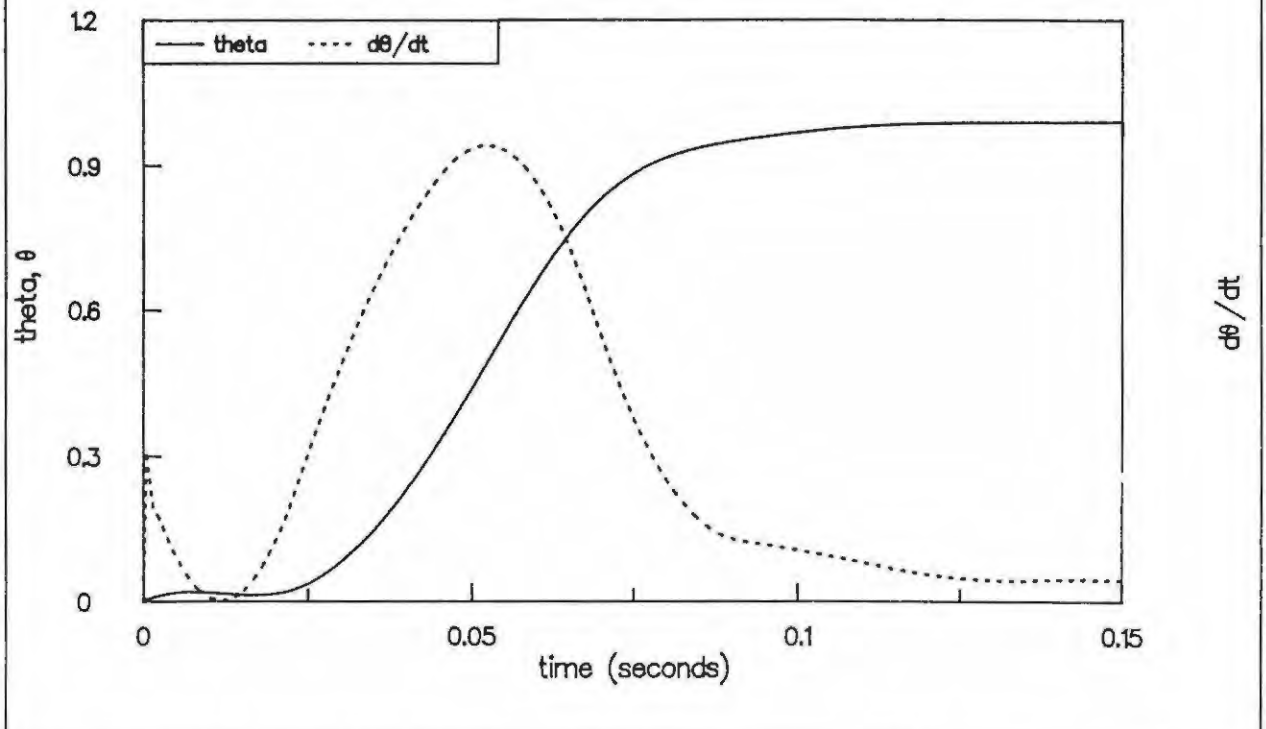

Figure 4.7 $(d\theta/dt)/\theta$ against θ for a typical temperature profile

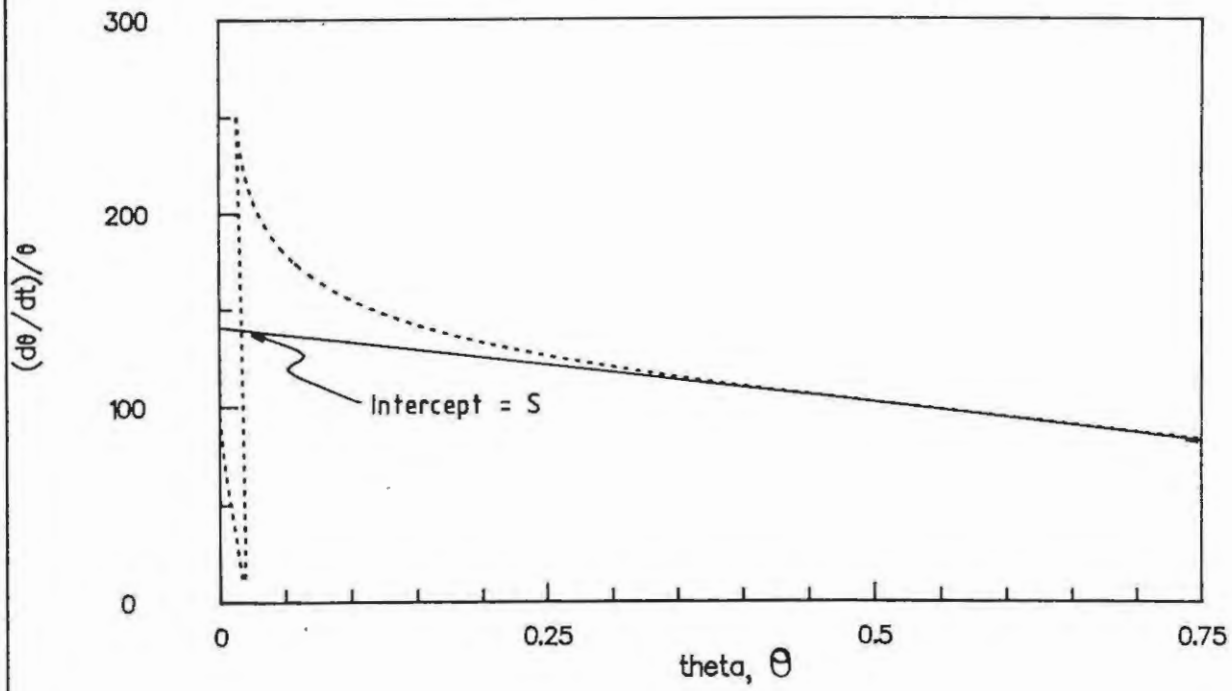

Figure 4.8 Alpha (α) and $d\alpha/dt$ against time

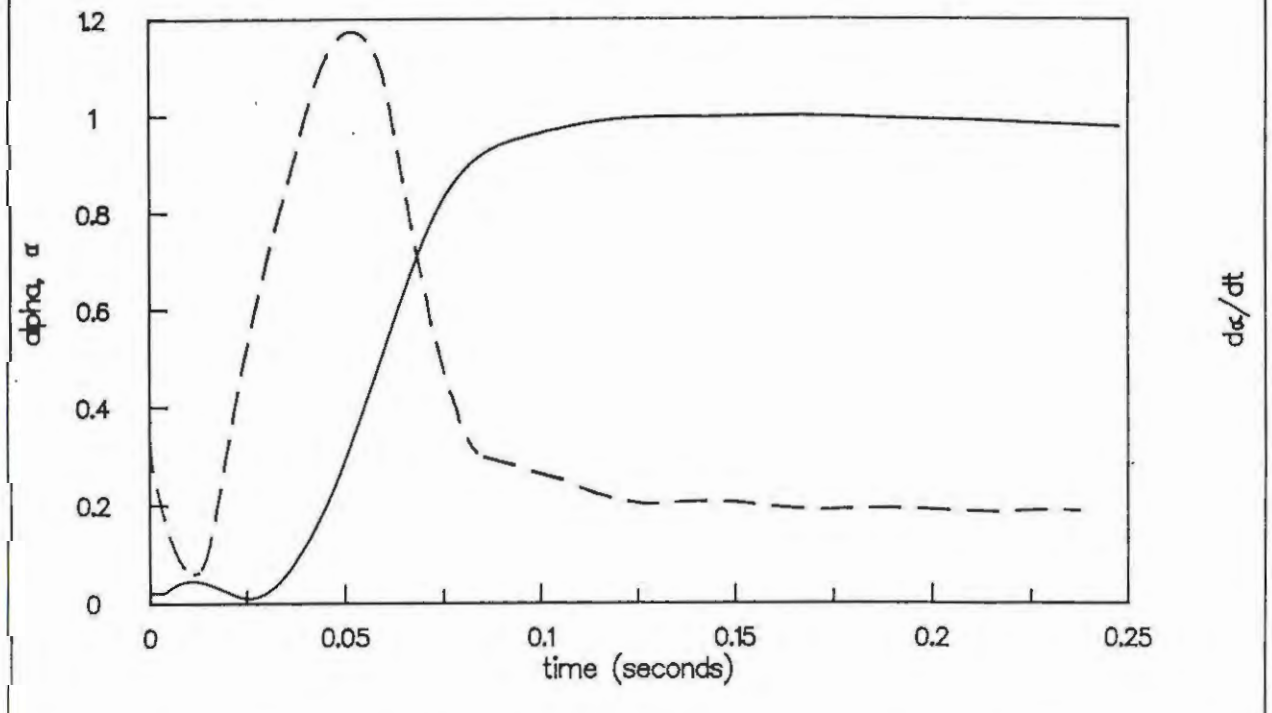

Hill obtained the fractional extent of reaction, α, from equation (4.4). A plot of α and $d\alpha/dt$ against t is shown in Figure 4.8. $h(\alpha)$ was calculated for various trial values of n and plotted against 1/T. n was adjusted until satisfactory linearity was achieved. E_a and ln A could then be calculated (equation 4.6) (Figure 4.9).

Leeds approach

The various contributions to the power function, G (equation (4.11)), are shown in Figure 4.10. α was calculated from partial area under the G_{exp} curve. Boddington *et al* used an iterative routine to minimise the sum

$$\Sigma \{(G_{exp}) - (G_{calc})\}^2$$

from which the kinetic parameters were obtained. A similar analysis was performed in this study. To simplify the problem, the following substitutions were made into equation (4.12)

$$y_i = (G_{exp})_i \; ; \qquad x_i = 1-\alpha_i \; ; \qquad z_i = 1/T \; ;$$

$$a = U_{ad}A \quad \text{and} \quad b = E_a/R$$

Then

$$f = y_i - a(x_i)^n \exp(-bz_i) \qquad \ldots(4.19)$$

a, b and n were adjusted until the the squares of the difference between G_{exp} and G_{calc} was a minimum. Two BMDP (18) routines were used to calculate a,b, and n.

(i) BMDP1R based on the linear regression of the natural log form of equation (4.19) and

(ii) BMDP3R based on a non-linear regression of the same equation.

Values of a,b and n obtained from BMDP1R, were used as initial estimates for the non-linear regression analysis. Figure 4.11 shows the results after linear regression analysis (G_{cal}-l) and after non-linear regression analysis (G_{cal}-nl). Also shown is the experimentally obtained curve for the power function (G_{exp}).

Figure 4.9 h(α) against 1/T for a typical temperature profile

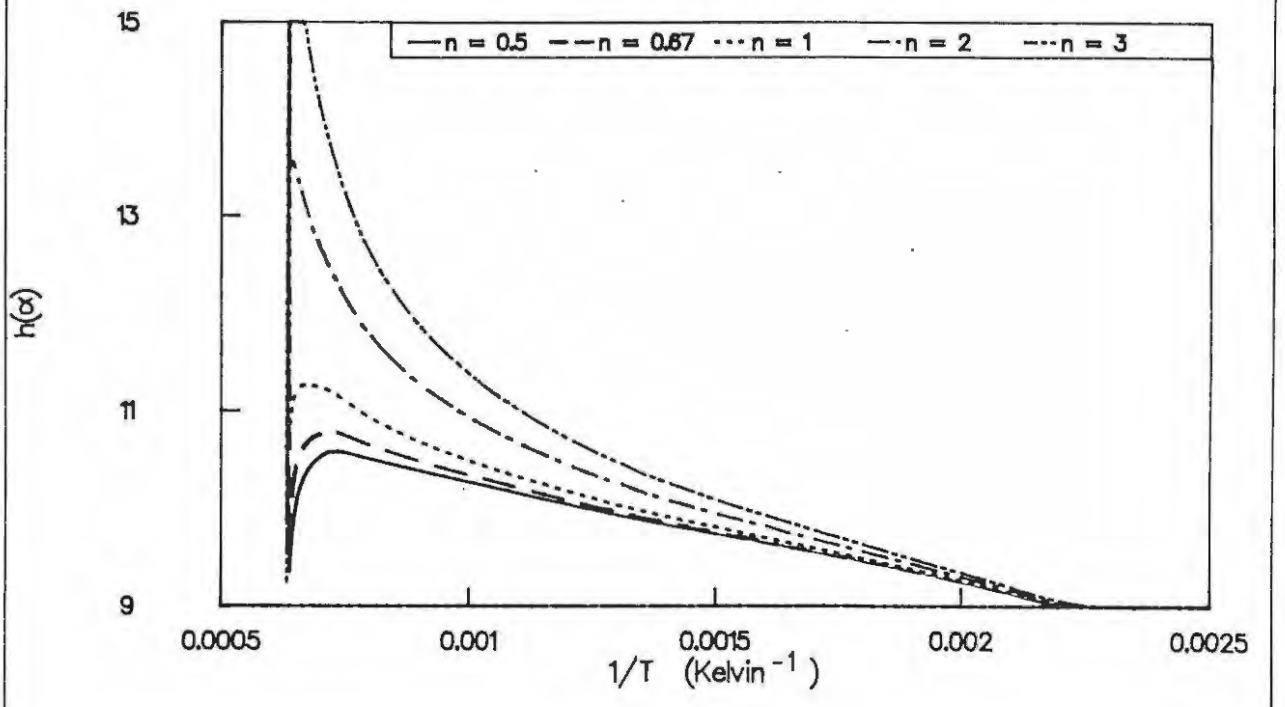

Figure 4.10 Leeds power functions for a typical temperature profile

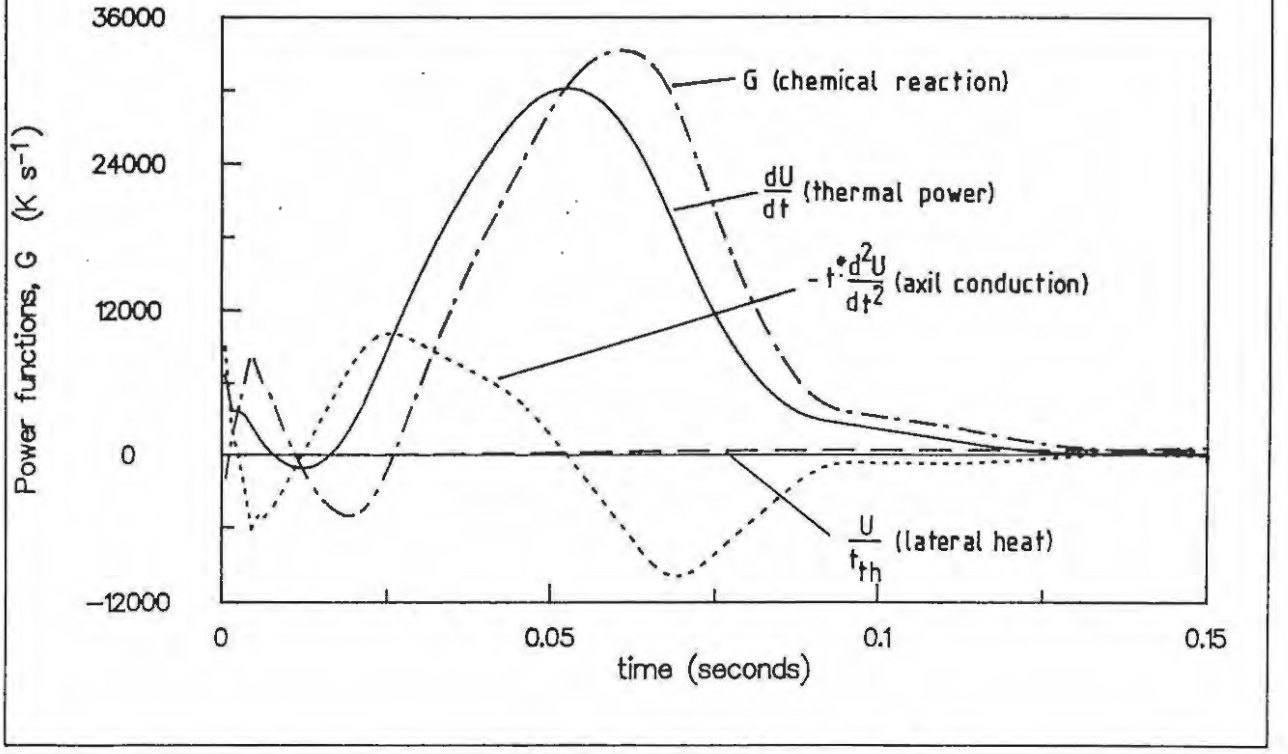

Figure 4.11 Comparison of experimental and calculated power functions

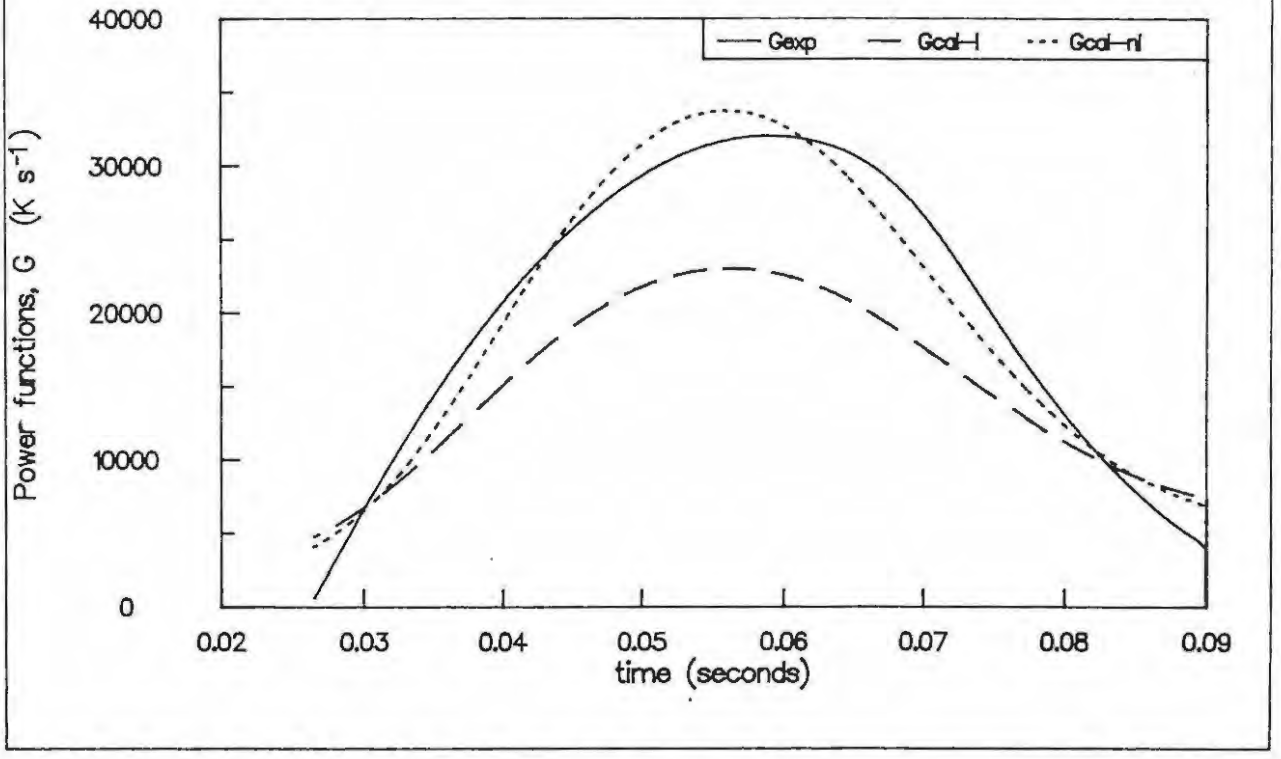

SCHEME 4.1

Schematic layout of the steps involved in analysis of temperature profiles using the Hill approach

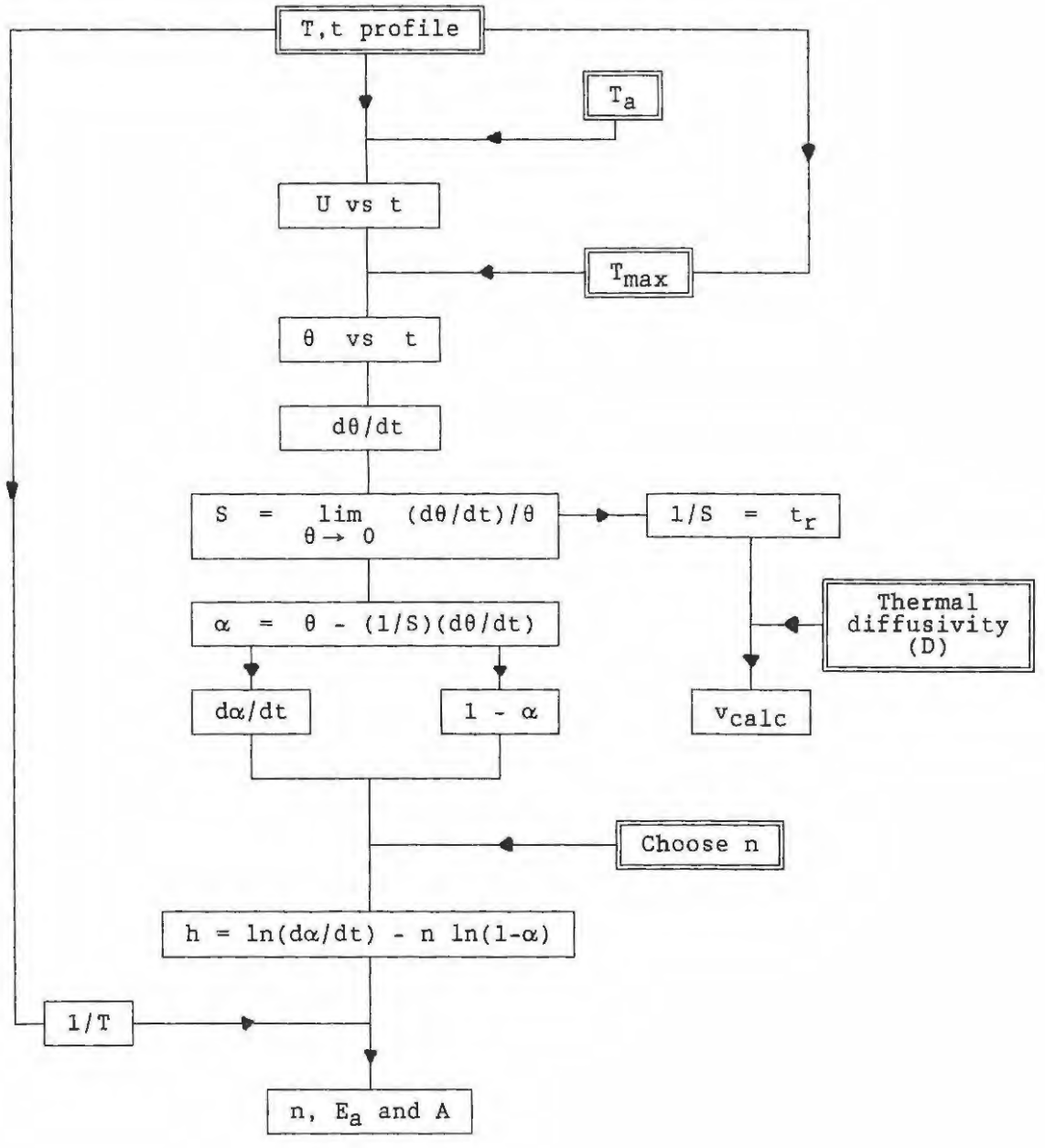

SCHEME 4.2

Schematic layout of the steps involved in analysis of temperature profiles using the Leeds approach

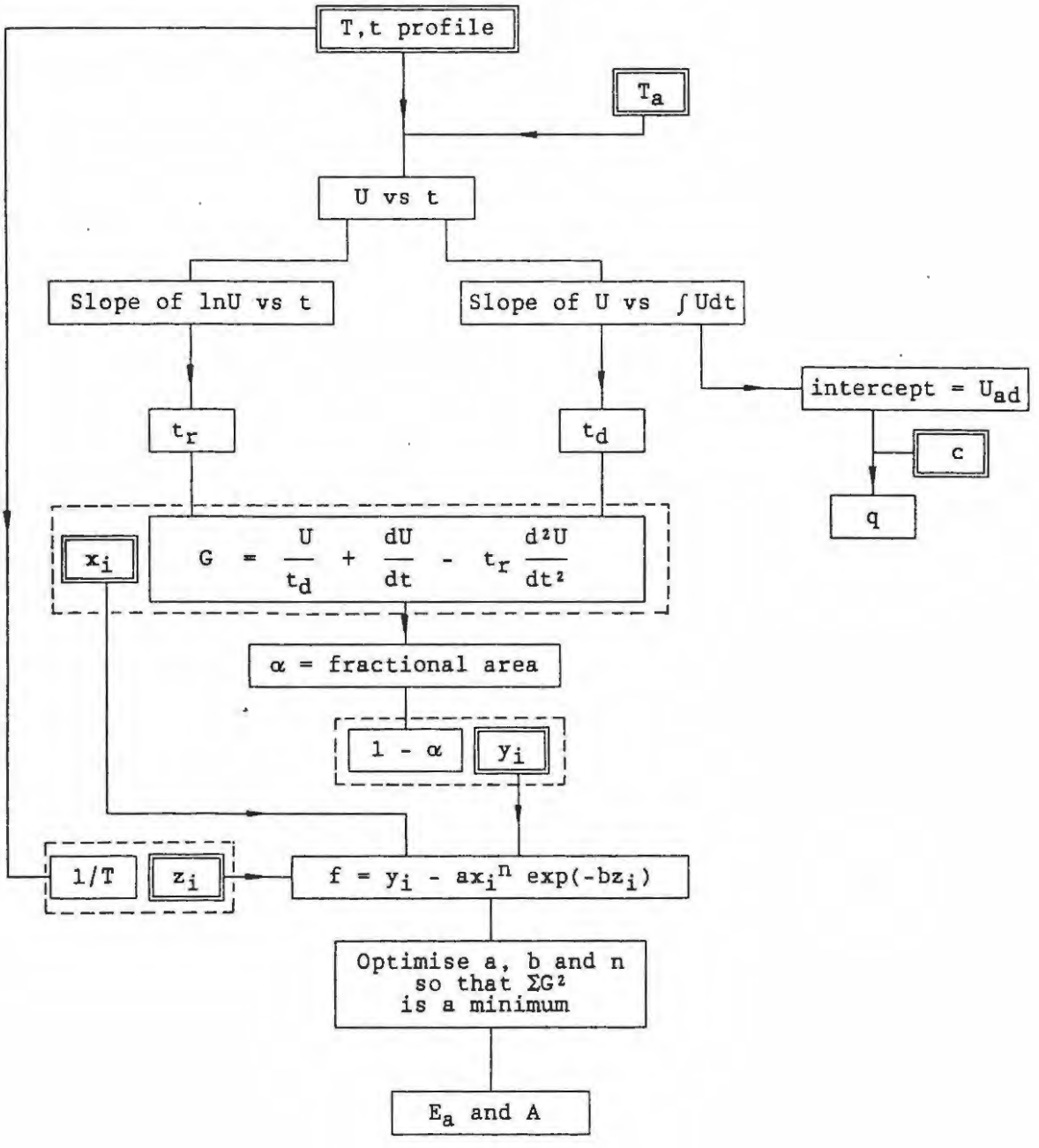

4.10 References

1. T. Boddington, P.G. Laye, J.R.G. Pude and J. Tipping, Combust. Flame, **47** (1982) 235.
2. Z.A. Munzir and J.B. Holt, "*Combustion and Plasma Synthesis of High-Temperature Materials*", VCH Publishers, New York, 1990.
3. A.G. Merzhanov, Dolk. Acad. Nauk. SSSR, **233** (1977) 1130.
4. A.P. Aldushin and A.G. Merzhanov, Dokl. Akad. Nauk SSSR, **236** (1977) 1133.
5. E. Mallard and H.L. Le Chatelier, Ann. Mines, **4** (1895) 274.
6. F. Booth, Trans. Faraday Soc., **49** (1953) 272.
7. R.A.W. Hill, L.E. Sutton, R.B. Temple and A. White, Research, 3 (1950) 569.
8. R.A.W. Hill, L.E. Sutton, R.B. Temple and A. White, 4th Symposium on Combustion, (1958) 349.
9. T. Boddington, P.G. Laye, J.R.G. Pude and J. Tipping, Comb. Flame, **63** (1986) 359.
10. T. Boddington, A. Cottrell and P.G. Laye, Comb. Flame, **79** (1990) 234.
11. T. Boddington, A. Cottrell and P.G. Laye, Comb. Flame, **76** (1989) 63.
12. T. Boddington, P.G. Laye, J. Tipping and D. Whalley, 8th Int. Pyro. Sem., (1982) p. 736.
13. M.W. Beck, "*Intersolid Combustion Reactions in Pyrotechnic Systems*", PhD. Thesis, Rhodes *University, 1984.*
14. M.W. Beck and M.E. Brown, 10th Int. Pyro. Sem., (1985) paper 14.
15. R.L. Drennan, "*Binary and Ternary Pyrotechnic Systems containing Manganese, Molybdenum, Barium Peroxide and Strontium Peroxide*", PhD. Thesis, Rhodes University, 1991.
16. R.L. Drennan and M.E. Brown, to be published.
17. K. Ebert, H. Edeser and T.L. Isenhour, "*Computer Applications in Chemistry*", VCH Verlag, 1989, p. 337.
18. H. Borchardt and F. Daniels, J. Am. Chem. Soc., **79** (1957) 41.

5. CHOICE OF SYSTEMS FOR STUDY

5.1 Experimental limitations

Although silicon is widely used as a fuel in several pyrotechnic systems, only the silicon and lead oxide systems have been thoroughly studied (see Section 2). The starting point of this research was to find pyrotechnic systems which were suitable for further study. The following restrictions were placed on the choice of systems:

(i) the system should be binary (to avoid unnecessary complication);

(ii) the oxidant used should be readily available and inexpensive;

(iii) compositions should be stable on storage;

(iv) compositions should burn with little or no mass transport;

(v) the maximum reaction temperatures reached during combustion should be less than 1700°C so that noble-metal thermocouples can be used for temperature measurement and

(vi) burning rates should not be faster than the responses of the sensors used in monitoring combustion.

5.2 Results of preliminary experiments

Binary pyrotechnic mixtures were prepared (see Section 3) consisting of between 10 and 40% (in increments of 10%) silicon (by mass) and an oxidant, chosen rather arbitrarily, from a range of available oxidants. A list of all the oxidants examined is given in Table 5.1. Those compositions which sustained burning are shown in Table 5.2. Also listed in Table 5.2 are some of the qualitative burning characteristics which were noted in these preliminary experiments.

5.3 Conclusions

The various systems listed in Table 5.2 below, showed a variety of burning characteristics. Many of the binary systems, although capable of sustaining combustion over a wide range of compositions, failed to qualify for further study because of the restrictions placed on the maximum temperature measurable in this study. Temperature profiles were only obtained, over a wide range of compositions, for the Si/Sb_2O_3, Si/Fe_2O_3 and Si/SnO_2 binary systems and these systems were thus chosen for further study.

The Si/KNO_3 system was also chosen for detailed study because the low melting point of KNO_3 (334°C) almost certainly means that reaction will occur in the molten phase.

TABLE 5.1

Table of oxidants tested in binary combination with silicon as fuel

Chromates	Dichromates	Oxides
K_2CrO_4	$Na_2Cr_2O_7$	CuO
$PbCrO_4$	$K_2Cr_2O_7$	Cu_2O
Na_2CrO_4		Fe_2O_3
$BaCrO_4$		MnO_2
		MoO_3
Nitrates	**Peroxides**	PbO_2
KNO_3	BaO_2	Pb_3O_4
$Ba(NO_3)_2$	SrO_2	Sb_2O_3
$Sr(NO_3)_2$		SnO_2
$Pb(NO_3)_2$	**Phosphates**	TiO_2
	K_2HPO_4	V_2O_3
	KH_2PO_4	V_2O_5
Sulphates	**Sulphides**	**Other**
$ZnSO_4$	Sb_2S_3	BaS_2O_3
$MgSO_4$		$KMnO_4$
$BaSO_4$		

TABLE 5.2

Some preliminary results of binary Si/oxidant mixtures

Mixture (% Si)	v_{exp}[a] (mm s^{-1})	% mass loss	Thermocouple shorted?	General comments
$BaCrO_4$				
20	2.49	5	Yes	Slightly gassy. Obtained one profile (30% Si) T_{max} = 1368°C).
30	2.60	4	Yes	
40	2.84	2	Yes	
K_2CrO_4				
20	2.63	6	Yes	Slightly gassy.
30	2.90	4	Yes	
40	5.58	3	Yes	
Na_2CrO_4				
20	-	-	-	Gassy mixture.
30	-	-	-	
40	2.80	10	Yes	
$PbCrO_4$				
20	7.24	15	Yes	Very gassy.
30	13.01	15	Yes	
40	-	-	Yes	
$K_2Cr_2O_7$				
20	6.89	7	Yes	Gassy to very gassy.
30	9.51	9	Yes	No profiles captured.
40	14.16	13	Yes	
$Na_2Cr_2O_7$				
20	3.08	12	Yes	Hot mixture.[b]
30	2.99	7	Yes	
40	2.88	5	Yes	
Cu_2O[c]				
20		2		These mixtures only burn when uncompacted.
30		2		
40		2		Cool mixture.[d]
PbO_2				
20		18		Mixtures too gassy and burning is violent. t/c[e] shorted. Very hot[f].
30		15		
40				
SrO_2				
10		>93		Reaction is dangerously violent. Did not attempt to pack into channels[g].
20		>95		
30		~100		
40		~100		
Sb_2O_3				
20	1.31	3	No	Very little gas produced. Thermocouple ok.
30	7.01	2	No	
40	8.30	2	No	
50	8.60	2	No	

TABLE 5.2 (continued)

Mixture (% Si)	v_{exp}[a] (mm s^{-1})	% mass loss	Thermocouple melted ?	General comments
MnO_2				
20	5.04	4	Yes	Mixture is slightly gassy. Very hot[e].
30	6.57	4	Yes	
40	6.64	2	Yes	
SnO_2				
20	4.09	2	No	Slightly gassy. t/c survived.
30	9.30	2	No	
40	17.50	1	No	
Fe_2O_3				
20	2.33	2	No	Gasless. t/c survived.
30	3.67	1	No	
40	3.82	2	No	
$KMnO_4$				
10	1.71	12	Yes	Gassy t/c shorted.
20	4.17	11	Yes	Hot mixture[c].
30	9.35	15	Yes	
KNO_3				
20	3.01	30	Yes	Mixture very gassy.
30	1.45	32	Yes	Burns hot[c].
40	2.80	26	Yes	

(a) Mean of 2 runs
(b) Channel reaches red heat
(c) 50% CuO/Cu_2O (as oxidant) mixtures have better burning characteristics, but as loose powders only.
(d) Slightly incandescent and a slow burning front
(e) t/c = thermocouple
(f) Channel reaches orange-red heat
(g) Small quantities (~5 mg) burn with intense white flash

TABLE 5.3

Physical properties of the selected fuels and oxides

	Molar mass (g mol^{-1})	Density (g cm^{-3})	Melting (°C)	c_p (J $K^{-1}g^{-1}$)	$-\Delta H_f$ (kJ mol^{-1})
Si	28.08	2.33	1410	0.71	0
FeSi	83.93	6.10	~1300	0.57	-73.6
$CaSi_2$	96.26	2.50	~ 980	0.96*	-151
Sb_2O_3	291.50	5.45	650	0.35	696.6
Fe_2O_3	159.69	5.24	1565	0.65	824.2
KNO_3	101.11	2.11	334	0.95	495.0
SnO_2	150.69	6.95	1630	0.35	581.2

* See reference (1)

From Table 5.3 it can be predicted that because of the high melting points of Si, Fe_2O_3 and SnO_2, reactions in the Si/Fe_2O_3 and Si/SnO_2 systems could be expected to be solid-solid reactions and reactions in the systems, Si/Sb_2O_3 and Si/KNO_3, may involve solid-liquid and solid/gas reactions. Sb_2O_3 is known, from a detailed study of the $Sb/KMnO_4$ system (2,3) to be volatile at temperatures above 500°C. There is also considerable information available on the role of KNO_3 as an oxidant (4-6).

5.4 **Outline of studies on the four binary systems**

The thermal behaviour of the individual constituents and of samples of the binary compositions were examined using thermogravimetry (TG) and differential scanning calorimetry (DSC). The techniques are described in Section 3 and the results in Section 6.

Burning rates of the binary systems over a range of compositions were determined simultaneously with the recording of temperature profiles (Section 3). The effects of compaction, of the specific surface area (SSA) of the silicon (Table 3.4) and of various additives including water, on the burning rates and temperature profiles were examined.

5.5 **References**

1. D.K. Nordstrom and J.L. Munoz, "*Geochemical Thermodynamics*", Blackwell Scientific Publications, 1986, p. 350.
2. M.W. Beck and M.E. Brown, 10th Int. Pyro. Sem., (1986), paper 14.
3. M.W. Beck and M.E. Brown, Comb. Flame, **65** (1986) 263.
4. A.P. Glazkova, Yu A. Kazarova and A.V. Saveljev, 5th Symp. Stability Explosives, Bästad, (1977) 588.
5. E.S. Freeman, J. Am. Chem. Soc., **79** (1959) 11.
6. R.A. Rugunanan, "*Intersolid Pyrotechnic Reactions of Blackpowder*", MSc. Thesis, Rhodes University, 1988.

6. THERMAL ANALYSES

6.1 Introduction

Thermogravimetry (TG) and differential scanning calorimetry (DSC) were used to examine the thermal behaviour in inert and oxidising atmospheres of the Si/Sb_2O_3, Si/KNO_3, Si/Fe_2O_3 and Si/SnO_2 pyrotechnic systems, in relation to the behaviour of the individual constituents. The use of $FeSi_7$ and $CaSi_2$ as alternative fuels to Si, and the behaviour of ternary systems with silicon as fuel, and two oxidants, were also examined.

The thermoanalytical results were complemented by infrared spectra of solid products in KBr disks and X-ray powder diffraction (XRD). The materials and apparatus are described in Section 3.

All thermal analysis results shown are the mean of from three to five runs and errors are calculated from range estimates of the results.

The processes occurring during combustion of a pyrotechnic composition may be far removed (1) from those which may be able to be identified during thermal analysis experiments, where the samples are small and the experimental conditions are such that thermal runaway (2) may be avoided.

6.2 Thermal behaviour of the fuels

6.2.1 *Silicon*

DSC curves of silicon powder heated in N_2 showed no significant thermal event up to 720°C. TG curves (Figure 6.1, curve a) showed a slight mass loss of 0.2 ± 0.1% between 50 and 700°C due, probably, to the desorption of surface impurities. The sample began to gain in mass above 720°C., probably due to slow reaction of silicon with residual traces of oxygen, and this gain was still continuing at the upper temperature limit of 1000°C. A similar gain in mass was observed when a sample, previously purged in flowing nitrogen for up to 10 hours, was heated. It is unlikely that this gain in mass was due to the nitridation of Si since this reaction, to form Si_3N_4, is reported (3) to occur at temperatures greater than 1200°C.

The infrared spectrum of a sample of untreated silicon showed a weak absorption band between 1300 and 1000 cm^{-1} due to SiO_2 which is formed as a result of the spontaneous surface oxidation of silicon on exposure to oxygen.

The TG curves of silicon heated to 950°C in oxygen (Figure 6.1, curve b) showed a gradual mass loss of 0.2 ± 0.1% between 50 and 500°C. Beyond 550°C and up to 950°C, the TG curves showed a gain

Figure 6.1 TG traces of silicon heated at 20°C min^{-1}

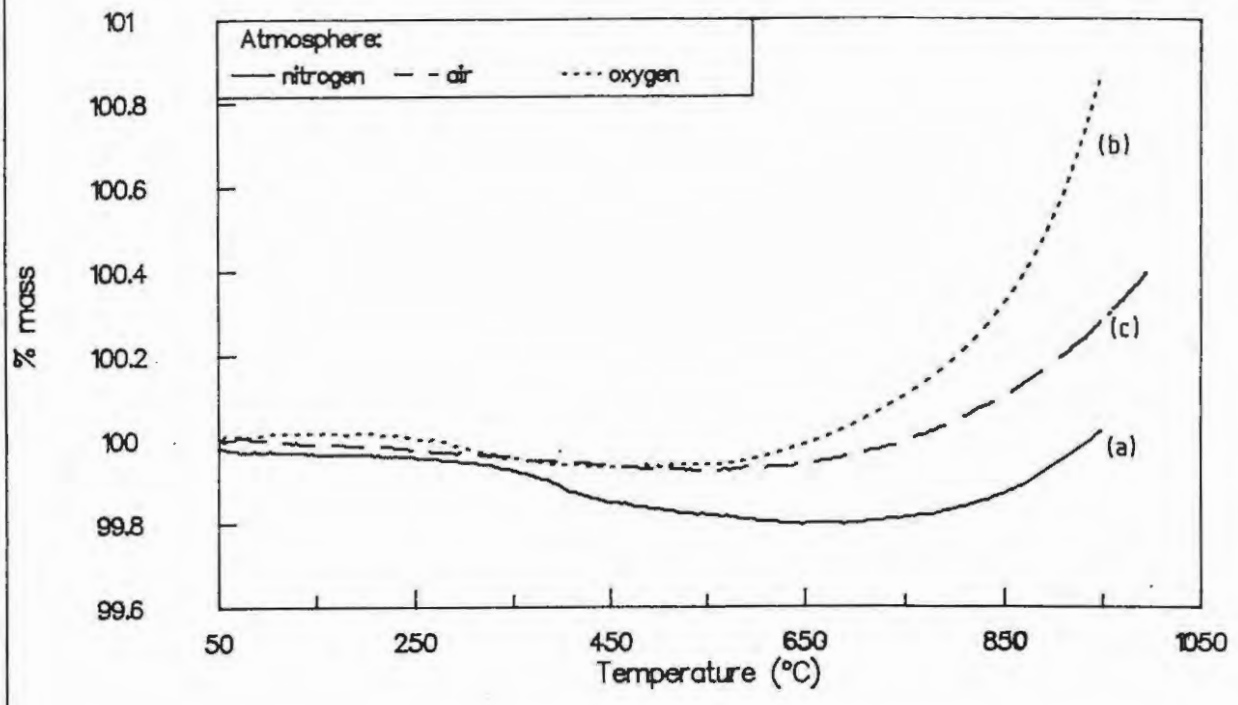

Figure 6.2 TG traces of $FeSi_7$ heated at 20°C min^{-1}

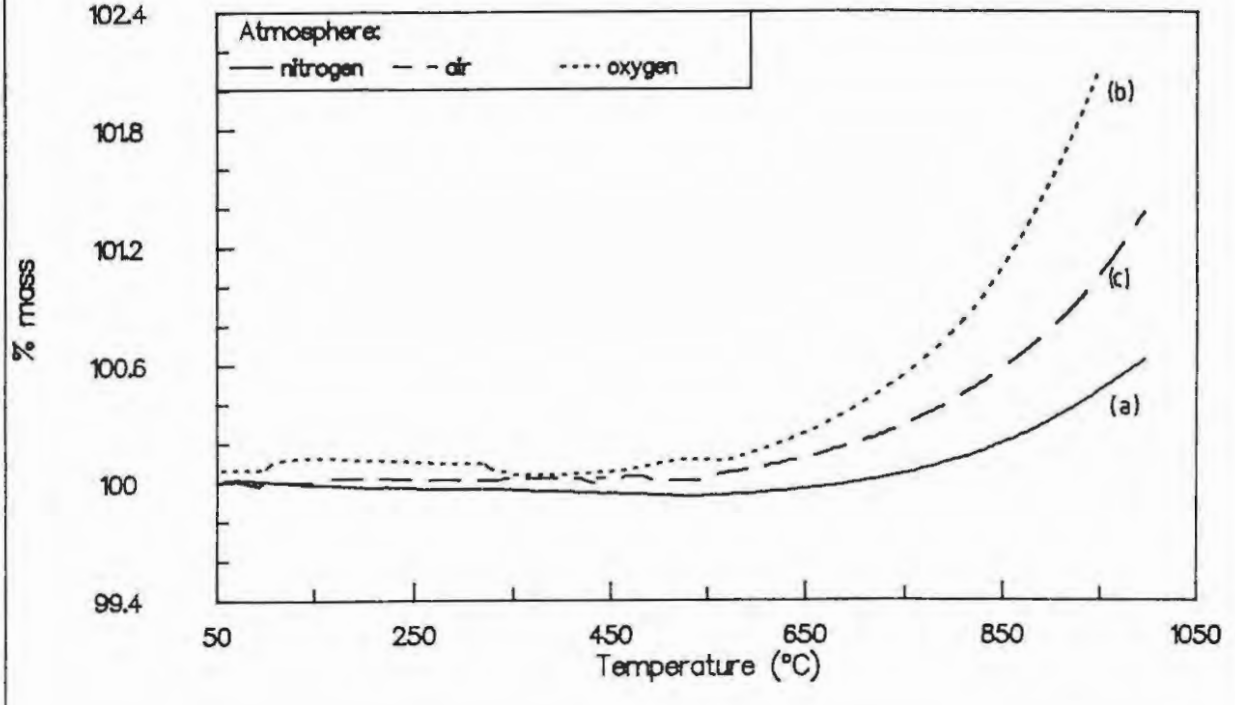

in mass of 0.9 ± 0.1% due to the oxidation of silicon. The rate of oxidation becomes acceleratory beyond 850°C and is still continuing at the upper temperature limit (950°C) of the heating programme.

The TG curves of samples of silicon, heated to 1000°C in air, (Figure 6.1, curve c), showed a mass loss, similar to that observed in nitrogen and in oxygen, of 0.2 ± 0.1% up to 660°C. A gain in mass of 0.6 ± 0.2% starting at ~700°C, similar to that in nitrogen, confirmed the sensitivity of the powder to oxidation above ~600°C.

The infrared spectrum of the product of oxidation in air and O_2 showed a main peak at 1230 cm^{-1} and a shoulder between 1100 and 1000 cm^{-1} (peak at 1070 cm^{-1}) due to SiO_2.

DSC curves of silicon, heated to 720°C in air and in oxygen, showed no significant thermal event. This upper limit is just near the onset of slow oxidation in the TG runs.

6.2.2 *Ferrosilicon*

DSC curves of $FeSi_7$ heated to 720°C in nitrogen showed no significant thermal event. TG curves showed a slight mass loss of 0.3 ± 0.2% between 50 and 600°C (Figure 6.2, curve a). This is followed by a gain in mass of 0.5 ± 0.2% on further heating to 950°C. A similar curve was obtained when a sample of $FeSi_7$ which had been purged for 10 hours in nitrogen, was heated.

A weak absorption band between 1500 and 900 cm^{-1} was observed in the infrared spectrum of untreated $FeSi_7$. No apparent change in the absorption characteristics was noted for a sample of $FeSi_7$ heated in N_2.

The TG curves of $FeSi_7$ heated in oxygen showed a mass gain of 2.1 ± 0.1% between 500 and 950°C (see Figure 6.2, curve b). When a sample of $FeSi_7$ was heated under similar conditions in air (Figure 6.2, curve c), a gain in mass of 1.3 ± 0.1% over the same temperature range was observed. The oxidation of $FeSi_7$ therefore occurs more readily in oxygen. DSC traces of $FeSi_7$ heated at 10°C min^{-1} in air and at 20°C min^{-1} in oxygen showed only a slight drift in the exothermic direction from ~580°C. Only SiO_2 could be detected in the infrared spectrum of $FeSi_7$ which had previously been heated to 950°C in oxygen.

6.2.3 *Calcium silicide*

In the TG curves of $CaSi_2$ heated in nitrogen, a mass loss of 0.2 ± 0.1% occurred between 50 and 650°C (see Figure 6.3, curve a). On further heating to 950°C, a gain in mass of 2.0 ± 0.3% occurred. This was ascribed to reaction with traces of O_2 in the purge gas. The DSC traces showed no significant deviations from the baseline.

The infrared spectrum of a sample of $CaSi_2$ heated to 950°C in nitrogen showed a weak absorption band between 1300 and 1000 cm^{-1}. A sample of untreated $CaSi_2$ showed similar characteristics.

Figure 6.3 TG traces of $CaSi_2$ heated at 20°C min^{-1}

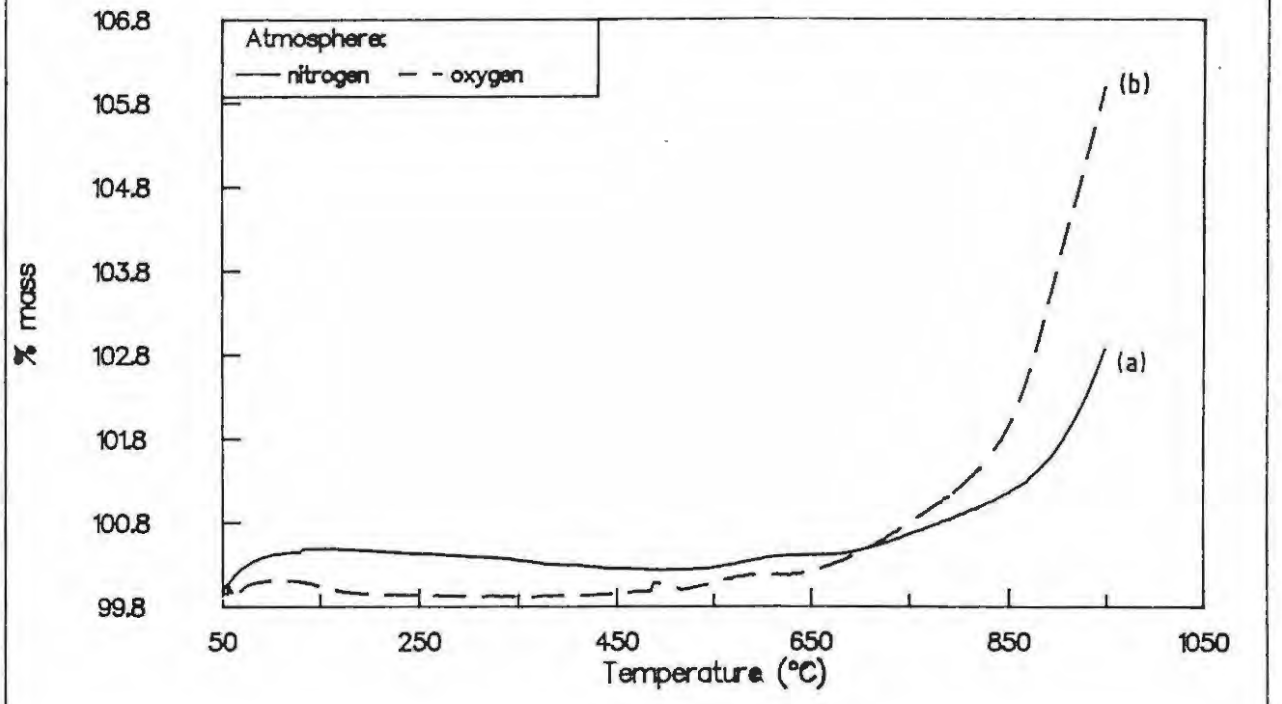

Figure 6.4 TG traces for Sb_2O_3 heated at 20°C min^{-1}

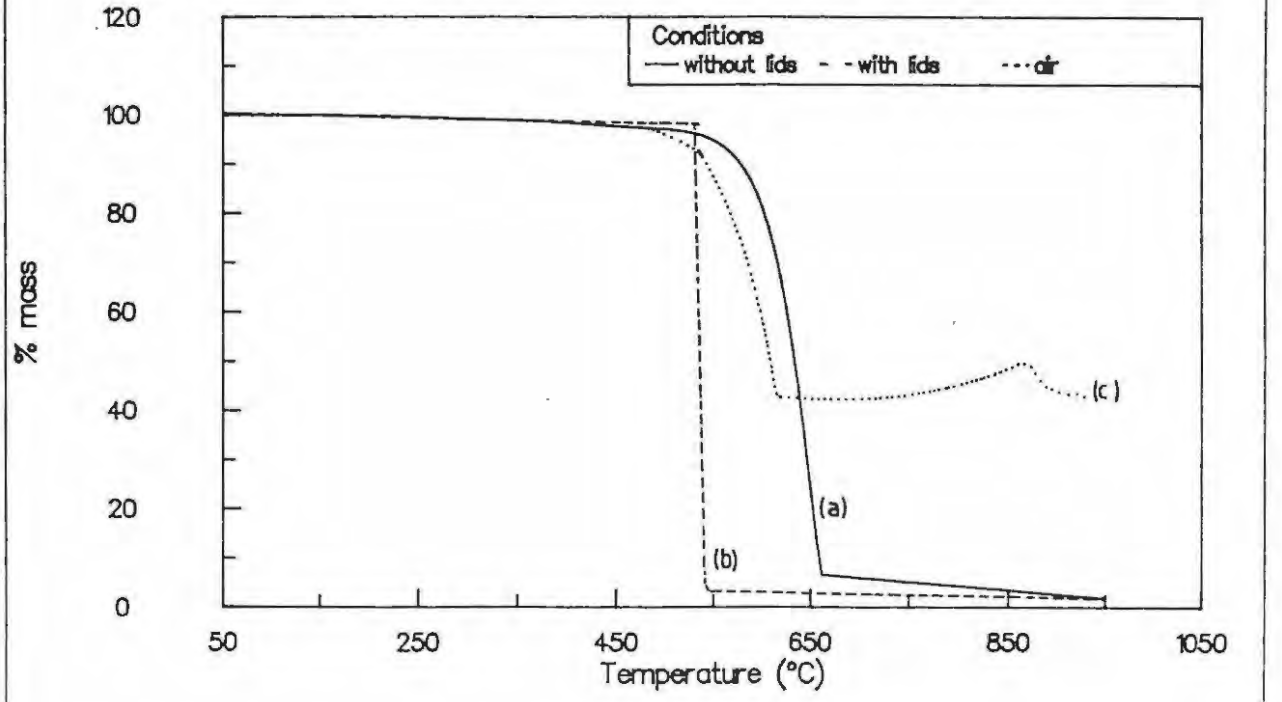

The TG curve of $CaSi_2$ heated in oxygen (Figure 6.3, curve b) showed a mass loss of 0.2 ± 0.1% between 50 and 560°C. Between 580 and 950°C, a gain in mass of 5.8 ± 0.1%, due to the oxidation of $CaSi_2$ was observed. The expected mass gain for the complete oxidation of $CaSi_2$

$$2CaSi_2(s) + 5O_2 \rightarrow 2CaO(s) + 4SiO_2(s)$$

is 54 %. The rate at which the sample mass increases is greatest beyond 850°C. The corresponding DSC curves showed only a slight deviation of the baseline in the exothermic direction starting at~600°C. The infrared spectrum of $CaSi_2$ heated in O_2 showed no absorptions other than those observed for SiO_2.

6.3 **Thermal behaviour of the oxidants**

6.3.1 *Antimony(III) oxide*

When Sb_2O_3 was heated to 1000°C in N_2 in platinum pans without lids (Figure 6.4, curve a), a rapid mass loss of 91.2 ± 1.0% occurred from 500 to 620°C. A large portion of Sb_2O_3 therefore sublimed at temperatures below its melting point (656°C). A further slower mass loss of 3.1 ± 1.3%, occurred between 620 and 800°C, in which the remainder of the Sb_2O_3 vapourised. The total mass loss over the temperature range 50 to 800°C was 97.8 ± 1.6%.

On heating samples in sample pans with lids, a very rapid mass loss of 97.8 ± 2.0% was observed between 520 and 580°C (see Figure 6.4, curve b).

The infrared spectrum of the untreated Sb_2O_3 compared well with that of cubic Sb_2O_3 with peaks at 820 and 380 cm^{-1} (4), as did the spectrum of a sample of the sublimed Sb_2O_3 which had collected on the cooler parts of the TG furnace.

The DSC curve for Sb_2O_3, heated in N_2 (Figure 6.5, curve a), showed the expected broad endotherm between 300 and 580°C due to sublimation of Sb_2O_3. This is followed by two not very reproducible endotherms at 624 and 681°C. The first endotherm is due to the cubic to orthorhombic crystalline transition of Sb_2O_3 and the second due to the melting of Sb_2O_3.

The DSC curve of Sb_2O_3 in air (Figure 6.5, curve b), showed an exotherm between 500 and 650°C due to the oxidation of Sb_2O_3 by gaseous oxygen

$$2Sb_2O_3(s) + O_2(g) \rightarrow 2Sb_2O_4(s)$$

The change in enthalpy for this reaction was -0.81 ± 0.21 kJ $(g\ Sb_2O_3)^{-1}$ compared to the expected value of -0.75 kJ $(g\ Sb_2O_3)^{-1}$ (ΔH = -218 kJ $(mol\ Sb_2O_3)^{-1}$). This exotherm occurred in a similar temperature range to the mass loss due to sublimation observed in the TG traces, suggesting that, in air, sublimation and oxidation of Sb_2O_3 occur simultaneously.

The TG curve for Sb_2O_3 in air (Figure 6.4, curve c), showed that the mass loss, ascribed to the sublimation of Sb_2O_3, began at ~510°C, but the loss of 63.3 ± 2.9% was less than that (~92%) observed in nitrogen. The residue after this initial mass loss consisted of Sb_2O_3 and some Sb_2O_4. After a further

Figure 6.5 DSC traces of Sb_2O_3 heated at 20°C min^{-1}

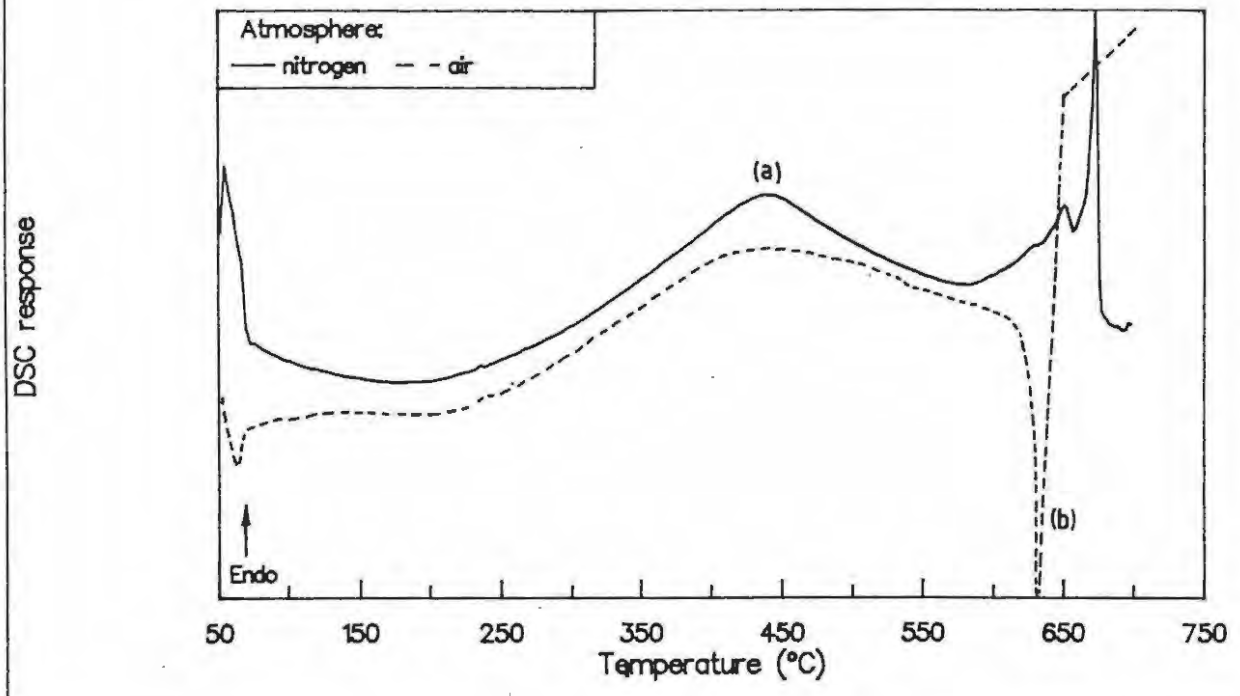

Figure 6.6 TG traces of KNO_3 heated at 10°C min^{-1}

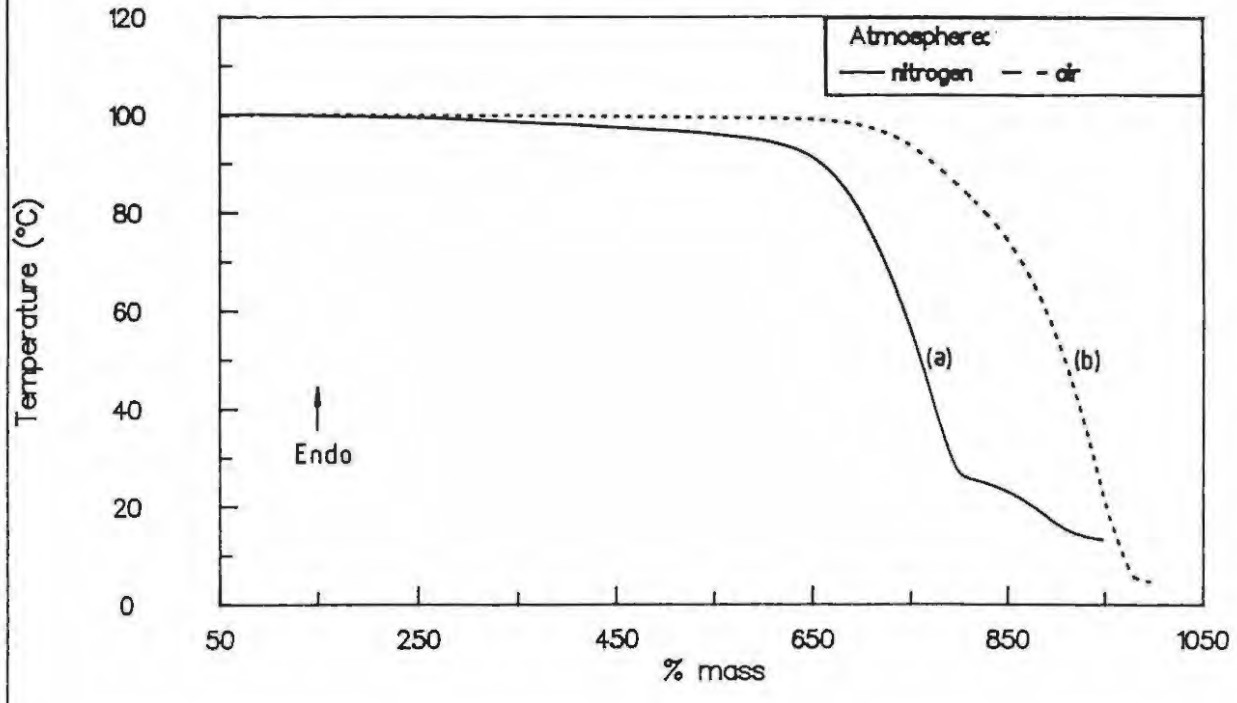

mass loss of 1.7 ± 0.9% between 600 and 760°C, a gain in mass of 3.8 ± 1.1% (or 6.2 ± 2.2% of the sample mass after the initial mass loss) occurred between 760 and 900°C (see Figure 6.4, curve c). This gain in mass is probably due to the oxidation of unreacted Sb_2O_3 (expected gain in mass is 5.5% per g of Sb_2O_3). A further mass loss of between 12 and 27% occurred above 910°C and this stage was incomplete at the upper temperature limit of 1000°C. The onset of this mass loss corresponds to the decomposition of Sb_2O_4 (910°C).

The infrared spectrum of the residue after heating to 1000°C in air confirmed the formation of Sb_2O_4 with an absorption peak at 735 cm^{-1}, a shoulder at 760 cm^{-1}, and a peak at 635 cm^{-1}, with a shoulder at 670 cm^{-1}. Further Sb_2O_4 peaks occurred at 595, 525, 465 and 370 cm^{-1}. The formation of Sb_2O_5 during oxidation cannot be ruled out since (4) the infrared spectrum of Sb_2O_5 closely resembles that of Sb_2O_4.

TG and DTA curves of Sb_2O_3 in N_2 reported by Golunski *et al* (4) showed that for cubic Sb_2O_3 (senarmontite) the mass loss which began at 640°C was ~100% after heating to 1000°C (4). Agrawal *et al* (5) reported however, that a mass loss occurs at as low as 430°C. The DTA curves for cubic Sb_2O_3 (4) showed an irreversible endotherm at 628°C due to the cubic to orthorhombic (valentinite) phase transition. This was followed at ~640°C by a reversible endotherm due to the melting of valentinite. Thermal analyses of orthorhombic Sb_2O_3 showed slightly different characteristics to cubic Sb_2O_3: only a reversible endotherm due to melting was observed at 643°C and mass loss due to vaporisation began at 625°C and was ~90% after heating to 1000°C. XRD analysis (4) showed that no chemical decomposition of Sb_2O_3 had occurred on being heated to 1000°C in nitrogen.

There are conflicting reports about the thermal stability of Sb_2O_3 in air. According to Agrawal *et al* (5), oxidation of cubic Sb_2O_3 occurs above 510°C and proceeds in two stages. The gain in mass for the first stage between 510 and 600°C was 4.5% (expected mass gain for complete oxidation was 5.9%). The second stage between 630 and 670°C showed a mass gain of ~1%. The authors claimed (5) that during the first stage, small quantities of orthorhombic Sb_2O_3 were formed at ~570°C. The orthorhombic Sb_2O_3 was apparently more stable than cubic Sb_2O_3, so the oxidation of the former occurs at 630°C. The DTA curves of Golunski *et al* (4) showed that the oxidation of cubic Sb_2O_3 in air began only at 575°C, while the oxidation of orthorhombic Sb_2O_3 was first noticable at 463°C. In the DSC traces of Sb_2O_3 in air, two exotherms (onset 337 and 442°C) were also reported (6). The first exotherm is due to the oxidation of the surfaces of the Sb_2O_3. Oxidation of the bulk occurred at a higher temperature during the second exotherm.

6.3.2 *Iron(III) oxide*

TG curves of samples of Fe_2O_3, heated in either nitrogen or in air, showed a small almost linear mass loss of ~0.6% between 60 and 940°C. DSC traces in N_2 and in air showed no significant thermal event below the limit of 720°C.

The infrared spectrum of Fe_2O_3 had a broad absorption band with a peak at 535 cm^{-1}, a sharp peak at 475 cm^{-1}, a weak sharp peak at 380 cm^{-1} followed by a strong band with peak at 335 cm^{-1}. There was no change in the infrared spectrum of a sample of Fe_2O_3 (m.pt. 1565°C) after it had been heated to 1000°C and cooled.

6.3.3 *Tin(IV) oxide*

TG curves of SnO_2, heated in N_2, showed only an approximately linear mass loss of up to ~1% which is incomplete by 1000°C. No thermal event was observed in the DSC trace of SnO_2 in nitrogen. The infrared spectrum of the residue compared well with the spectrum of the untreated SnO_2 and showed a strong broad multiplet between 750 and 370 cm^{-1}, a strong sharp peak at 320 and a sharp peak at 265 cm^{-1}. SnO_2 melts only at much higher temperatures (1630°C).

The TG curves of SnO_2, heated at 10°C min^{-1} in air, showed an initial slight mass gain which was lost again above 360°C, followed by a further gradual mass loss of 1.0 ± 0.1% which was incomplete at 1000°C. DSC curves were similar to those observed in nitrogen. No significant changes were observed in the infrared spectrum of SnO_2 which had been heated to 1000°C in air.

6.3.4 *Potassium nitrate*

In the TG curve for KNO_3, heated at 10°C min^{-1} in N_2 (see Figure 6.6, curve a), decomposition occurred in two partially-overlapping stages (500 to 770°C and 770 to 1000°C). The mass loss between 500 and 770°C was 72.0 ± 1.2% and 14.0 ± 1.0% between 770 and 1000°C.

According to Freeman (7), decomposition of KNO_3 occurs between 650 and 750°C to the nitrite, followed at 800°C by

$$2KNO_2(l) \rightarrow K_2O(l) + 2NO(g) + O_2(g)$$

while, according to Serotkin (8), K_2O is not formed until 1000°C and decomposition is only complete above 1200°C. The mass of the residue in N_2 (12.1 ± 1.8% of the original) is less than expected for K_2O and supports reports of volatilisation of K_2O (m. pt. 380°C) (9).

In the TG curve for KNO_3 heated at 10°C min^{-1} in air, decomposition occurred above 500°C and proceeded through a rapid mass loss (84.8 ± 1.2%) between 500 and 920°C, followed by a slower mass loss of 7.1 ± 1.1% between 920 and 1000°C. The two-stage mass loss observed in N_2 was not resolved in the trace for KNO_3 in air (see Figure 6.6, curve b). The total mass loss in air of 91.9% was greater than the 86.0% observed in nitrogen.

The DSC curves in N_2 (20°C min^{-1}) (Figure 6.7, curve a) and air (10°C min^{-1}) (Figure 6.7, curve b) were similar, confirming the onset of endothermic decomposition at about 500°C after the rhombic-to-trigonal crystalline phase transition at 116°C and melting at 325°C.

Figure 6.7 DSC traces of KNO_3 heated at 20°C min^{-1}

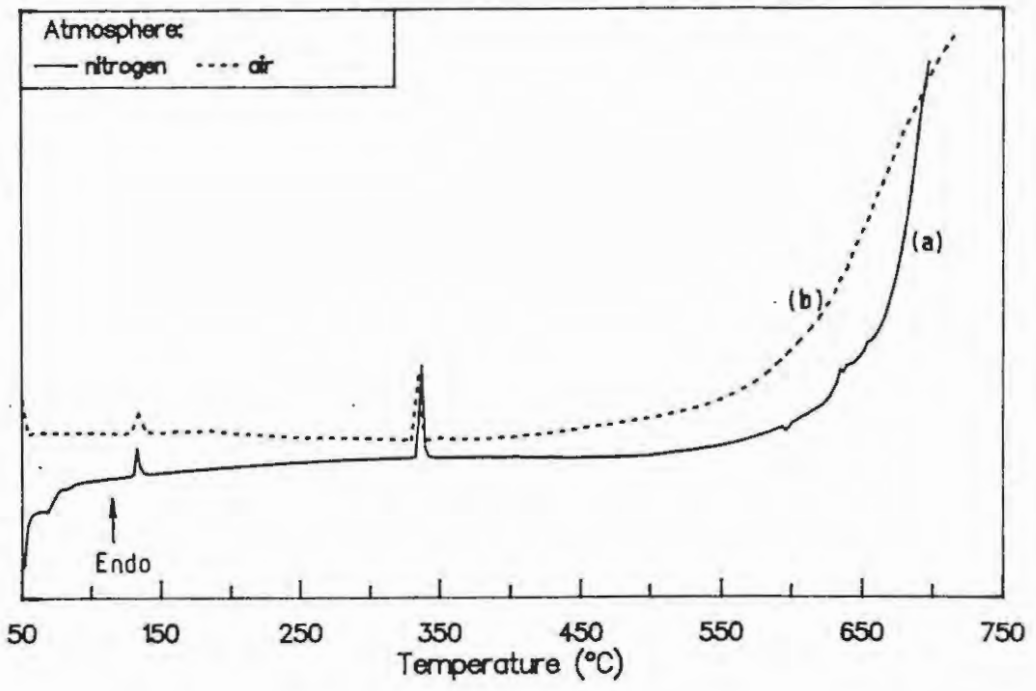

Figure 6.8 DSC traces of 40% Si/Sb_2O_3 heated at 20°C min^{-1} in nitrogen and 10°C min^{-1} in air. (Note heating decreased in air on account of strongly exothermic reaction)

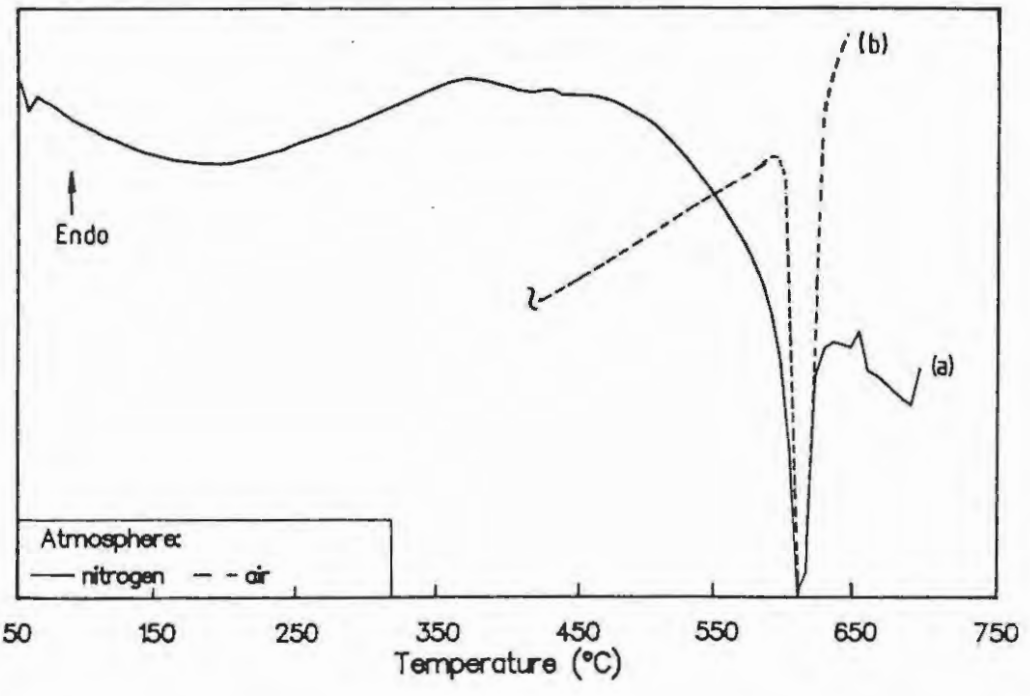

6.3.5 *Comments*

The individual oxidants, described above, behaved very differently on heating. Fe_2O_3 and SnO_2 show very little change over the temperature range accessible (< 1000°C). Neither melts, decomposes in inert atmosphere, or oxidises significantly in air. Sb_2O_3 sublimed readily and may also melt and/or oxidise further in air. KNO_3 melted at relatively low temperatures (325°C) and decomposed readily in the melt. With these differences in behaviour, the oxidants, on binary combination with silicon as fuel, could be expected to show significant differences in reactivity.

6.4 Thermal behaviour of the binary Si/oxidant systems

All the binary Si systems sustain combustion over a range of compositions (see Sections 7 - 10), with similar maximum temperatures (~1300°C) reached during approximately adiabatic combustion, but with different linear burning rates.

6.4.1 *The Si/Sb_2O_3 system*

In the DSC traces of a 40% Si/Sb_2O_3 composition in nitrogen (Figure 6.8, curve a), an exotherm from 590 to 615°C with a change in enthalpy of -0.53 ± 0.13 kJ (g of mixture)$^{-1}$, was observed. This exotherm occurred in the temperature range during which sublimation of Sb_2O_3 occurred when it is heated alone. If the reaction

$$3Si(s) + 2Sb_2O_3(g) \rightarrow 3SiO_2(s) + 4Sb(s) \quad ...(6.1)$$

is assumed to occur during this exotherm, the change in enthalpy, calculated from standard enthalpies of formation, would be -1.82 kJ (g mixture)$^{-1}$.

DSC curves of the above composition in air (Figure 6.8, curve b) showed an exotherm between 600 and 680°C and the change in enthalpy was -0.74 ± 0.19 kJ (g mixture)$^{-1}$. This exotherm occurred in a similar temperature range to that in which the sublimation and oxidation of Sb_2O_3 was observed in air (Figure 6.5, curve b).

The TG traces for the 40% Si/Sb_2O_3 composition heated to 1000°C in N_2 in platinum pans without lids (Figure 6.9, curve a), showed a mass loss of 48.5 ± 0.4% between 420 and 630°C followed by a further mass loss of 8.5 ± 1.5% between 650 and 995°C. Calculations based on TG mass losses showed that only < 5% of the total silicon in the mixture had reacted with Sb_2O_3 compared to the expected 46.5%

When the sample pans were covered with lids (see Figure 6.9, curve b), the mass loss was only 6.1 ± 0.3% over the temperature range 520 to 570°C, followed immediately by a slower mass loss of 3.6 ± 0.4% (580 to 995°C). Only ~20% of the total silicon had reacted despite attempts at preventing the escape of Sb_2O_3 vapour. The presence of SiO_2 was detected in the infrared spectrum of the residue.

Figure 6.9 TG traces of 40% Si/Sb_2O_3 heated at 20°C min^{-1} in nitrogen in sample pans without and with lids

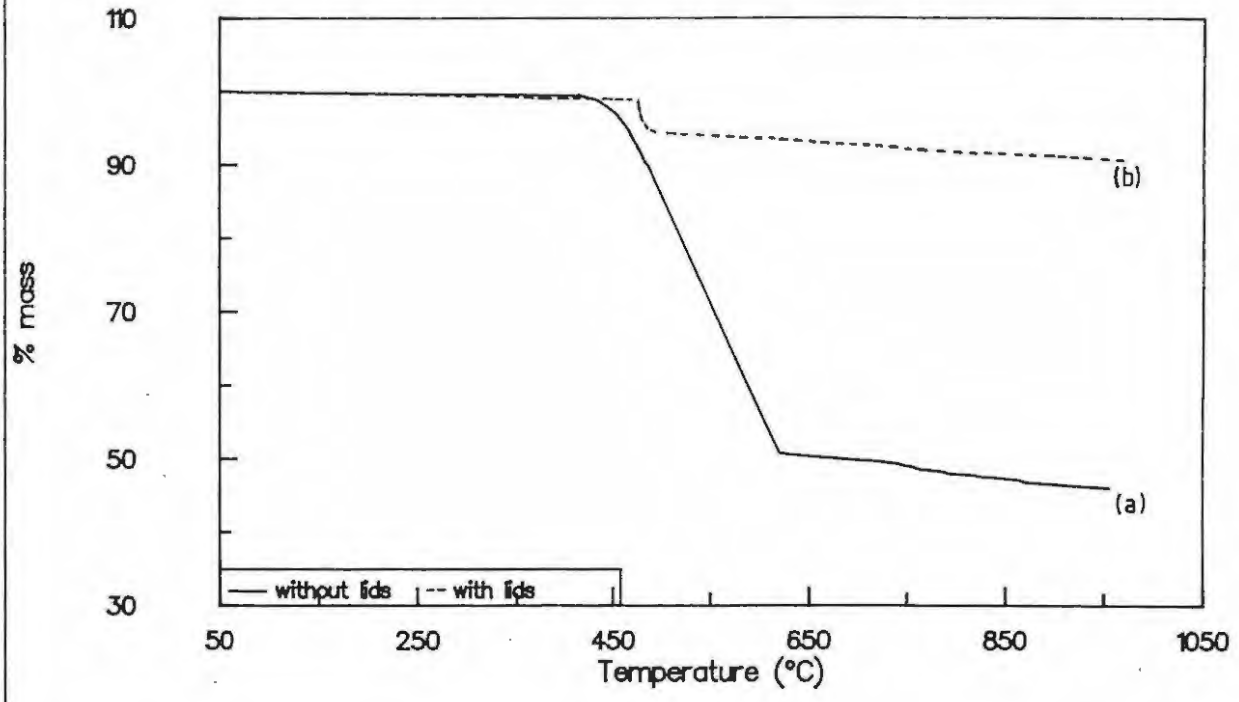

Figure 6.10 TG traces of 40% Si/Sb_2O_3 heated at 20°C min^{-1} in air in sample pans without and with lids

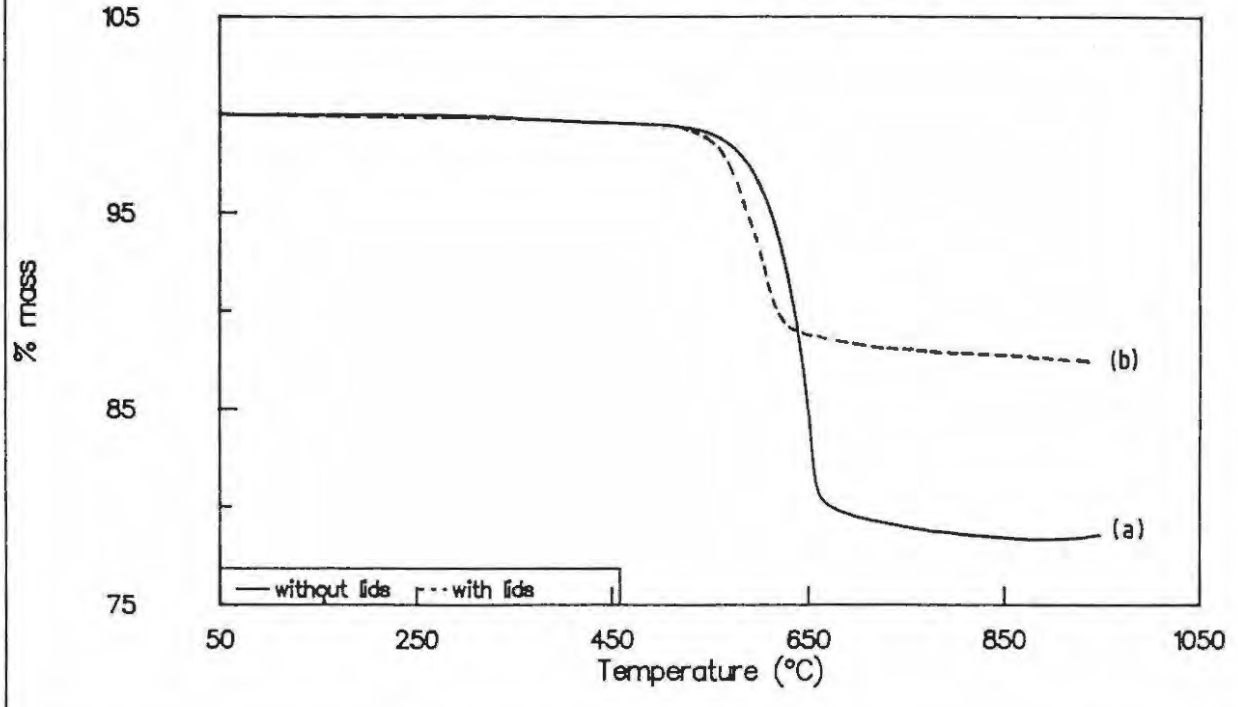

The infrared spectrum of a sample heated to 700°C showed the usual SiO_2 absorptions as well as additional absorption peaks at 705, 595, 545, 475, 380 and 330 cm^{-1} which are characteristic of orthorhombic Sb_2O_3 (4).

A summary of the observed and expected mass losses for a 40% Si/Sb_2O_3 mixture are shown in Table 6.1. Calculations are based on the amount of Sb_2O_3 left after sublimation (case 1) and after heating to 1000°C (case 2). The mass loss above ~630°C is assumed to be due to the vaporisation of unreacted Sb_2O_3. The residues are assumed to consist of Sb, SiO_2 and unreacted Si only, according to reaction 6.1.

TABLE 6.1

Comparison of the calculated* mass loss and enthalpy of reaction for the 40% Si/Sb_2O_3 mixture heated in nitrogen with experimental values

Details	% mass loss at onset temperature		Mass of residue (%)		$-\Delta H$ (kJ (g of mixture)$^{-1}$)		mass % of total Si[2] reacted
	520°C	630°C	m_{exp}	m_{calc}	DSC	Calc[1]	
Complete[3]	0	0	0.0	100	-	1.37	46.5
No lids:							
case 1	48.5	-	52.5	51.2	-	0.26	4.2
case 2	48.5	8.5	43.0	41.7	-	0.26	1.2
With lids:							
case 1	6.1	-	93.9	93.9	0.53	0.57	19.3
case 2	6.1	3.5	90.3	90.3	-	0.57	18.0

* Calculated for 1 g of mixture
1 Calculated on the on the basis of the mass of Sb_2O_3 left sublimation
2 Calculated from TG data, referes to the % of silicon oxidised in the mixture
3 For complete reaction between constituents without sublimation of oxidant
case 1: calculated on mass loss between 420 and 630°C only
case 2: calculation includes mass loss after 630°C
mcalc calculated mass percent of residue

The TG curve of 40% Si/Sb_2O_3 in air in platinum pans without lids (Figure 6.10, curve a) showed that sublimation begins at ~410°C. The mass loss observed between 410 and 610°C was 43.4 ± 2.8%. This region of rapid mass loss is followed by a slower mass loss of 1.2 ± 0.5% over the temperature range 610 to 910°C. Between 910 and 1000°C a slight and not very reproducible mass loss of ~1%, due to the decomposition of Sb_2O_4 was observed. When the sample pans were covered with lids, a rapid mass loss of 10.5 ± 2.3% was observed between 470 and 700°C (Figure 6.10, curve b).

DSC traces of the above composition, heated at various heating rates in air, showed an exotherm over the range 580 to 620°C. Enthalpy values measured from these DSC curves (Table 6.2) were not very reproducible and varied according to mass of the sample and the heating rate used.

TABLE 6.2

ΔH values measured from the DSC traces of 40% Si/Sb_2O_3 compositions heated either in nitrogen or in air

Heating rate (°C min^{-1})	-ΔH (kJ (g of mixture)$^{-1}$)	
	Nitrogen	Air
10	0.21 ± 0.10	0.61 ± 0.14
20	0.53 ± 0.13	0.74 ± 0.19
50	0.43 ± 0.20	0.93 ± 0.19
100	0.46 ± 0.14	0.61 ± 0.14

The changes in enthalpy measured for the composition in air are generally greater than those observed in nitrogen as a result of a contribution made by the reaction of Sb_2O_3 with gaseous O_2. For mixtures heated in nitrogen, maximum ΔH was reached at 20°C min^{-1}, with no further increase with increased heating rate. The infrared spectrum of the residue after heating to 1000°C showed the presence of SiO_2 and trace amounts of the oxidant.

6.4.2 *The Si/Fe_2O_3 system*

On heating samples of loose powders of 35% Si/Fe_2O_3 to 1000°C in nitrogen, or in air, the slow mass loss, over the range 50 to 1000°C, of 0.6 ± 0.2% was similar to that observed on heating Fe_2O_3 alone. The infrared spectrum of the residue showed the strong presence of Fe_2O_3. DSC curves in nitrogen and also in air showed no thermal event over the temperature range of the instrument. Similar results were obtained when compacted samples were used and also when either the heating rate ($\leq$ 150°C min^{-1}) or the sample mass (<30 mg) was varied. Thus the process responsible for propagation of combustion of this composition could not be readily initiated under the conditions applying, and within the temperature limits of the thermal analysis equipment.

6.4.3 *The Si/SnO_2 system*

The TG curves of a 30% Si/SnO_2 composition in nitrogen, or in air, showed a slight mass loss (1.5 ± 0.6%) over the range 50 to 1000°C. The DSC trace, in N_2 and in air, showed no thermal event between 50 and 720°C. Increasing the heating rate (≤150°C min^{-1}) or the sample mass (<30 mg) did not result in any exothermic reaction.

The infrared spectrum of the residues after heating in nitrogen and in air, showed only the characteristic absorption bands of SnO_2. Again it was not possible to initiate a self-sustaining reaction in this composition, as loose powders or as compacted pellets, under typical thermoanalytical conditions.

6.4.4 *The Si/KNO_3 system*

A typical TG curve for a 30% Si/KNO_3 mixture, heated at 20°C min^{-1} in N_2, (Figure 6.11, curve a) showed a single mass loss of 23.3 ± 0.8%. The extent of the loss and the temperature range over which the loss occurs, varied with composition (10) of the mixture as shown in Table 6.3. However, the onset temperature for this mass loss, which varied within narrow limits between 560 and 575°C for the compositions examined, appears to be independent of composition.

A DSC curve for 30% Si/KNO_3, heated at 10°C min^{-1} in N_2, is shown in Figure 6.12. The crystalline and melting transitions of KNO_3 are evident as is the onset of endothermic decomposition of KNO_3 (~500°C). Upon this endotherm is superimposed a strong exothermic spike at ~660°C, characteristic of ignition. When the proportion of Si in the composition was increased, the resulting DSC curve for a sample in nitrogen showed a similar sharp exotherm at ~600°C. The onset temperature of the exotherms varied between 570 and 640°C and generally occurred within the same temperature range as the mass loss observed in the TG curves. If it is assumed that the reaction which occurs during this exotherm is

$$2Si(s) + 2KNO_3(l) \rightarrow 2SiO_2(s) + K_2O(l) + N_2(g) + 0.5O_2(g)$$

the enthalpy of reaction, determined from standard enthalpies of formation, is -4.3 kJ (g mixture)$^{-1}$ (or -590.7 kJ (mol KNO_3)$^{-1}$). The maximum enthalpy of reaction, determined from DSC traces, was -2.29 kJ (g mixture)$^{-1}$ and occurred at approximately 40% Si (see Table 6.4).

The TG curve of a 30% Si/KNO_3 composition in air (Figure 6.11, curve b) showed a single mass loss. The extent of mass loss depended on the composition of the mixture and generally decreased with decreasing oxidant content (see Table 6.4). The DSC curves of the above composition showed the usual endothermic transitions. The onset of the exothermic reaction between the decomposing oxide and solid silicon occurred at ~600°C and was incomplete at 720°C, which is the upper temperature limit of the instrument. A broad exotherm was observed between 570 and 700°C for a 60% Si/KNO_3 composition heated at 10°C min^{-1} (Figure 6.13).

Figure 6.11 TG traces of 30% Si/KNO_3 heated at 20°C min^{-1}

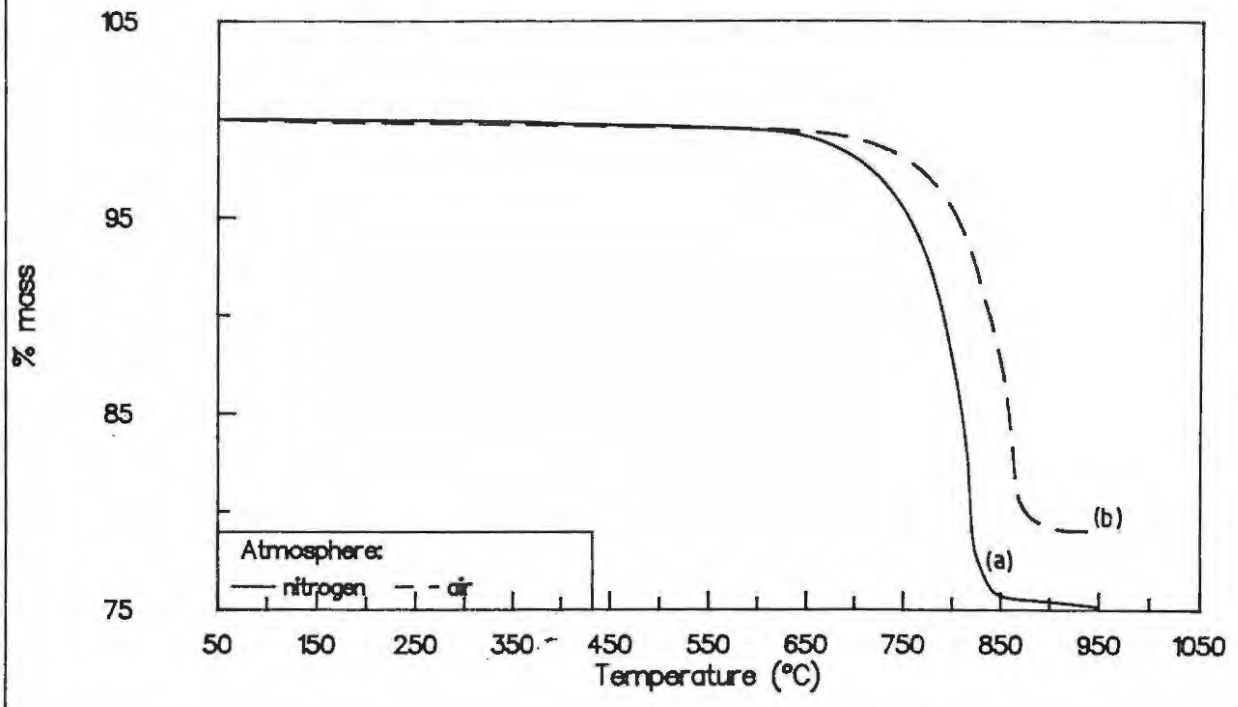

Figure 6.12 DSC trace of 30% Si/KNO_3 heated at 10°C min^{-1} in nitrogen

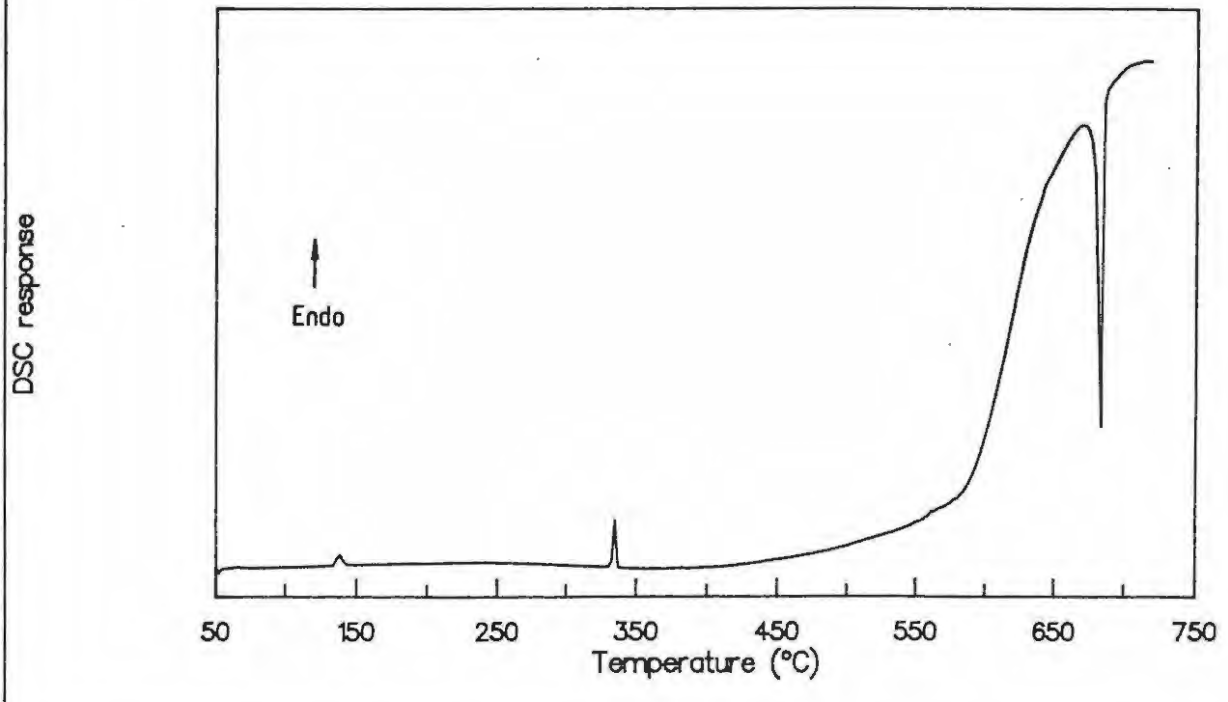

TABLE 6.3

Summary of TG and DSC data

for the Si/KNO_3 system heated in nitrogen

% Si	TG		DSC		$-\Delta H^*$ (kJ g^{-1})
	Temperature range (°C)	% change in mass	Temperature range (°C)	$-\Delta H$ (kJ g^{-1})	
20	570 to 950	36.8 ± 2.6	-	-	4.22
30	570 to 910	23.3 ± 0.8	660 to 680	0.97 ± 0.02	4.09
40	565 to 860	17.3 ± 2.0	640 to 680	2.39 ± 0.03	3.51
50	570 to 790	11.7 ± 0.8	600 to 720	1.90 ± 0.04	2.92
60	560 to 760	10.7 ± 0.6	600 to 710	1.00 ± 0.02	2.34
70	560 to 690	7.6 ± 0.4	620 to 650	0.43 ± 0.02	1.75
80	575 to 653	4.5 ± 0.4	570 to 620	0.34 ± 0.03	1.17

* Calculated from standard enthalpies of formation.

TABLE 6.4

Summary of TG and DSC data

for the Si/KNO_3 system heated in air

% Si	TG		DSC	
	Temperature range (°C)	% change in mass	Temperature range (°C)	$-\Delta H$ (kJ (g mixture)$^{-1}$)
20	560 to 960	35.2 ± 1.2	570 to 650	0.72 ± 0.01
30	570 to 930	20.7 ± 0.2	570 to >720	-
40	560 to 850	14.9 ± 0.1	570 to >720	-
50	540 to 750	12.9 ± 0.1	570 to >720	-
60	540 to 720	10.9 ± 0.4	570 to 700	1.64 ± 0.01
70	580 to 720	6.9 ± 0.2	570 to 660	1.16 ± 0.02
80	550 to 670	5.4 ± 0.1	570 to 640	0.66 ± 0.03

Figure 6.13 DSC trace for 60% Si/KNO_3 heated at 10°C min^{-1} in nitrogen

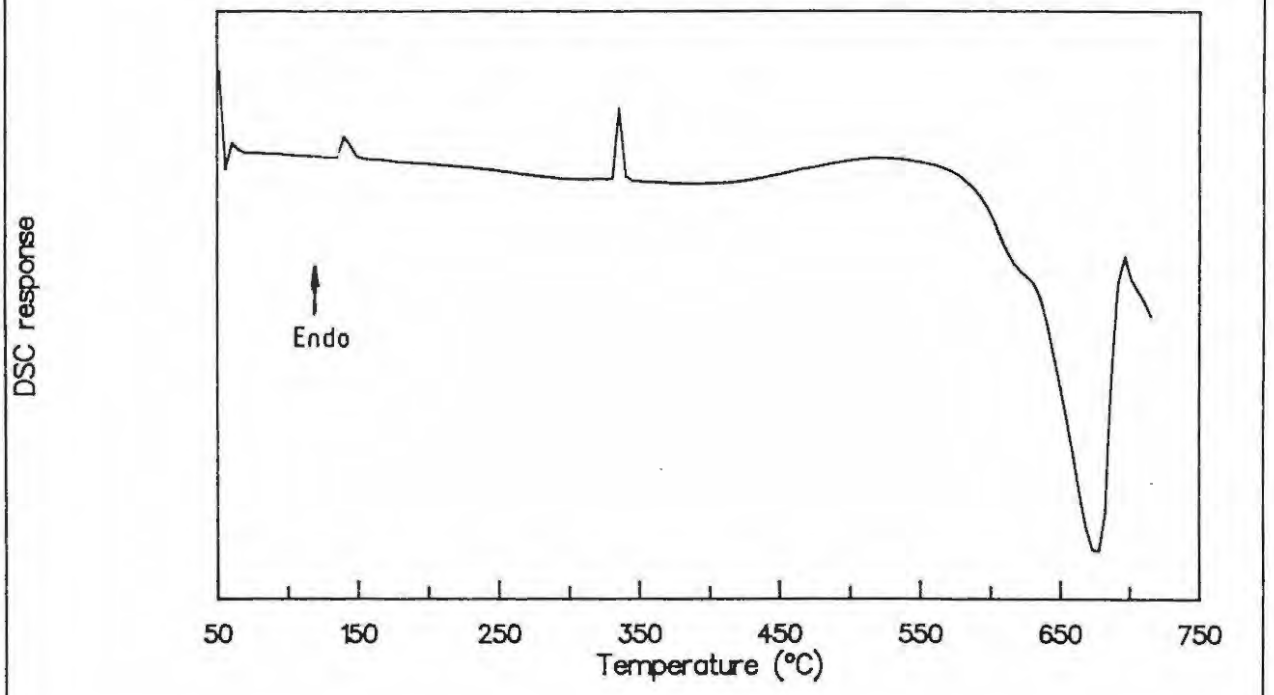

Figure 6.14 DSC trace of 40% $FeSi_7/Sb_2O_3$ heated at 20°C min^{-1} in nitrogen

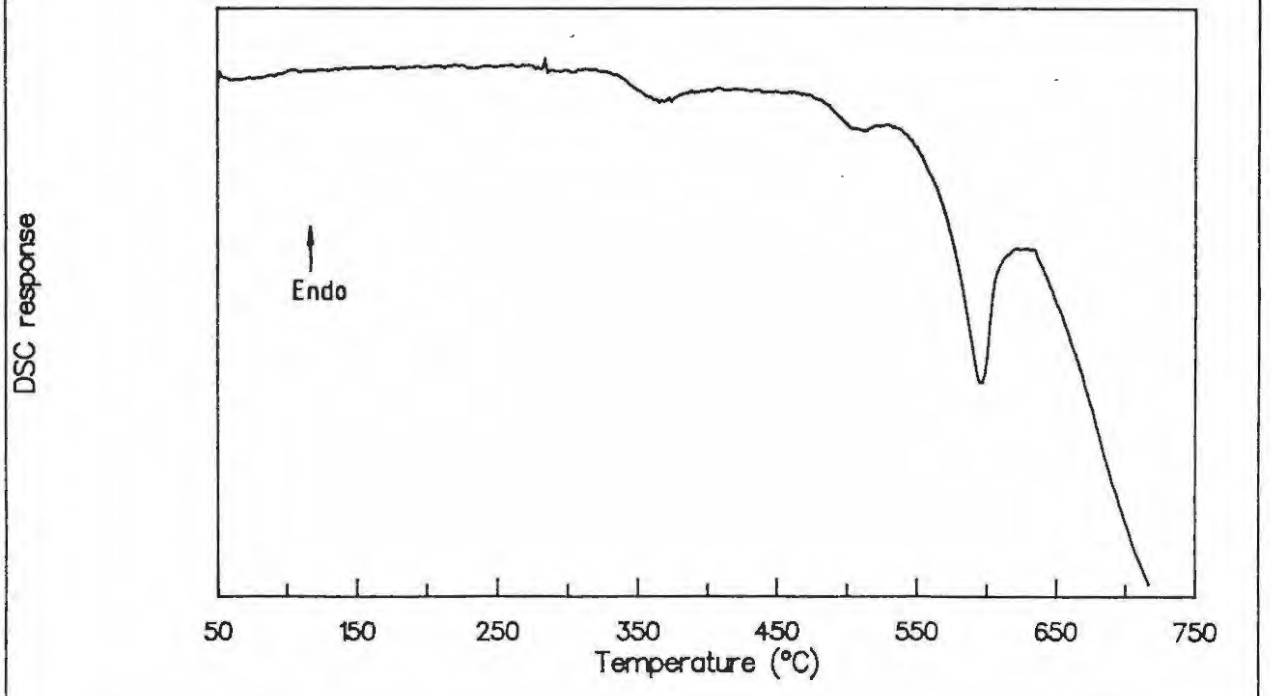

The infrared spectra of the thermal analysis residues showed the strong presence of SiO_2. The absorption bands due to KCO_3, $KHCO_3$ and KOH were also detected. These compounds were probably formed on contact with moisture during the preparation of the KBr disks.

6.5 Thermal behaviour of the $FeSi_7$/oxidant systems

Binary systems in which $FeSi_7$ and $CaSi_2$ were added separately to the various oxidants, were examined using TG and DSC. All the results reported in this section have been carried out in flowing nitrogen atmospheres only.

6.5.1 *The $FeSi_7/Sb_2O_3$ system*

The DSC traces of a 40% $FeSi_7/Sb_2O_3$ mixture (Figure 6.14) showed a single exotherm between 510 and 635°C. Because of the volatility of Sb_2O_3 (see section 6.3.1), the change in enthalpy for the exotherm was not very reproducible and varied between -0.34 kJ (g mixture)$^{-1}$ (using sample pans with lids) and -0.06 kJ (g mixture)$^{-1}$ (using sample pans without lids). TG curves obtained using open sample pans, showed a rapid mass loss of 49.0 ± 2.0% between 430 and 620°C. This was followed by a gradual mass loss of ~2% on further heating to 950°C. Infrared spectra of the residues showed the characteristic absorptions of SiO_2 and only traces of Sb_2O_3.

6.5.2 *The $FeSi_7/Fe_2O_3$ system*

The DSC traces of pressed, as well as loose, powdered samples of 35% $FeSi_7/Fe_2O_3$ showed no thermal events when heated. Only a steady mass loss of ~0.5% was noted between 200 and 950°C. The presence of Fe_2O_3 and weak SiO_2 bands only, could be identified in the infrared spectra of residues. No reaction between $FeSi_7$ and Fe_2O_3 therefore occurred.

6.5.3 *The $FeSi_7/SnO_2$ system*

The TG traces of pressed and of loose powders of a 45% $FeSi_7/SnO_2$ composition heated in nitrogen showed a slight mass loss of 0.4 ± 0.1% between 50 and 800°C. A slight increase in mass of 0.2 ± 0.1%, which is still continuing at 950°C, occurred above 850°C. DSC traces showed no significant deviation from the baseline. Infrared spectra of the residues confirmed that no interaction occurred between the fuel and the oxidant on heating to 950°C.

6.5.4 *The $FeSi_7/KNO_3$ system*

A typical DSC trace for 85% $FeSi_7/KNO_3$ is shown in Figure 6.15. The usual endothermic crystalline transition and melting of KNO_3, at 132 and 345°C respectively, were followed by two exothermic events. The first exotherm was broad and flat (onset at 460 ± 10°C) and overlapped the second exotherm (onset 590 ± 5°C). The second exotherm is complex and showed several spikes. The changes in enthalpy for the first and second exotherms were 0.03 ± 0.01 and 0.29 ± 0.07 kJ (g mixture)$^{-1}$ respectively.

TG curves of the above mixture showed a single mass loss of 5.8 ± 1.2% over the temperature range 350 to 850°C. The mass loss above 550°C was rapid.

The infrared spectrum of the residue after heating to 950°C showed the strong presence of SiO_2 and of K_2CO_3 and $KHCO_3$. The latter carbonates arise from a possible reaction between K_2O and atmospheric CO_2 and H_2O vapour (see section 6.4.4).

6.6 Thermal behaviour of $CaSi_2$/oxidant systems

6.6.1 *The $CaSi_2/Sb_2O_3$ system*

DSC traces of a 40% $CaSi_2/Sb_2O_3$ mixture (Figure 6.16) showed a broad endotherm between 470 and 720°C (onset 471 ± 3°C) due to sublimation of Sb_2O_3. Superimposed on this endotherm is a sharp exotherm due to reaction between fuel and oxidant (onset 565 ±5°C). The change in enthalpy for this reaction varied between -0.25 and 0.11 kJ (g mixture)$^{-1}$ and depended on the mass of the sample used. A mass loss of 35.3 ± 1.2% occurred between 500 and 570°C in the open sample pans used for thermogravimetry, so, most of the oxidant escaped as volatiles before reacting with the fuel. A gradual mass loss of ~1.2% occurred between 650 and 950°C. Infrared spectra of the residues obtained after heating the sample to 950°C in the TG showed that no significant reaction occurred between the fuel and oxidant.

6.6.2 *The $CaSi_2/Fe_2O_3$ system*

The DSC trace of a pressed sample of a 35% $CaSi_2/Fe_2O_3$ mixture showed no thermal event. The infrared spectra of the residues of samples heated under similar conditions to 950°C in the TG confirmed that no reaction occurred between the constituents of this mixture.

Figure 6.15 DSC trace of 85% $FeSi_7/KNO_3$ heated at 20°C min^{-1} in nitrogen

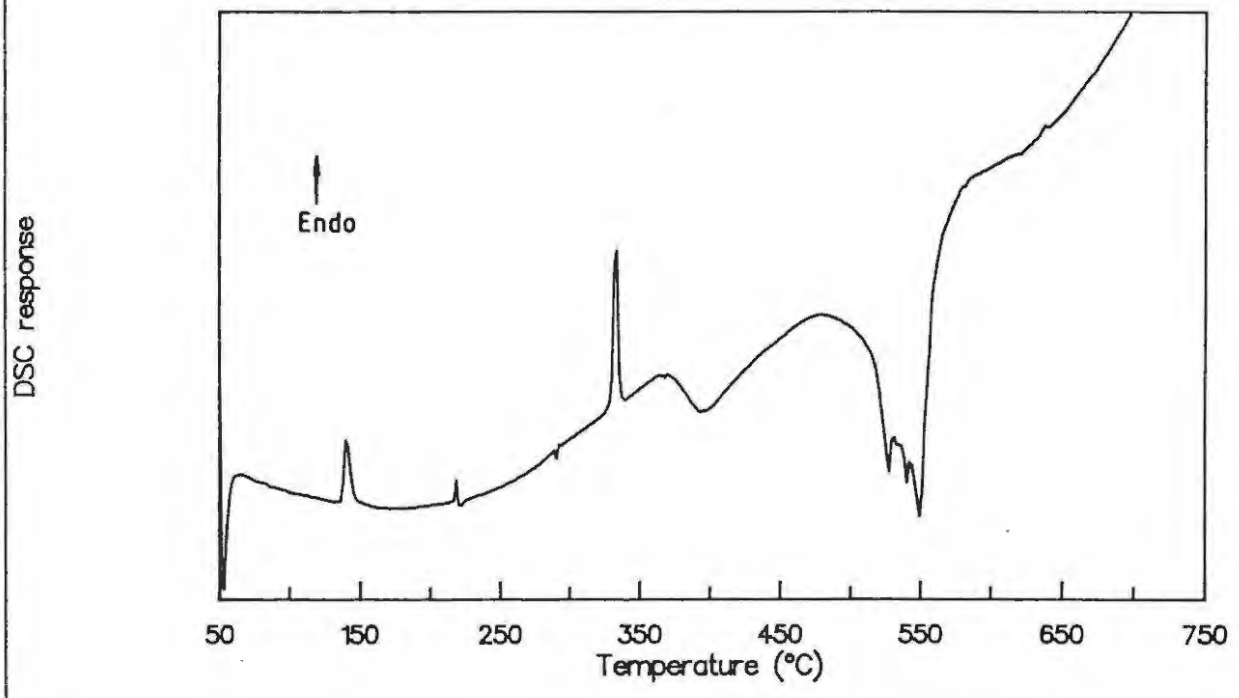

Figure 6.16 DSC trace of 40% $CaSi_2/Sb_2O_3$ heated at 20°C min^{-1} in nitrogen

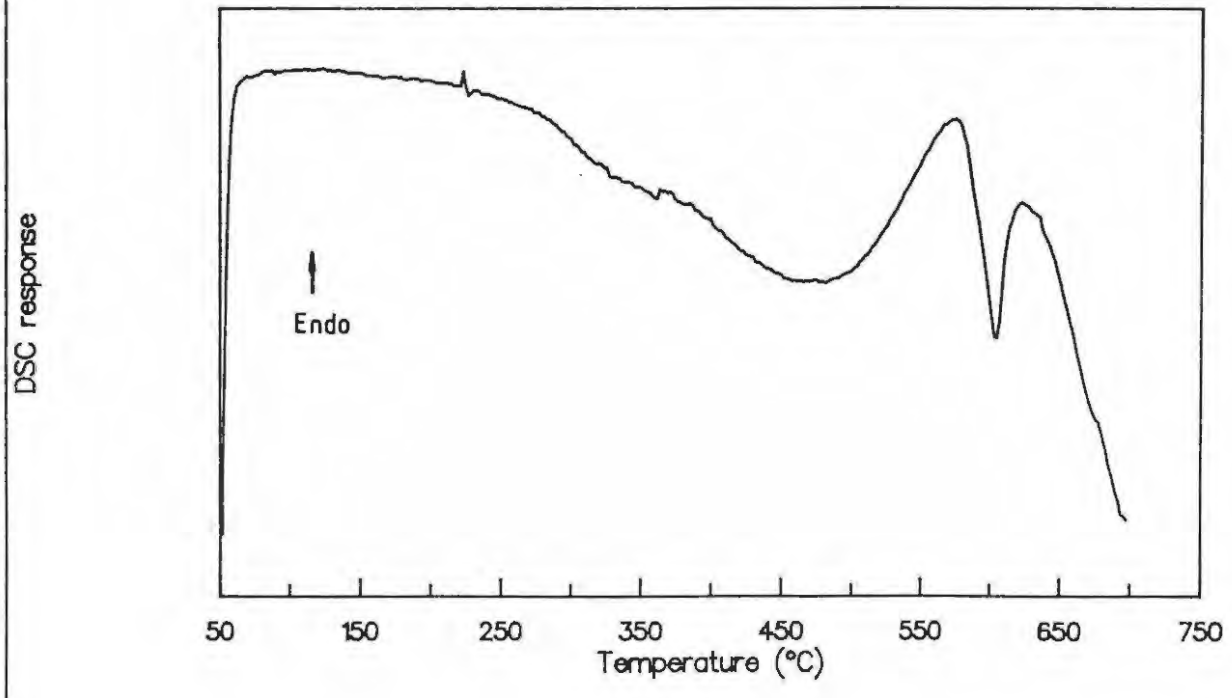

6.6.3 *The $CaSi_2/SnO_2$ system*

A slight mass loss of ~0.3% was observed in the TG curves of pressed samples of a 45% $CaSi_2/SnO_2$ mixture on heating from 50 to 900°C. No thermal events occurred when similar samples were heated in the DSC. Infrared spectra of the residue showed only the strong presence of SnO_2.

6.6.4 *The $CaSi_2/KNO_3$ system*

A typical DSC trace for an 85% $CaSi_2/KNO_3$ composition showed the usual endothermic processes due to KNO_3 (Figure 6.17). This was followed by two overlapping exotherms above 450°C. The first exotherm (520 to 590°C) is a broad process (ΔH = -0.16 ± 0.1 kJ (g mixture)$^{-1}$) which overlaps the second exothermic spike (595 to 690°C). The exothermic spike is usually an indication of ignition and the measured change in enthalpy was not reproducible. Similar exothermic spikes were observed for several mixtures, 25%, 40%, 65% and 85% $CaSi_2$ by mass. TG curves of the 85% $CaSi_2/KNO_3$ composition showed a continuous mass loss (8.3 ± 2.4%) starting at 390°C and mass loss is complete at 795°C. Mass loss occurred slowly initially and became rapid at ~540°C. A further mass loss of ~1.2% occurred above 800°C. The ignition residues showed the strong presence of SiO_2 and $KHCO_3$ and K_2CO_3.

6.7 **Thermal analysis of silicon with two oxidants**

Various ternary mixtures with silicon as fuel were examined using DSC in nitrogen as the main technique. The aim of this study was to induce a reaction, within the temperature limits of the DSC, in the Si/Fe_2O_3 and Si/SnO_2 systems through use of a third oxidant (either Sb_2O_3 or KNO_3) which is known to react with Si below the temperature limit of the DSC (730°C). The results below are for ternary systems in which the proportion by mass of the fuel was kept constant at 40%. The mass ratio of the two oxidants was varied such that the proportion by mass of the oxidants combined was kept at 60%.

6.7.1 *The $Si/SnO_2/Fe_2O_3$ system*

The DSC traces of various mixtures of the above composition in which only the mass ratios of SnO_2 and Fe_2O_3 were varied, showed no thermal event. This was confirmed by infrared spectra of the residues. No changes in the DSC curves were noted when either the heating rate or the mass of the sample was varied.

Figure 6.17 DSC trace of 85% $CaSi_2/KNO_3$ heated at 20°C min^{-1} in nitrogen

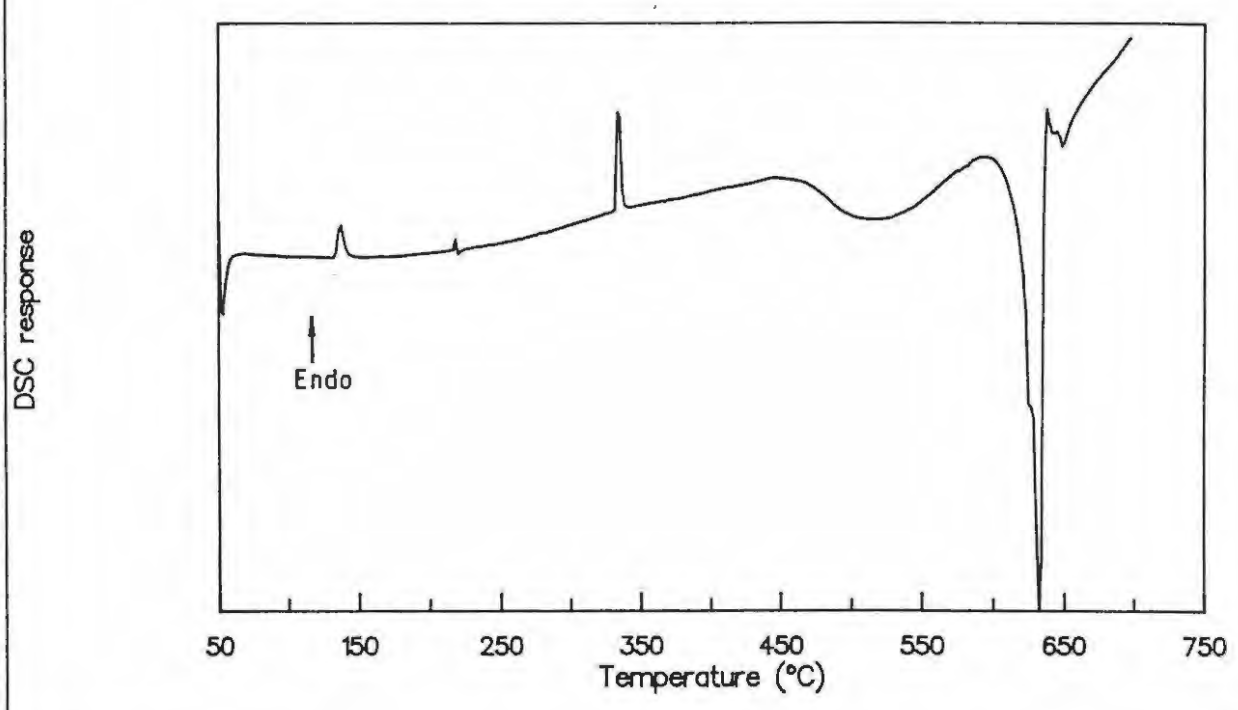

Figure 6.18 DSC trace of 40% Si/45% Fe_2O_3/15% KNO_3 heated at 20°C min^{-1} in nitrogen

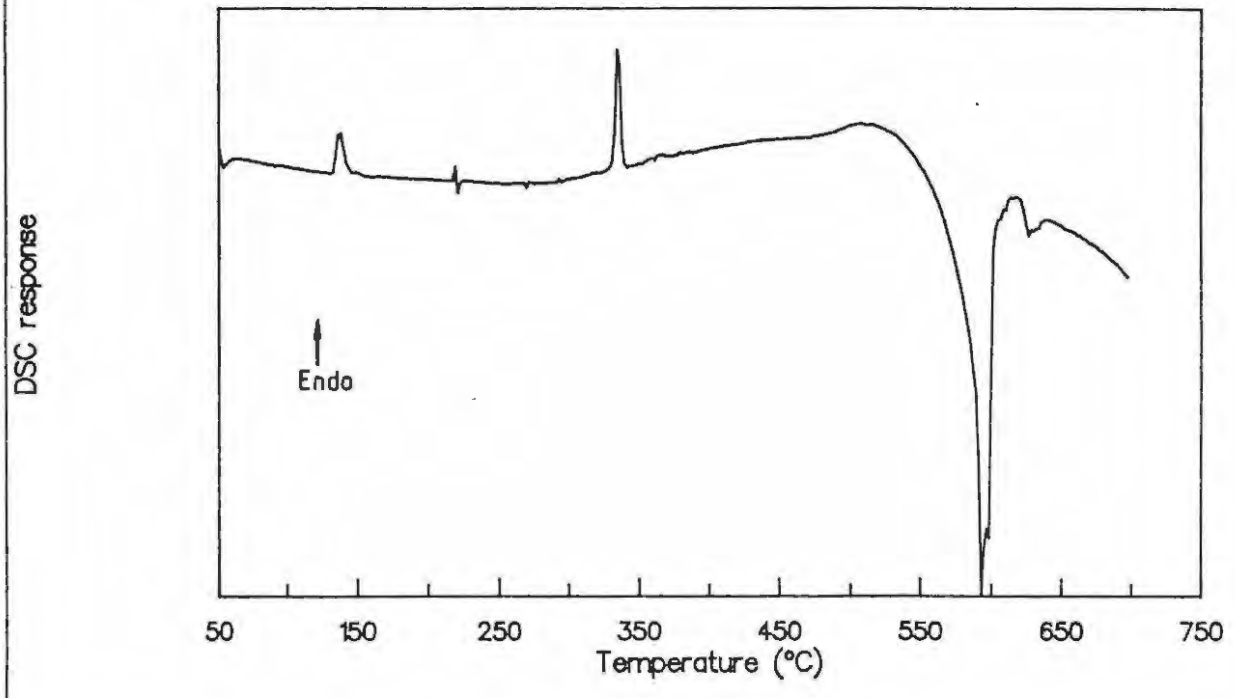

6.7.2 *The $Si/Fe_2O_3/KNO_3$ system*

The DSC trace of the ternary system of 40% Si, 45% Fe_2O_3 and 15% KNO_3 (Figure 6.18) showed a strong exothermic spike, associated with ignition of the sample, between 520 and 640°C (ΔH = -0.39 ± 0.08 kJ (g of mixture)$^{-1}$). Other mass percent ratios of KNO_3 and Fe_2O_3 gave violent exotherms (ignition temperature of 530 ± 7°C) which caused the sample pans to move. The infrared spectra of the ignition residue showed the strong presence of SiO_2 only and confirmed that Fe_2O_3 had reacted during the exothermic reaction.

6.7.3 *The $Si/Fe_2O_3/Sb_2O_3$ system*

The DSC traces of the $Si/Fe_2O_3/Sb_2O_3/$ system were similar to the DSC curves recorded for the Si/Sb_2O_3 system alone. The exotherm due to reaction between Si and Sb_2O_3 is superimposed on the endotherm due to the sublimation of Sb_2O_3 (see Figure 6.19).

The ΔH values measured from DSC curves (see Table 6.5) decreased with a decrease in the Sb_2O_3 content of the mixture. The presence of Fe_2O_3 had apparently no effect on the DSC curves of the ternary mixture. This was confirmed using infrared spectroscopy.

TABLE 6.5

Summary of DSC data for various $Si/Fe_2O_3/Sb_2O_3$ mixtures

% KNO_3	% SnO_2	Range* (°C)	Onset (°C)	- ΔH kJ (g mixture)$^{-1}$
60	0	590 to 615	592 ± 5	0.55 ± 0.02
45	15	560 to 620	570 ± 12	0.28 ± 0.03
30	30	561 to 600	571 ± 10	0.28 ± 0.02
15	45	580 to 610	580 ± 12	0.24 ± 0.01
0	60	-	-	-

* Refers to the temperature range of the exotherm

Figure 6.19 DSC trace of 40% Si/30% Fe_2O_3/30% Sb_2O_3 heated at 20°C min^{-1} in nitrogen

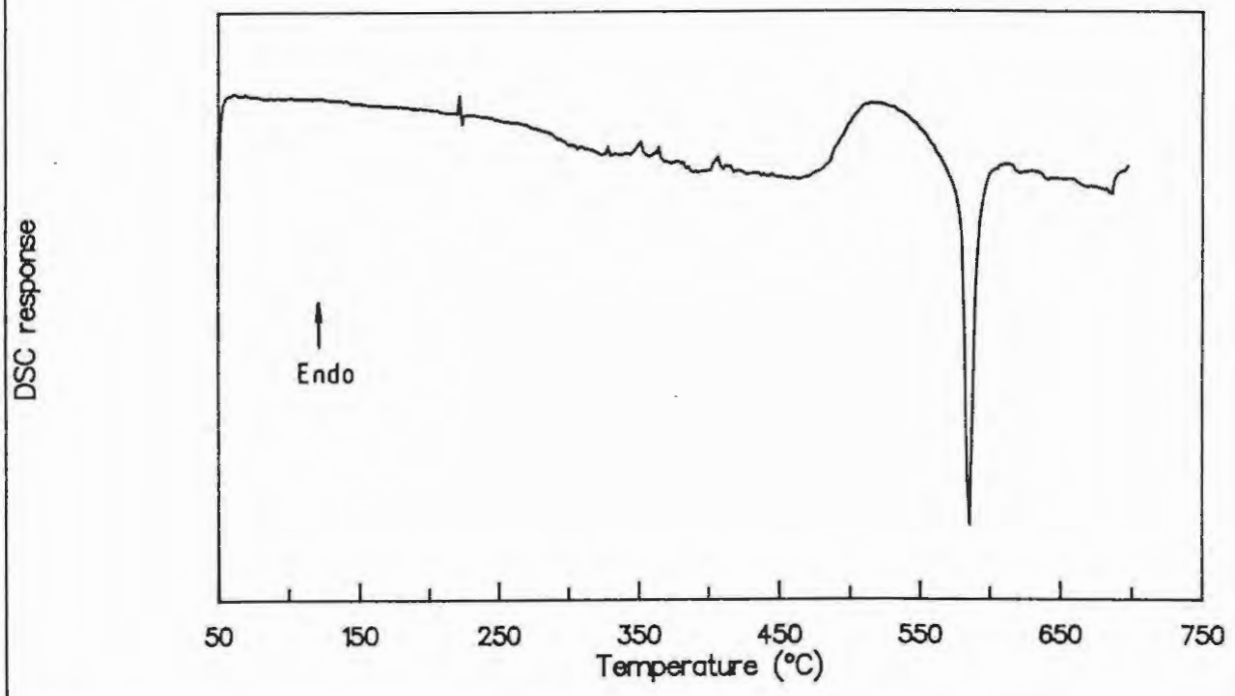

Figure 6.20 DSC trace of 40% Si/45% SnO_2/15% KNO_3 heated at 20°C min^{-1} in nitrogen

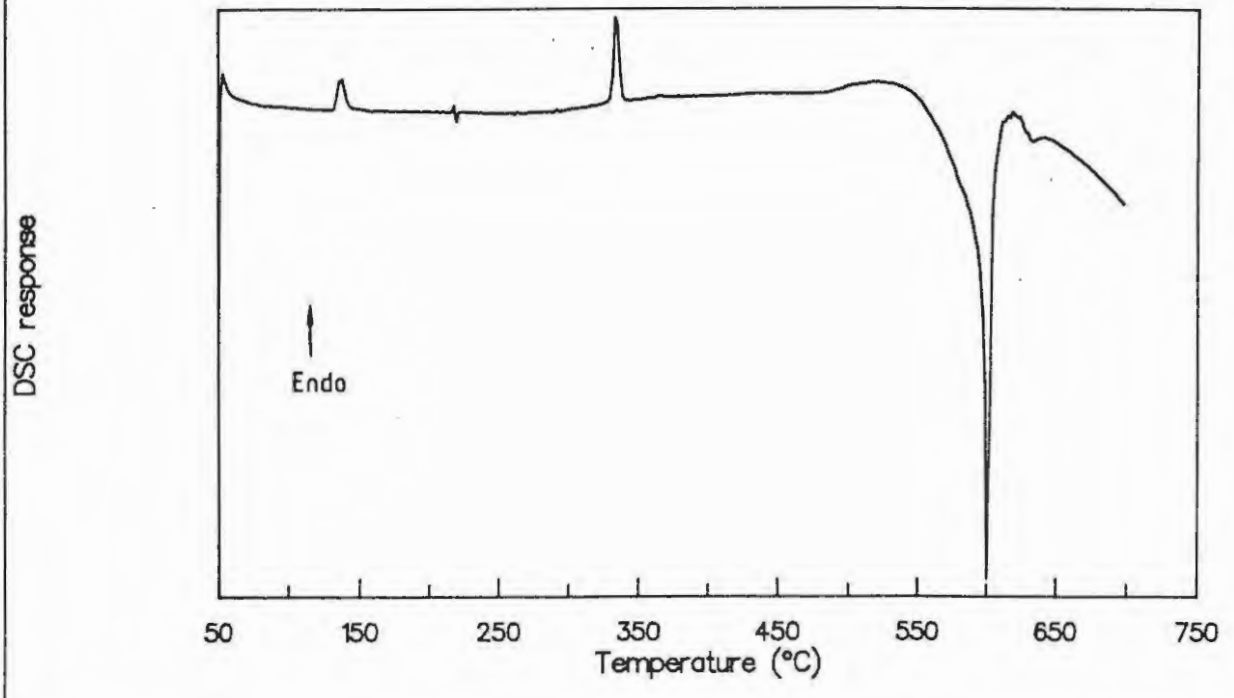

6.7.4 *The $Si/SnO_2/KNO_3$ system*

A typical DSC trace of the above ternary system (Figure 6.20) showed a single exotherm between 540 and 700°C (see Table 6.6).

TABLE 6.6

Summary of DSC data for various $Si/SnO_2/KNO_3$ mixtures

% KNO_3	% SnO_2	Range* (°C)	Onset (°C)	$-\Delta H$ kJ (g of mixture)$^{-1}$
60	0	540 to 720	545 ± 5	2.39 ± 0.40
45	15	540 to 580	538 ± 2	ignited
30	30	540 to 698	542 ± 11	0.61 ± 0.08
15	45	540 to 625	541 ± 9	0.41 ± 0.08
0	60	No exotherm	observed	-

* Refers to the temperature range of the exotherm

The temperature range in which the exotherm occurred corresponds to that for a reaction between Si and KNO_3 only. Samples which contained 45% KNO_3 and 15% SnO_2 gave a strong exothermic spike but the exothermicity decreased with increasing SnO_2. The infrared spectrum of the residue showed the presence of SiO_2 and also SnO_2. The involvement of SnO_2 in the reaction between Si and KNO_3 could not be confirmed.

6.7.5 *The $Si/SnO_2/Sb_2O_3$ system*

DSC traces of the above mixtures showed, typically, a single exotherm (onset at ~620°C) superimposed on a broad endotherm (between 480 and 680°C) due to sublimation of Sb_2O_3 (see Figure 6.21). The characteristics of the DSC traces of the various mixtures examined are summarised in Table

Figure 6.21 DSC traces of 40% Si/15% SnO_2/45% Sb_2O_3 heated at 20°C min^{-1} in nitrogen

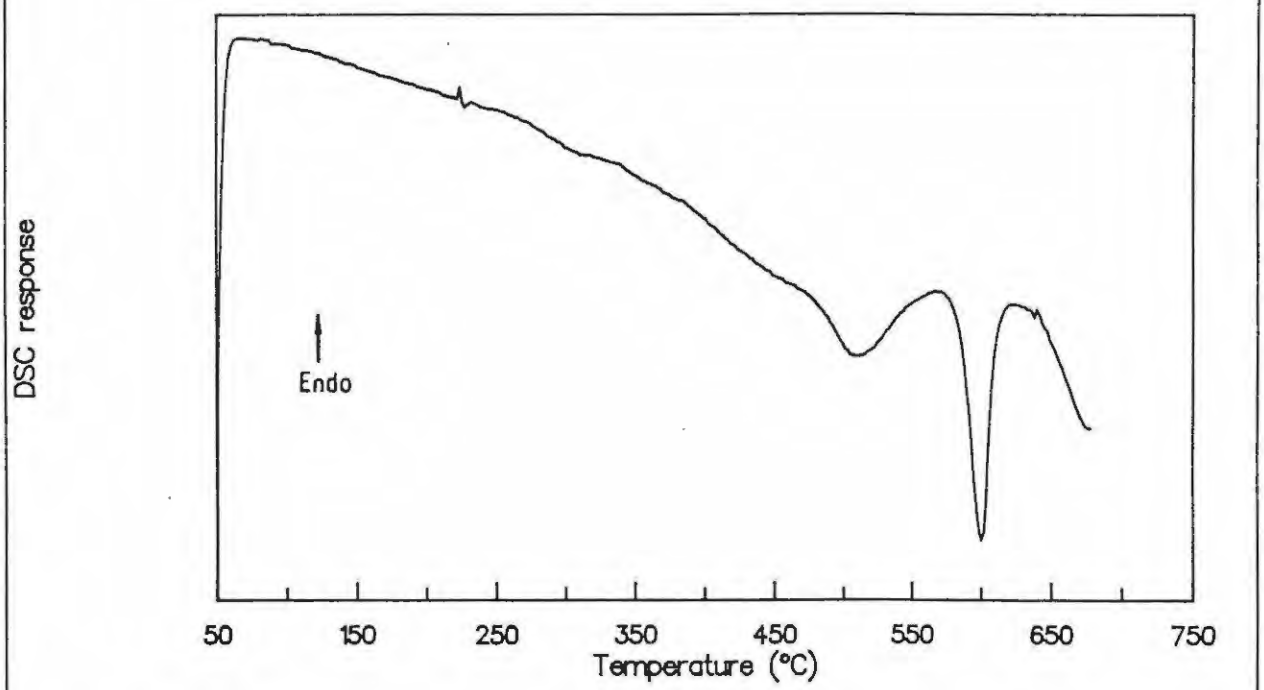

Figure 6.22 DSC traces of 40% Si/15% KNO_3/45% Sb_2O_3 heated at 20°C min^{-1} in nitrogen

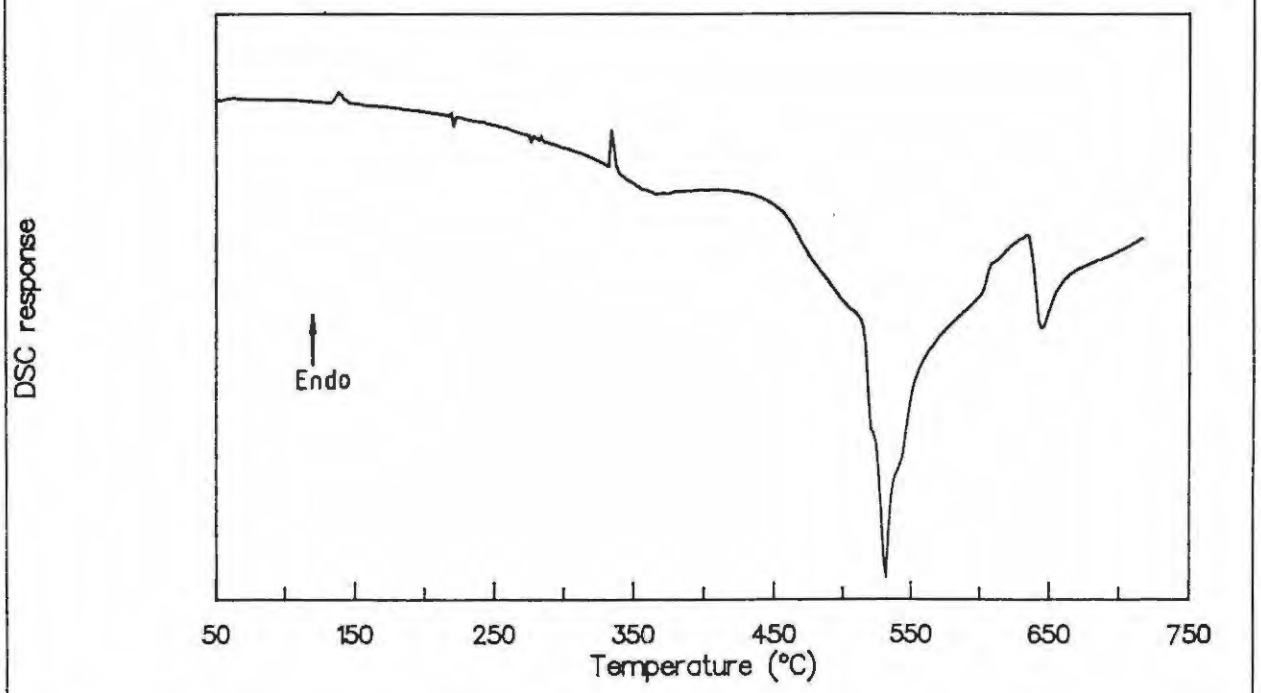

6.7. The change in enthalpy of the exotherm decreased with decreasing Sb_2O_3. So, SnO_2 could not be induced to react with Si in the presence of Sb_2O_3. The DSC traces of the binary 40% Si/SnO_2 mixture showed, as expected, no thermal event. The infrared spectra of the residues showed the presence of SiO_2 and SnO_2.

TABLE 6.7

Summary of DSC data for various $Si/SnO_2/Sb_2O_3$ mixtures

% Sb_2O_3	% SnO_2	Range* (°C)	Onset (°C)	$-\Delta H$ kJ (g of mixture)$^{-1}$
60	0	590 to 615	590 ± 5	0.53 ± 0.01
45	15	560 to 625	566 ± 5	0.23 ± 0.03
30	30	530 to 620	537 ± 5	0.26 ± 0.02
15	45	520 to 550	530 ± 12	0.03 ± 0.01
0	60	No exotherm	observed	-

* Refers to the temperature range of the exotherm

6.7.6 *The $Si/KNO_3/Sb_2O_3$ system*

DSC curves of ternary mixtures consisting of Si, Sb_2O_3 and KNO_3 showed two exotherms (see Figure 6.22). ΔH for the first (between 400 and 620°C) and second (between 630 and 700°C) exotherms increased and decreased, respectively, with increasing Sb_2O_3 (see Table 6.8). The exotherm due to Si and Sb_2O_3 alone ($\Delta H = -0.53 \pm 0.01$ kJ (g mixture)$^{-1}$) occurred between 590 and 620°C, and that between Si and KNO_3 ($\Delta H = -1.00 \pm 0.02$ kJ (g mixture)$^{-1}$) between 600 and 720°C. The ΔH values for the first and second exotherms for the ternary mixtures were not consistent with those expected for the Si/Sb_2O_3 and Si/KNO_3 reactions, respectively. Therefore, the reaction during the first exotherm probably involves all three ingredients. It is likely that the reaction between Si and Sb_2O_3 predominates in the first exotherm and residual KNO_3 then reacts at a higher temperature during the second exotherm.

TABLE 6.8

Summary of DSC data for various $Si/KNO_3/Sb_2O_3$ mixtures

% KNO_3	% Sb_2O_3	Range* (°C)	Onset (°C)	$-\Delta H$ kJ (g of mixture)$^{-1}$
60	0	590 to 720	600 ± 10	2.39 ± 0.04
45	15	390 to 575 630 to 695	400 ± 10 644 ± 10	0.59 ± 0.06 0.61 ± 0.04
30	30	480 to 590 650 to 705	492 ± 13 675 ± 15	0.98 ± 0.03 0.22 ± 0.01
15	45	430 to 621 630 to 690	446 ± 21 631 ± 1	1.44 ± 0.05 0.19 ± 0.02
0	60	590 to 615	590 ± 4	0.53 ± 0.01

* Refers to the temperature range of the exotherm

6.8 **Kinetics from thermal analysis**

6.8.1 *Introduction*

The extraction of kinetic information from programmed temperature thermal analysis curves for heterogeneous reactions is a controversial field. Many methods have been used to analyse experimental data. A method suggested by Borchardt and Daniels (11) is used in this section to extract kinetic information from TG as well as DSC traces recorded for various binary Si/oxidant systems.

The Borchardt and Daniels method assumes the usual form of the rate equation

$$\frac{d\alpha}{dt} = k\,(1-\alpha)^n$$

so,

$$k = (d\alpha/dt)/(1-\alpha)^n$$

and

$$k = A \exp(-E_a/RT)$$

Use is also made of the relationship

$$\frac{d\alpha}{dt} = \frac{d\alpha}{dT} \cdot \frac{dT}{dt} = \frac{d\alpha}{dT}\phi$$

where ϕ is the heating rate. E_a and A may thus be calculated from a plot of ln k against 1/T. The value of n can be adjusted until satisfactory linearity is achieved.

Kinetic analysis is only appropriate where the thermal analysis curve is simple. An example of a suitable DSC trace is shown in Figure 6.23. This represents the exothermic reaction of the 40% Si/Sb_2O_3 composition. The DSC response is assumed to be proportional to $d\alpha/dt$ and hence the partial area under an exotherm or endotherm is a measure of α (see Figures 6.23 and 6.24). A value of n is selected by trial and error until a plot of ln k against 1/T is suitably linear (Figure 6.25).

The following DSC and TG curves were analysed according to the Borchardt and Daniels method:

(i) TG curve for the oxidation of Si in air

(ii) TG curve for the oxidation of Si in oxygen

(iii) DSC exotherm of the reaction of 40% Si/Sb_2O_3

(iv) DSC exotherm of the reaction of 30% Si/KNO_3

(v) DSC exotherm of the reaction of 60% Si/KNO_3

6.8.2 *Results*

A summary of the kinetic parameters obtained is shown in Table 6.9. The TG curve for the oxidation of silicon in O_2 is shown in Figure 6.26. Also shown is a plot of α against T. The extent of the total reaction at 950°C is small (0.008). The plot of ln k against 1/T is therefore not very sensitive to the value of n (see Figure 6.27). Satisfactory linearity was obtained for n = 1. The activation energies obtained for samples heated in oxygen were greater than those obtained for the runs in air. However, the values for E_a in O_2 ($\sim$84 kJ mol^{-1}) are significantly lower than the $\sim$130 kJ mol^{-1} reported (12-14) in the literature (see section 2.2). The literature values were determined for the high-temperature oxidation of a silicon substrate with a thick SiO_2 film (12,13) (see Section 2.2).

The results of the kinetic analysis of the exotherm in the DSC trace for a 40% Si/Sb_2O_3 mixture (Figure 6.23 to 6.25) showed that the values of E_a were sensitive to the value of n. Of those tried, a value of n = 1 gave the best value of the correlation coefficient, r.

The activation energies obtained for 30% Si/KNO_3 and for a 60% Si/KNO_3 were very different (see Table 6.9). The values for the activation energies of the 30% Si/KNO_3 mixture are much greater than those observed for the 60% Si/KNO_3 and are probably unrealistic (see Table 6.9). The region of interest for the exotherm for a 60% Si/KNO_3 mixture is shown in Figure 6.28. Best correlation coefficients were obtained when n = 2 (see Figure 6.29).

TABLE 6.9

Kinetic analysis of nonisothermal thermal analysis curves

System	n	E_a (kJ mol^{-1})	ln (A min^{-1})	r*
Si in air	0.5	62.6 ± 5.5	-3.74 ± 1.53	0.85
	0.67	62.7 ± 5.5	-3.74 ± 1.55	0.85
	1	62.8 ± 5.4	-3.74 ± 1.54	0.85
	2	63.0 ± 5.5	-3.73 ± 1.55	0.85
Si in O_2	0.5	83.9 ± 18.1	3.99 ± 1.17	0.85
	0.67	84.0 ± 18.2	4.03 ± 1.14	0.85
	1	84.5 ± 18.3	4.11 ± 1.07	0.86
	2	85.9 ± 18.3	4.35 ± 0.88	0.72
40% Si/Sb_2O_3	0.5	251.4 ± 11.6	36.39 ± 1.87	0.88
	0.67	280.5 ± 9.6	41.02 ± 1.53	0.92
	1	338.7 ± 8.3	50.26 ± 1.52	0.98
	2	513.4 ± 14.5	78.0 ± 2.12	0.95
30% Si/KNO_3	0.5	1216.1 ± 122.5	154.83 + 6.21	0.68
	0.67	1428.9 ± 108.0	182.37 ± 6.02	0.78
	1	3131.0 ± 101.5	402.74 ± 7.27	0.96
	2	3109.2 ± 101.3	400.01 ± 7.94	0.96
60% Si/KNO_3	0.5	509.2 ± 105.0	78.15 ± 2.56	0.74
	0.67	610.7 ± 125.9	94.16 ± 3.08	0.74
	1	813.3 ± 167.5	126.15 ± 4.11	0.75
	2	1421.7 ± 292.3	222.13 ± 7.19	0.91

* r = correlation coefficient

Figure 6.23 DSC and α trace for 40% Si/Sb_2O_3 heated at 20°C min^{-1} in nitrogen

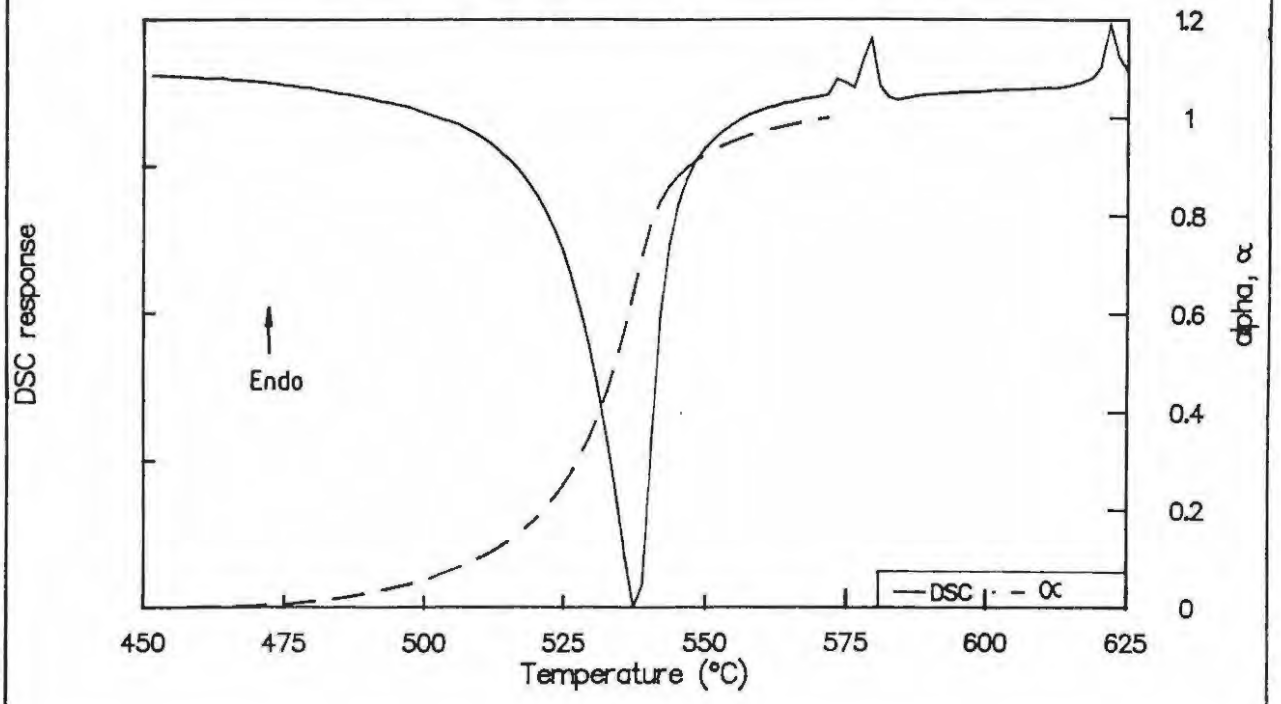

Figure 6.24 α - time and dα - time curves for 40% Si/Sb_2O_3

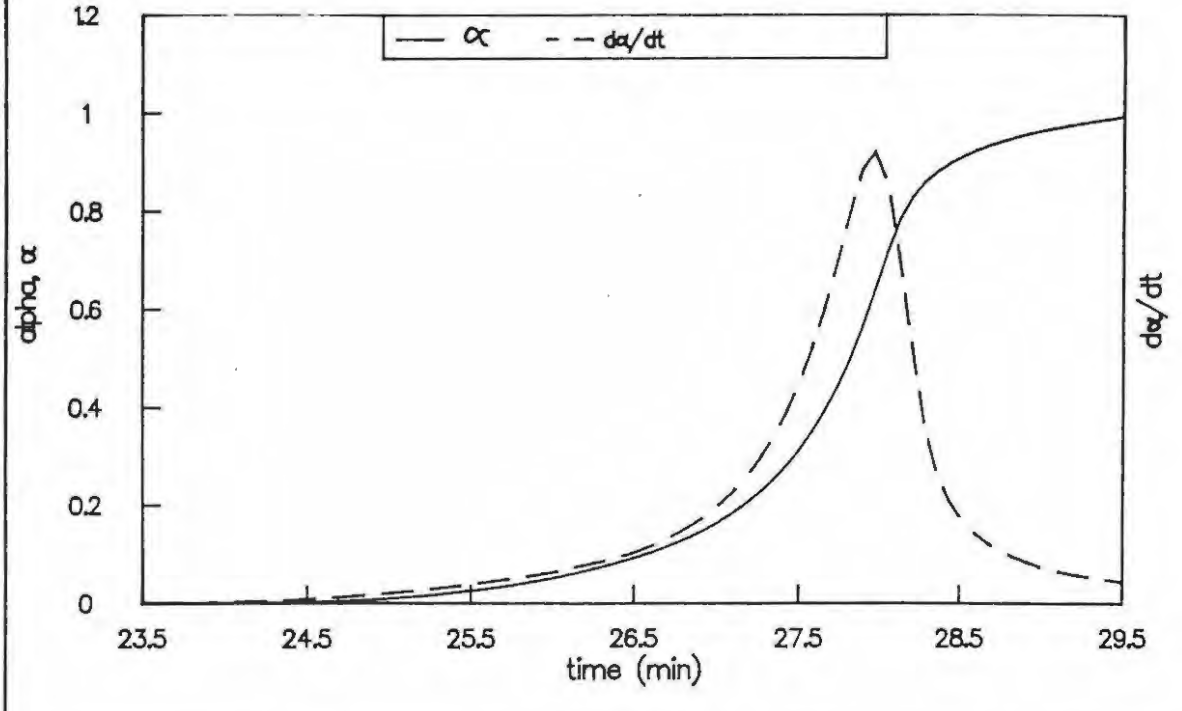

Figure 6.25 Arrhenius plot for 40% Si/Sb_2O_3 heated at 20°C min^{-1} in nitrogen

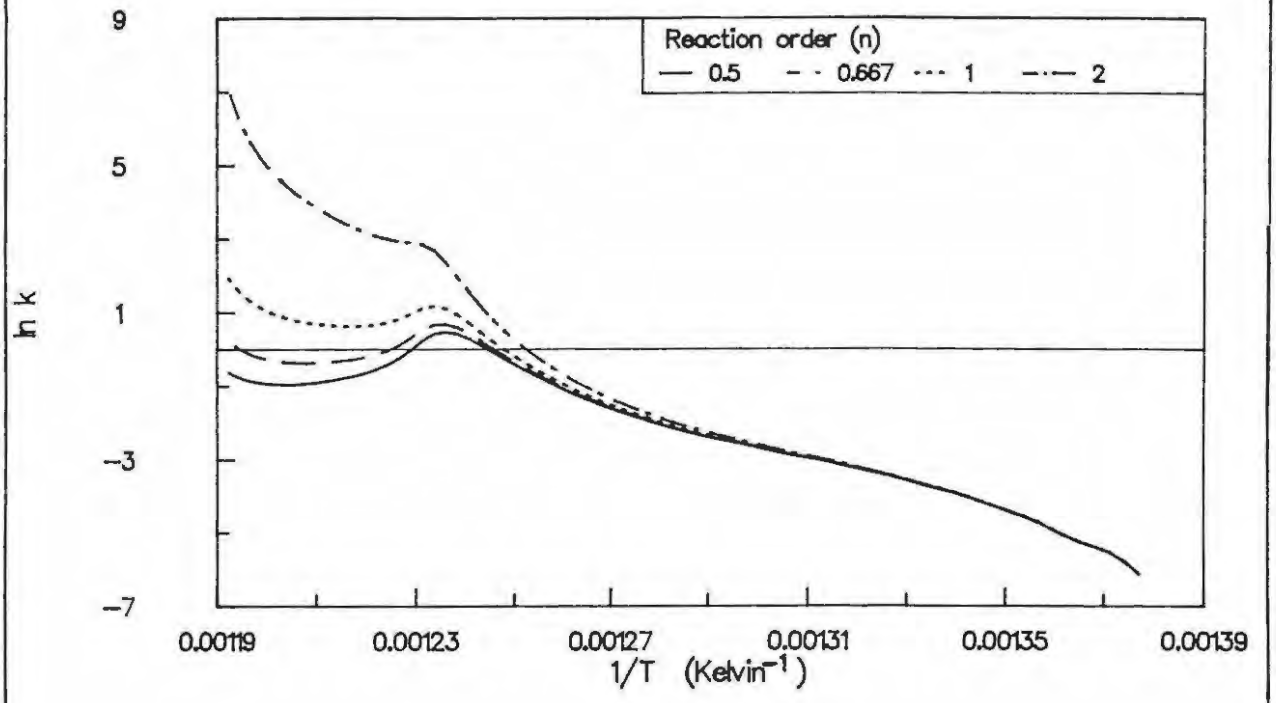

Figure 6.26 TG and α trace for Si heated at 20°C min^{-1} in O_2

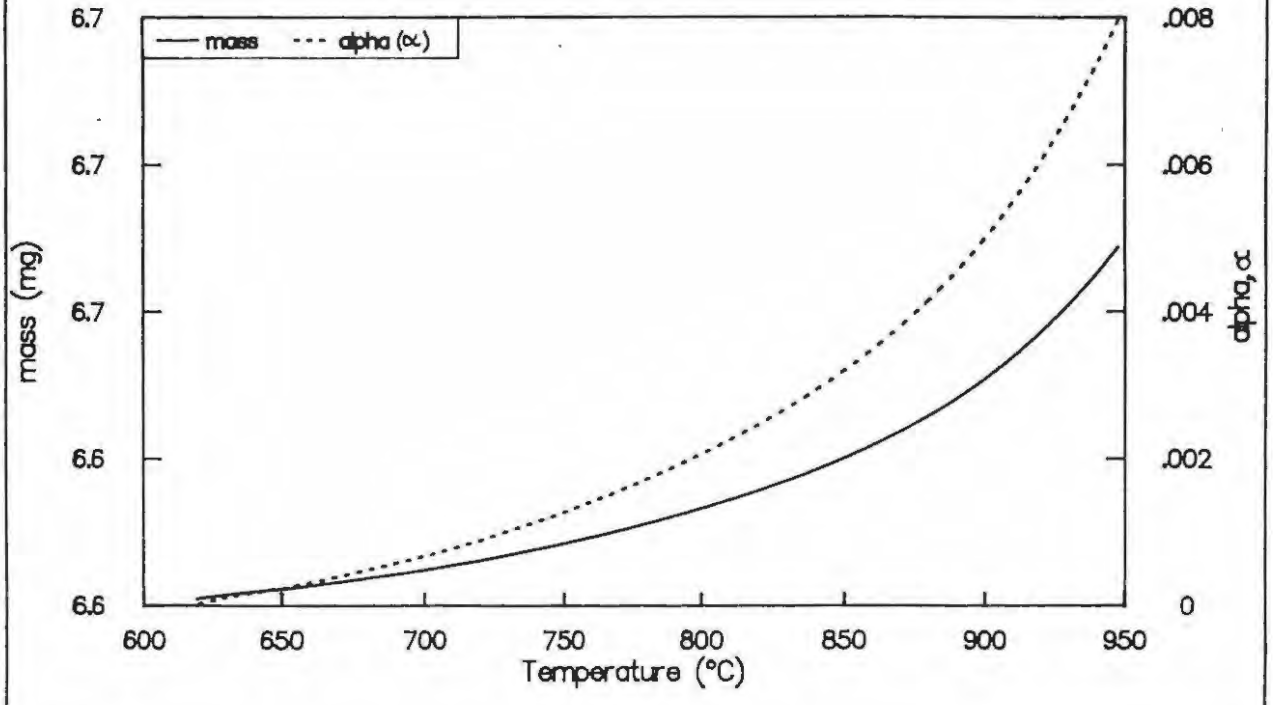

Figure 6.27 Arrhenius plot for silicon heated at 20°C min^{-1} in oxygen

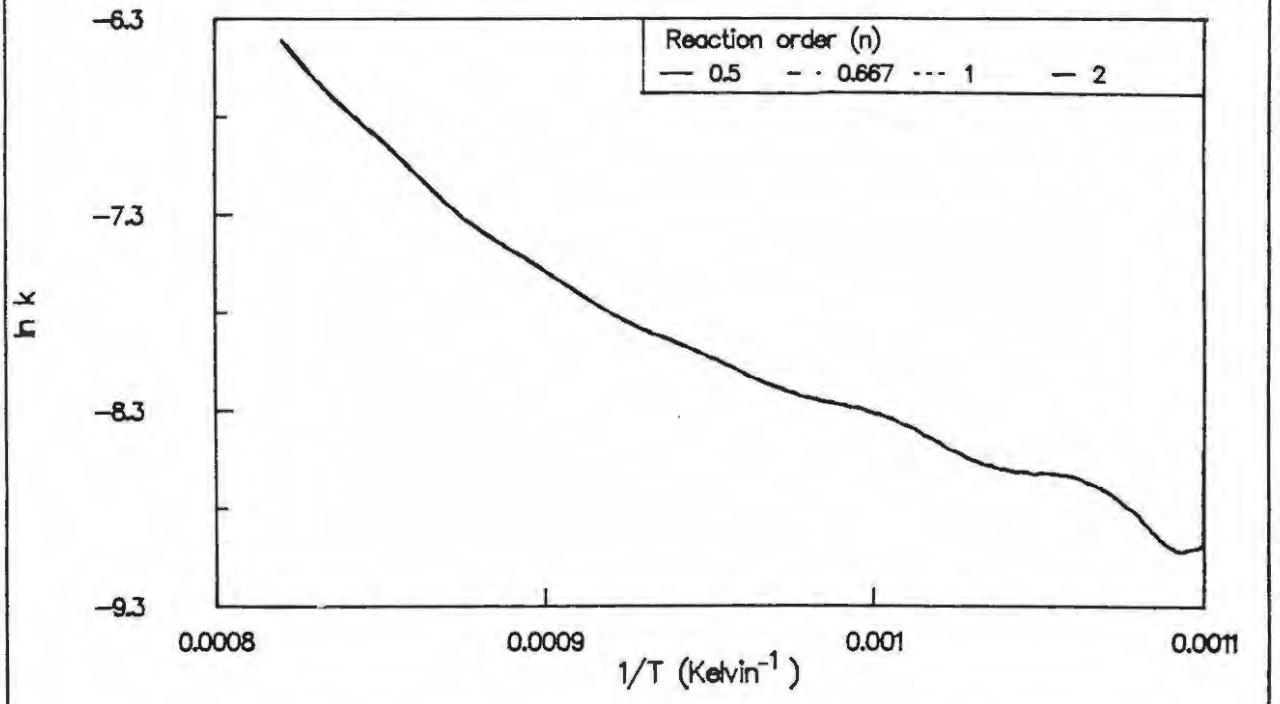

Figure 6.28 DSC and α trace for 60% Si/KNO_3 heated at 20°C min^{-1} in nitrogen

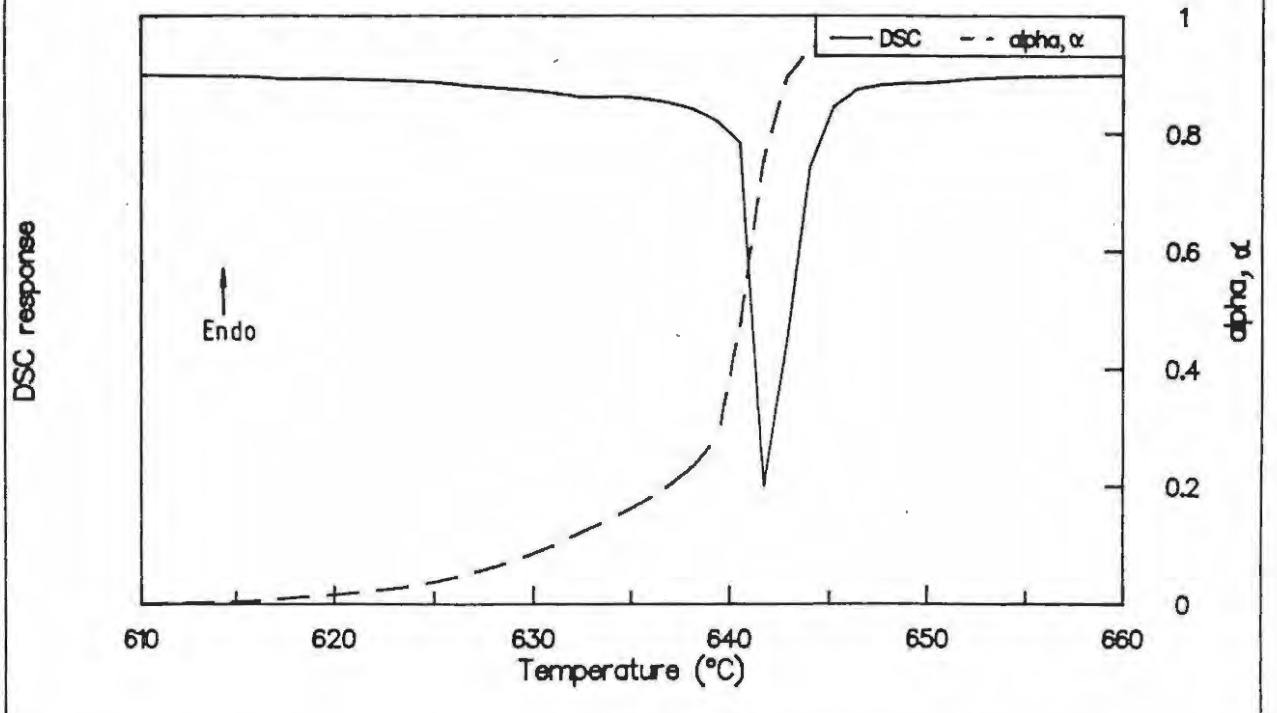

Figure 6.29 Arrhenius plot for 60% Si/KNO_3 heated at 20°C min^{-1} in nitrogen

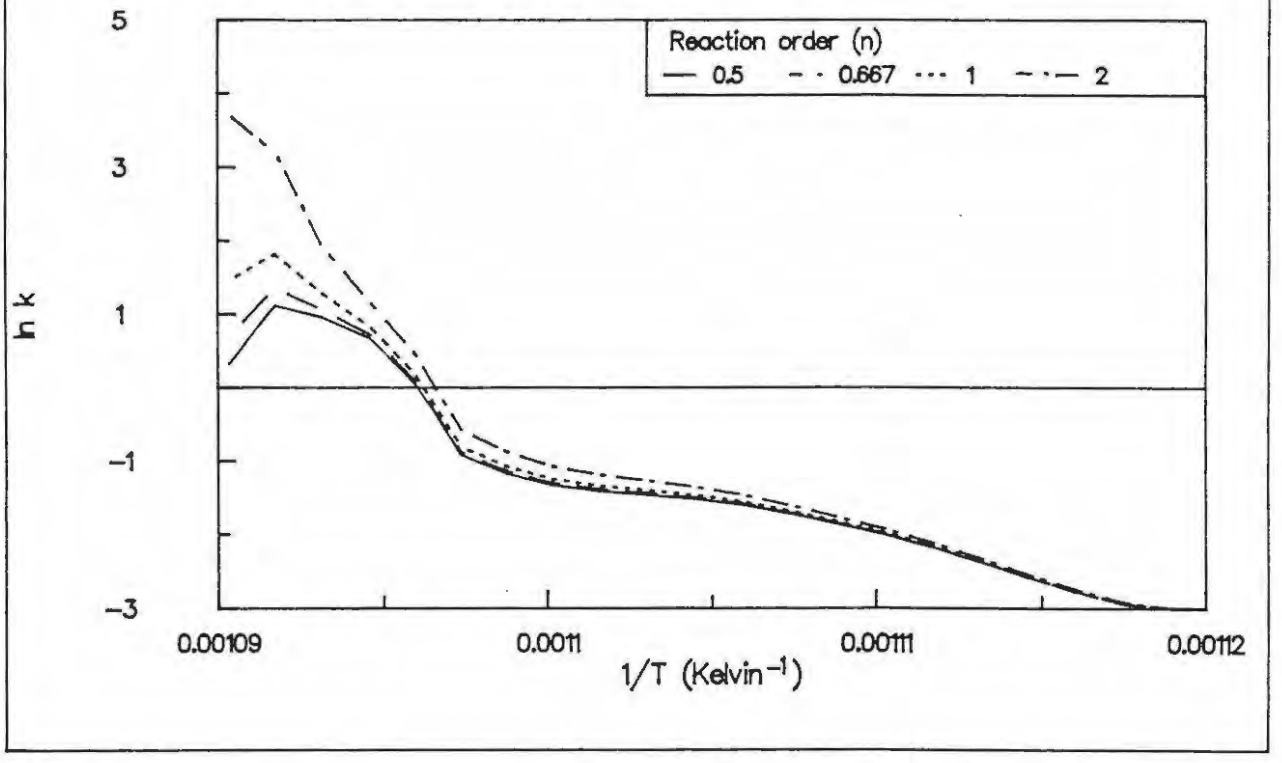

6.9 References

1. P.G. Laye and E.L. Charsley, Thermochim. Acta, **120** (1987) 329.
2. M.E. Brown, Thermochim. Acta, **148** (1989) 521.
3. G Braun, G. Bowden, K. Henkel and H. Rossbach, J. Thermal Anal., **33** (1988) 479.
4. S.E. Golunski, T.G. Nevell and M.I. Pope, Thermochim. Acta, **51** (1981) 153.
5. Y.K. Agrawal, A.L. Shashimohan and A.B. Biswas, J. Thermal Anal., **7** (1975) 635.
6. P.W. Centres, R.L. Wright, F.D. Price and C.J. Klenke, Physics and Chemistry of Glasses, **30** (1989) 149.
7. E.S. Freeman, J. Amer. Chem. Soc., **79** (1957) 383.
8. G.D. Serotkin, Zh. Neorg. Khim., 4 (1959)11.
9. G. Krishnamohan, E.M. Kurian and K.R.K. Rao, 8th Int. Pyro. Sem., (1982) 404.
10. M.E. Brown and R.A. Rugunanan, Thermochim. Acta, **134** (1988) 57.
11. H.J. Borchardt and F. Daniels, J. Am. Chem. Soc., **79** (1957) 41.
12. N. Mott, "*Conduction in Non-Crystalline Materials*", Oxford University Press, 1987.
13 S. Rigio, F. Rochet, B. Agius and A. Straboni, J. Electrochem. Soc., **129** (1982) 867.
14. B.E. Deal and A.S. Grove, J. App. Phys., **36** (1965) 3770.

7. COMBUSTION OF THE Si/Sb_2O_3 SYSTEM

7.1 Effect of composition

Binary Si/Sb_2O_3 mixtures ranging from 20 to 50% by mass of silicon, showed self-propagating combustion on suitable ignition and mixtures which contained more or less than these proportions of silicon failed to ignite. Mixtures with 20 to 25% silicon were slightly gassy (mass loss ~3%) and this caused movement of the sample and electrical shorting of the thermocouple during burning. A mass loss of ~1% after burning, was observed for samples with between 30 and 50% silicon indicating that the burning was essentially gasless.

The temperature profiles of mixtures with 30 to 50% silicon showed a smooth rise to maximum temperature (T_{max}) (see Figure 7.1) followed by cooling. Temperature profiles recorded for a given mixture were reasonably reproducible (see Figure 7.2). A slight, but not very reproducible, change in the slope of the rise-to-T_{max} at ~650°C, which corresponds to the temperature at which Sb_2O_3 melts (m.pt. 656°C), was observed (Figure 7.3). The first derivative of the rise region of the temperature profile (see Figure 7.3) showed two overlapping peaks. This change in the rate is probably due to the formation of molten Sb_2O_3 (see section 6.3).

The linear burning rates (v_{exp}) and mass burning rates (m_{exp}) of the Si/Sb_2O_3 compositions are given in Table 7.1.

TABLE 7.1

Burning rates for the Si/Sb_2O_3 system

(<53 μm Si, pressed 1 min at 55 MPa)

% Si	Density (g cm^{-3})	Porosity factor, ε	v_{exp} (mm s^{-1})	m_{exp} (g s^{-1})	T_{max} (°C)
20	2.87 ± 0.10	0.41	1.56 ± 0.20	0.18 ± 0.02	shorted
25	2.62 ± 0.04	0.44	3.25 ± 0.10	0.21 ± 0.01	shorted
30	2.59 ± 0.04	0.43	6.30 ± 0.29	0.50 ± 0.02	1301 ± 21
35	2.39 ± 0.07	0.45	8.71 ± 0.42	0.58 ± 0.02	1282 ± 13
40	2.25 ± 0.05	0.47	8.52 ± 0.33	0.63 ± 0.02	1178 ± 18
45	2.20 ± 0.11	0.46	8.73 ± 0.14	0.57 ± 0.04	1177 ± 14
50	2.09 ± 0.05	0.46	7.25 ± 0.11	0.48 ± 0.01	1056 ± 15

Figure 7.1 Temperature profiles for the Si/Sb_2O_3 system

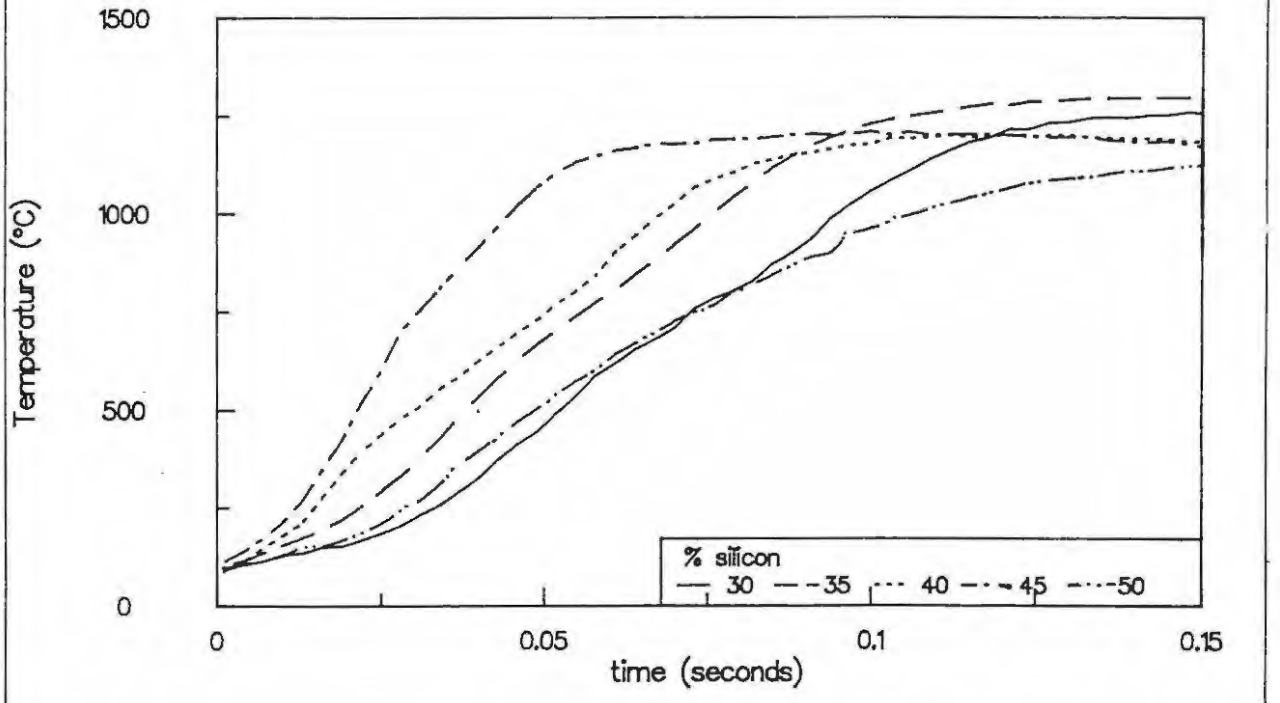

Figure 7.2 Temperature profiles of 40% Si/Sb_2O_3 mixtures showing reproducibility

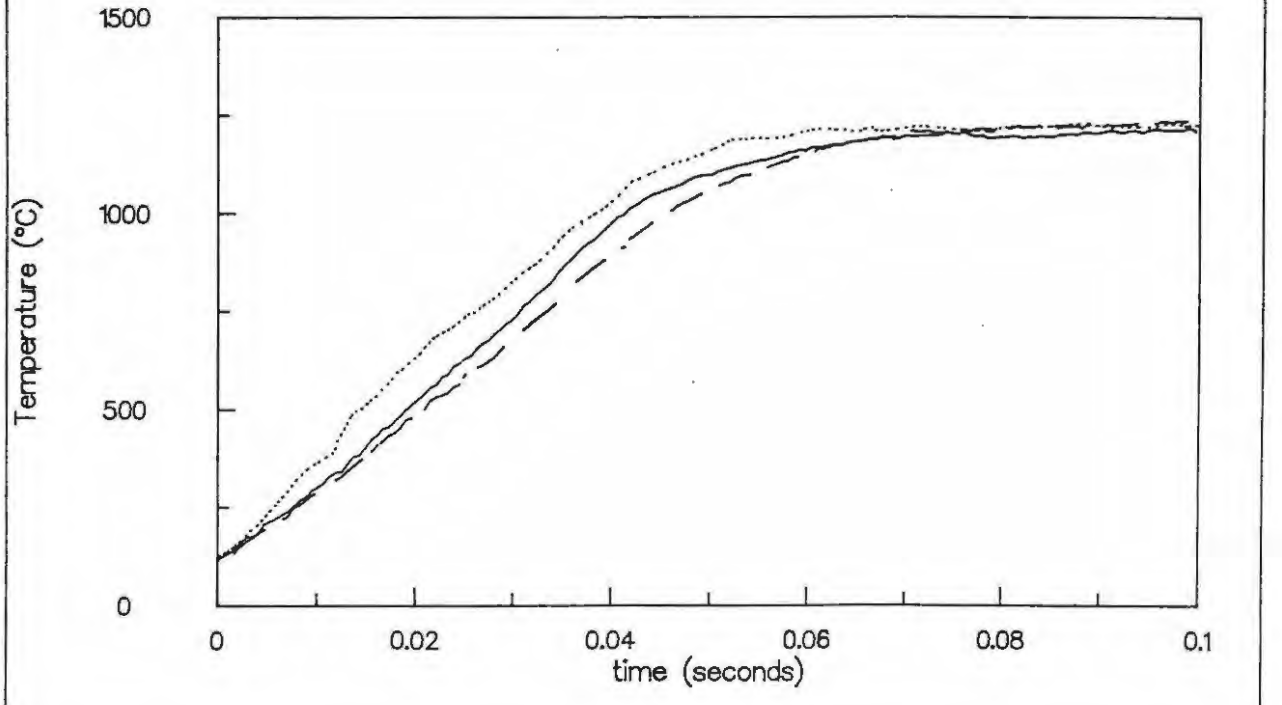

Figure 7.3 Temperature profile of a 45% Si/Sb_2O_3 mixture showing first derivative

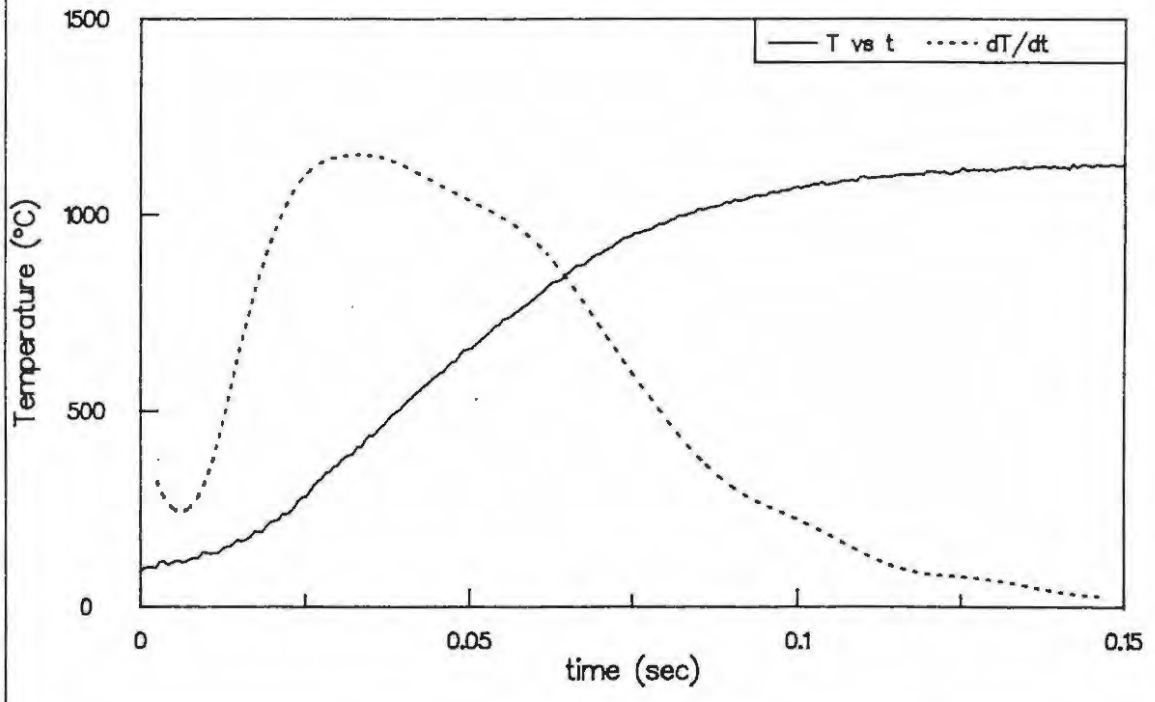

Figure 7.4 Burning rates of the Si/Sb_2O_3 system

(<53 μm Si, pressed 1 min at 55 MPa)

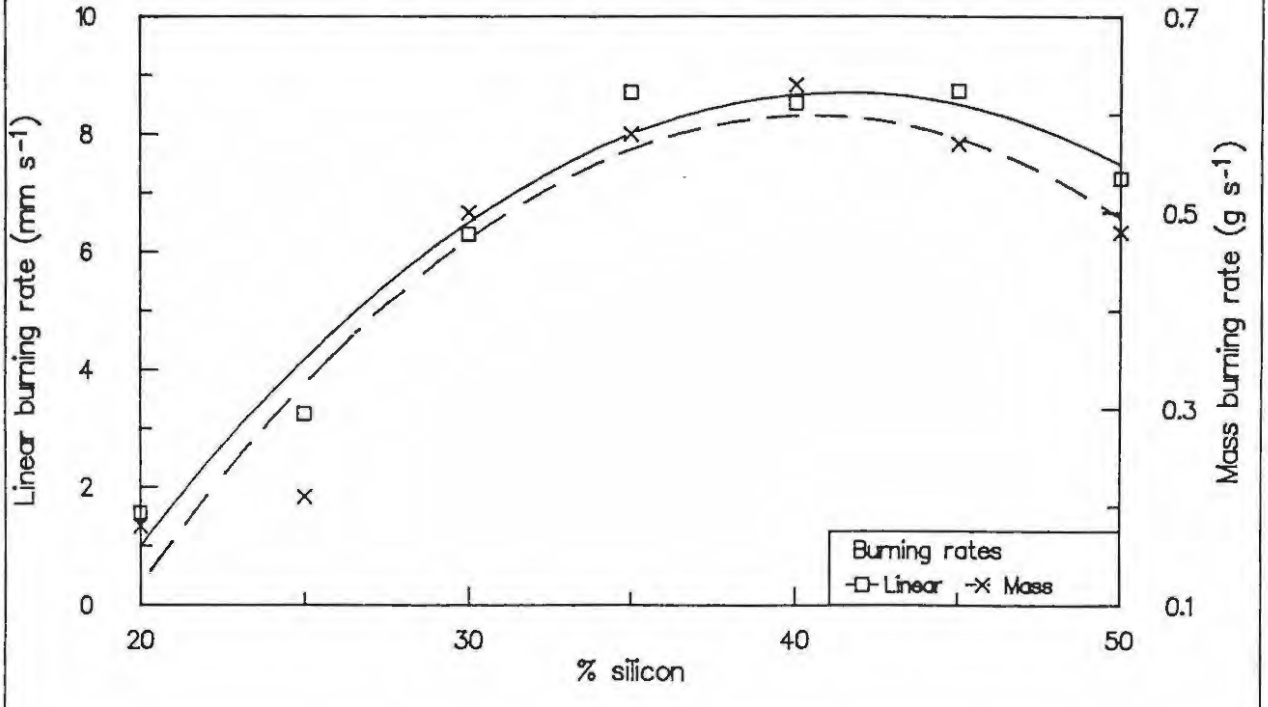

The porosity factor, ε, is given by

$$\varepsilon = \frac{\rho_s - \rho_e}{\rho_s - \rho_g}$$

where ρ_s is the density of the pure bulk solid, ρ_g is the density of the trapped gas (in this case, air) and ρ_e is the density of the compacted powdered mixture. Since $\rho_s >> \rho_g$,

$$\varepsilon = (1 - \rho_e/\rho_s)$$

In a plot of the burning rate against % Si (Figure 7.4), the maximum v_{exp} and m_{exp} occurred at approximately 43% Si. The maximum recorded temperatures (~1300°C) occurred at 30% Si (see Table 7.1) and decreased with increasing silicon to approximately 1060°C at 50% Si.

Scanning electron micrographs of a sample of an unreacted 40% Si/Sb_2O_3 mixture and samples after combustion are shown in Plate 7. The formation of solidified molten material confirmed the involvement of a molten phase during reaction. The micrographs also showed the presence of crystalline structures embedded in a solidified melt (see Plate 7.2 to 7.6) and of channels which were formed during the evolution of gaseous products during burning (see Plate 7.2, 7.3 and 7.6). Channel formation, is however, not extensive. Cavities in the frozen melt, due to pockets of trapped gas, were also observed.

The presence of vitreous SiO_2 (absorption band 1400 to 800 cm^{-1}) was detected in the infrared spectrum for the combustion residues of various Si/Sb_2O_3 mixtures. In the X-ray diffraction (XRD) patterns of the combustion residues, Si, unreacted Sb_2O_3 and Sb were identified. The few relatively low-intensity unidentified XRD peaks were probably due to the formation of antimony silicates and possibly anitimony silicides. Although the silicate ion is infrared active (1175 to 950 and 550 to 450 cm^{-1}) (1), only weak SiO_4^- absorptions could be identified in the range 550 to 450 cm^{-1}. Silicides are generally not infrared active (1). Although infrared spectra showed intense SiO_2 absorptions, the lack of XRD patterns of SiO_2 and of other silicates indicate that the silicon oxides formed were non-crystalline.

The main reaction which is proposed to occur during combustion, based on the predominant products identified by infrared spectroscopy and XRD, is

$$3Si(s) + 2Sb_2O_3(s \text{ or } g) \rightarrow 3SiO_2(s) + 4Sb(l) \quad ...(7.1)$$

The reaction has an expected ΔH = -444.4 kJ $(mol\ Si)^{-1}$. The stoichiometric proportion of Si is 12.6% and the calculated heat output is 1.97 kJ $(g\ mixture)^{-1}$.

According to McLain (2), the difference between the compositions at which v_{exp} is a maximum (~40% Si) and the stoichiometric composition (see section 7.1.2) is expected to be large if the thermal conductivity, λ, (see section 12) of the fuel (λ for Si = 0.35 W m^{-1} K^{-1}) is greater than that of the oxidant (λ for Sb_2O_3 = 0.24 W m^{-1} K^{-1}). The higher thermal conductivity of the fuel promotes faster burning as its mass ratio in the mixture increases. The formation of a layer of the oxide also prevents further oxidation of the bulk of the silicon particles so the actual stoichiometric composition is considerably greater than the calculated one based on complete reaction.

Plate 7 Scanning electron micrographs of the combustion residues of 40% Si/Sb_2O_3 mixtures

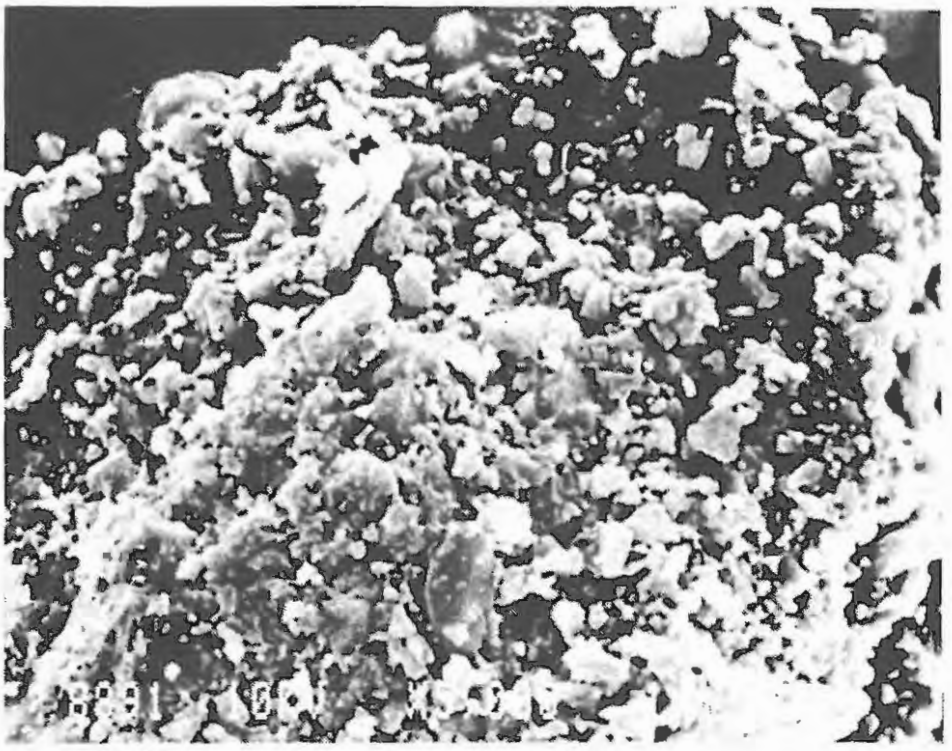

Plate 7.1 Unreacted material (magnified 5000 X)

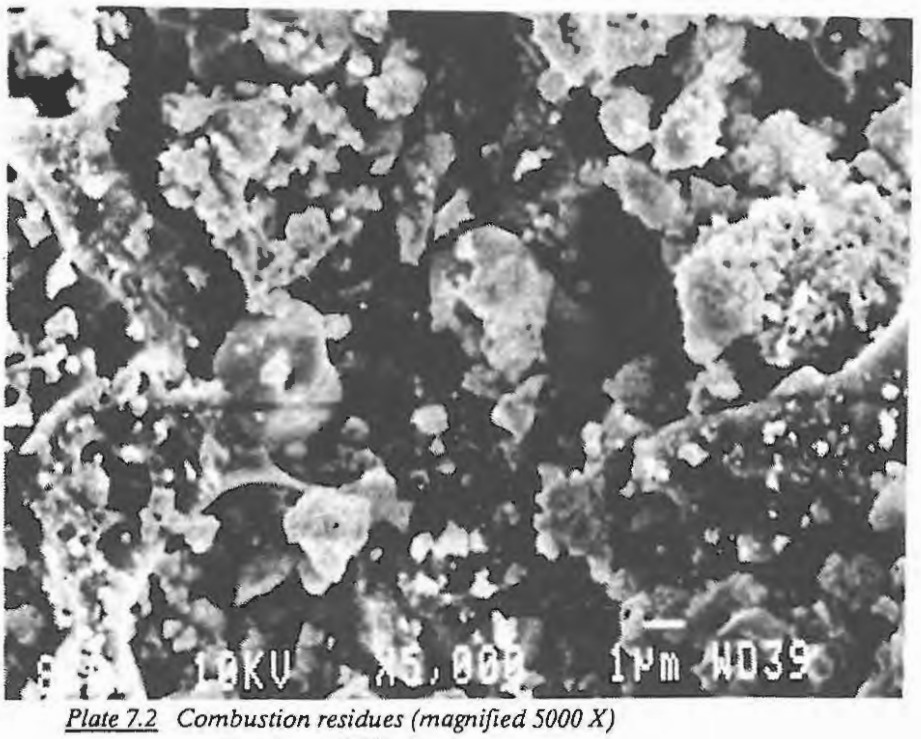

Plate 7.2 Combustion residues (magnified 5000 X) showing solidified melts

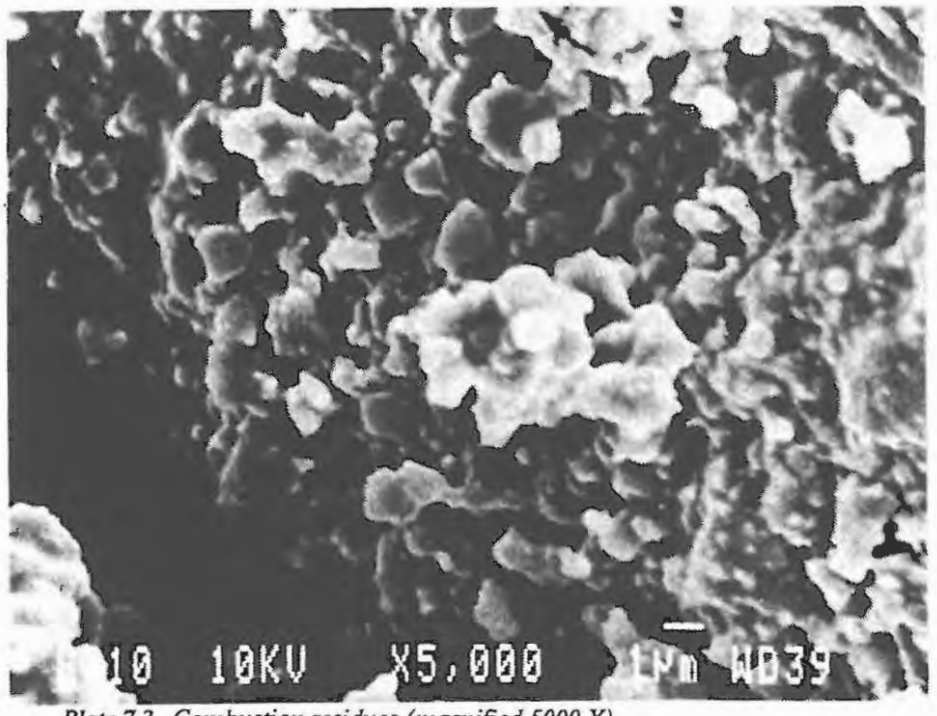

Plate 7.3 *Combustion residues (magnified 5000 X) showing solidified melts and recrystallisation*

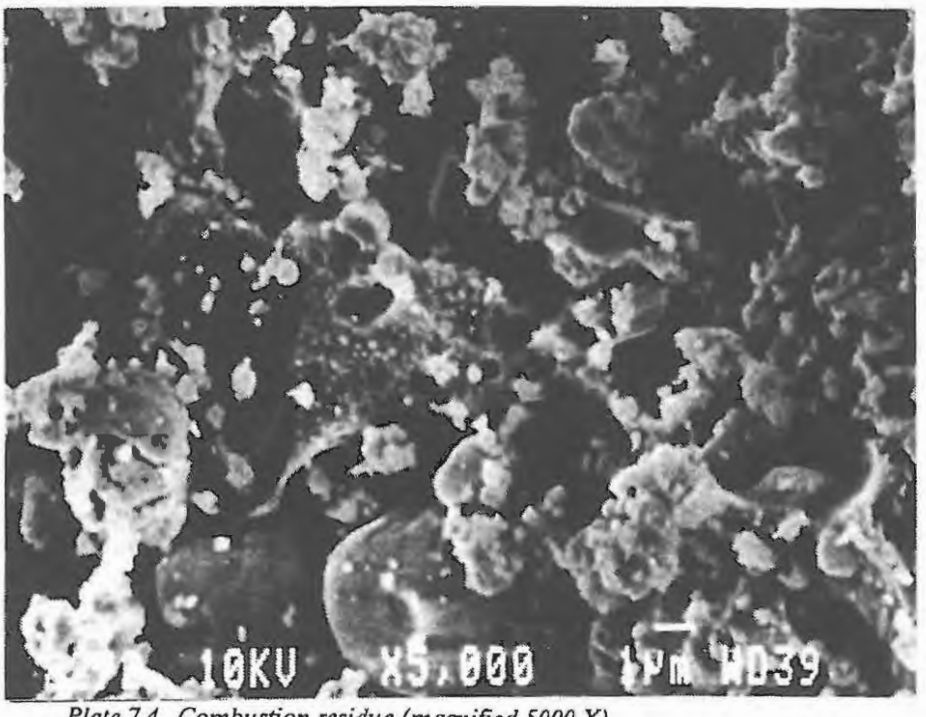

Plate 7.4 *Combustion residue (magnified 5000 X) showing gas cavities*

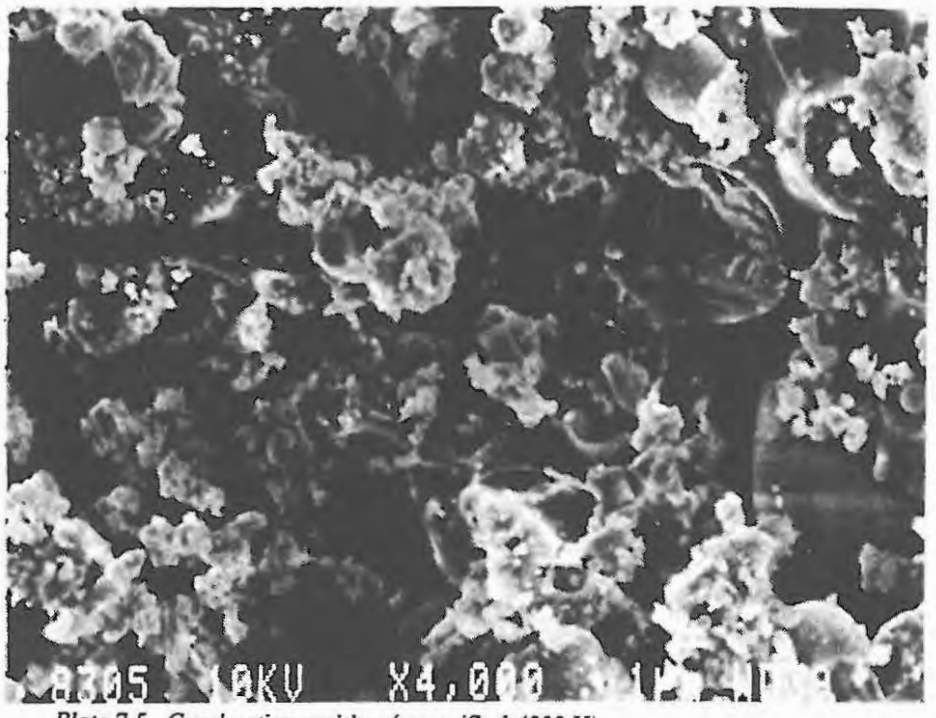

Plate 7.5 *Combustion residue (magnified 4000 X) showing cavities and the formation of channels*

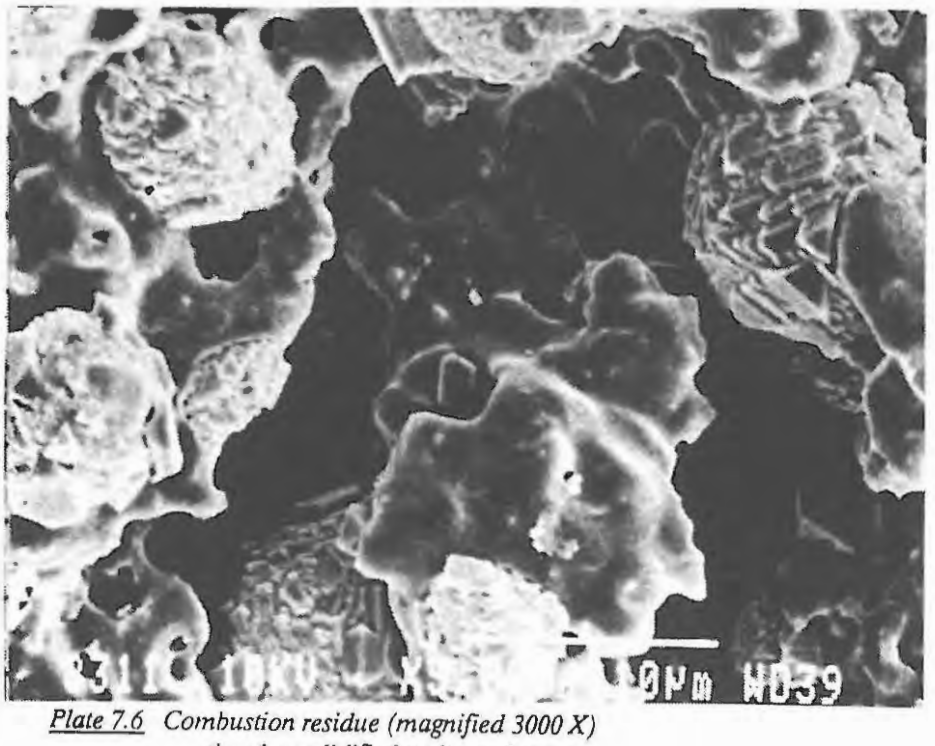

Plate 7.6 *Combustion residue (magnified 3000 X) showing solidified melts and some recrystallisation*

7.1.1 *Kinetic aspects*

The kinetic parameters obtained from temperature profiles analysed according to the Hill approach (3,4) (see section 4) for the Si/Sb_2O_3 system are listed in Table 7.2.

TABLE 7.2

Kinetic parameters calculated from the temperature profiles of Si/Sb_2O_3 compositions using the Hill approach

Parameter	% Si	Order of reaction (n)			
		0.5	0.667	1	2
(i) E_a (kJ mol^{-1})	30	5.7 ± 1.4	8.5 ± 2.0	14.1 ± 3.2	31.0 ± 6.8
	35	13.2 ± 1.5	14.3 ± 1.3	16.6 ± 1.0	23.7 ± 0.1
	40	11.3 ± 2.3	12.3 ± 2.2	14.3 ± 1.7	20.7 ± 1.0
	45	9.7 ± 1.5	11.3 ± 1.6	14.5 ± 2.2	24.1 ± 4.4
	50	4.3 ± 1.3	6.0 ± 1.2	9.4 ± 1.1	19.5 ± 1.5
(ii) ln (A/ s^{-1})	30	11.0 ± 0.7	11.3 ± 0.7	12.4 ± 1.0	15.3 ± 1.5
	35	11.3 ± 0.3	11.6 ± 0.3	12.0 ± 0.2	23.7 ± 0.1
	40	10.7 ± 0.4	11.0 ± 0.3	11.5 ± 0.3	13.3 ± 0.2
	45	10.8 ± 0.9	11.2 ± 0.9	11.8 ± 0.2	13.7 ± 0.6
	50	10.0 ± 0.3	10.3 ± 0.3	11.0 ± 0.2	13.5 ± 0.3

The values of E_a from the Hill analysis (Table 7.2) depended on the composition of the mixture and also varied with the value chosen for the reaction order, n. Plots of $h(\alpha)$ against 1/T were not very sensitive to n and satisfactory linearity was generally obtained only when $n \leq 1$. The activation energies for $n > 0.67$ varied only slightly with composition. When n was ≤ 0.67, the activation energies had a more marked dependence on the mass ratio of silicon in the mixture.

Activation energies derived from the Leeds approach (5,6) (Table 7.3) also depended on the composition of the mixture. The calculated reaction orders were all greater than 0.5 (except for 30% Si/Sb_2O_3) and less than 1.

TABLE 7.3

Kinetic parameters calculated from temperature profiles of Si/Sb_2O_3 compositions using the Leeds approach

% Si	n	a x 10^4	b	E_a (kJ mol^{-1})	ln (A/s^{-1})
Linear regression					
30	0.36 ± 0.04	10.55 ± 0.25	902 ± 30	7.50 ± 0.26	3.29 ± 0.29
35	0.55 ± 0.07	12.13 ± 0.34	2173 ± 306	18.07 ± 2.55	4.91 ± 0.36
40	0.63 ± 0.07	11.51 ± 0.91	1597 ± 575	13.28 ± 4.73	4.39 ± 0.89
45	0.58 ± 0.06	11.37 ± 0.37	1554 ± 502	12.92 ± 4.18	4.20 ± 0.36
50	0.54 ± 0.14	10.71 ± 0.85	1134 ± 237	9.43 ± 4.47	3.69 ± 0.85
Non-linear regression					
30	0.32 ± 0.09	10.23 ± 0.10	564 ± 137	4.69 ± 1.14	2.97 ± 0.14
35	0.61 ± 0.11	12.76 ± 0.85	2774 ± 432	23.07 ± 3.02	5.55 ± 0.86
40	0.87 ± 0.02	12.60 ± 0.80	2920 ± 687	17.79 ± 2.98	5.49 ± 0.78
45	0.62 ± 0.14	11.91 ± 0.50	2290 ± 630	15.43 ± 3.06	4.74 ± 0.50
50	0.55 ± 0.24	10.54 ± 0.79	2458 ± 247	7.44 ± 3.77	3.51 ± 0.80

A plot of E_a from both the Hill and Leeds approach against % Si, is shown in Figure 7.5. Only the Hill-E_a values for n = 0.5 to 1 and Leeds-E_a values derived from the non-linear regression analysis of the temperature profiles are shown. The Leeds-E_a values were slightly larger than those derived from the Hill approach (for $n \leq 1$), but the overall trends were similar. There was good agreement between the values of n, which gave satisfactory linear plots of $h(\alpha)$ versus 1/T in the Hill approach, and those calculated from the Leeds approach. Considerable differences between the values of ln A derived from the Hill and the Leeds analysis were noted.

For powdered systems, the most feasible kinetic model is the contracting volume model in which n = 0.67 (7). The Hill E_a for the Si/Sb_2O_3 system at n = 0.67 ranged from 6 to 14 kJ mol^{-1}. From applying the Leeds analysis, the activation energies measured ranged from 7.5 to 18 kJ mol^{-1}.

Figure 7.5 Activation energies from the Hill and Leeds analysis of the Si/Sb_2O_3 system

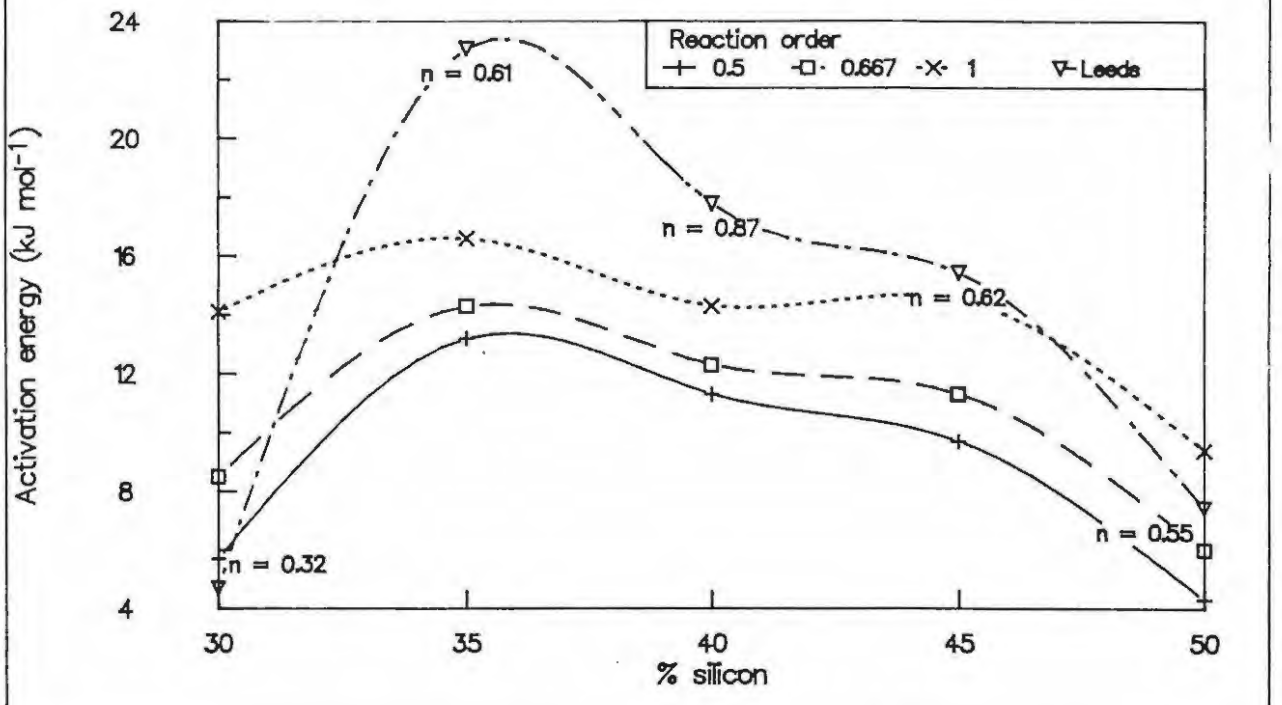

Figure 7.6 Temperature profiles of 40% Si/Sb_2O_3 mixtures at various densities

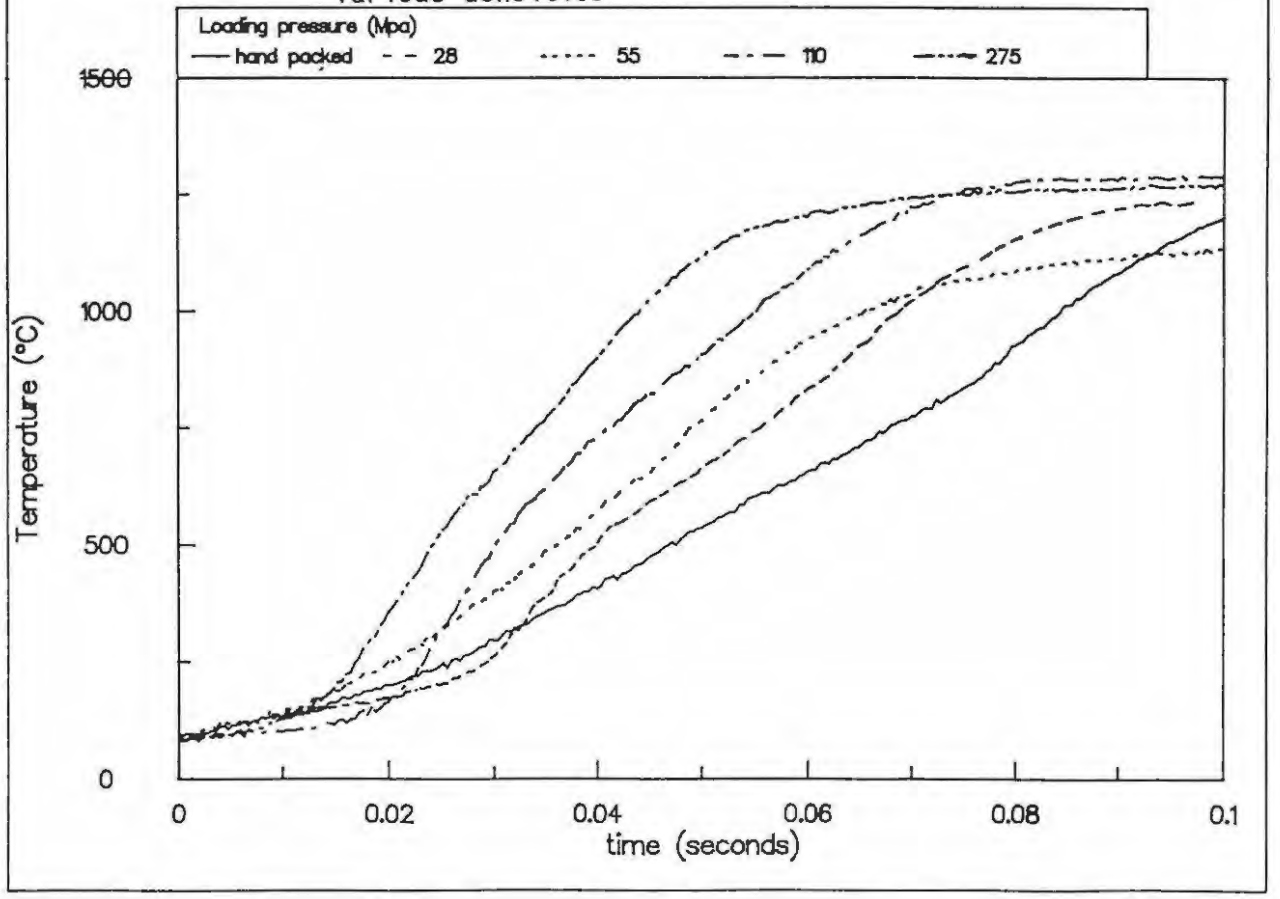

7.1.2 *Thermochemical aspects*

The maximum reaction temperatures (T_{max}), the maximum excess temperatures (U_{max}) and the maximum adiabatic temperature rises (U_{ad}) for various Si/Sb_2O_3 compositions are listed in Table 7.4.

Enthalpies of combustion for the various compositions, measured using bomb calorimetry, (ΔH_{exp}), are listed in Table 7.5, together with ΔH_{calc}, the change in enthalpy for reaction (7.1) calculated from standard enthalpies of formation (298 K). The heat outputs, q, for the various Si/Sb_2O_3 mixtures were calculated from values of U_{ad} from the temperature profiles and the heat capacities of the reactants at $T_{ad} = U_{ad} + 298 \sim 1600$ K ($c(Si) = 0.961$ J K^{-1} g^{-1} and $c(Sb_2O_3) = 0.667$ J K^{-1} g^{-1}).

TABLE 7.4

Summary of temperatures from temperature profiles of the Si/Sb_2O_3 system

% Si	T_{max} (C°)	U_{max} (C°)	U_{ad} (C°)
30	1301 ± 14	1274	1434 ± 34
35	1282 ± 12	1256	1356 ± 26
40	1179 ± 12	1177	1231 ± 23
45	1177 ± 35	1152	1209 ± 13
50	1057 ± 38	1032	1127 ± 8

Maximum ΔH_{exp} occurred at 20% silicon compared to the value of ~13% calculated from reaction (7.1). The composition at which ΔH is a maximum is usually taken as the stoichiometric composition (2). The results obtained using bomb calorimetry compare favourably with the calculated values (ΔH_{calc}) for the silicon-rich compositions (40 to 50% Si). The values of q were lower than those measured using bomb calorimetry, although the trends were similar. The lower values may arise from the occurrence of one or more of the sublimation of Sb_2O_3, melting of Sb_2O_3 and/or melting of Sb.

TABLE 7.5

Thermodynamic data for Si/Sb_2O_3 compositions

% Si	Heat capacity (J K^{-1} g^{-1}) (298 K)	Heat capacity (J K^{-1} g^{-1}) (1600 K)	q (kJ (g mixture)$^{-1}$) (1600 K)	$-\Delta H_{exp}$ (kJ (g mixture)$^{-1}$)	$-\Delta H_{calc}$ (kJ (g mixture)$^{-1}$)
20	0.420	0.726	-	1.48 ± 0.02	1.83
25	0.438	0.741	-	-	1.72
30	0.465	0.755	1.08 ± 0.03	1.38 ± 0.02	1.60
35	0.475	0.770	1.04 ± 0.02	-	1.49
40	0.493	0.785	0.97 ± 0.02	1.32 ± 0.01	1.37
45	0.511	0.799	0.97 ± 0.02	-	1.26
50	0.530	0.814	0.92 ± 0.02	1.14 ± 0.05	1.14

7.1.3 *Burning rates from temperature profiles*

The various time parameters, t_r and t_d, determined from the temperature profiles for various Si/Sb_2O_3 mixtures, are listed in Table 7.6. Also shown are values of the thermal diffusivity (D) of the mixtures (see Section 12). Calculated burning rates, v_{calc} (without correction for the thermocouple wire-diameter), are listed together with the experimentally obtained burning rates (v_{exp}) in Table 7.6.

TABLE 7.6

Time parameters for Si/Sb_2O_3 mixtures

% Si	t_r (x 10^{-3} s)	t_d (seconds)	Thermal diffusivity (mm^2 s^{-1})	Burning rates (mm s^{-1})	
				v_{exp}	v_{calc}
30	22.3 ± 4.1	1.59 ± 0.21	0.128 ± 0.023	6.30 ± 0.29	2.40 ± 0.44
35	23.3 ± 2.5	1.22 ± 0.22	-	8.71 ± 0.42	-
40	23.9 ± 1.3	1.34 ± 0.49	0.140 ± 0.080	8.52 ± 0.33	2.42 ± 0.13
45	30.0 ± 3.5	1.79 ± 0.59	-	8.73 ± 0.40	-
50	29.0 ± 4.2	3.31 ± 1.10	0.151 ± 0.070	7.25 ± 0.11	2.28 ± 0.33

The agreement between v_{calc} and v_{exp} is poor. Boddington *et al* (5,6) found a similar difference between experimental and calculated burning rates for the $W/K_2Cr_2O_7$ system. They suggested that this difference is due to the effect of using a thermocouple of a finite diameter to capture temperature profiles, and suggested a method for correcting the profiles for the effect of the thermocouple diameter (see Section 7.1.4).

7.1.4 *Effect of thermocouple diameter*

Thermocouples of various diameters were used to measure temperature profiles of the 40% Si/Sb_2O_3 composition. The various parameters obtained from the analysis of these temperature profiles are shown in Tables 7.7 to 7.10. The temperature profiles showed an increase in the rise-time to T_{max} with increasing thermocouple diameter, but the maximum temperature measured ($\sim$1245°C) was not affected.

Boddington *et al* (5,6,8) have shown that, for more accurate kinetic parameters, corrections have to be made for the finite size and hence delayed response of the thermocouple. The Hill kinetic parameters for temperature profiles captured with thermocouples of various diameters are listed in Table 7.8.

TABLE 7.7

Temperature and time parameters from temperature profiles of a 40% Si/Sb_2O_3 composition using thermocouples of various diameters

tc diameter (mm)	Temperature data (°C)			Time parameters (seconds)	
	T_{max}	U_{max}	U_{ad}	$t_r \times 10^{-3}$	t_d
0.05	1183 ± 22	1159	1262 ± 32	5.2 ± 0.4	4.7 ± 6.2
0.10	1204 ± 15	1179	1266 ± 17	13.4 ± 0.1	5.5 ± 1.6
0.20	1212 ± 12	1188	1272 ± 30	24.8 ± 1.5	3.2 ± 2.5
0.30	1182 ± 7	1157	1274 ± 11	33.1 ± 3.8	5.1 ± 1.6

TABLE 7.8

Kinetic parameters (Hill approach) calculated from the temperature profiles of a 40% Si/Sb_2O_3 composition using thermocouples of various diameters

TC diameter (mm)	Activation energy (kJ mol^{-1})			
	n = 0.50	n = 0.67	n = 1	n = 2
0.05	7.1 ± 1.2	8.6 ± 2.6	11.6 ± 1.8	20.7 ± 2.1
0.10	10.3 ± 1.4	11.4 ± 3.1	13.6 ± 4.0	20.3 ± 6.2
0.20	12.7 ± 0.6	13.8 ± 0.7	15.9 ± 1.0	22.4 ± 1.5
0.30	10.3 ± 1.0	11.0 ± 1.2	13.4 ± 1.3	18.2 ± 1.9

Within the error limits, the activation energy was not dependent on the diameter of the wire.

The calculated burning velocity obtained from the rise times (t_r) of the profiles, may be corrected by extrapolation of a linear plot of t_r against the square of the thermocouple diameter, d, to obtain the rise time at zero thermocouple diameter (5). For the 40% Si/Sb_2O_3 system the relationship was $(t_r/ms)_d$ = (295 ± 68)(d/mm) + (8.63 ± 4.70) (correlation coefficient r = 0.90).

7.2 Effect of compaction

Samples of 40% Si/Sb_2O_3 were pressed for 1 minute under various loading pressures and then burnt. The burning rates are listed in Table 7.9. The corresponding temperature profiles showed a decrease in the rise-time to T_{max} with an increase in the density of the mixture (Figure 7.6). T_{max} decreased, initially, with increasing density but then increased with further increase in compaction of the sample (see Table 7.9). Both v_{exp} and m_{exp} (Figure 7.7) showed similar behaviour.

An increase in mass burning rate with increasing sample density is usually taken as supporting the proposal that the reaction between fuel and oxidant is a solid-solid reaction (2). Combustion of the Si/Sb_2O_3 system almost certainly occurs between molten Sb_2O_3 (m.pt. 650°C) or Sb_2O_3 vapour (see section 6.3.1)) and solid silicon.

Figure 7.7 Burning rate of 40% Si/Sb_2O_3 mixtures at various densities (<53 μm Si, pressed 1 min)

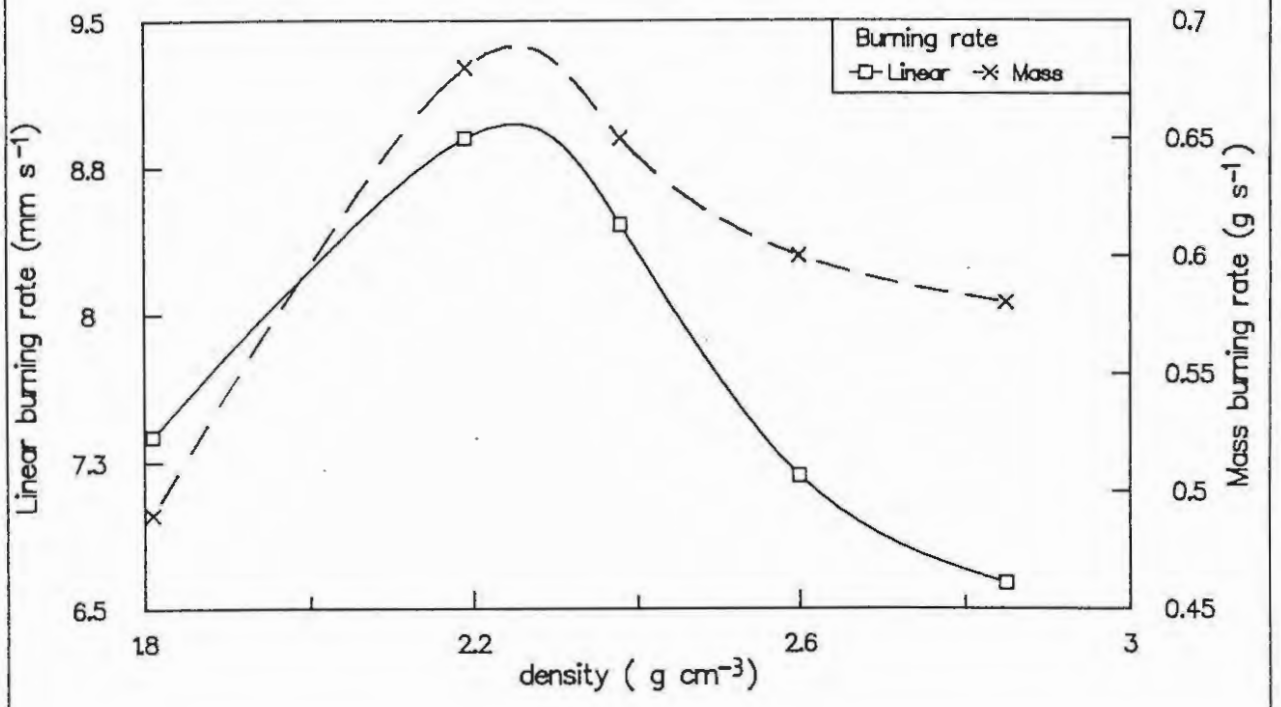

Figure 7.8 Effect of SSA of Si on the temperature profiles of 40% Si/Sb_2O_3 mixtures (pressed for 1 min at 55 MPa)

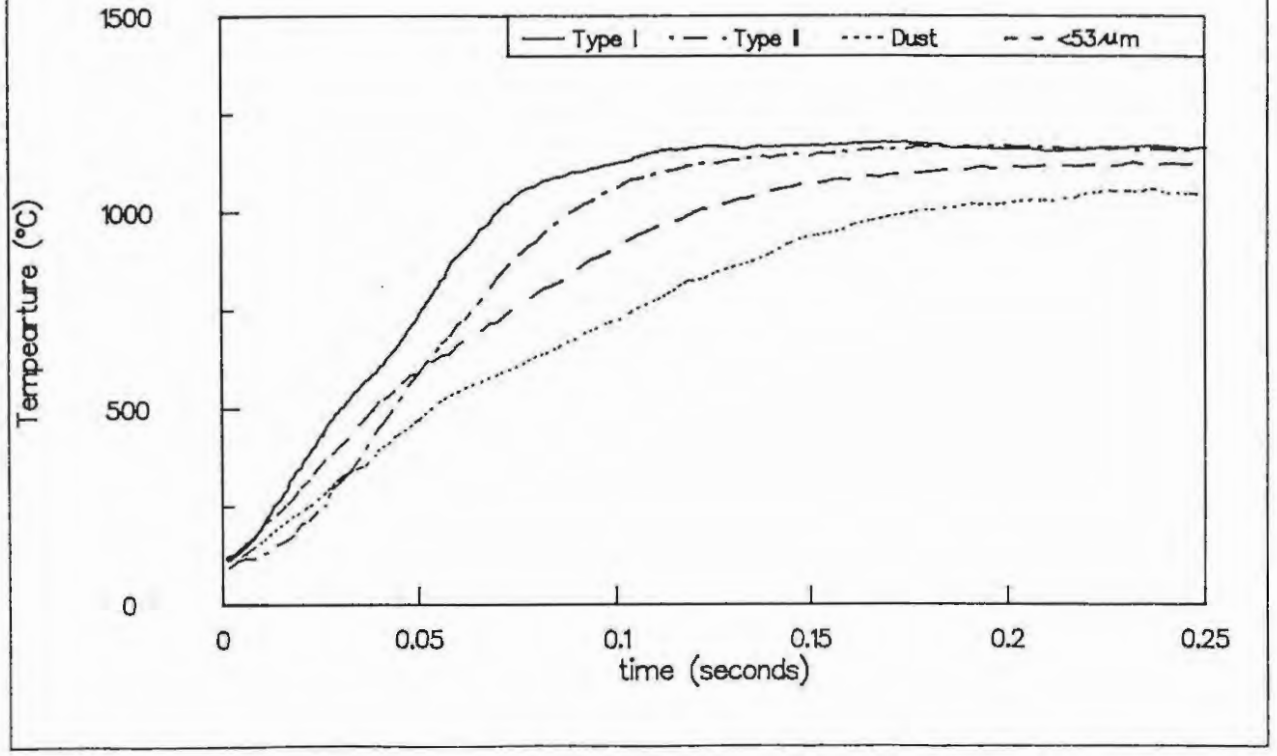

TABLE 7.9

Burning rates of samples of 40% Si/Sb_2O_3 pressed to various densities (<53 μm Si)

Loading pressure (MPa)	Density (g cm^{-3})	Porosity factor ε	v_{exp} (mm s^{-1})	m_{exp} (g s^{-1})	T_{max} (°C)
HP*	1.81 ± 0.07	0.57	7.38 ± 0.21	0.49 ± 0.01	1402 ± 13
28	2.19 ± 0.04	0.48	8.90 ± 0.49	0.68 ± 0.01	1259 ± 9
55	2.38 ± 0.05	0.47	8.46 ± 0.13	0.65 ± 0.01	1257 ± 11
110	2.60 ± 0.04	0.38	7.18 ± 0.19	0.60 ± 0.02	1313 ± 5
275	2.85 ± 0.09	0.32	6.63 ± 0.22	0.58 ± 0.01	1301 ± 8

* Manually pressed only

The density of the composition has a marked effect on the time parameters of the temperature profile (see Table 7.10) and both t_r and t_d decreased with increasing compaction.

Within the error limits, the activation energies (calculated by either the Hill approach (Table 7.11) or the Leeds approach (Table 7.12)) were not very sensitive to the density of the mixture.

TABLE 7.10

Time parameters derived from temperature profiles of a 40% Si/Sb_2O_3 composition at various densities

Loading pressure (MPa)	Density (g cm^{-3})	Time parameters (seconds)	
		$t_r \times 10^{-3}$	t_d
0	1.81 ± 0.07	17.7 ± 0.2	2.47 ± 1.3
23	2.19 ± 0.04	10.7 ± 0.3	2.59 ± 0.2
55	2.25 ± 0.05	13.4 ± 1.9	2.25 ± 2.3
110	2.60 ± 0.04	10.6 ± 2.5	1.84 ± 0.8
275	2.85 ± 0.09	9.9 ± 0.1	1.00 ± 0.9

TABLE 7.11

Kinetic parameters (Hill approach) calculated from the temperature profiles of a 40% Si/Sb_2O_3 composition at various densities

Density ($g\ cm^{-3}$)	Activation energy ($kJ\ mol^{-1}$)			
	0.50	0.67	1	2
1.81 ± 0.07	12.4 ± 2.9	13.8 ± 2.6	16.5 ± 2.0	24.8 ± 0.2
2.19 ± 0.04	9.6 ± 0.3	11.3 ± 0.6	14.6 ± 0.3	24.7 ± 1.5
2.25 ± 0.05	11.0 ± 2.4	12.5 ± 2.1	15.5 ± 1.7	24.6 ± 1.0
2.60 ± 0.04	11.8 ± 0.7	13.1 ± 0.2	15.6 ± 0.8	23.2 ± 2.5
2.85 ± 0.09	13.5 ± 2.0	15.0 ± 2.1	19.0 ± 2.3	27.0 ± 2.9

TABLE 7.12

Kinetic parameters (Leeds approach) calculated from temperature profiles of Si/Sb_2O_3 compositions at various densities

Density ($g\ cm^{-3}$)	n	a x 10^4	b	E_a ($kJ\ mol^{-1}$)	ln (A/s^{-1})
Linear regression					
1.81 ± 0.07	0.52 ± 0.14	7.63 ± 2.17	1314 ± 171	10.9 ± 1.4	3.9 ± 0.3
2.19 ± 0.04	0.21 ± 0.11	7.68 ± 2.03	729 ± 81	6.1 ± 0.9	4.0 ± 0.3
2.25 ± 0.05	0.63 ± 0.27	14.59 ± 10.1	1598 ± 575	13.3 ± 4.8	4.4 ± 0.9
2.60 ± 0.04	0.47 ± 0.10	15.86 ± 6.46	1630 ± 250	13.6 ± 5.8	4.8 ± 0.9
2.85 ± 0.09	0.46 ± 0.08	34.27 ± 11.1	1734 ± 63	14.4 ± 0.5	5.6 ± 0.3
Non-linear regression					
1.81 ± 0.07	0.61 ± 0.21	15.04 ± 10.9	1512 ± 721	12.6 ± 6.0	4.3 ± 0.9
2.19 ± 0.04	0.24 ± 0.09	7.26 ± 3.01	726 ± 93	6.0 ± 1.3	4.1 ± 0.3
2.25 ± 0.05	0.87 ± 0.02	13.43 ± 2.66	2290 ± 630	19.0 ± 5.2	5.5 ± 0.8
2.60 ± 0.04	0.73 ± 0.16	18.58 ± 13.6	2196 ± 877	18.3 ± 7.3	5.5 ± 1.0
2.85 ± 0.09	0.58 ± 0.20	35.87 ± 15.3	1690 ± 78	14.0 ± 1.7	5.6 ± 0.4

7.3 Effect of particle-size

40% Si/Sb_2O_3 compositions were prepared in which silicon samples of various particle-sizes were used (see Table 7.13). The burning rates measured are also listed in Table 7.13 and the corresponding temperature profiles are shown in Figure 7.8.

TABLE 7.13

Burning rates of 40% Si/Sb_2O_3 compositions with silicon of various specific surface areas (pressed 1 min at 55 MPa)

Silicon	Specific surface area ($m^2\ cm^{-3}$)	Density ($g\ cm^{-3}$)	v_{exp} ($mm\ s^{-1}$)	m_{exp} ($g\ s^{-1}$)
Type I	1.03	2.10 ± 0.10	7.73 ± 0.21	0.54 ± 0.06
<53 μm	2.04	2.35 ± 0.09	8.52 ± 0.13	0.63 ± 0.02
Dust	2.81	2.42 ± 0.12	8.93 ± 0.25	0.67 ± 0.06
Type II	5.40	2.41 ± 0.09	9.15 ± 0.17	0.69 ± 0.02

There is a slight increase in the burning rate with an increase in the specific surface area of the fuel. Trends for the temperature profiles were not very clear since the differences lie within the limits of variation of the profiles for individual mixtures.

7.4 Effect of additives

The burning of pyrotechnic compositions may be modified by the deliberate addition of diluents which may either be chemically active or inert. Various proportions of two inert diluents, SiO_2 and Al_2O_3, were added separately to a 40% Si/Sb_2O_3 mixture and burnt and the corresponding temperature profiles are shown in Figure 7.9 and 7.10. Plots of the linear burning rates containing various proportions of either SiO_2 or Al_2O_3 (Table 7.14) are shown in Figure 7.11. Mixtures of 40% Si/Sb_2O_3 with 7% SiO_2 or 9% Al_2O_3 ignited, but burning was not sustained. Both v_{exp} and T_{max} decrease with increasing proportions of diluent added and this decrease is greatest for SiO_2.

Similar proportions of water as a diluent were also added to a 40% Si/Sb_2O_3 mixture. Burning was accompanied by the release of water vapour from the samples ahead of the burning front. The slope of the rise regions of the temperature profile were generally unaffected by the moisture content (Figure 7.12a and 7.12b). Maximum temperatures in the presence of water were approximately constant within the

range of uncertainty for the 40% Si/Sb_2O_3 composition. There is also an increase in the induction time of the temperature profile with increasing water content of the sample. Burning rates decreased sharply with increasing water content (Figure 7.11). The effect was greater than that of the other additives and is only exceeded by the slowing effect of decreasing the Si content (Table 7.1). Burning failed at 3% water compared to the 5 and 7% for SiO_2 and Al_2O_3 respectively.

TABLE 7.14

Burning rates of the 40% Si/Sb_2O_3 composition with various proportions of diluents (<53 μm Si, 1 min at 55 MPa)

% additive	Density ($g\ cm^{-3}$)	v_{exp} ($mm\ s^{-1}$)	m_{exp} ($g\ s^{-1}$)	T_{max} (°C)
SiO_2				
0	2.26 ± 0.04	7.99 ± 0.27	0.62 ± 0.02	1257 ± 11
2	2.32 ± 0.01	7.52 ± 0.21	0.54 ± 0.03	1234 ± 31
3	2.24 ± 0.03	6.03 ± 0.24	0.42 ± 0.02	1233 ± 21
5	2.17 ± 0.03	4.44 ± 0.17	0.32 ± 0.02	1190 ± 21
Al_2O_3				
0	2.26 ± 0.04	7.99 ± 0.27	0.62 ± 0.02	1257 ± 11
2	2.29 ± 0.02	7.77 ± 0.11	0.54 ± 0.03	1243 ± 4
3	2.28 ± 0.01	8.01 ± 0.21	0.56 ± 0.02	1254 ± 3
5	2.26 ± 0.03	6.36 ± 0.18	0.44 ± 0.02	1229 ± 31
7	2.25 ± 0.03	5.76 ± 0.16	0.40 ± 0.01	1216 ± 17
H_2O				
0	2.32 ± 0.11	8.52 ± 0.11	0.65 ± 0.01	1248 ± 11
1	2.65 ± 0.06	6.68 ± 0.09	0.60 ± 0.05	1266 ± 22
2	2.92 ± 0.18	5.93 ± 0.12	0.48 ± 0.02	1272 ± 19
3	2.41 ± 0.07	2.59 ± 0.14	0.23 ± 0.01	1260 ± 12

Previous workers showed that oxidation of silicon is enhanced in the presence of moisture and oxygen compared to that of oxygen alone (see Section 2.2). This effect could not be confirmed when moist pyrotechnic mixtures of Si and Sb_2O_3 were combusted.

Figure 7.9 Temperature profiles of 40% Si/Sb_2O_3 mixtures with various proportions of SiO_2

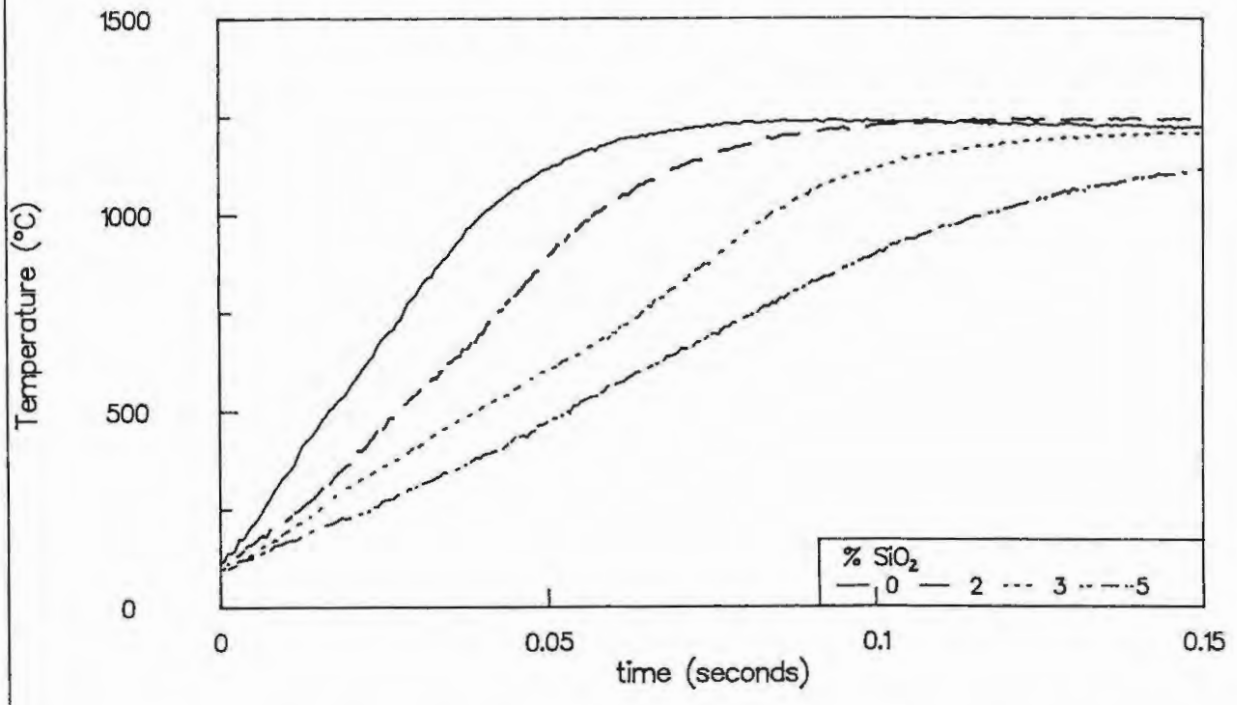

Figure 7.10 Temperature profiles of 40% Si/Sb_2O_3 mixtures with various proportions of Al_2O_3

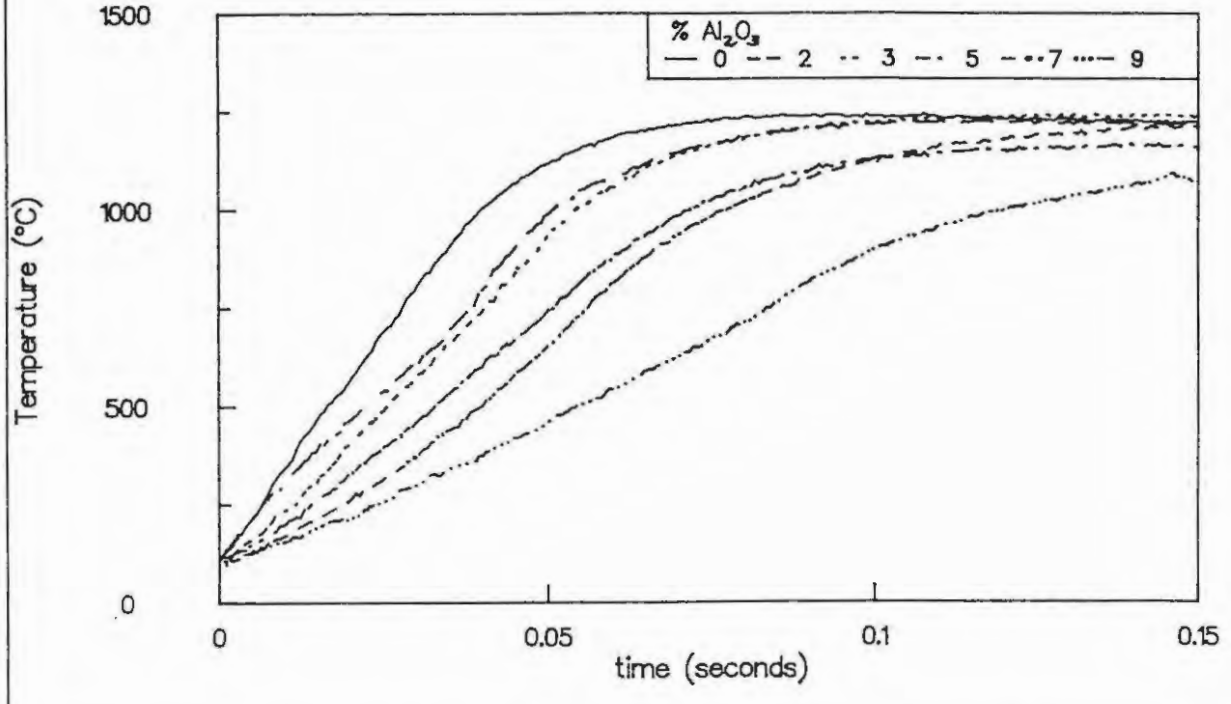

Figure 7.11 Linear burning rates of 40% Si/Sb_2O_3 mixtures with various diluents (<53 μm Si, pressed 1 min at 55 MPa)

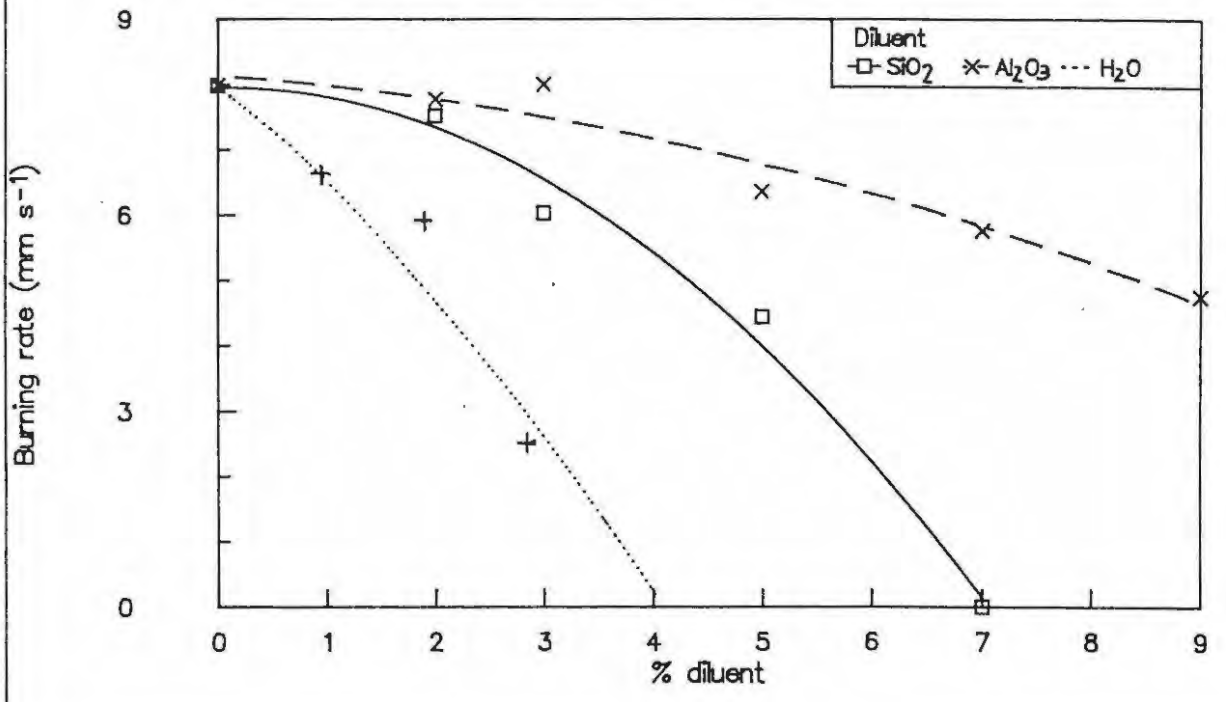

Figure 7.12a Temperature profiles of 40% Si/Sb_2O_3 mixtures with 0 to 2% moisture

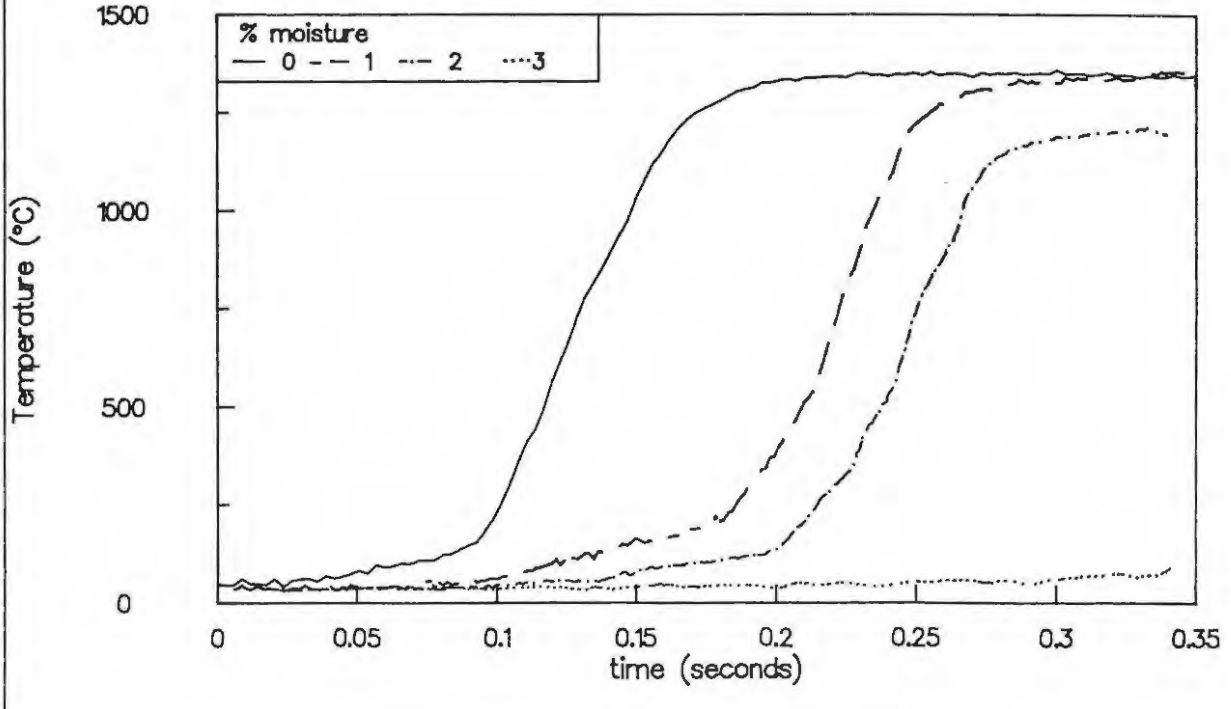

Figure 7.12b Temperature profiles of a 40% Si/Sb_2O_3 mixture with 3% moisture

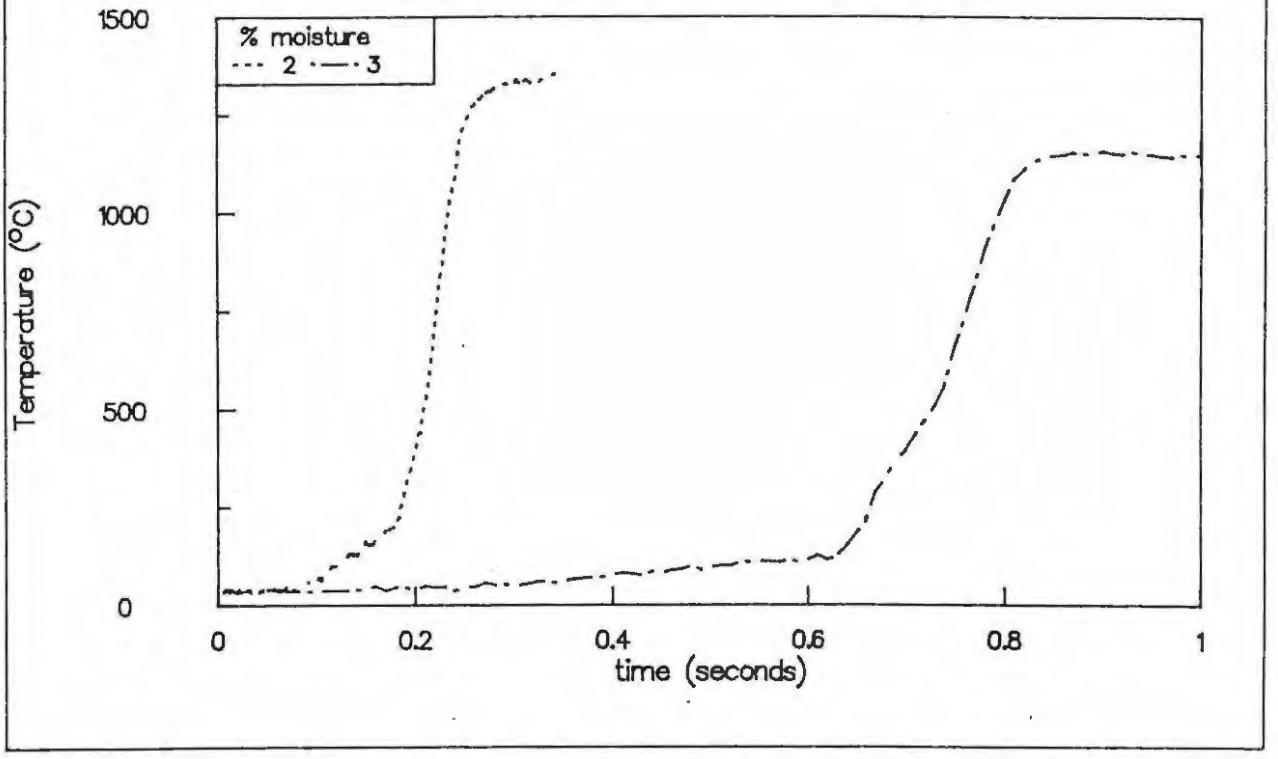

7.5 Comments

Further discussion of these results in relation to the other binary systems is given in section 13.

7.6 References

1. R.A. Nyquist and R.O. Kagel, "*Infrared Spectra of Inorganic Compounds*, Academic Press, New York, 1971.
2. J.H. McLain, "*Pyrotechnics: From the Viewpoint of Solid State Chemistry*", The Franklin Institute Press, Philadelphia, Pennsylvania, 1980.
3. R.A.W. Hill, L.E. Sutton, R.B. Temple, A. White and T.L. Cottrell, Research, **3** (1950) 569.
4. R.A.W. Hill and T.L. Cottrell, 4th Symp. Combustion, (1953) 349.
5. T. Boddington, P.G. Laye, J.R.G. Pude and J. Tipping, Comb. Flame, **47** (1982) 235.
6. T. Boddington, P.G. Laye, J.R.G. Pude and J. Tipping, Comb. Flame, **63** (1986) 359.
7. M.E. Brown, D. Dollimore and A.K. Galwey, "*Reactions in the Solid State*", Comprehensive Chemical Kinetics, Vol. 22, Elsevier, 1980.
8. T. Boddington, A. Cottrell and P.G. Laye, Comb. Flame, **76** (1989) 63.

8. COMBUSTION OF THE Si/Fe_2O_3 SYSTEM

8.1 Effect of composition

Binary Si/Fe_2O_3 mixtures with from 20 to 40% silicon sustained combustion and failure occurred below and above these limits. Temperature profiles for the various compositions are shown in Figure 8.1. The profiles are complex showing at least three fairly distinct stages:

(i) a relatively slow rise in temperature after triggering ($T_{(i)}$). This not very reproducible, possibly because of the triggering level,

(ii) a first sigmoid segment which overlaps (at $T_{(ii)-(iii)}$)

(iii) a second (presumably) sigmoid segment which leads to a maximum temperature, T_{max}, values of which are given in Table 8.1.

TABLE 8.1

Features of the temperature profiles recorded during the burning of various Si/Fe_2O_3 mixtures

% Si	T_{max} (°C)	U (C°)	U_{ad} (°C)	$T_{(ii)-(iii)}$ (°C)
20	1225 ± 10	1202	1352 ± 67	~ 900
25	1221 ± 38	1200	1385 ± 77	~ 650
30	1253 ± 16	1230	1375 ± 115	~ 700
35	1166 ± 24	1140	1375 ± 28	~ 800
40	1150 ± 10	1127	1358 ± 31	~ 600

Replicate temperature profiles for a composition containing 35% silicon are shown in Figure 8.2. The profiles are not very reproducible and are complex. The rise-to-T_{max} occurs over 150 to 300 ms and maximum temperatures varied from 1100 to 1250°C. A plot of the derivative of a smoothed temperature profile of a 35% Si/Fe_2O_3 mixture (Figure 8.3) showed at least two well-defined peaks and it thus appears that the burning of Si/Fe_2O_3 compositions is at least a two-stage process. The poor reproducibility of the profiles for individual compositions makes it difficult to detect trends caused by varying the silicon content. Beyond T_{max} there is some indication of further exothermic processes which are probably caused by solidification of molten products during cooling. The maximum reaction temperatures are well below the melting points of the fuel, Si (1410°C) and the oxidant, Fe_2O_3 (1565°C).

Figure 8.1 Temperature profiles for the Si/Fe_2O_3 system

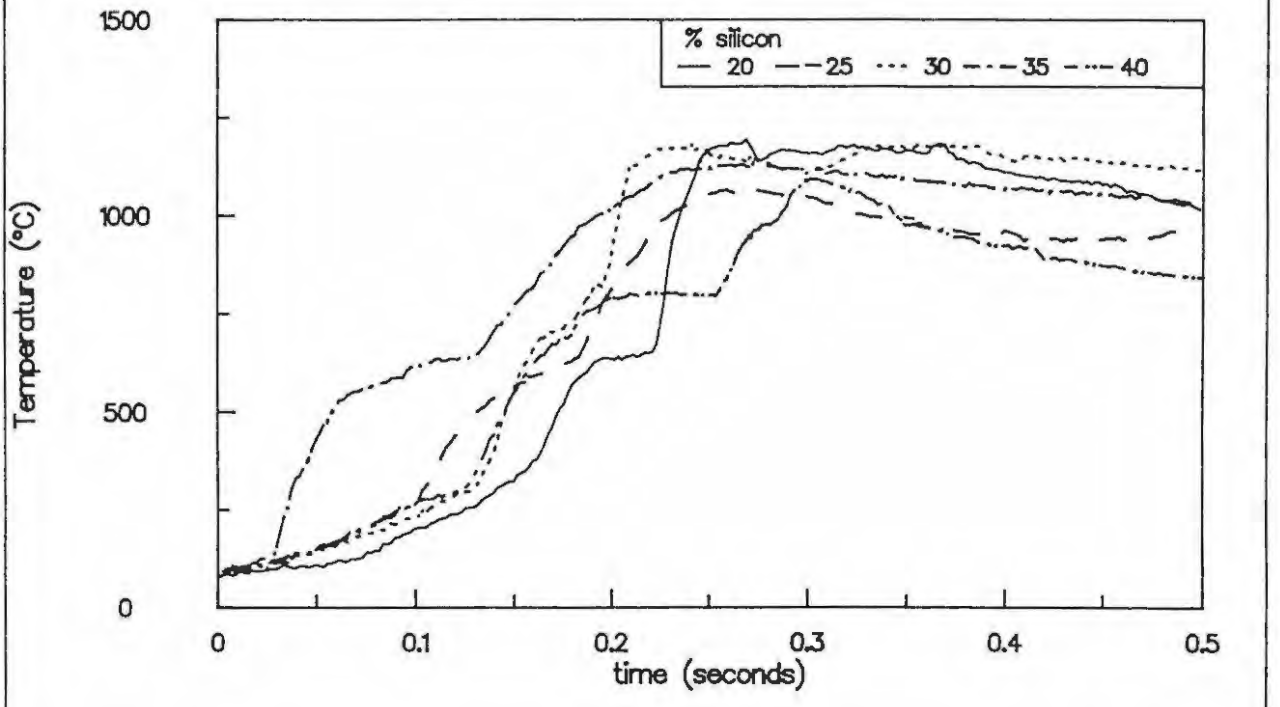

Figure 8.2 Temperature profiles of 35% Si/Fe_2O_3 mixtures showing reproducibility

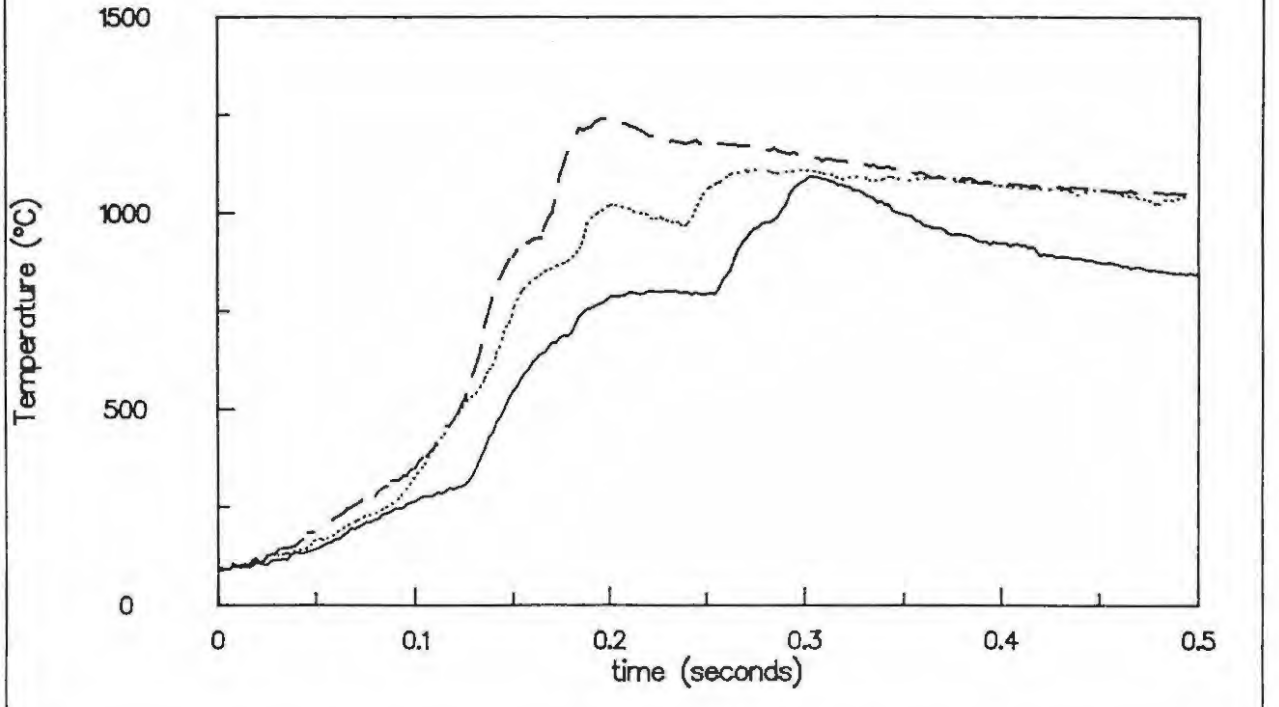

Figure 8.3 Temperature profile of a 35% Si/Fe_2O_3 mixture showing first derivative

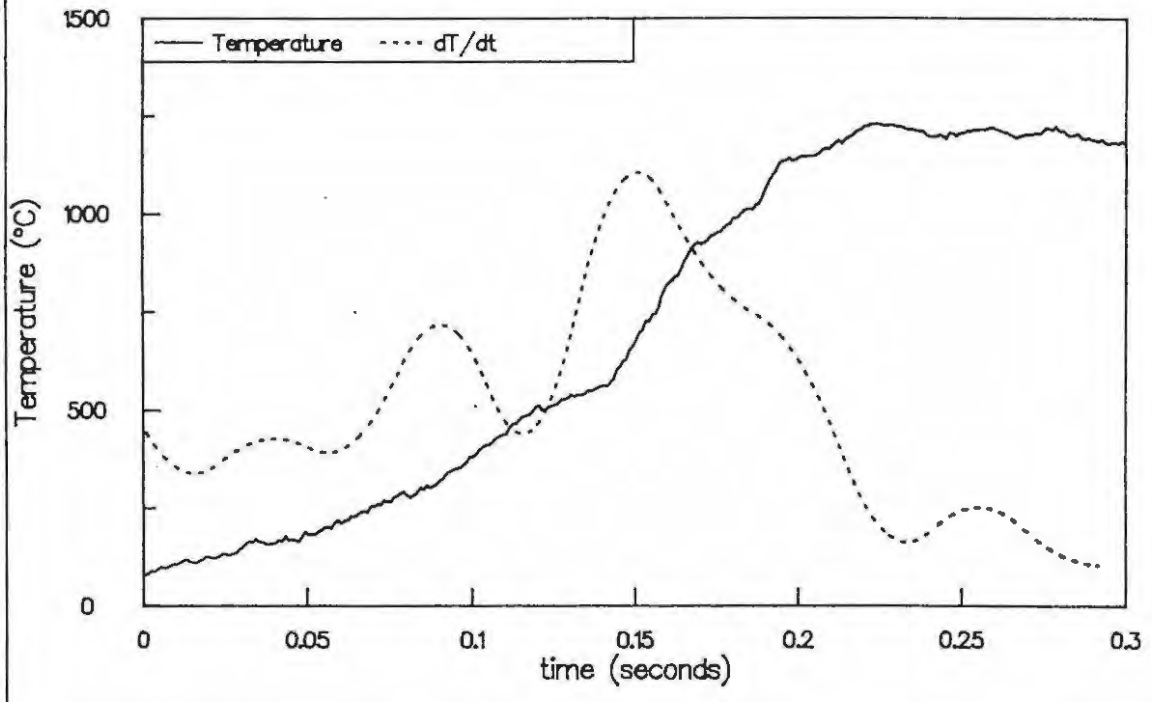

Figure 8.4 Burning rates for the Si/Fe_2O_3 system (<53 μm Si, pressed 1 min at 55 MPa)

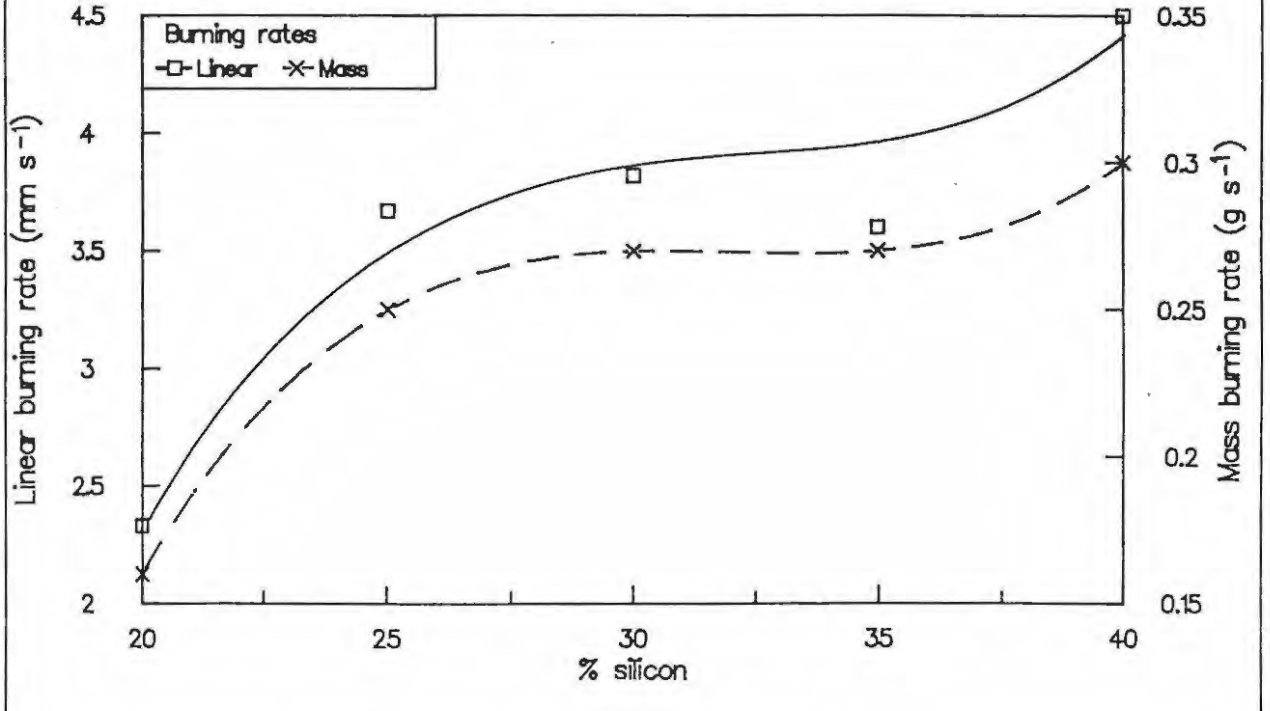

The region of approximately constant temperature is suggested (1) to indicate either the occurrence of two zones of chemical reaction or simultaneous chemical reaction and phase transition. Two-stage profiles have been reported by Hill (2,3) for combustion of Mo/$KMnO_4$ and Fe/$KMnO_4$ compositions. The explanation put forward was that in the first stage Mo or Fe diffused into the dislocation network of the $KMnO_4$ structure, followed by reaction on the surfaces of the mozaic bloeks to yield a complex product. The second stage was the penetration of the Mo or Fe species into the mozaic blocks themselves. The first stage corresponded to between 8 and 15% of the total heat evolved by the reaction. Such an explanation is unlikely to apply in the Si/Fe_2O_3 system.

Burning rates of various Si/Fe_2O_3 compositions are listed in Table 8.2.

TABLE 8.2

Burning rates for the Si/Fe_2O_3 system

(<53 μm Si, pressed for 1 min at 55 MPa)

% Si	Density (g cm^{-3})	Porosity factor ε	v_{exp} (mm s^{-1})	m_{exp} (g s^{-1})
20	2.14 ± 0.01	0.54	2.33 ± 0.17	0.16 ± 0.01
25	2.29 ± 0.02	0.49	3.67 ± 0.08	0.25 ± 0.01
30	2.36 ± 0.08	0.46	3.82 ± 0.12	0.27 ± 0.02
35	2.20 ± 0.02	0.48	3.60 ± 0.10	0.27 ± 0.03
40	2.10 ± 0.03	0.49	4.54 ± 0.21	0.30 ± 0.02

The linear (v_{exp}) and mass burning (m_{exp}) rates (Figure 8.4) increase most between 20 and 25% silicon and then remain approximately constant from 25 to 35% with a slight increase to a maximum at 40% silicon. It is unusual for the maximum burning rate to occur at a composition at one of the extremes of the range. Only a slight mass loss (~4%) was observed after burning, indicating no significant loss of gaseous oxygen from the system during combustion. The 35% Si/Fe_2O_3 mixture was chosen for further study.

The extreme redox reaction between Si and Fe_2O_3 is

$$3Si(s) + 2Fe_2O_3(s) \rightarrow 3SiO_2(s) + 2Fe(s) \qquad ...(8.1)$$

The stoichiometric composition corresponding to this reaction is 21% silicon, and the calculated change in enthalpy is -355 kJ (mol Si)$^{-1}$ or -2.64 kJ (g mixture)$^{-1}$. Another possible reaction is

$$Si(s) + 2Fe_2O_3(s) \rightarrow SiO_2(s) + 4FeO(s) \qquad ...(8.2)$$

(stoichiometric composition is 8.1% silicon and the calculated ΔH is -325 kJ (mol Si)$^{-1}$ or -0.94 kJ (g mixture)$^{-1}$).

Several other products are possible such as ferrosilicon or iron silicates. The infrared spectra of residues of Si/Fe_2O_3 combustion showed that SiO_2 is the predominant product. Only Fe and Fe_2SiO_4 were identified from the XRD patterns. The presence of both SiO_2 and Fe_2SiO_4 (fayalite) suggests that the two products are either formed independently in reaction (8.1) above and in

$$3Si(s) + 4Fe_2O_3(s) \rightarrow 3Fe_2SiO_4(s) + 2Fe(s) \quad ...(8.3)$$

(stoichiometric composition 11.7% Si, ΔH = -381.6 kJ (mol Si)$^{-1}$), or -0.94 kJ (g mixture)$^{-1}$), or in a single reaction

$$2Si(s) + 2Fe_2O_3(s) \rightarrow SiO_2(s) + Fe_2SiO_4(s) + 2Fe(s) \quad ...(8.4)$$

(stoichiometric composition 15.0% Si, ΔH = -353.5 kJ (mol Si)$^{-1}$) or -1.88 kJ (g mixture)$^{-1}$. Phase diagrams of the FeO-SiO_2-Fe_2O_3 system (4) show that fayalite crystallises out of FeO-SiO_2 systems only at low Fe_2O_3 contents, in the region of 1150°C. The various mixtures of Si and Fe_2O_3 have maximum reaction temperatures between 1100 and 1300°C (see Table 8.2) and these temperatures are well below the melting point of Fe and its various oxides (see Table 8.3).

TABLE 8.3

Physical properties of the oxides of iron and of SiO_2

Property	Fe	FeO	Fe_3O_4	Fe_2O_3	Fe_2SiO_4	SiO_2
% oxygen (by mass)	0	22	28	30	31	53
melting point (°C)	1537	1369	1594	1565	1503	1470
$-\Delta H_f$ (kJ mol^{-1})	0	272.5	1120.5	825.8	1482.7	905.2
Mol mass (g mol^{-1})	55.9	71.9	231.5	159.7	203.8	60.1

If it is assumed that FeO is one of the decomposition products of Fe_2O_3, then phase diagrams (4) show a eutectic point for the FeO-SiO_2 system at approximately 1170°C (at given binary composition). The melting points of both SiO_2 and FeO are sufficiently lowered for SiO_2 and FeO to form Fe_2SiO_4. The Fe_2SiO_4 need not thus be formed by direct reaction between Fe_2O_3 and Si.

Scanning electron micrographs of the combustion product of a 35% Si/Fe_2O_3 mixture showed the extensive formation of solidified melts (Plate 8.2 to 8.4). A micrograph of an unburnt mixture is shown in Plate 8.1. Some of the residues appeared to be unreacted particles (Plate 8.3 and 8.4). There was no indication of extensive channel formation expected when gaseous products are evolved during reaction confirming that reaction between Si and Fe_2O_3 occurs mainly in the condensed phase.

Plate 8 Scanning electron micrographs of the combustion residues of 35% Si/Fe_2O_3 mixtures

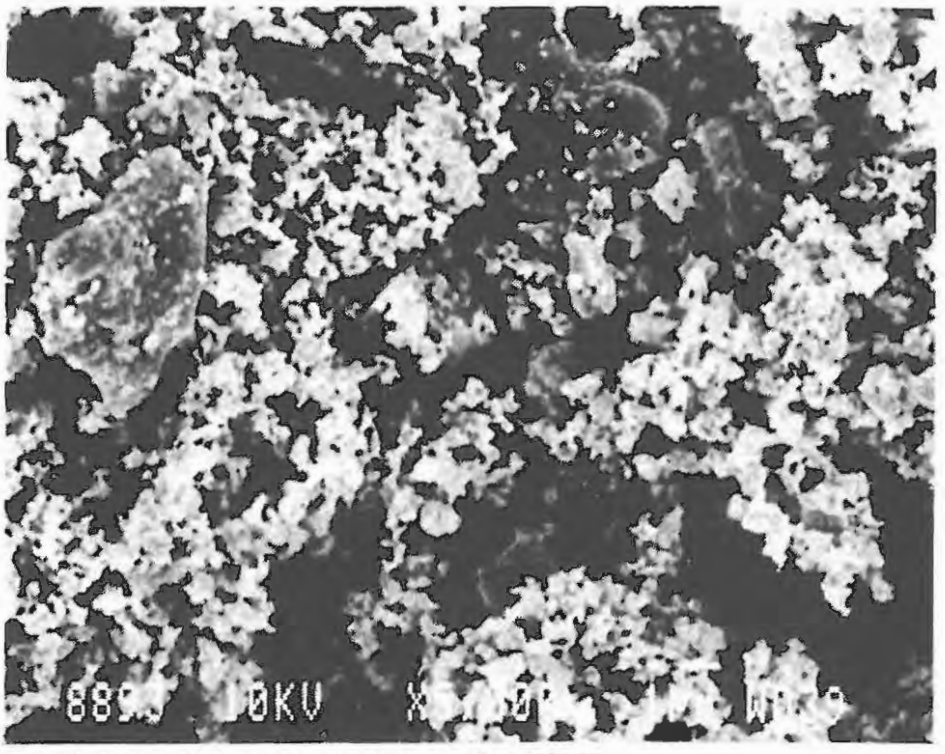

Plate 8.1 Unreacted material (magnified 5000 X)

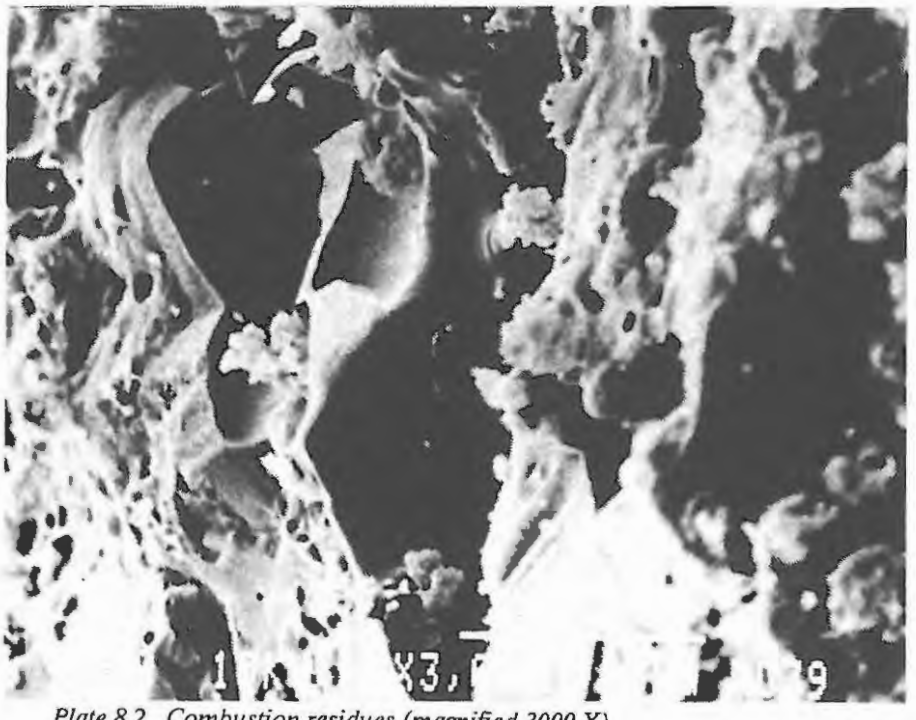

Plate 8.2 Combustion residues (magnified 3000 X) showing solidified melts

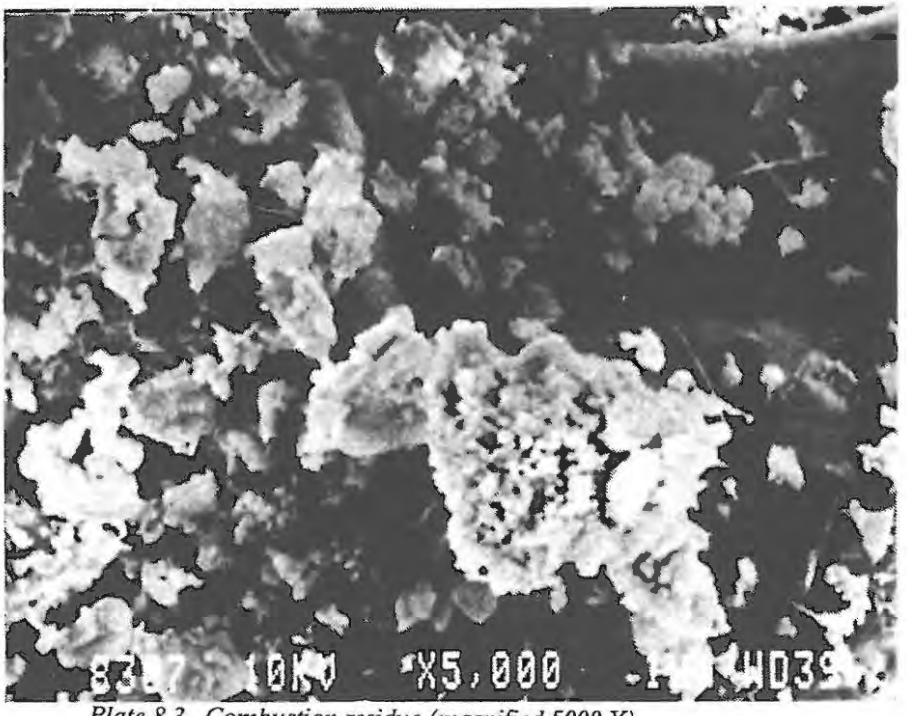

Plate 8.3 *Combustion residue (magnified 5000 X) showing solidified melts and unreacted particles*

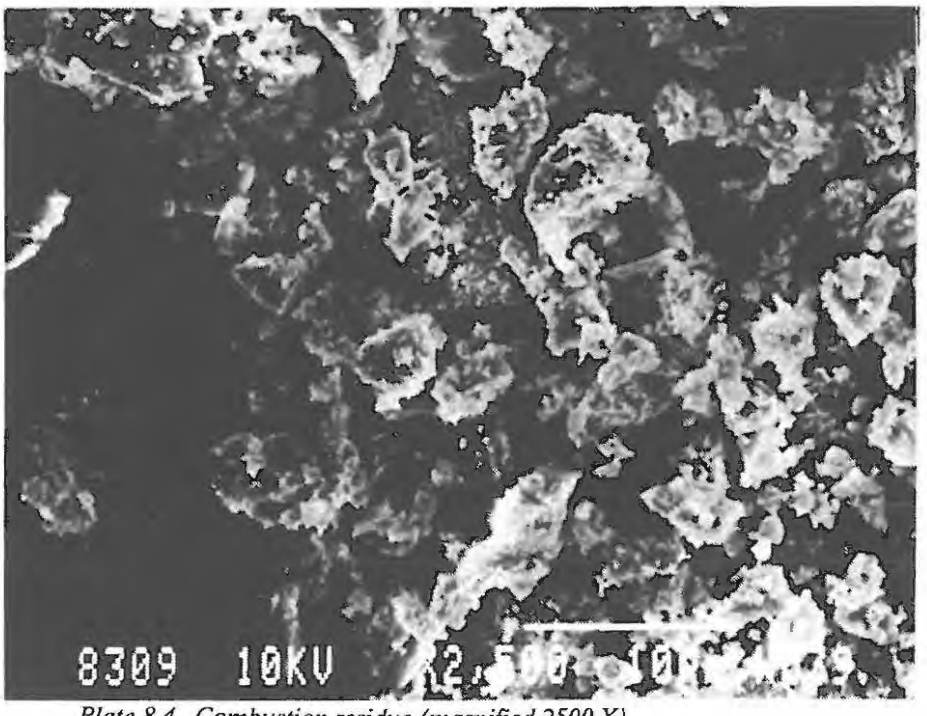

Plate 8.4 *Combustion residue (magnified 2500 X) showing unreacted particles*

8.1.1 *Thermochemical aspects*

The enthalpies of combustion were determined using bomb calorimetry (ΔH_{exp}) and the results are shown in Table 8.4.

The heat outputs, q, of the burning mixtures were also estimated from the heat capacities of the constituents, their respective proportions in the mixture and the adiabatic temperature rises, U_{ad}, (Table 8.6). An average T_{ad} (U_{ad} + 298) of 1600 K and the heat capacities of the solid reactants at 1600 K were used (0.961 J K^{-1} g^{-1} for Si and 1.376 J K^{-1} g^{-1} for Fe_2O_3 (4)).

TABLE 8.4

Thermochemical data for Si/Fe_2O_3 compositions

% Si	Heat capacity (J K g)$^{-1}$ 298 K	Heat capacity (J K g)$^{-1}$ 1600 K	U_{ad} (°C)	q (kJ (g mixture)$^{-1}$) 1600 K	$-\Delta H_{exp}$ (kJ (g mixture)$^{-1}$)	$-\Delta H_{calc}$ (kJ (g mixture)$^{-1}$) reaction: (8.1) (8.4)
20	0.664	1.293	1352 ± 67	1.75 ± 0.08	1.91 ± 0.06	2.53 (1.84)
25	0.667	1.272	1385 ± 77	1.76 ± 0.10	-	2.50 (1.73)
30	0.671	1.252	1375 ± 115	1.72 ± 0.04	1.88 ± 0.02	2.33 (1.61)
35	0.674	1.231	1375 ± 28	1.69 ± 0.04	1.82 ± 0.06	2.16 (1.49)
40	0.677	1.210	1358 ± 31	1.64 ± 0.04	1.79 ± 0.03	2.00 (1.38)

The agreement between ΔH_{exp} and ΔH_{calc} for reaction (8.4) is good at <30% Si, but values for reaction (8.1) are closer at higher percentages of Si. Values calculated from U_{ad} are reasonable considering the assumptions made. Further adjustment for temperature and allowance for conversion of reactants to products could improve the agreement.

A maximum heat output at around 26% silicon was observed. The composition at which maximum enthalpy of reaction occurs is usually taken to be an indication of the stoichiometric composition. The 25% Si composition is expected to contain more Si than the calculated stoichiometric point since the silicon particles become coated with a layer of oxide which eventually prevents further oxidation of the bulk of the Si particle. Reaction temperatures are not sufficiently high to melt either the oxide or the silicon to expose unreacted fuel to oxidation.

If reaction (8.1)

$$3Si(s) + 2Fe_2O_3(s) \rightarrow 3SiO_2(s) + 4Fe(s) \quad ...(8.1)$$

were to occur in two stages, i.e. reaction (8.2)

$$Si(s) + 2Fe_2O_3(s) \rightarrow SiO_2(s) + 4FeO(s) \quad ...(8.2)$$

followed by:

$$2Si(s) + 4FeO(s) \rightarrow 2SiO_2(s) + 4Fe(s) \quad ...(8.5)$$

then the calculated enthalpies of the reaction stages would be $\Delta H_{(8.2)}$ = -333 kJ and $\Delta H_{(8.5)}$ = -756 kJ. If these two processes separately accounted for the two stages of the temperature profiles, and assuming a constant heat capacity, the temperature rises in the two stages would be 31% of T_{max} in the first and the remaining 69% in the second. From the actual profiles (see Table 8.1), the first stage tends to account for from 45% to 67% of the total temperature rise. The estimated U_{ad} on the basis of complete reaction, and using the heat capacities of the products at 1600 K (461 J K^{-1}), would be 2362 K, which is considerably higher than values obtained of about 1350 K (Table 8.1).

8.1.2 *Kinetic aspects*

Kinetic parameters for the temperature profiles for the various Si/Fe_2O_3 mixtures determined according to Hill *et al* (5,6) from the approximately linear regions for the two segments respectively, are listed in Table 8.5. Plots of E_a for the first segment (using the Hill approach) with the value of n ranging from 0.5 to 1, as well as those obtained by applying the Leeds approach are shown in Figure 8.5.

The kinetic parameters above were calculated by (i) using an S value obtained from the first segment to calculate α for the first and second segments and (ii) by using an S value calculated from the first and also from the second segment to calculate α for the first and second segments respectively. The values obtained using method (ii) were generally only slightly greater than those obtained by method (i). All the results shown in Table 8.5 were calculated by method (i).

The activation energy varied with the composition, as well as with the value chosen for n. Values of E_a for the second rise region were not very reproducible and were significantly greater than those determined for the first rise region (see Table 8.5). If the thermal properties of the mixture change during the first combustion stage, the S (or t_r) value for the second stage could change considerably.

A summary of the Leeds kinetic analysis of the first segments of the temperature profiles of the Si/Fe_2O_3 system is given in Table 8.6.

Kinetic parameters were derived for the two rise regions in each of the profiles for the various Si/Fe_2O_3 mixtures. The Hill E_a values for the two rise regions generally decreased with increasing silicon in the mixture. E_a values were sensitive to the value of n and were of the order of 20 kJ mol^{-1} (at n = 0.67). Values of n = 0.5 and 0.67 gave the best approximately linear plots of $h(\alpha)$ against 1/T. The E_a values for the second rise region were substantially greater (> 50 kJ mol^{-1}) than those derived from the first rise region. The Leeds analysis (7,8) was attempted for both the rise regions but no success was achieved when applied to the second rise region. Leeds reaction orders ranged from 0.54 to 0.78 for the mixtures examined.

TABLE 8.5

Kinetic parameters calculated from the first and second segments of the temperature profiles of mixtures of Si/Fe_2O_3 (using the Hill approach)

Region of profile	% Si	Order of reaction (n)			
		0.5	0.667	1	2
E_a (kJ mol^{-1})					
1st segment	25	19.5 ± 3.1	21.3 ± 3.3	24.0 ± 3.7	33.0 ± 6.7
2nd segment		51.9 ± 9.7	60.2 ± 3.5	76.1 ± 9.4	126.9 ± 15.0
1st segment	30	18.4 ± 3.8	19.4 ± 3.8	21.5 ± 3.6	27.6 ± 4.3
2nd segment		51.3 ± 12.4	60.4 ± 12.9	78.4 ± 13.2	132.7 ± 17.4
1st segment	35	17.8 ± 2.7	19.1 ± 2.6	21.7 ± 3.5	29.5 ± 2.8
2nd segment		46.5 ± 14.9	52.2 ± 15.5	63.4 ± 16.3	97.2 ± 21.6
1st segment	40	12.1 ± 3.5	12.9 ± 3.5	14.5 ± 3.4	16.1 ± 3.2
2nd segment		65.1 ± 21.6	72.6 ± 18.9	87.3 ± 16.7	131.8 ± 7.2
ln (A/s^{-1})					
1st segment	25	12.4 ± 0.9	12.7 ± 0.9	13.2 ± 0.9	14.9 ± 1.1
2nd segment		14.6 ± 2.4	15.7 ± 2.3	17.7 ± 2.1	23.9 ± 1.5
1st segment	30	11.6 ± 0.7	11.8 ± 0.7	12.5 ± 0.5	13.6 ± 0.5
2nd segment		14.6 ± 1.7	15.7 ± 1.7	17.8 ± 2.3	24.2 ± 4.3
1st segment	35	12.3 ± 0.3	12.5 ± 0.3	13.0 ± 0.5	14.4 ± 1.0
2nd segment		13.4 ± 0.2	14.3 ± 0.2	16.2 ± 1.0	21.7 ± 3.3
1st segment	40	10.7 ± 0.9	10.9 ± 0.9	11.3 ± 0.8	12.5 ± 0.8
2nd segment		16.6 ± 3.5	17.6 ± 3.4	19.5 ± 2.3	25.1 ± 0.9

The agreement between kinetic parameters calculated from the Hill and Leeds approach is poor due to the complexity of the profiles and the cumulative effects of the many stages in the analysis. The low values of the activation energies obtained, however, support proposed diffusion controlled reaction mechanisms for pyrotechnic reactions.

Figure 8.5 Activation energies from the Hill and Leeds analysis of the first rise region of profiles for the Si/Fe_2O_3 system

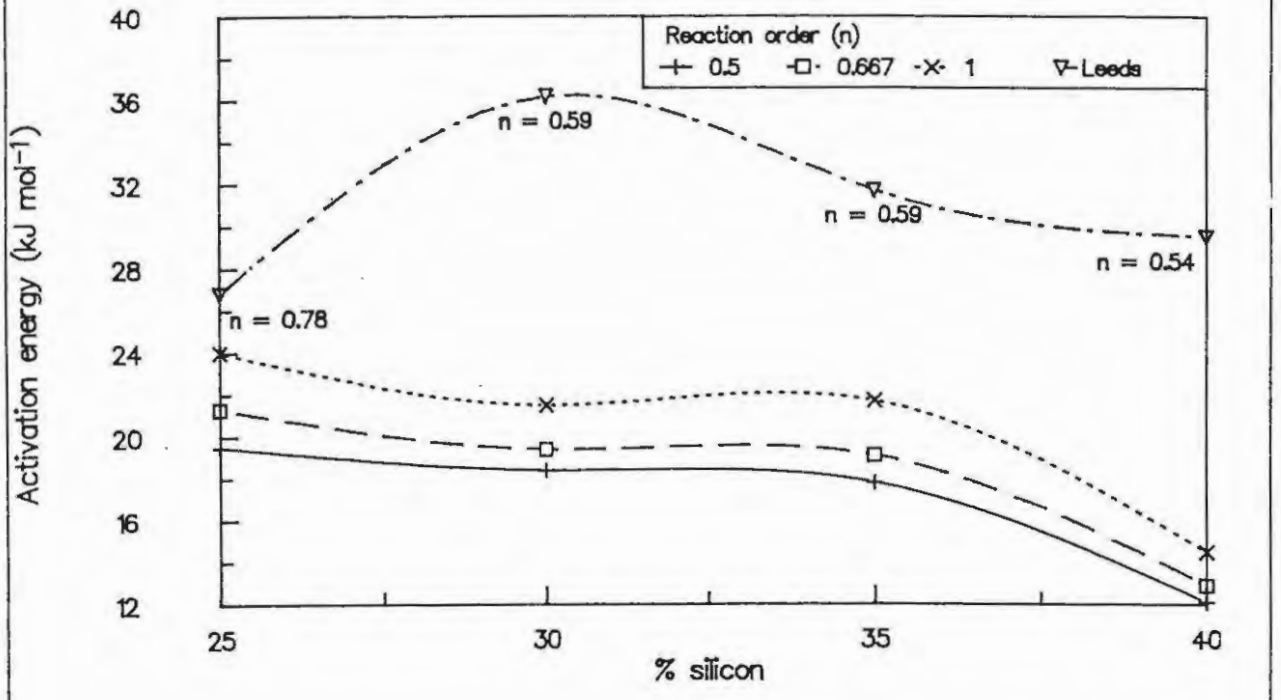

Figure 8.6 Temperature profiles of 35% Si/Fe_2O_3 mixtures pressed to various densities

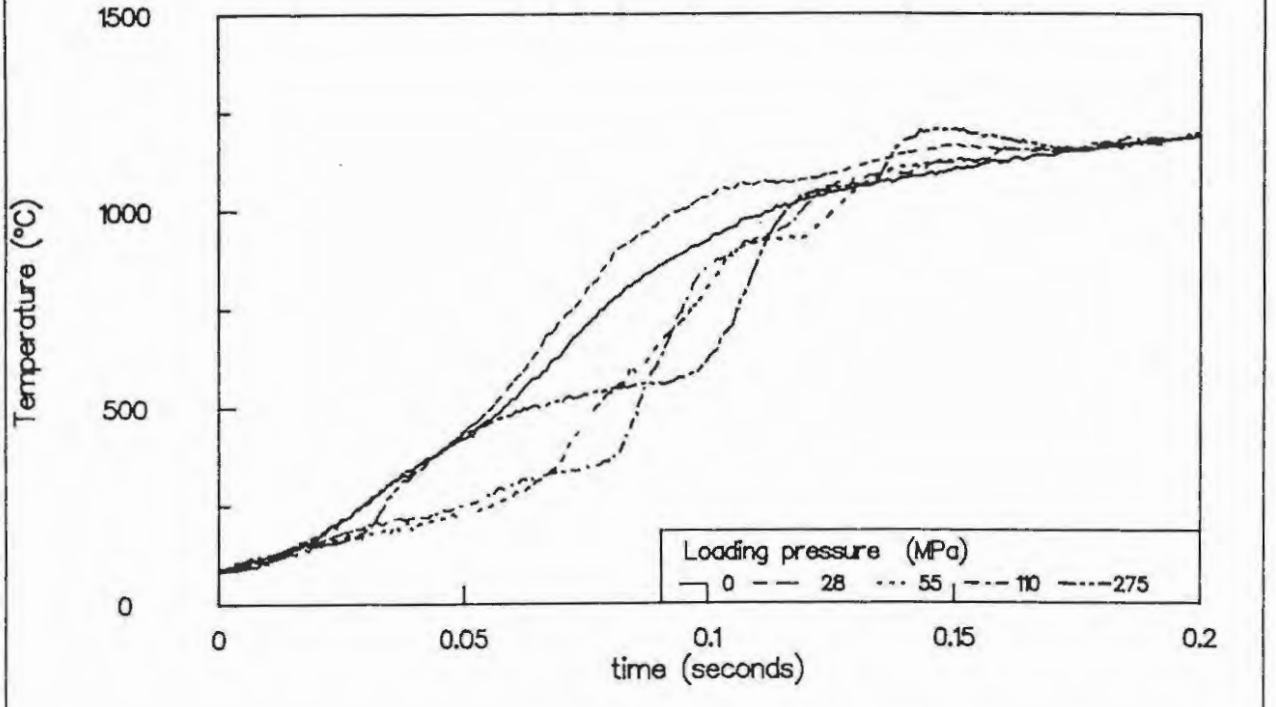

TABLE 8.6

Kinetic parameters calculated from the first segments of the temperature profiles of Si/Fe_2O_3 compositions using the Leeds Approach

% Si	n	a x 10^4	b	E_a (kJ mol^{-1})	ln (A/s^{-1})
Linear regression					
25	0.58 ± 0.02	12.3 ± 2.1	2364 ± 911	19.7 ± 2.2	5.05 ± 2.07
30	0.48 ± 0.04	14.5 ± 4.1	3808 ± 576	29.1 ± 3.3	7.42 ± 0.45
35	0.47 ± 0.08	13.6 ± 2.1	7185 ± 902	26.0 ± 4.7	9.61 ± 1.87
40	0.38 ± 0.09	14.7 ± 2.1	3423 ± 921	28.5 ± 3.6	7.59 ± 1.77
Non-linear regression					
25	0.78 ± 0.11	16.3 ± 6.3	3219 ± 1316	26.8 ± 8.6	6.36 ± 1.23
30	0.59 ± 0.12	15.5 ± 2.7	5778 ± 1978	36.2 ± 3.7	8.53 ± 2.02
35	0.59 ± 0.13	13.2 ± 4.1	5722 ± 1901	31.7 ± 7.5	8.90 ± 2.02
40	0.54 ± 0.02	13.5 ± 3.9	2526 ± 1026	29.5 ± 4.8	6.34 ± 1.85

8.1.3 *Burning rates*

The t_r values for the Si/Fe_2O_3 system, for the first segment of the profiles are shown in Table 8.7.

TABLE 8.7

Time parameters and burning rates for a 35% Si/Fe_2O_3 mixture

% Si	t_r (x 10^{-3} s)	t_d (seconds)	Thermal diffusivity, D (mm^2 s^{-1})	Burning rates (mm s^{-1})	
				v_{exp}	v_{calc}
25	30.2 ± 1.2	2.4 ± 0.7	0.154 ± 0.041	2.33 ± 0.17	2.25 ± 0.59
30	59.9 ± 0.1	3.7 ± 0.2	0.161 ± 0.069	3.67 ± 0.08	1.63 ± 0.68
35	58.0 ± 2.7	3.9 ± 0.3	0.148 ± 0.080	3.82 ± 0.12	1.59 ± 0.86
40	44.7 ± 1.3	3.9 ± 0.2	0.153 ± 0.070	3.60 ± 0.10	1.85 ± 0.84
50	-	-	0.156 ± 0.029	4.54 ± 0.21	-

The calculated burning rates $v_{calc} = (D/t_r)^{1/2}$ (without correction for the thermocouple diameter) do not compare well with the experimental values. This is discussed further in Section 12.

8.2 Effect of compaction

The temperature profiles of samples of 35% Si/Fe_2O_3, pressed under various loading pressures to the densities given in Table 8.8, showed the usual complex behaviour (see Figure 8.6). The temperature profiles of hand packed mixtures were less complex and more reproducible. The burning rate data for these samples are also given in Table 8.8.

The maximum reaction temperature decreased initially (with an increase in sample density from 1.57 to 2.07 g cm^{-3}) but increased thereafter. A plot of the linear burning rate versus sample density (Figure 8.7) showed an initial decrease on compaction, to a minimum at ~1.9 g cm^{-3}, followed by an increase with further increase in density. Because the interparticle contact between the reactants is improved by increasing the compaction of the mixture, the burning rate of reactions which occur predominantly between solids is expected to increase (9).

TABLE 8.8

Burning rates of samples of 35% Si/Fe_2O_3 pressed to various densities (<53 μm Si)

Loading pressure (MPa)	Density (g cm^{-3})	Porosity factor ε	v_{exp} (mm s^{-1})	m_{exp} (g s^{-1})	T_{max} (°C)
0 Hand packed	1.57 ± 0.08	0.63	5.73 ± 0.20	0.37 ± 0.01	1263 ± 9
28 (0.5 tons)	2.07 ± 0.02	0.51	3.78 ± 0.12	0.29 ± 0.01	1125 ± 19
55 (1 ton)	2.20 ± 0.02	0.48	4.10 ± 0.14	0.35 ± 0.01	1166 ± 24
110 (2 tons)	2.43 ± 0.04	0.42	4.97 ± 0.10	0.38 ± 0.01	1205 ± 13
275 (5 tons)	2.58 ± 0.03	0.39	5.01 ± 0.10	0.41 ± 0.01	1223 ± 11

Figure 8.7 Burning rate of 35% Si/Fe_2O_3 at various densities

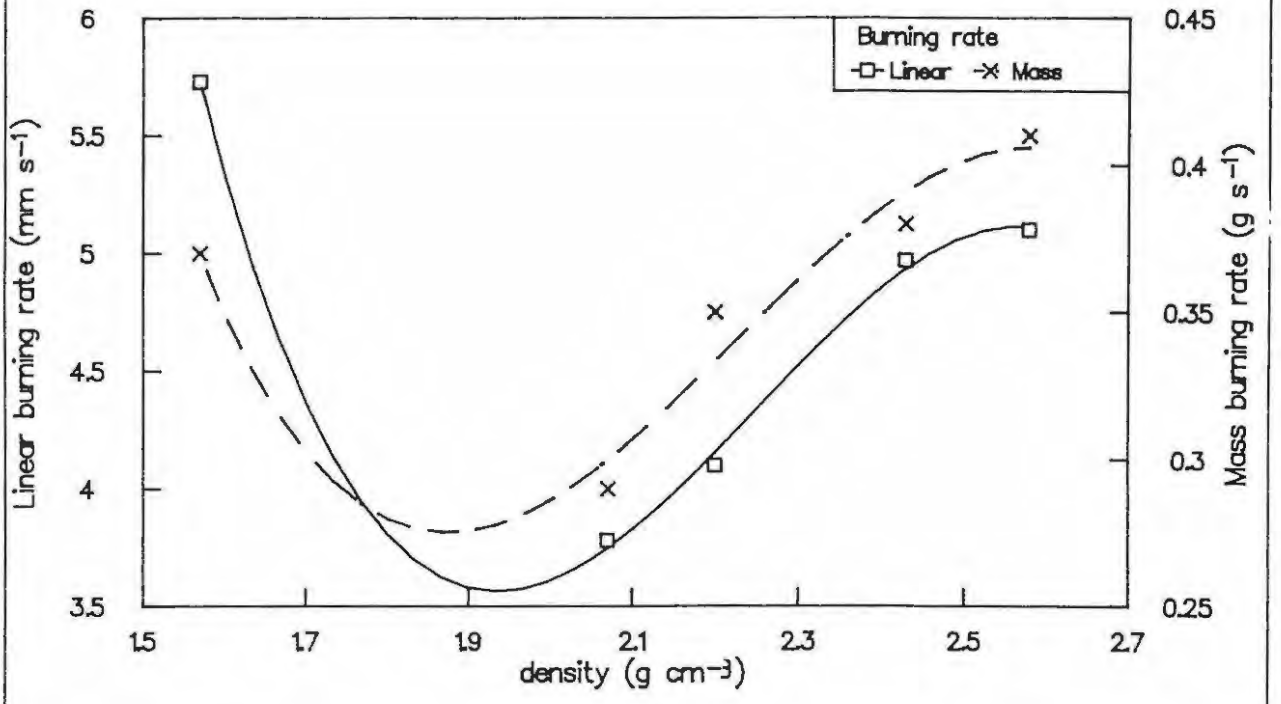

Figure 8.8 Effect of SSA of Si on the temperature profiles of a 35% Si/Fe_2O_3 mixture (pressed for 1 min at 55 MPa)

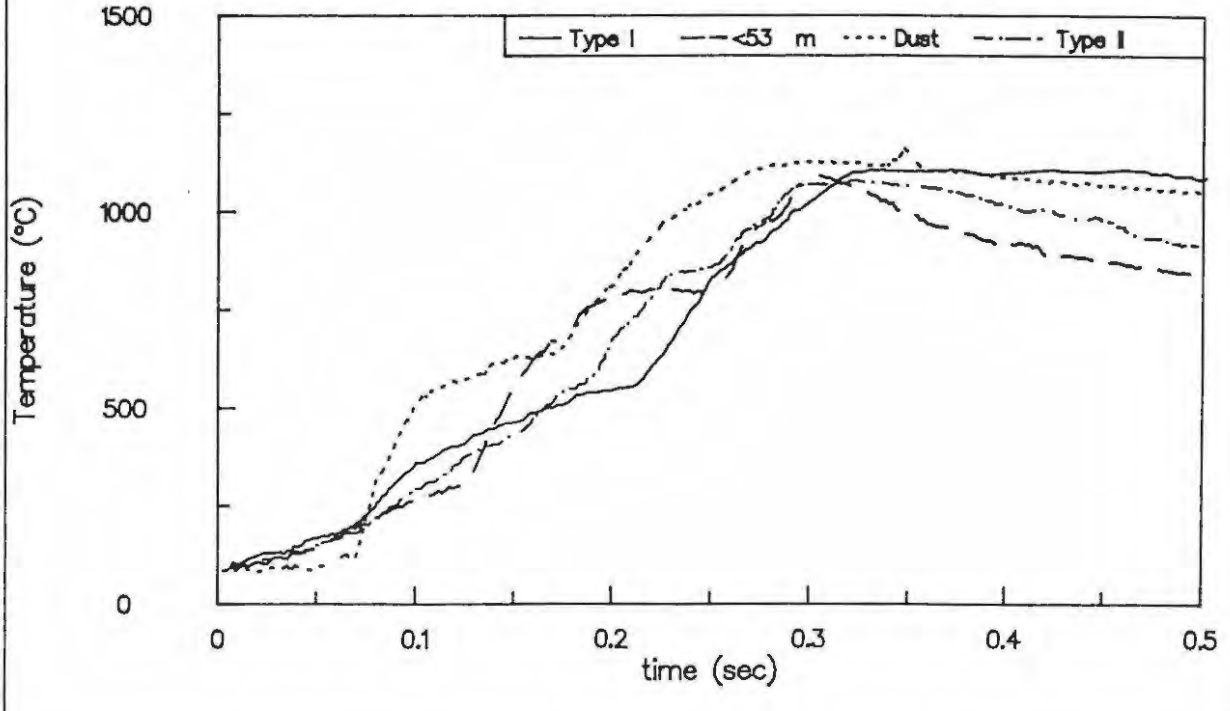

8.3 Effect of particle-size

The burning rates for 35% Si/Fe_2O_3 mixtures (Table 8.9) increased only slightly with increasing surface area of the silicon particles. The temperature profiles were also complex (see Figure 8.8).

TABLE 8.9

Burning rates of 35% Si/Fe_2O_3 with silicon samples of various specific surface areas

Silicon	Specific surface area (m^2 cm^{-3})	Density (g cm^{-3})	v_{exp} (mm s^{-1})	m_{exp} (g s^{-1})
Type I	1.03	2.23 ± 0.03	3.35 ± 0.06	0.29 ± 0.04
<53 μm	2.04	2.19 ± 0.02	3.72 ± 0.04	0.27 ± 0.02
Dust	2.81	2.19 ± 0.04	3.80 ± 0.06	0.31 ± 0.04
Type II	5.40	2.17 ± 0.05	3.94 ± 0.07	0.30 ± 0.03

8.4 Effect of additives

Various proportions of two powdered solids, SiO_2 and Al_2O_3, were added separately as inert diluents to 35% Si/Fe_2O_3 mixtures. Similar proportions of water, as an additive, were also added to the above binary mixture. These diluted compositions were then burnt in the usual manner.

The temperature profiles recorded for 35% Si/Fe_2O_3 which contained SiO_2 or Al_2O_3 as diluents are shown in Figures 8.9 and 8.10, respectively. A decrease in the slope of the rise part of the profile with an increase in the diluent content was observed. The temperature profiles for the 35% Si/Fe_2O_3 mixtures with diluents were still complex. The rise regions appear to be less well-defined in the presence of SiO_2 (see Figure 8.10).

The burning rates of 35% Si/Fe_2O_3 mixed with various proportions of the diluents are shown in Table 8.10. Plots of the burning rate versus proportion of additive (Figure 8.11), showed that the burning rate decreased with increasing diluent content. Burning failed beyond 9% SiO_2 and beyond 7% Al_2O_3. The maximum reaction temperatures for the mixtures remained relatively unchanged.

Samples of Si/Fe_2O_3 with various moisture contents did not sustain reproducible burning when pressed, but burning could be sustained when manually pressed only. Burning rates decreased sharply with increasing H_2O content (Table 8.10). The temperature profiles obtained (Figure 8.12) change from

Figure 8.9 Temperature profiles of 35% Si/Fe_2O_3 mixtures with various proportions of SiO_2

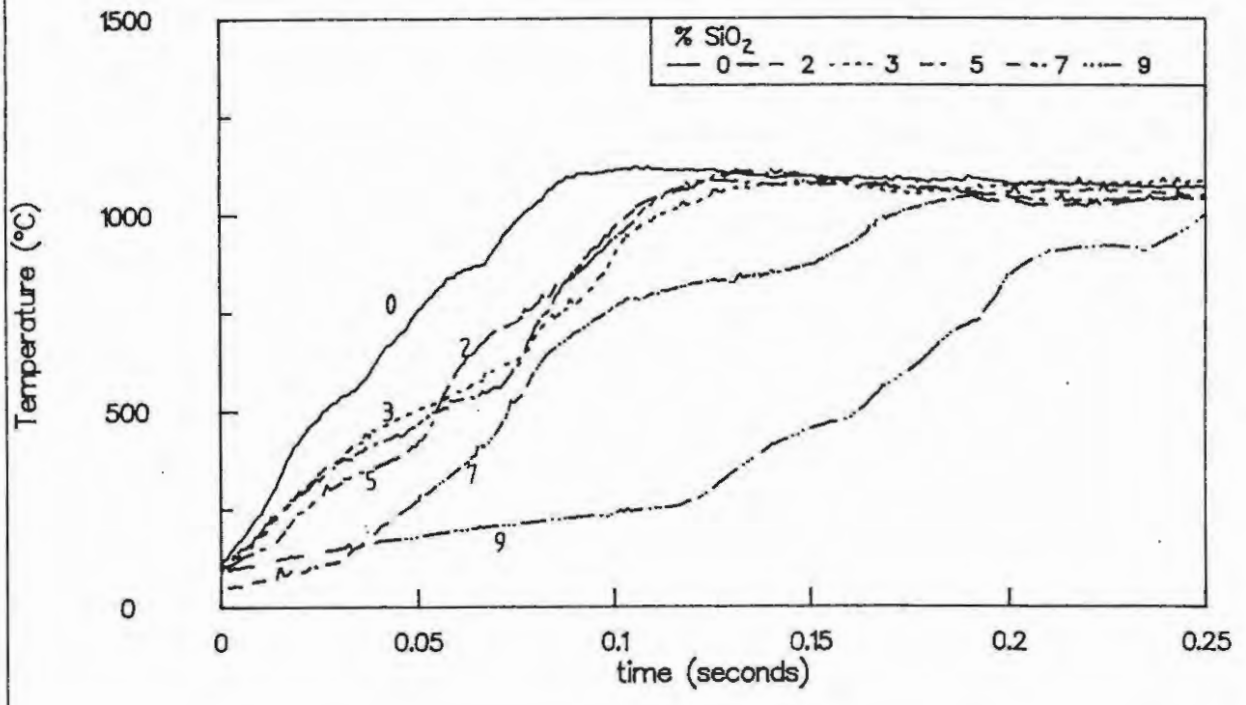

Figure 8.10 Temperature profiles of 35% Si/Fe_2O_3 mixtures with various proportions of Al_2O_3

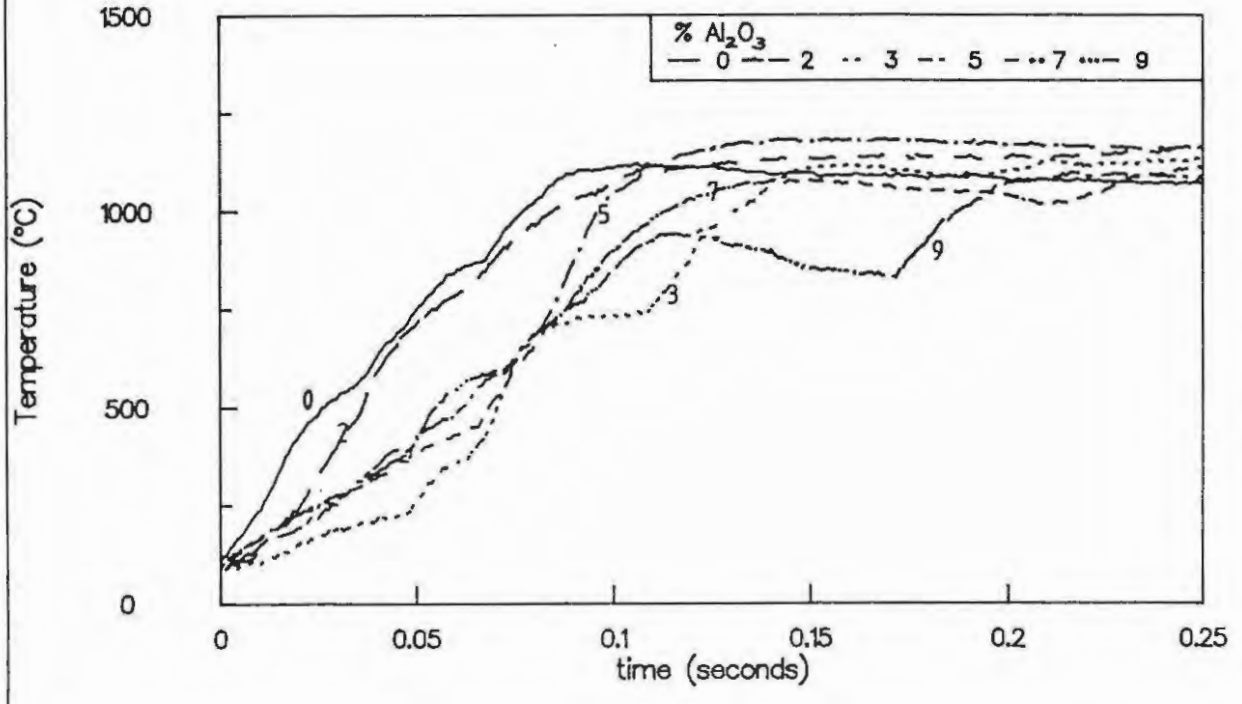

complex (at 0% water) to simple (>2% water). The maximum reaction temperature recorded for the above mixtures increased with increasing moisture content of the samples. There is an expected increase in the time taken to reach maximum temperature with increasing water content.

TABLE 8.10

Burning rates of the 35% Si/Fe_2O_3 mixture with various proportions of additives

(<53 μm Si, pressed for 1 min at 55 MPa)

% additive	Density (g cm^{-3})	v_{exp} (mm s^{-1})	m_{exp} (g s^{-1})	T_{max} (°C)
		SiO_2		
0	2.28 ± 0.08	4.87 ± 0.10	0.33 ± 0.01	1139 ± 9
2	2.15 ± 0.03	4.28 ± 0.11	0.28 ± 0.01	1107 ± 11
3	2.17 ± 0.02	3.72 ± 0.13	0.25 ± 0.01	1101 ± 24
5	2.11 ± 0.04	2.85 ± 0.16	0.18 ± 0.01	1069 ± 29
7	2.11 ± 0.03	2.73 ± 0.10	0.18 ± 0.02	1053 ± 35
9	1.99 ± 0.03	2.39 ± 0.29	0.15 ± 0.02	1034 ± 34
12	WOULD NOT	IGNITE	-	
		Al_2O_3		
0	2.28 ± 0.08	4.87 ± 0.10	0.33 ± 0.01	1139 ± 9
2	2.25 ± 0.01	4.51 ± 0.12	0.31 ± 0.01	1123 ± 16
3	2.24 ± 0.02	4.29 ± 0.11	0.30 ± 0.01	1120 ± 13
5	2.15 ± 0.02	3.64 ± 0.17	0.25 ± 0.01	1115 ± 9
7	2.15 ± 0.03	3.51 ± 0.15	0.23 ± 0.01	1090 ± 35
9	WOULD NOT	IGNITE	-	
		H_2O		
0*	1.26 ± 0.04	5.64 ± 0.20	0.29 ± 0.01	1148 ± 19
2*	1.28 ± 0.07	3.91 ± 0.25	0.19 ± 0.02	1192 ± 13
3*	1.49 ± 0.06	2.72 ± 0.24	0.14 ± 0.01	1309 ± 17
5*	WOULD NOT	IGNITE	-	

* Manually pressed

Figure 8.11 Linear burning rate of 35% Si/Fe_2O_3 mixture with various diluents (<53 μm Si, pressed for 1 min at 55 MPa)

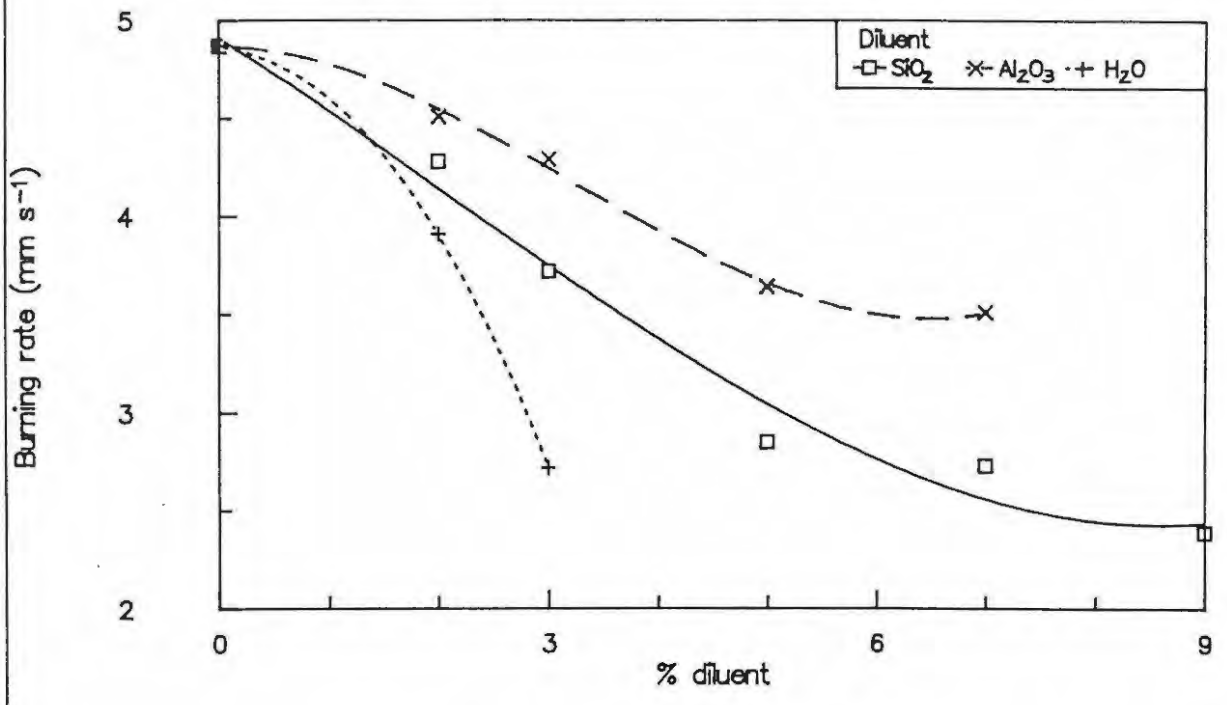

Figure 8.12 Temperature profiles of 35% Si/Fe_2O_3 mixtures with various moisture contents (<53 μm Si)

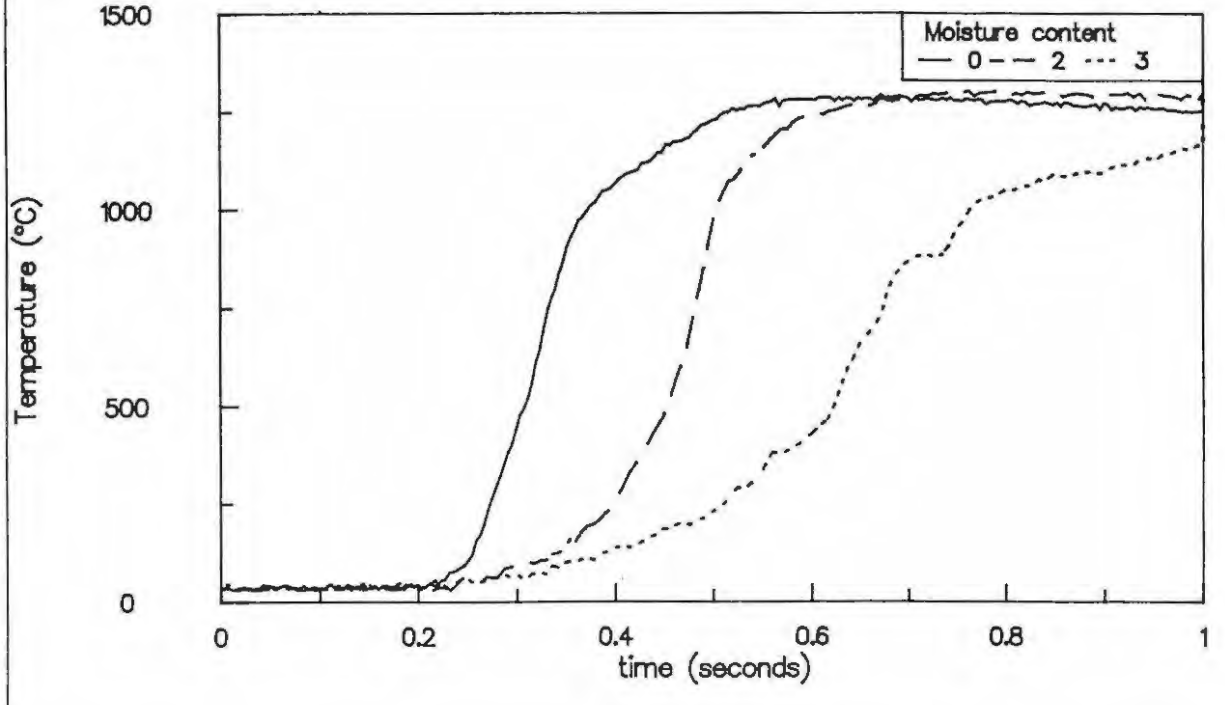

8.5 Comment

These results are discussed further, in relation to the other binary systems, in Section 13.

8.6 References

1. Z.A. Munzir and J.B. Holt (Eds.), "*Combustion and Plasma Synthesis of High Temperature Materials*", VCH Publishers, New York, 1971.
2. R.A.W. Hill and J.N. Welsh, Trans. Far. Soc. **55** (1959) 299.
3. R.A.W. Hill and A.A. Wallace, Nature, **178** (1956) 4535.
4. E.M. Levin, C.R. Robbins and H.F. McMurdie, "*Phase Diagrams for Ceramicists*", American Ceramic Society, Ohio, 1964.
5. R.A.W. Hill, L.E. Sutton, R.B. Temple, A. White and T.L. Cottrell, Research, **3** (1950) 569.
6. R.A.W. Hill and T.L. Cottrell, 4th Symp. Combustion, (1953) 349.
7. T. Boddington, P.G. Laye, J.R.G. Pude and J. Tipping, Comb. Flame, **47** (1982) 235.
8. T. Boddington, P.G. Laye, J.R.G. Pude and J. Tipping, Comb. Flame, **63** (1986) 359.
9. J.H. McLain, "*Pyrotechnics: From the Viewpoint of Solid State Chemistry*", The Franklin Institute Press, Philadelphia, Pennsylvania, 1980.

9. COMBUSTION OF THE Si/SnO_2 SYSTEM

9.1 Effect of composition

Binary mixtures of between 20 and 55% silicon (by mass) and SnO_2 burned reproducibly as pressed columns. Temperature profiles could not be captured for the gassy 20% Si/SnO_2 mixture. The burning of other compositions occurred without significant mass transport (mass loss after combustion was <2%). Temperature profiles for the various compositions are shown in Figure 9.1. The profiles for a given composition were fairly reproducible (Figure 9.2). Maximum temperatures recorded were of the order of 1350°C decreasing to about 1200°C at high % Si (see Table 9.1). These temperatures are well below the melting point of both the fuel (1410°C) and the oxidant (1630°C) so reaction occurred between solid reactants. The temperature profiles for 30 to 50% silicon showed decreased rise times at the extremes of composition (see Figure 9.1). The burning rates for the Si/SnO_2 compositions are listed in Table 9.1.

TABLE 9.1

Burning rates for the Si/SnO_2 system

(< 53 μm, pressed for 1 min at 55 MPa)

% Si	Density ($g\ cm^{-3}$)	Porosity factor ε	v_{exp} ($mm\ s^{-1}$)	m_{exp} ($g\ s^{-1}$)	T_{max} (°C)
20	3.11 ± 0.05	0.46	5.25 ± 0.06	0.53 ± 0.01	shorted
25	2.81 ± 0.02	0.49	7.54 ± 0.39	0.74 ± 0.04	1333 ± 22
30	2.70 ± 0.19	0.49	11.60 ± 0.64	1.09 ± 0.05	1357 ± 18
35	2.58 ± 0.07	0.49	14.78 ± 0.82	1.28 ± 0.10	1362 ± 23
40	2.55 ± 0.05	0.48	17.05 ± 1.29	1.39 ± 0.06	1343 ± 17
45	2.43 ± 0.03	0.48	15.68 ± 0.35	1.37 ± 0.09	1296 ± 24
50	2.37 ± 0.06	0.47	12.84 ± 0.49	0.99 ± 0.01	1258 ± 26
55	2.04 ± 0.03	0.48	9.11 ± 0.39	0.76 ± 0.04	1182 ± 12

A plot of the burning rates against % silicon (Figure 9.3) showed that maximum v_{exp} and m_{exp} occurred at approximately 43% silicon. The burning rates for mixtures with between 35 to 45% silicon were, however, not very different.

A scanning electron micrograph of a sample of an unburnt 45% Si/SnO_2 mixture is shown in Plate 9.1. Also shown are micrographs of the combustion residues (Plate 9.2 and 9.3). The residues showed evidence of the formation of a molten product during burning and also the formation of cavities, on subsequent cooling, due to trapped gases. There were still many powder-like particles present.

Figure 9.1 Temperature profiles for the Si/SnO_2 system

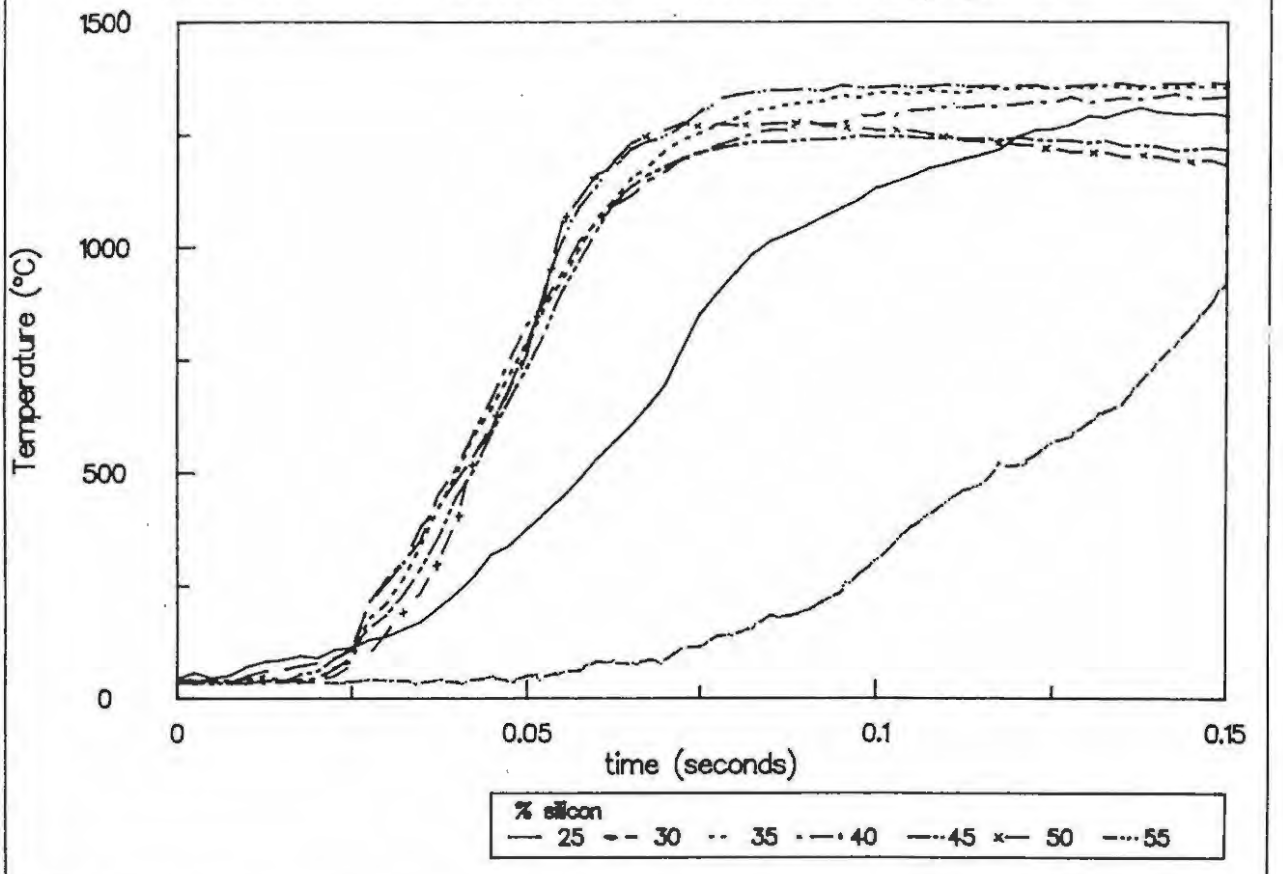

Figure 9.2 Temperature profiles of 45% Si/SnO_2 mixtures showing reproducibility

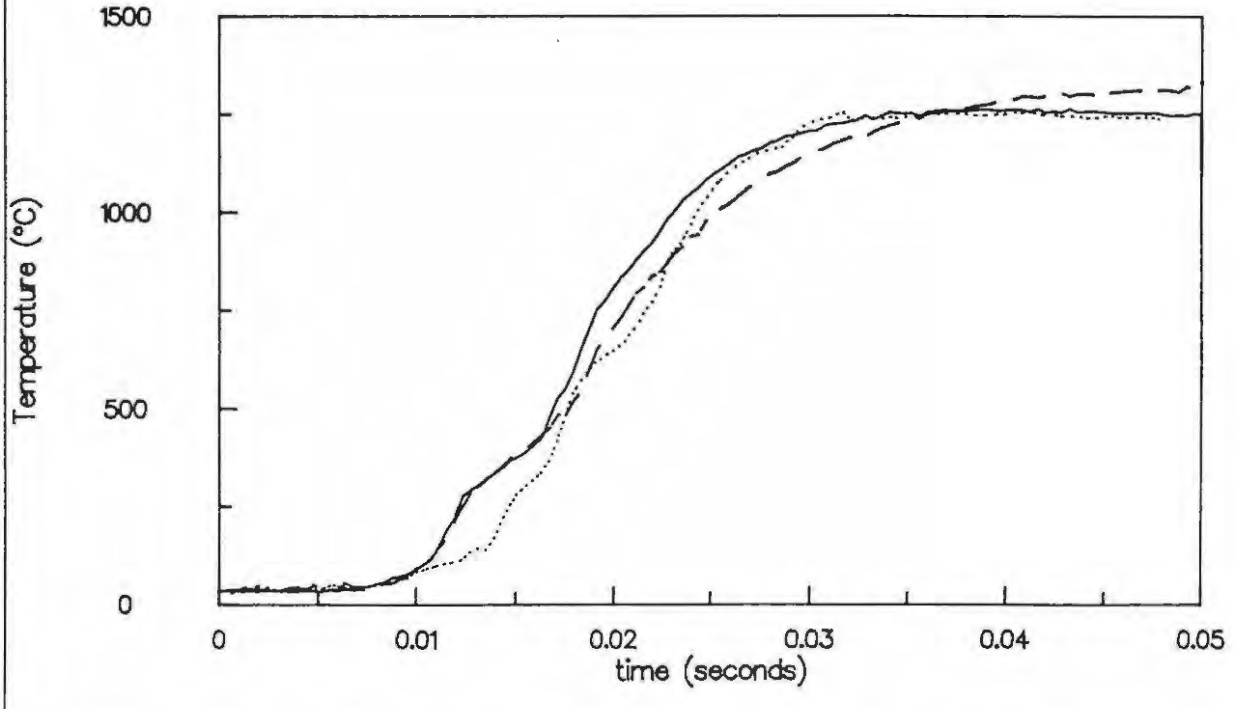

Figure 9.3 Burning rates of the Si/SnO_2 system (<53 μm Si, pressed 1 min at 55 MPa)

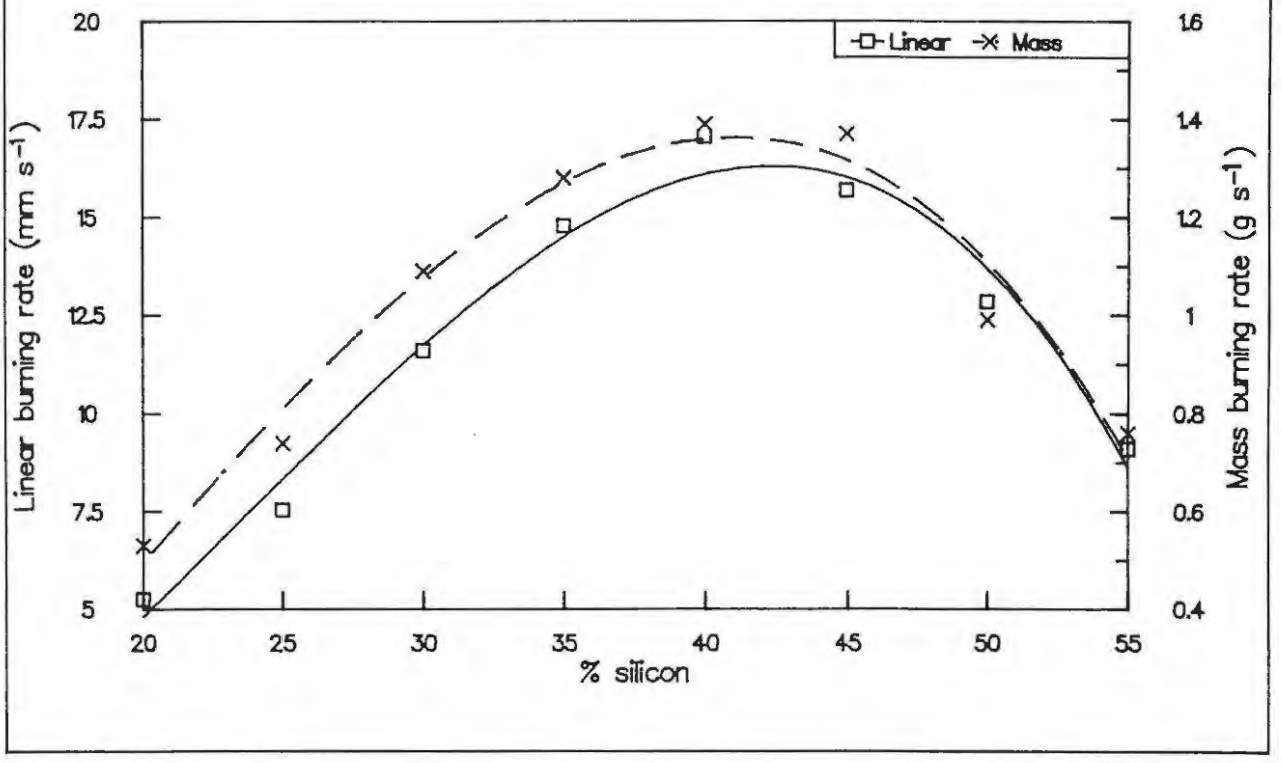

Plate 9 Scanning electron micrographs of the combustion residues of 45% Si/SnO_2 mixtures

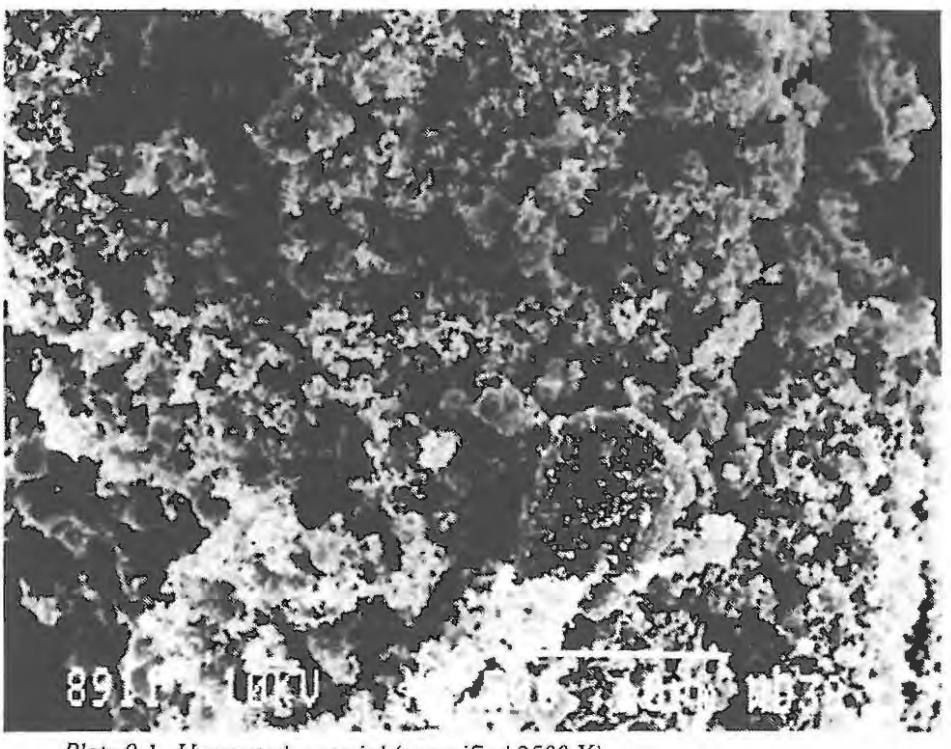

Plate 9.1 Unreacted material (magnified 2500 X)

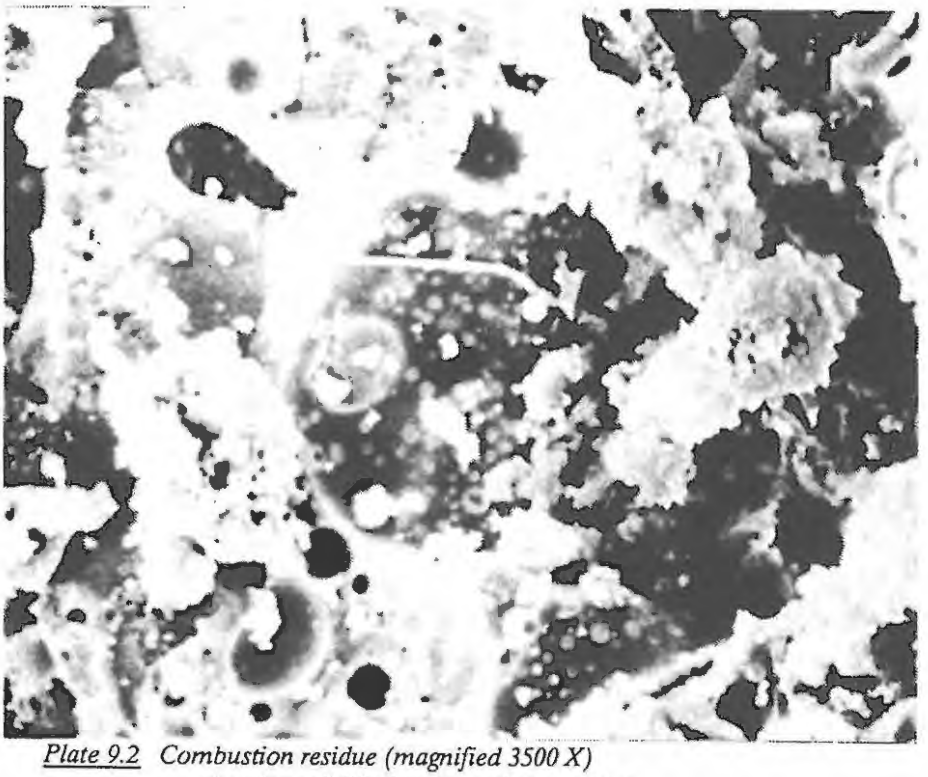

Plate 9.2 *Combustion residue (magnified 3500 X) showing solidified melts and gas cavities*

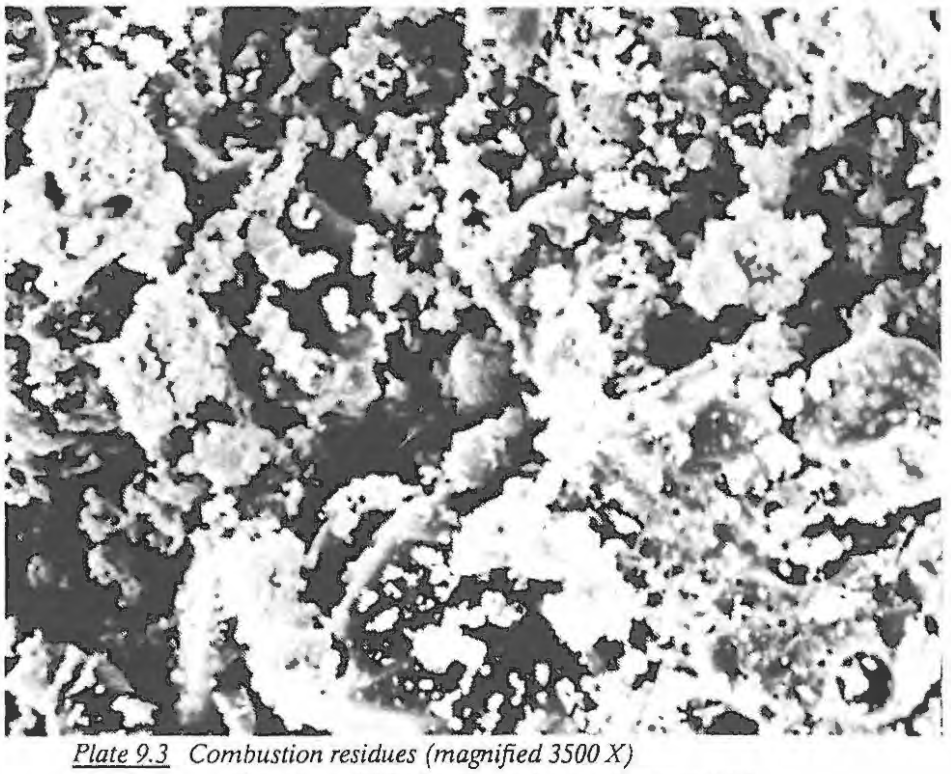

Plate 9.3 *Combustion residues (magnified 3500 X) showing solidified melts and some (presumably) unreacted particles*

Infrared spectra of the combustion residues showed only the strong presence of SiO_2. XRD patterns of the residues showed the presence of unreacted silicon, SnO_2 and traces of SnO. The most intense XRD patterns were those of metallic Sn. Some minor unidentified peaks were probably due to tin silicates. There were no apparent differences in the XRD patterns of the combustion residues of the various Si/SnO_2 compositions. Thus the reaction which occurs during combustion is proposed to be

$$Si(s) + SnO_2(s) \rightarrow SiO_2(s) + Sn(l) \quad ...(9.1)$$

The expected change in enthalpy for this reaction is -316.2 kJ (mol Si)$^{-1}$. The stoichiometric composition is ~15.7% Si and the calculated heat output is 1.77 kJ (g mixture)$^{-1}$. The melting point of tin is 232°C ($\Delta H_{melting}$ = 7.20 kJ mol^{-1}).

9.1.1 *Kinetic aspects*

The kinetic parameters for various Si/SnO_2 mixtures, are given in Tables 9.2 (Hill approach (1,2)) and 9.3 (Leeds approach (3,4)).

The Hill kinetic parameters were not very sensitive to the composition of the mixture, but depended more on the value chosen for the reaction order, n. Approximately linear plots of $h(\alpha)$ against 1/T were obtained for values of $n < 1$. The activation energies from the Leeds analysis (Table 9.3) were approximately similar to those derived from the Hill analysis except for the 55% Si/SnO_2 mixture. Leeds values were more sensitive to the composition of the mixture than the corresponding Hill values. Leeds reaction orders were between 0.4 and 1. The low activation energies (~10 kJ mol^{-1}) obtained from both Hill and Leeds approaches suggest a diffusion controlled reaction mechanism during combustion.

TABLE 9.2

Kinetic parameters calculated from temperature profiles of the Si/SnO_2 system using the Hill approach

Parameter	% Si	Order of reaction (n)			
		0.5	0.667	1	2
E_a (kJ mol^{-1})	25	8.9 ± 0.5	10.0 ± 0.1	12.3 ± 0.7	19.2 ± 3.0
	30	7.5 ± 1.0	9.3 ± 1.3	13.0 ± 1.9	19.1 ± 3.8
	35	6.3 ± 0.3	7.8 ± 0.3	10.6 ± 0.3	19.1 ± 0.3
	40	6.9 ± 2.7	8.5 ± 2.3	11.6 ± 1.5	21.0 ± 1.0
	45	6.0 ± 2.7	7.9 ± 0.5	11.6 ± 0.8	22.9 ± 1.9
	50	7.2 ± 0.7	9.1 ± 0.8	12.9 ± 0.9	24.1 ± 1.7
	55	9.8 ± 1.5	10.2 ± 1.6	18.2 ± 1.8	23.7 ± 1.7
ln (A/s^{-1})	25	10.4 ± 0.3	10.6 ± 0.4	11.1 ± 0.5	12.4 ± 1.0
	30	11.1 ± 0.1	11.6 ± 0.2	12.1 ± 0.2	13.9 ± 0.7
	35	11.1 ± 0.3	11.4 ± 0.3	12.0 ± 0.2	13.8 ± 0.3
	40	11.6 ± 0.6	12.0 ± 0.6	12.7 ± 0.6	14.7 ± 0.6
	45	11.8 ± 0.2	12.2 ± 0.2	12.9 ± 0.3	15.2 ± 0.1
	50	11.6 ± 0.4	12.0 ± 0.4	12.8 ± 0.4	15.2 ± 0.3
	55	11.7 ± 0.3	11.9 ± 0.3	12.8 ± 0.2	13.4 ± 0.2

TABLE 9.3

Kinetic parameters calculated from temperature profiles of Si/SnO_2 compositions using the Leeds Approach

% Si	n	a x 10^4	b	E_a (kJ mol^{-1})	ln (A/s^{-1})
Linear regression					
25	0.51 ± 0.06	35.80 ± 2.13	1654 ± 195	13.8 ± 1.6	6.49 ± 0.16
30	0.52 ± 0.02	26.31 ± 1.30	2040 ± 33	17.0 ± 0.2	5.21 ± 0.10
35	0.52 ± 0.03	6.55 ± 1.29	835 ± 101	6.9 ± 0.8	3.83 ± 0.21
40	0.43 ± 0.06	10.67 ± 1.94	1009 ± 215	8.4 ± 1.8	4.33 ± 0.19
45	0.60 ± 0.07	22.31 ± 4.45	1147 ± 113	9.5 ± 0.9	5.07 ± 0.23
50	0.54 ± 0.01	33.61 ± 7.02	1456 ± 125	12.1 ± 1.0	5.36 ± 0.43
55	0.50 ± 0.05	1638 ± 132	5101 + 371	42.4 ± 3.1	–
Non-linear regression					
25	0.95 ± 0.11	21.64 ± 6.62	2052 ± 276	17.1 ± 0.2	5.42
30	0.56 ± 0.02	19.39 ± 0.76	1657 ± 15	13.8 ± 0.1	4.91 ± 0.05
35	0.84 ± 0.06	20.46 ± 2.96	1341 ± 170	11.2 ± 0.2	4.99 ± 0.14
40	0.44 ± 0.07	9.50 ± 1.84	881 ± 219	7.3 ± 1.8	4.22 ± 0.20
45	0.82 ± 0.11	44.23 ± 0.62	1326 ± 231	11.0 ± 1.9	5.65 ± 0.47
50	0.51 ± 0.06	13.35 ± 0.21	1269 ± 15	10.6 ± 0.1	4.61 ± 0.01
55	0.56 ± 0.01	882 ± 64	4653 + 402	38.7 ± 3.3	–

Figure 9.4 illustrates the dependence of the activation energies on the composition of the mixture.

9.1.2 *Thermochemical aspects*

The characteristic temperatures of the profiles for the Si/SnO_2 system are listed in Table 9.4. Maximum T_{max} occurred at 35% Si.

The changes in enthalpy determined from bomb calorimetry (ΔH_{exp}) are listed in Table 9.5. Also listed are the expected changes in enthalpy (ΔH_{calc}) calculated from the standard enthalpies of formation of the reactants and products for reaction (9.1). The heat outputs, q, based on U_{ad} and the heat capacities of the solid reactants calculated at T_{ad} = ~1600 K (= U_{ad} + 298), are also listed (c(Si) = 0.961 J K^{-1} g^{-1} and $c(SnO_2)$ = 0.567 J K^{-1} g^{-1} at 1600 K).

Figure 9.4 Activation energies from the Hill and Leeds analysis of the temperature profiles of the Si/SnO_2 system

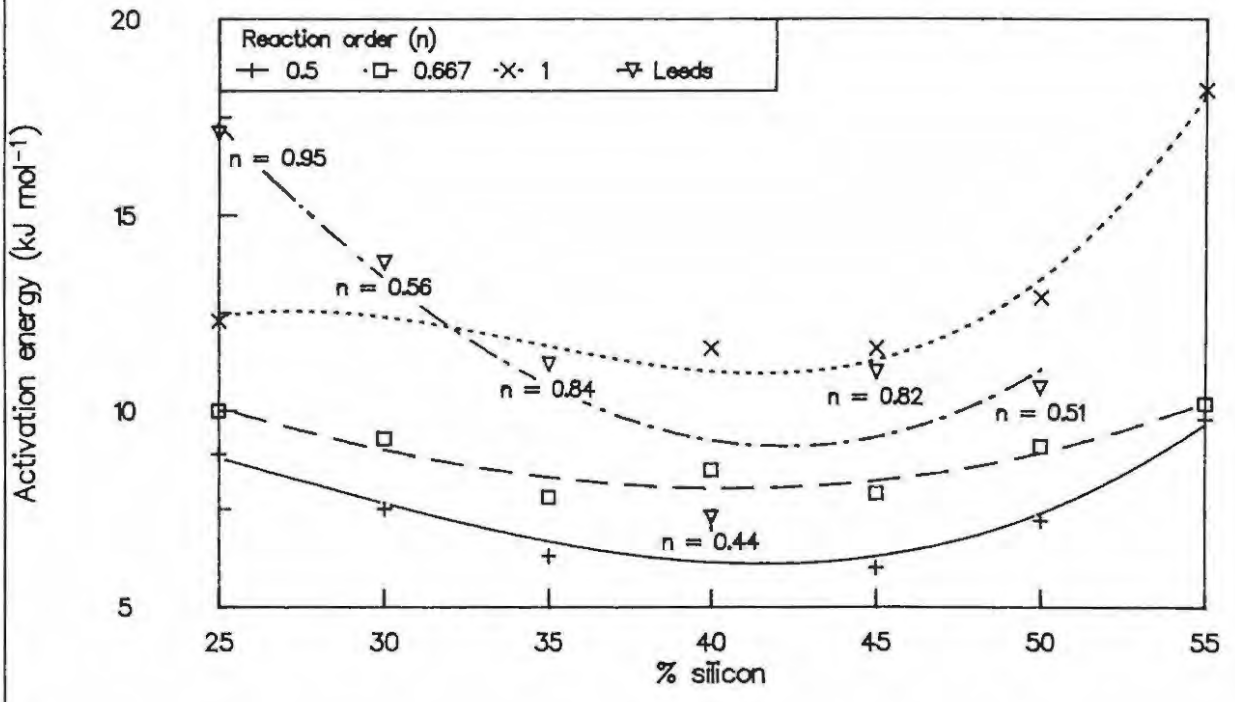

Figure 9.5 Temperature profiles of 45% Si/SnO_2 mixtures at various densities

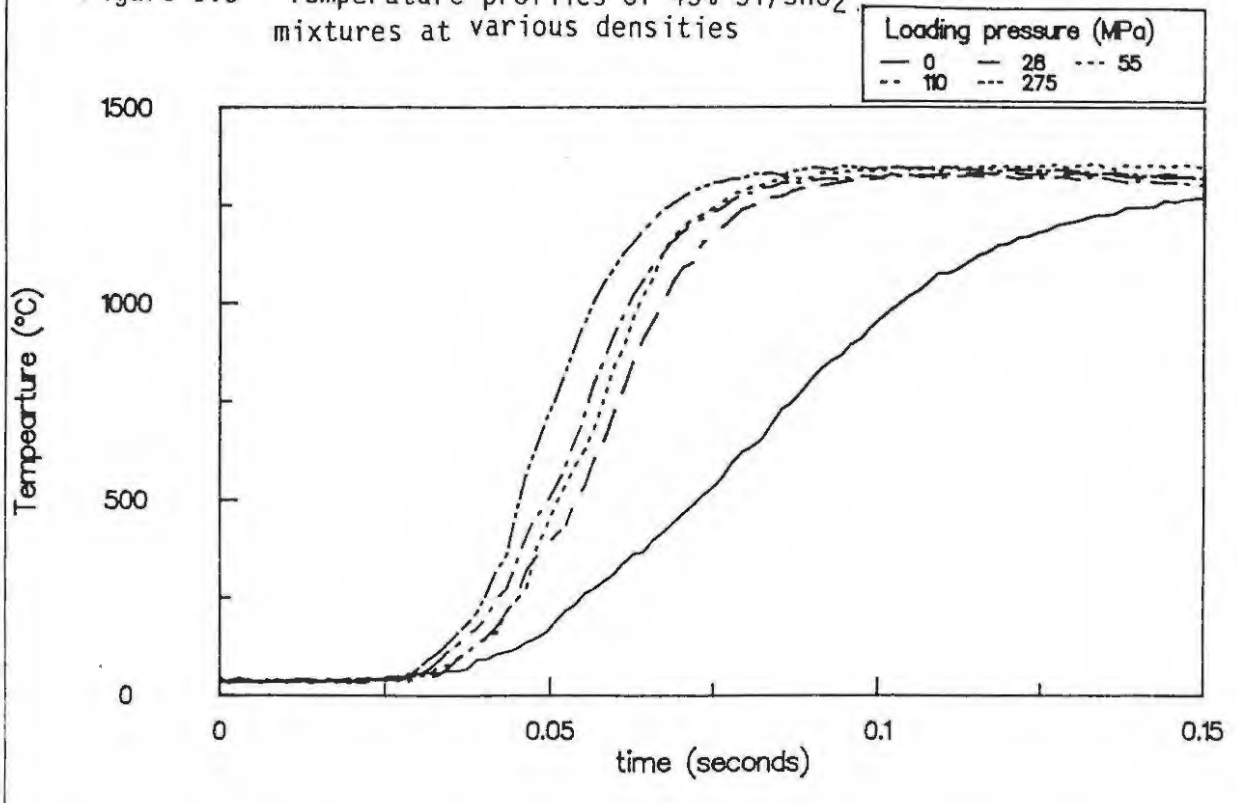

TABLE 9.4

Characteristic temperatures for the Si/SnO_2 system

% Si	T_{max} (C°)	U_{max} (C°)	U_{ad} (C°)
25	1333 ± 22	1311	1361 ± 36
30	1357 ± 18	1335	1413 ± 47
35	1362 ± 24	1342	1377 ± 32
40	1343 ± 24	1323	1376 ± 21
45	1296 ± 24	1276	1311 ± 12
50	1258 ± 26	1238	1279 ± 14
55	1182 ± 11	1163	-

TABLE 9.5

Thermochemical data for Si/SnO_2 compositions

% Si	Heat capacity (J K g^{-1}) 298 K	Heat capacity (J K g^{-1}) 1600 K	q (kJ (g mixture)$^{-1}$) 1600 K	$-\Delta H_{exp}$ (kJ (g mixture)$^{-1}$)	$-\Delta H_{calc}$ (kJ (g mixture)$^{-1}$)
20	0.422	0.646	-	1.42 ± 0.02	1.72
25	0.441	0.666	0.91 ± 0.03	-	1.61
30	0.459	0.685	0.97 ± 0.03	1.50 ± 0.01	1.50
35	0.477	0.705	0.97 ± 0.02	-	1.40
40	0.495	0.725	1.00 ± 0.02	1.36 ± 0.01	1.29
45	0.514	0.744	0.98 ± 0.02	1.22 ± 0.01	1.18
50	0.532	0.764	0.98 ± 0.02	1.14 ± 0.01	1.07
55	0.550	0.784	-	-	0.97
60	-	-	-	1.07 ± 0.02	0.86

There is good agreement between ΔH_{exp} and ΔH_{calc} for mixtures which contained between 30 and 50% Si by mass. The values obtained from the heat capacities (at 1600 K) and U_{ad} are lower, but agreement improves at higher Si content.

Maximum heat of reaction occurred at ~30% silicon compared to the expected value of 15.7% Si (see reaction 9.1). The composition at which maximum heat is evolved is usually taken as the stoichiometric composition. The observed maximum at 30% Si is consistent with the silicon particles becoming coated with a layer of oxide which prevents any further oxidation of the bulk of the Si particle. Reaction temperatures are not sufficiently high to melt either the oxide or the silicon to expose unreacted fuel to oxidation.

9.1.3 *Burning rates*

The various time parameters determined from the analysis of the temperature profiles of the Si/SnO_2 system are shown in Table 9.6. Also shown are the thermal diffusivities of the respective mixtures and the burning rates.

TABLE 9.6

Time parameters for the Si/SnO_2 system

% Si	t_r (x 10^{-3} s)	t_d (seconds)	Thermal diffusivity, D ($mm^2\ s^{-1}$)	Burning rates ($mm\ s^{-1}$)	
				v_{exp}	v_{calc}
20	-	-	0.229 ± 0.010	5.25 ± 0.06	-
25	15.6 ± 0.9	-	-	7.54 ± 0.39	-
30	13.9 ± 0.2	2.2 ± 1.3	0.235 ± 0.010	11.60 ± 0.64	4.11 ± 0.17
35	7.6 ± 0.8	3.6 ± 0.2	-	14.78 ± 0.64	-
40	7.5 ± 0.1	2.1 ± 0.4	0.208 ± 0.006	17.05 ± 1.29	5.26 ± 0.15
45	3.3 ± 0.4	1.6 ± 0.6	0.188 ± 0.032	15.68 ± 0.35	7.54 ± 0.80
50	9.4 ± 0.4	1.4 ± 0.2	0.174 ± 0.005	12.84 ± 0.49	4.47 ± 0.13
55	12.8 ± 0.5	-	-	9.11 ± 0.39	-

The rise times (t_r) showed a minimum at ~45% silicon. The decay times (t_d) decreased with increasing silicon. The agreement between experimental and calculated burning rates, v_{calc}, (without correction for the diameter of the thermocouples) was poor. In most systems where the composition at which maximum v_{exp} occurs is greater than the observed stoichiometric composition, the difference is usually due to a larger thermal conductivity value, (λ), of the fuel compared to the oxidant (5). The thermal conductivity (see section 12) of SnO_2 (λ = 0.40 W K^{-1} m^{-1}) is slightly higher than that Si (λ = 0.35 W K^{-1} m^{-1}), and

such differences are too small to account for the difference between the composition at which v_{exp} is a maximum (43% Si) and the stoichiometric composition (30% Si). The formation of molten tin as a product (see reaction (9.1)) would however increase the thermal conductivity considerably.This aspect is discussed further in section 12.

9.1.4 *Effect of thermocouple wire-diameter*

Various thermocouple diameters were used to capture temperature profiles of a 45% Si/SnO_2 mixture. Results are listed in Tables 9.7 to 9.8.

TABLE 9.7

Characteristic temperatures and time parameters from temperature profiles of a 45% Si/SnO_2 composition using thermocouples of various diameters

tc diameter (mm)	Temperature data (°C)			Time parameters (seconds)	
	T_{max}	U_{max}	U_{ad}	$t_r \times 10^{-3}$	t_d
0.05	1351 ± 13	1330	1348 ± 15	6.2 ± 1.3	2.2 ± 0.9
0.10	1352 ± 10	1330	1415 ± 7	10.2 ± 0.7	3.9 ± 0.8
0.20	1341 ± 11	1319	1378 ± 17	11.7 ± 1.5	4.1 ± 1.1
0.30	1336 ± 14	1315	1374 ± 11	14.1 ± 3.8	7.1 ± 1.4

The overall shape of the profiles and the values of T_{max} were not altered significantly when thermocouples of various diameters were used to capture data. The slope of the rise regions of the profiles decreased with increasing wire-diameter (d). Time parameters from the profiles increased with an increase in d. The relationship for t_r was $(t_r/ms) = (74 \pm 27)(d/mm)^{-2} + (8 \pm 2)$. Correction of the finite diameter of the thermocouple wire would thus decrease the calculated burning rates (Table 9.6). The apparent activation energies (Table 9.8) were not significantly affected by d.

TABLE 9.8

Kinetic parameters (Hill approach) calculated from the temperature profiles of a 45% Si/SnO_2 composition using thermocouples of various diameters

TC diameter (mm)	Activation energy (kJ mol^{-1})			
	n = 0.50	n = 0.67	n = 1	n = 2
0.05	6.5 ± 1.6	7.1 ± 1.5	10.4 ± 2.1	18.3 ± 2.5
0.10	8.9 ± 1.4	9.9 ± 1.4	11.7 ± 1.4	17.3 ± 1.3
0.20	9.5 ± 0.7	10.3 ± 0.9	11.8 ± 1.1	18.3 ± 1.7
0.30	7.0 ± 0.3	8.3 ± 0.3	10.8 ± 0.5	18.4 ± 1.3

9.2 Effect of compaction

Samples of 45% Si/SnO_2 were pressed under various loading pressures to the densities given in Table 9.9 and burnt in the usual way. The temperature profiles obtained (Figure 9.5), show a marked decrease in rise-time on initial compaction, but little change thereafter. Both v_{exp} and m_{exp} increased with an increase in the density of the sample (Table 9.9). A plot of the linear and mass burning rates against density for the 45% Si/SnO_2 mixtures (Figure 9.6) showed an almost linear increase in the burning rate as the sample density increased and strongly indicates that burning occurs between solid reactants (5).

TABLE 9.9

Burning rates of samples of 45% Si/SnO_2 pressed to various densities (< 53 μm Si)

Loading pressure (MPa)	Density (g cm^{-3})	Porosity factor ε	v_{exp} (cm s^{-1})	m_{exp} (g s^{-1})
Hand packed	1.71 ± 0.05	0.64	11.28 ± 0.74	0.72 ± 0.03
28 (0.5 tons	2.33 ± 0.02	0.52	14.13 ± 0.24	1.07 ± 0.02
55 (1 ton)	2.53 ± 0.08	0.48	15.22 ± 0.52	1.28 ± 0.01
110 (2 tons)	2.63 ± 0.03	0.46	16.25 ± 0.71	1.42 ± 0.04
275 (5 tons)	2.66 ± 0.07	0.45	16.79 ± 0.88	1.41 ± 0.03

Figure 9.6 Burning rates for 45% Si/SnO_2 mixtures at various densities (<53 μm Si, pressed for 1 min)

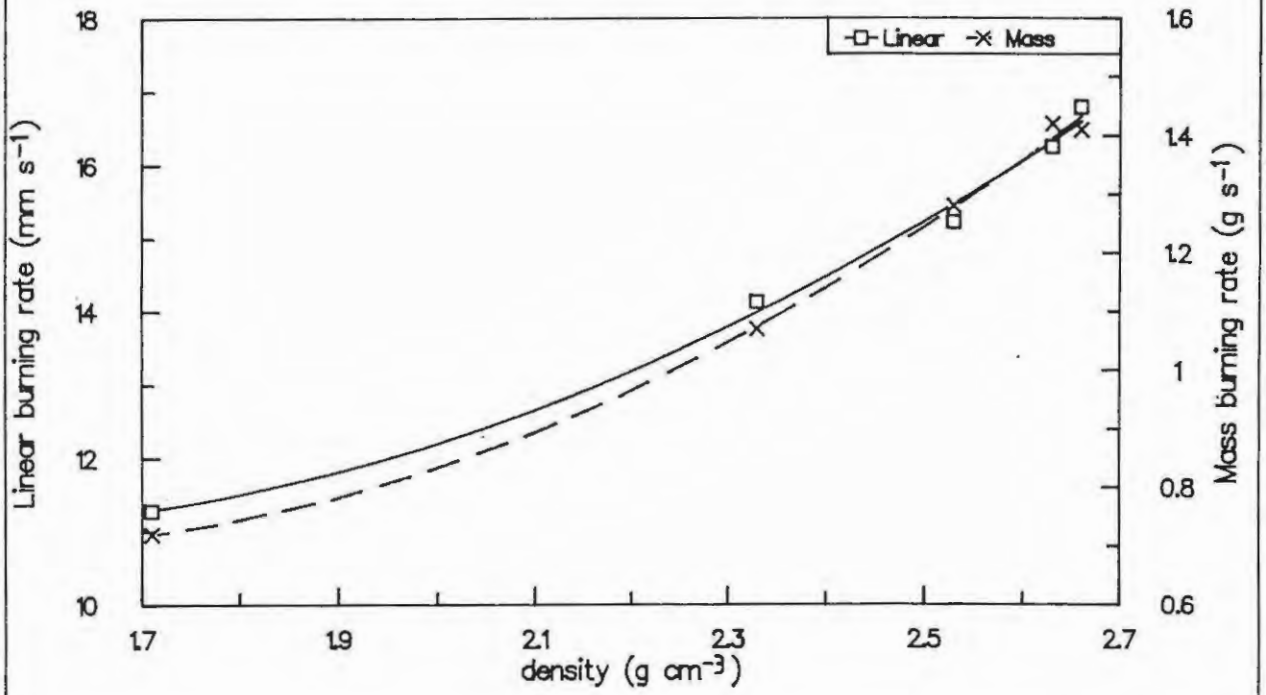

Figure 9.7 Effect of SSA of Si on the temperature profiles of a 45% Si/SnO_2 mixture (pressed 1 min at 55 MPa)

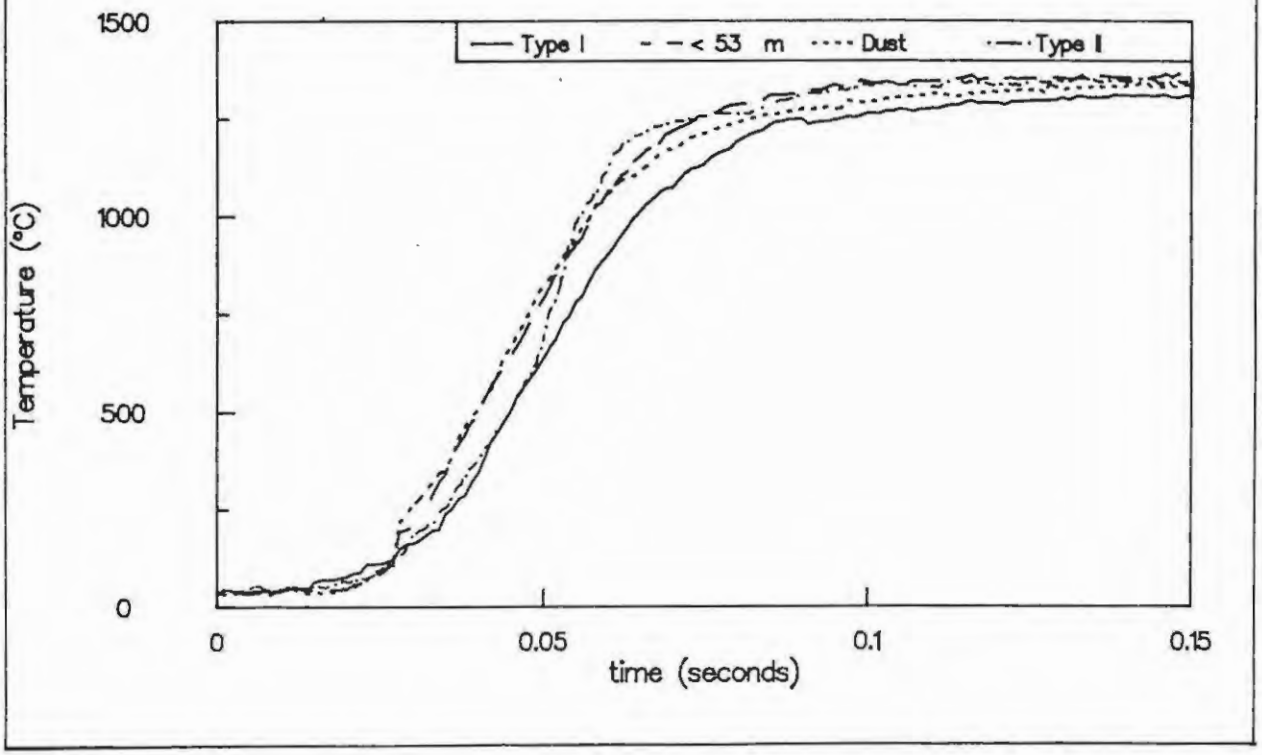

9.2.1 *Kinetic aspects*

The characteristics of temperature profiles of a 45% Si/SnO_2 composition pressed to various densities are listed in Table 9.10 and 9.11.

TABLE 9.10

Temperature parameters calculated from temperature profiles of samples of a 45% Si/SnO_2 composition at various densities

Loading pressure (MPa)	Density (g cm^{-3})	Temperature data (°C)		
		T_{max}	U_{max}	U_{ad}
0	1.71 ± 0.05	1356 ± 13	1331	1382 ± 25
23	2.33 ± 0.02	1342 ± 27	1316	1430 ± 20
55	2.53 ± 0.08	1352 ± 10	1330	1414 ± 10
110	2.63 ± 0.03	1338 ± 7	1313	1465 ± 11
275	2.66 ± 0.07	1401 ± 90	1378	1451 ± 50

TABLE 9.11

Time parameters derived from temperature profiles of a 45% Si/SnO_2 composition at various densities

Loading pressure (MPa)	Density (g cm^{-3})	Time parameters (seconds)	
		$t_r \times 10^{-3}$	t_d
0	1.71 ± 0.05	16.3 ± 1.1	8.3 ± 0.6
23	2.33 ± 0.02	9.9 ± 0.9	1.4 ± 0.2
55	2.53 ± 0.08	10.2 ± 0.4	1.6 ± 0.6
110	2.63 ± 0.03	7.9 ± 0.1	2.1 ± 0.3
275	2.66 ± 0.07	6.7 ± 1.2	2.5 ± 0.4

TABLE 9.12

Kinetic parameters (Hill approach) calculated from the temperature profiles of a 45% Si/SnO_2 composition at various densities

Density ($g\ cm^{-3}$)	Activation energy ($kJ\ mol^{-1}$)			
	n = 0.50	n = 0.67	n = 1	n = 2
1.71 ± 0.05	13.5 ± 1.2	14.7 ± 1.2	17.2 ± 1.0	24.5 ± 0.6
2.33 ± 0.02	11.2 ± 2.9	12.7 ± 2.8	15.7 ± 2.5	24.6 ± 1.5
2.53 ± 0.08	10.0 ± 2.7	11.9 ± 0.5	15.6 ± 0.8	26.9 ± 1.9
2.63 ± 0.03	13.5 ± 0.3	14.9 ± 0.4	17.8 ± 0.7	26.3 ± 1.7
2.66 ± 0.07	13.1 ± 1.2	15.4 ± 1.2	17.9 ± 1.5	25.7 ± 2.7

TABLE 9.13

Kinetic parameters (Leeds Approach) calculated from temperature profiles of a 45% Si/SnO_2 composition at various densities

Density ($g\ cm^{-3}$)	n	a x 10^4	b	E_a ($kJ\ mol^{-1}$)	ln (A/s^{-1})
Linear regression					
1.71 ± 0.05	0.59 ± 0.06	5.52 ± 1.18	1107 ± 103	9.2 ± 0.9	3.7 ± 0.2
2.33 ± 0.02	0.52 ± 0.12	14.78 ± 0.20	1349 ± 197	11.2 ± 1.6	4.6 ± 0.1
2.53 ± 0.08	0.67 ± 0.01	26.73 ± 0.10	1258 ± 6	10.5 ± 0.1	5.2 ± 0.1
2.63 ± 0.03	0.52 ± 0.04	22.51 ± 1.03	1573 ± 101	13.1 ± 0.8	5.0 ± 0.1
2.66 ± 0.07	0.61 ± 0.09	38.48 ± 2.61	1510 ± 85	12.6 ± 0.7	5.3 ± 0.1
Non-linear regression					
1.71 ± 0.05	0.99 ± 0.08	18.31 ± 3.35	1678 ± 61	14.0 ± 0.5	4.9 ± 0.2
2.33 ± 0.02	0.66 ± 0.24	33.52 ± 26.9	1632 ± 624	13.8 ± 5.1	5.2 ± 0.7
2.53 ± 0.08	0.91 ± 0.04	58.20 ± 7.77	1535 ± 64	12.8 ± 0.5	6.0 ± 0.1
2.63 ± 0.03	0.56 ± 0.10	15.78 ± 89.5	1261 ± 173	10.5 ± 4.8	4.7 ± 0.3
2.66 ± 0.07	0.92 ± 0.13	72.33 ± 31.2	1859 ± 745	15.5 ± 6.2	6.1 ± 0.5

The maximum temperatures recorded for the profiles increased only slightly with increasing density. As expected, the characteristic times of the profiles depended markedly on the density of the mixture. The decay time for the uncompacted sample is considerably greater than for those samples which were compacted.

The Hill kinetic parameters from temperature profiles (see Table 9.12, page 147) were very sensitive to the density of the sample and increased with increasing compaction. Leeds E_a values showed no trends (see Table 9.13, page 147).

9.3 **Effect of particle-size**

The burning rate of 45% Si/SnO_2 compositions increased slightly for Si samples with a large specific surface area (see Table 9.14).

The temperature profiles in Figure 9.7 show that any trend is smaller than the scatter caused by limited reproducibility.

TABLE 9.14

Burning rates of 45% Si/SnO_2 with silicon samples of various specific surface areas

Silicon	Specific surface area ($m^2\ cm^{-3}$)	Density ($g\ cm^{-3}$)	v_{exp} ($mm\ s^{-1}$)	m_{exp} ($g\ s^{-1}$)
Type I	1.03	2.61 ± 0.08	15.55 ± 1.12	1.31 ± 0.08
<53 μm	2.04	2.46 ± 0.09	15.39 ± 0.75	1.47 ± 0.09
Dust	2.81	2.51 ± 0.07	17.05 ± 1.29	1.30 ± 0.05
Type II	5.40	2.59 ± 0.08	18.63 ± 1.41	1.52 ± 0.17

9.4 **Effect of additives**

The burning rates of 45% Si/SnO_2 with various proportions of either SiO_2 or Al_2O_3 (Table 9.15) decreased with increasing diluent content (see Figure 9.8). Combustion was sustained for up to 15% (by mass) of diluent. Mixtures which contained 17% Al_2O_3 sustained combustion as loose powders only. The temperature profiles (Figures 9.9 and 9.10) showed an increase in rise-time of the profile and a decrease in T_{max} with an increase in the diluent content.

Figure 9.8 Burning rates for 45% Si/SnO_2 mixtures with various diluents (<53 μm Si, pressed for 1 min at 55 MPa)

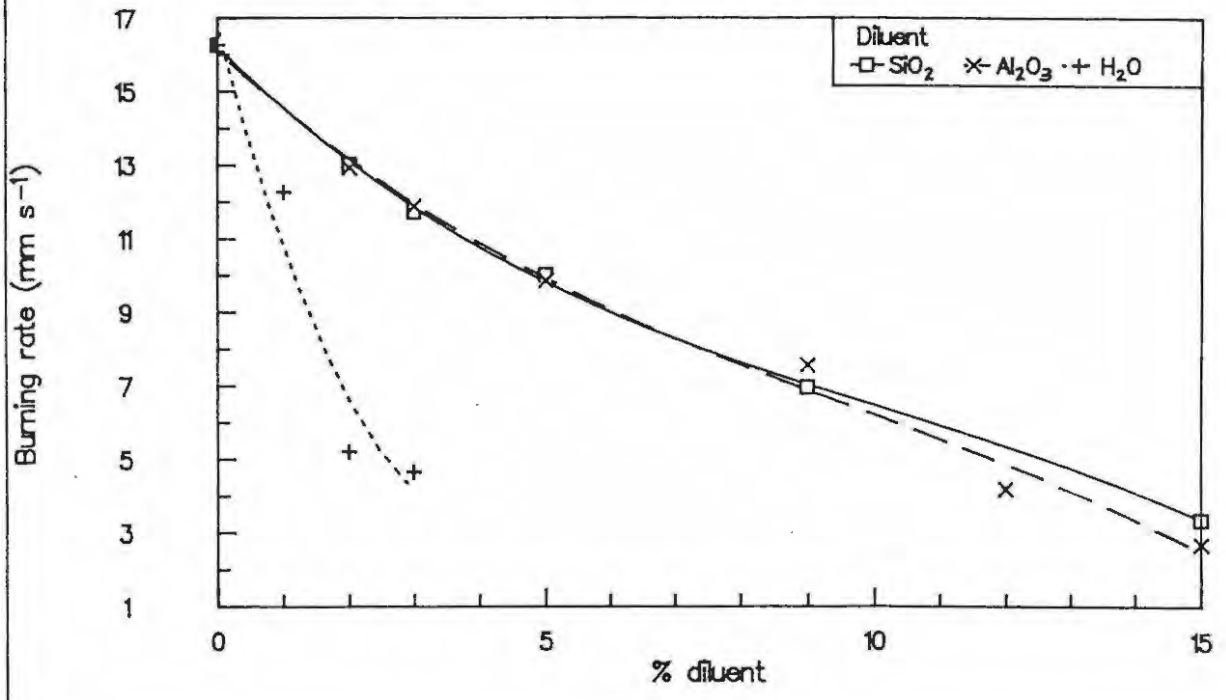

Figure 9.9a Temperature profiles of 45% Si/SnO_2 mixtures with various proportions of SiO_2

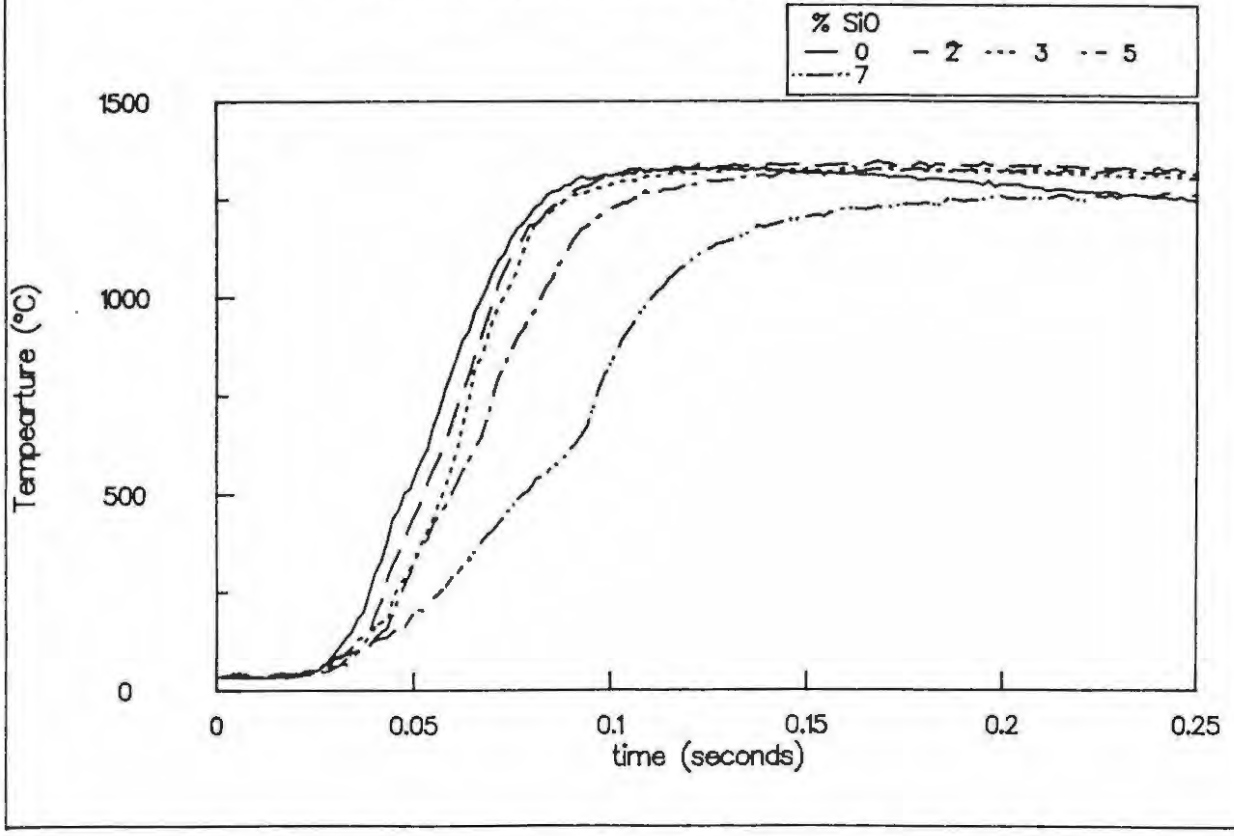

Figure 9.9b Temperature profiles of 45% Si/SnO_2 mixtures with 12 and 15% SiO_2

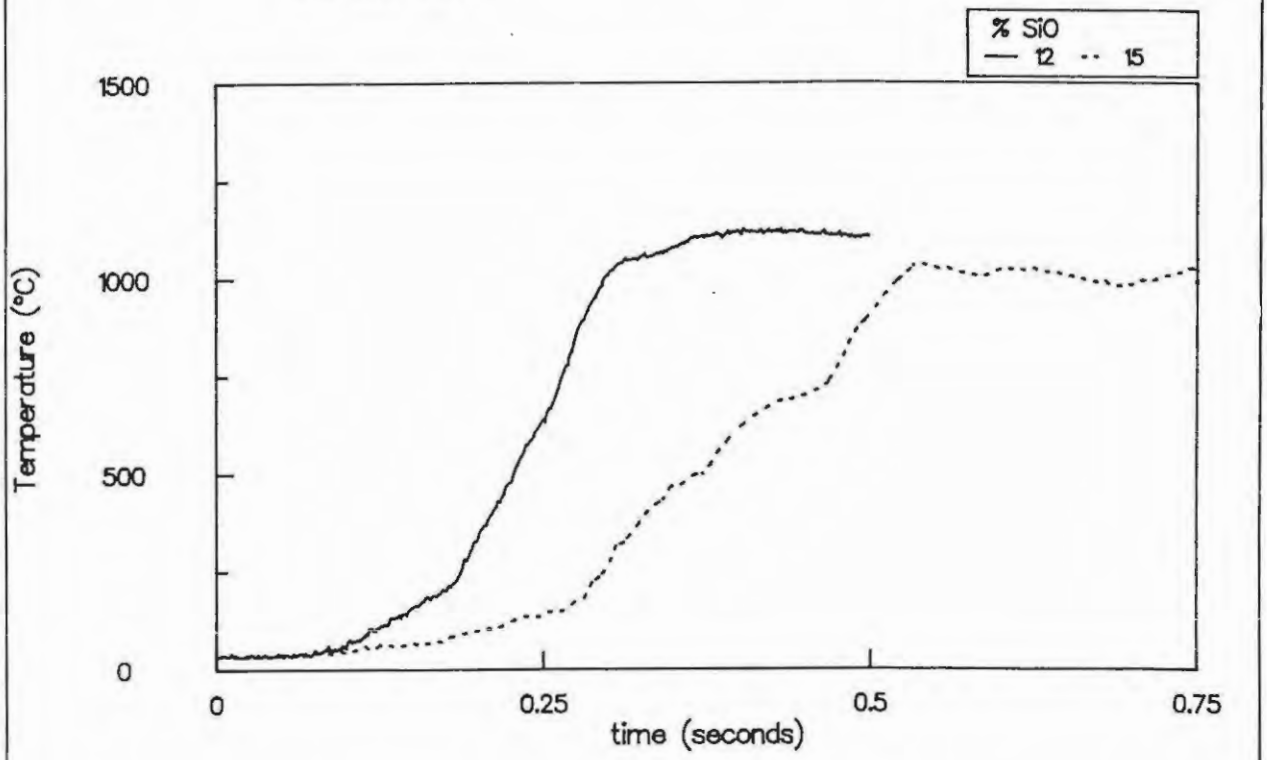

Figure 9.10 Temperature profiles of 45% Si/SnO_2 mixtures with various proportions of Al_2O_3

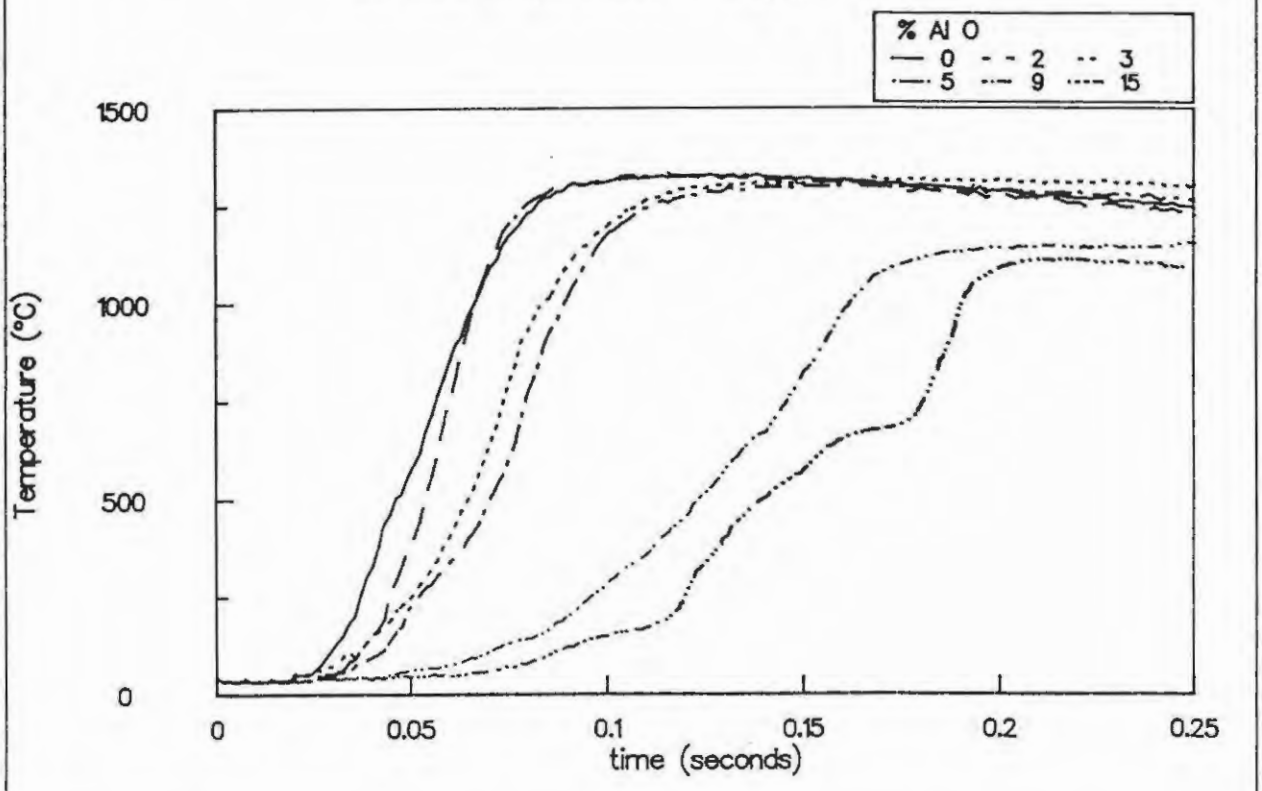

Temperature profiles for 45% Si/SnO_2 with various moisture contents are shown in Figure 9.11. There is an increase in the rise-time with increasing water content, but also, an apparent "induction period" which may be related to mass transport of water. The maximum reaction temperature remained approximately constant for all the mixtures examined. The burning rates (see Table 9.15) decreased with increasing water content to 3% after which burning failed (Figure 9.11).

Figure 9.11 Temperature profiles of 45% Si/SnO_2 mixtures with various moisture contents

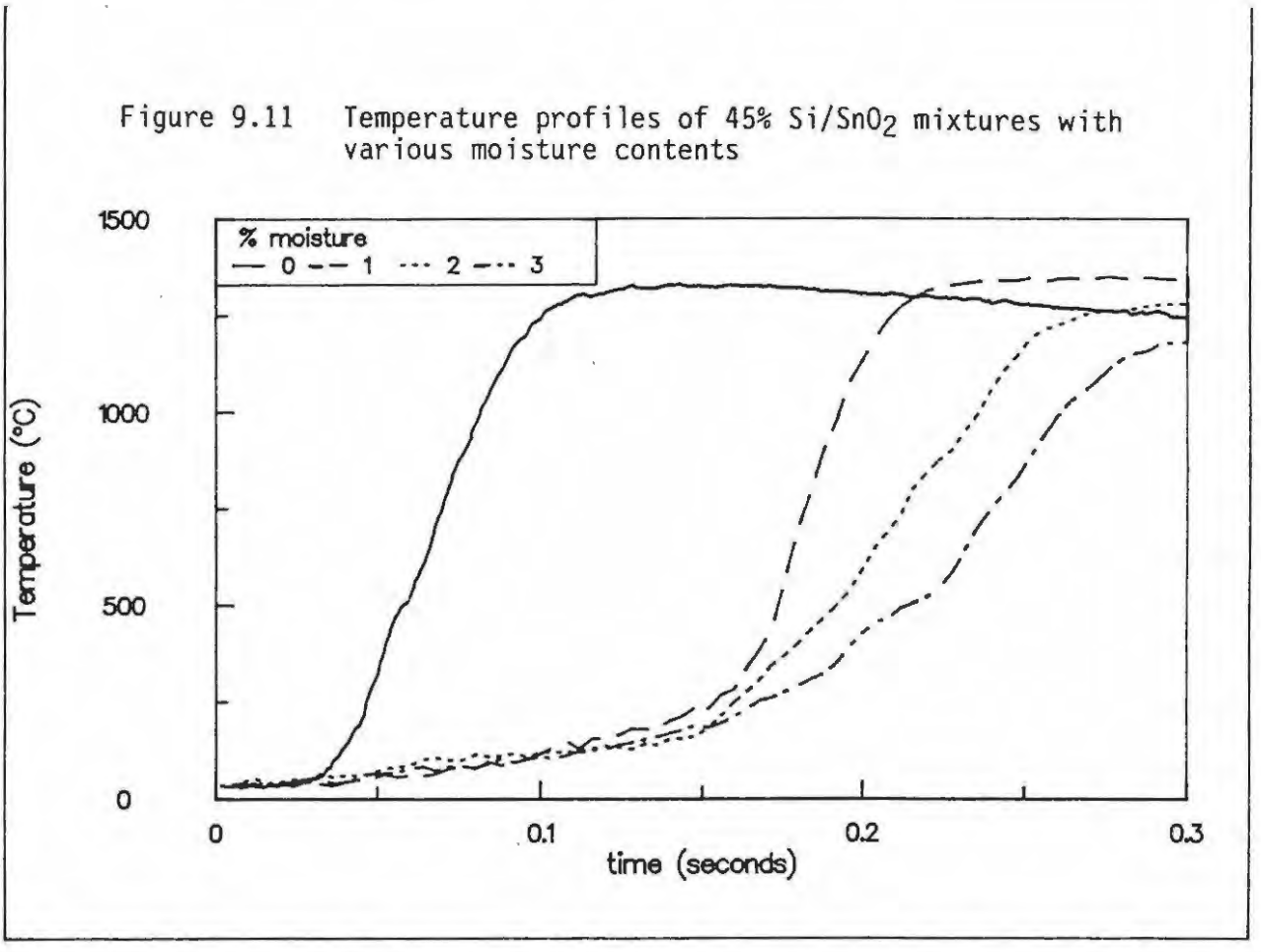

TABLE 9.15

Burning rates of 45% Si/SnO_2 mixtures with various proportions of diluents

% diluent	Density ($g\ cm^{-3}$)	v_{exp} ($mm\ s^{-1}$)	m_{exp} ($g\ s^{-1}$)	T_{max} (°C)
SiO_2				
0	2.44 ± 0.04	16.27 ± 0.28	1.24 ± 0.02	1348 ± 16
2	2.50 ± 0.07	13.03 ± 0.27	1.02 ± 0.06	1336 ± 8
3	2.42 ± 0.02	11.74 ± 0.10	0.89 ± 0.02	1323 ± 8
5	2.44 ± 0.05	10.02 ± 0.20	0.76 ± 0.03	1295 ± 17
9	2.41 ± 0.09	6.96 ± 0.17	0.51 ± 0.02	1239 ± 37
15	2.37 ± 0.06	3.36 ± 0.39	0.27 ± 0.02	1142 ± 40
Al_2O_3				
0	2.44 ± 0.04	16.27 ± 0.28	1.24 ± 0.02	1348 ± 16
2	2.40 ± 0.03	12.93 ± 0.63	0.97 ± 0.03	1347 ± 11
3	2.32 ± 0.04	11.89 ± 0.42	0.88 ± 0.05	1321 ± 27
5	2.31 ± 0.03	9.86 ± 0.13	0.71 ± 0.07	1307 ± 21
7	2.24 ± 0.05	7.55 ± 0.10	0.53 ± 0.01	1267 ± 4
12	2.14 ± 0.09	4.18 ± 0.23	0.29 ± 0.04	1143 ± 21
15	2.06 ± 0.08	2.68 ± 0.12	0.17 ± 0.07	1092 ± 25
H_2O				
0	2.44 ± 0.04	17.50 ± 0.19	1.47 ± 0.02	1352 ± 27
1	2.59 ± 0.03	12.27 ± 0.38	1.07 ± 0.07	1355 ± 8
2	2.90 ± 0.50	5.20 ± 0.76	0.36 ± 0.08	1321 ± 24
3*	1.83 ± 0.04	4.66 ± 0.35	0.29 ± 0.01	1343 ± 11

* Manually pressed

9.5 Comment

Further discussion of the above results, in relation to other binary Si/oxidant systems is given in section 13.

9.6 References

1. R.A.W. Hill, L.E. Sutton, R.B. Temple, A. White and T.L. Cottrell, Research, **3** (1950) 569.
2. R.A.W. Hill and T.L. Cottrell, 4th Symp. Combustion, (1953) 349.
3. T. Boddington, P.G. Laye, J.R.G. Pude and J. Tipping, Comb. Flame, **47** (1982) 235.
4. T. Boddington, P.G. Laye, J.R.G. Pude and J. Tipping, Comb. Flame, **63** (1986) 359.
5. J.H. McLain, "*Pyrotechnics: From the Viewpoint of Solid State Chemistry*", The Franklin Institute Press, Philadelphia, Pennsylvania, 1980.

10. COMBUSTION OF THE Si/KNO_3 SYSTEM

10.1 Effect of composition

Mixtures of 20 to 90% silicon, by mass, and KNO_3 sustained burning on ignition. The burning of all mixtures, especially KNO_3-rich mixtures, was very gassy causing large quantities of unburnt material to be ejected from the pressed sample. The mass loss on burning ranged from 32% (for 30% silicon) to 15% (for 90% silicon) and included unburnt silicon particles, particularly in silicon-rich mixtures. Maximum reaction temperatures were beyond the range of the thermocouple material for all compositions except 90% Si/KNO_3 where a maximum reaction temperature of 1032 ± 53°C was measured. The temperature profiles of some compositions showed a normal thermocouple response up to approximately 400°C. At this temperature the molten KNO_3 (melting point 334°C) causes an acceleration in the reaction. The temperature then rapidly exceeds the melting point of the thermocouple junction.

Temperature profiles obtained for 90% Si/KNO_3 (Figure 10.1) were not very reproducible and the thermoeouple wires were often electrically shorted against the channel due to the movement of the sample during burning. The profiles showed a discontinuity at approximately 450°C, and this temperature corresponds approximately to the melting and onset of decomposition of KNO_3 and may indicate the approximate temperature at which the mixture ignites.

Burning rates for various Si/KNO_3 compositions are listed in Table 10.1. A plot of the burning rate against silicon content (see Figure 10.2) showed that the burning rate increased with an increase in the silicon content of the mixture and maximum burning rate occurred at 85% silicon. Burning rates for 20 and 90% Si/KNO_3 could not be obtained because of erratic burning. Samples of material were ejected from both ends of the channel by the gassy reaction particularly at high silicon contents. The above burning rate curve is similar to that reported in the literature (1,2). Previous workers (1,2) reported a maximum burning rate at ~80% silicon in closed systems.

The combustion products were very hygroscopic and quickly formed a strongly alkaline residue on being exposed to the atmosphere. The infrared spectra showed the strong presence of SiO_2, CO_3^{2-}, HCO_3^- and OH^-. These ions probably arise from a reaction between K_2O, CO_2 and atmospheric moisture after the residues have cooled. XRD patterns showed only the presence of unreacted silicon and traces of KNO_3 and K_2CO_3. The intense absorption bands for SiO_2 in the infrared speetra indicated that the formation of amorphous SiO_2 was extensive. The following reaction is suggested as a possibility:

$$2Si(s) + 2KNO_3(l) \rightarrow 2SiO_2(s) + K_2O(s) + N_2(g) + 0.5O_2(g) \quad ...(10.1)$$

The change in enthalpy (calculated from standard enthalpies of formation) for the above reaction is -590.7 kJ $(mol\ Si)^{-1}$. The stoichiometric point occurs at 25% silicon (calculated heat output is 4.38 kJ (g of

Figure 10.1 Temperature profiles of 90% Si/KNO_3 mixtures

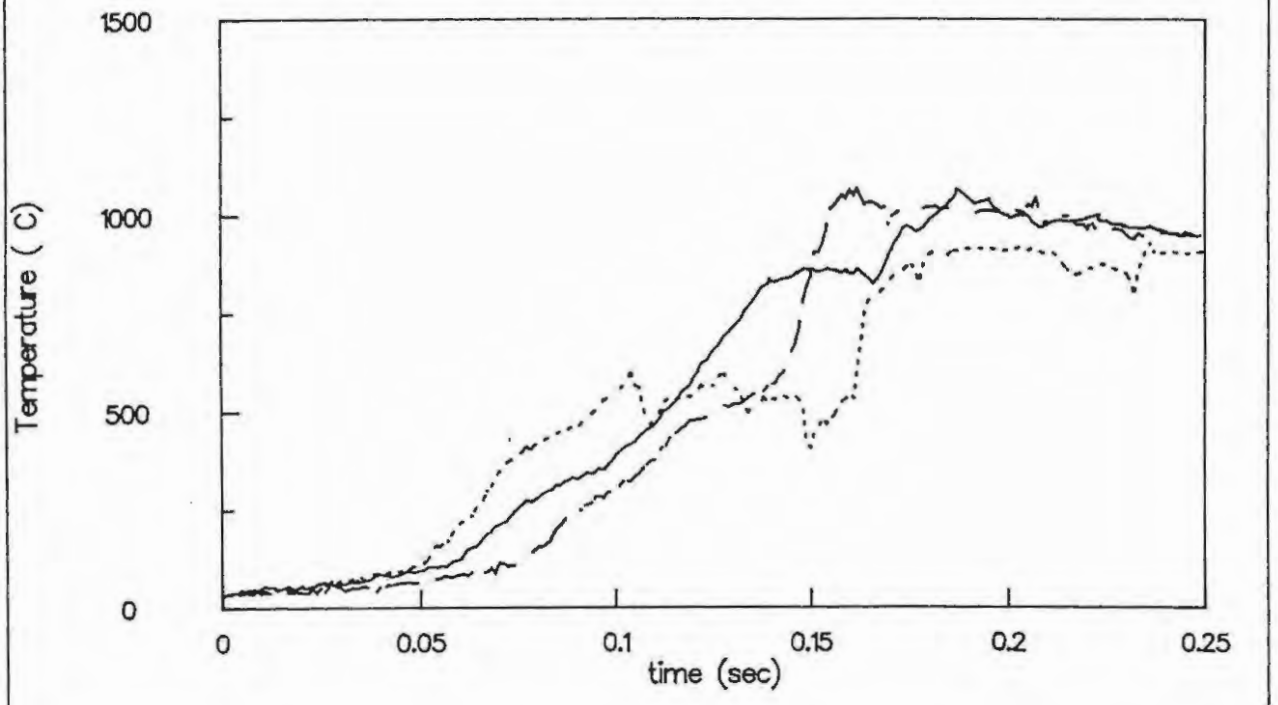

Figure 10.2 Burning rates for the Si/KNO_3 system (<53 μm Si pressed for 1 min at 55 MPa

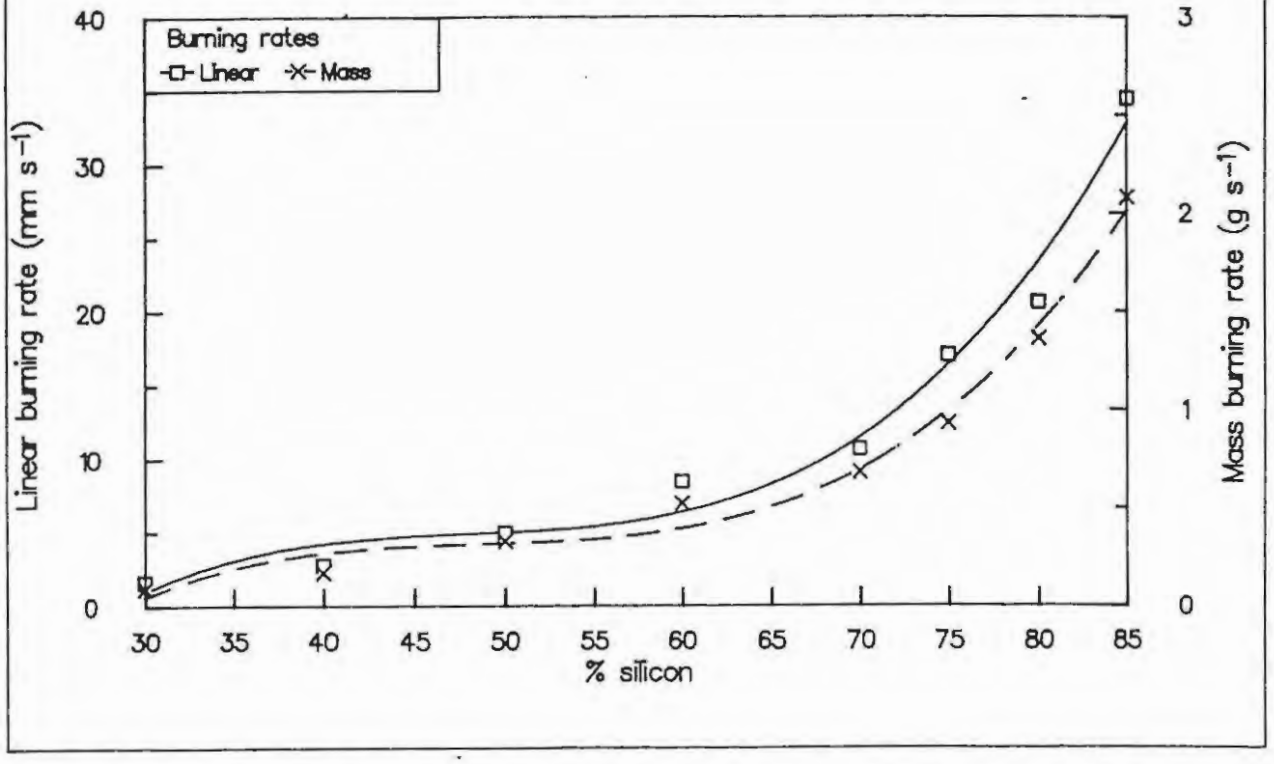

TABLE 10.1

Burning rates for the Si/KNO_3 system

% Si	Density (g cm^{-3})	Porosity factor ε	v_{exp} (mm s^{-1})	m_{exp} (g s^{-1})
20	1.76 ± 0.02	0.18	-	-
30	1.71 ± 0.06	0.21	1.65 ± 0.21	0.09 ± 0.04
40	1.77 ± 0.04	0.20	2.78 ± 0.16	0.17 ± 0.06
50	1.74 ± 0.02	0.22	4.96 ± 0.39	0.33 ± 0.05
60	1.68 ± 0.07	0.25	8.43 ± 1.00	0.52 ± 0.08
70	1.67 ± 0.10	0.26	10.68 ± 1.54	0.68 ± 0.03
75	1.60 ± 0.04	0.30	17.05 ± 1.25	0.93 ± 0.06
80	1.57 ± 0.05	0.31	20.63 ± 2.26	1.36 ± 0.09
85	1.59 ± 0.09	0.31	34.47 ± 3.33	2.08 ± 0.41
90	1.57 ± 0.04	0.32	-	-

mixture)$^{-1}$). Previous workers have suggested (1) that the reaction

$$3Si(s) + 2KNO_3(l) \rightarrow 3SiO_2(s) + 2K(s) + N_2(g) \quad ...(10.2)$$

(expected ΔH = -574.5 kJ (mol Si)$^{-1}$, stoichiometric composition is 31.6% Si and the calculated heat output is 5.98 kJ (g mixture)$^{-1}$) is the predominant reaction which occurs during combustion. The formation of metallic potassium is unlikely since any potassium formed is more likely to undergo further oxidation under the extreme oxidising conditions of burning of pyrotechnic mixtures. Scanning electron micrographs of the combustion residues did not provide much information. The samples rapidly absorbed atmospheric water and formed concentrated solutions.

The calculated and experimental enthalpies of combustion of selected mixtures are listed in Table 10.2. Also shown in Table 10.2 are the approximate maximum temperatures calculated from the equation $U_{ad} = q/c$ where q is taken as equal to $-\Delta H_{exp}$. Values of the heat capacities at 298 K are c(Si) = 0.712 J K^{-1} g^{-1} and c(KNO_3(s)) = 0.952 J K^{-1} g^{-1}. Both values will increase with temperature and KNO_3 melts at 607 K. A values was not found for the heat capacity of KNO_3(l), but if it is assumed to be similar to that of K_2SO_4(l), the value at 298 K is 1.15 J K^{-1} g^{-1} (3). The value of Si(s) increases by 35% to 0.961 J K^{-1} g^{-1} at 1600 K. Allowing a similar increase in the value of KNO_3(l) for increasing temperature, a value of 1.55 J K^{-1} g^{-1} was estimated. Using these values, the heat capacities of the mixtures were estimated as given in Table 10.2.

TABLE 10.2

Enthalpies of combustion for the Si/KNO_3 system

% Si	c ($J\ K^{-1}\ g^{-1}$)	$-\Delta H_{exp}$ ($kJ\ g^{-1}$)	$-\Delta H_{calc}$ ($kJ\ g^{-1}$)	Predicted U_{ad} (K)
20	1.43	4.35 ± 0.06	4.21	3040
30	-	-	4.09	-
40	1.32	4.14 ± 0.04	3.80	3140
50	-	-	2.92	-
60	1.20	2.54 ± 0.06	2.34	2117
70	-	-	1.75	-
80	1.08	2.10 ± 0.02	1.17	1944

The maximum enthalpy of combustion occurred at ~20% Si and decreased with increasing silicon. Similar trends were reported (4). The predicted U_{ad} values are probably far from accurate, but the trend is correct since for the only profiles obtained (90% Si), U_{ad} was about 900 K and all other compositions were very much hotter burning.

10.2 Effect of compaction

To examine the effect of density on the burning rate, two compositions consisting of 40% Si and 80% Si by mass were compacted under various loads and burnt. The former composition is very gassy (~30% mass loss on burning) while the latter is slightly less gassy (21% mass loss on burning). Temperature profiles could not be recorded for either mixture. For the 40% Si/KNO_3 mixtures pressed up to 10 MPa, large sample masses were ejected from the unburnt end of the channel. Samples pressed at 275 MPa failed to sustain burning. The burning of 80% Si/KNO_3 showed similar characteristics. The burning rates for these two compositions at various densities are listed in Table 10.3.

The burning rates for 40% Si/KNO_3 showed a slight decrease with increasing density. Burning rates for 80% Si/KNO_3 pressed to various densities, were similar up to 55 MPa. At 110 MPa a dramatic decrease in the burning rate was observed. Burning failed when the 80% Si/KNO_3 was pressed at 275 MPa.

TABLE 10.3

Burning rates of 40 and 85% Si/KNO_3 mixtures at various densities

Load (MPa)	Density ($g\ cm^{-3}$)	Porosity factor ε	v_{exp} ($mm\ s^{-1}$)	m_{exp} ($g\ s^{-1}$)
(a) 40% Si/KNO_3				
Hand packed	1.50 ± 0.47	0.32	2.95 ± 0.10	0.18 ± 0.02
28 (0.5 tons	1.55 ± 0.04	0.30	2.94 ± 0.23	0.17 ± 0.09
55 (1 ton)	1.77 ± 0.04	0.20	2.75 ± 0.16	0.17 ± 0.06
110 (2 tons)	1.88 ± 0.09	0.15	2.71 ± 0.12	0.16 ± 0.03
275 (5 tons)	1.94 ± 0.10	0.12	BURNING	FAILED
(b) 80% Si/KNO_3				
Hand packed	1.50 ± 0.47	0.34	19.81 ± 1.01	1.16 ± 0.02
28 (0.5 tons	1.55 ± 0.29	0.32	20.45 ± 1.23	1.39 ± 0.09
55 (1 ton)	1.58 ± 0.21	0.30	21.50 ± 2.31	1.39 ± 0.11
110 (2 tons)	1.78 ± 0.09	0.22	6.88 ± 0.73	0.37 ± 0.03
275 (5 tons)	1.88 ± 0.03	0.17	BURNING	FAILED

10.3 **Effective of additives**

SiO_2 was the only diluent added to the 80% Si/KNO_3 mixtures and the burning rates are given in Table 10.4.

Burning could be sustained when up to 60% SiO_2 by mass was added to the 80% Si/KNO_3 mixtures. The burning rates decreased as the proportion of SiO_2 was increased. The mixtures containing upto 60% SiO_2 were still very gassy and temperature profiles could not be recorded.

The burning rates of a 40% Si/KNO_3 mixture at various moisture contents are listed in Table 10.4. Burning was not sustained for mixtures with greater than 3% moisture. The burning rates for mixtures containing up to 2% moisture were similar and a decrease was noted at 3% moisture.

TABLE 10.4

Burning rates of 80% Si/KNO_2 mixtures with various proportions of SiO_2

% additive	Density (g cm^{-3})	v_{exp} mm s^{-1})	m_{exp} (g s^{-1})
SiO_2			
0	1.57 ± 0.05	20.63 ± 2.26	1.36 ± 0.09
10	1.58 ± 0.07	12.65 ± 0.29	0.67 ± 0.05
20	1.34 ± 0.02	6.11 ± 0.18	0.28 ± 0.02
60	1.13 ± 0.05	1.62 ± 0.20	0.07 ± 0.01
H_2O			
0	1.76 ± 0.09	2.85 ± 0.41	0.19 ± 0.02
1	1.79 ± 0.06	2.80 ± 0.28	0.18 ± 0.03
2	1.78 ± 0.08	2.78 ± 0.32	0.18 ± 0.02
3	1.75 ± 0.08	2.15 ± 0.42	0.13 ± 0.03

10.4 Kinetic aspects

The only profiles obtained were for 90% Si/KNO_3 (Figure 10.1) and these were too irregular to warrant kinetic analysis.

10.5 Comments

The above results are further discussed in Section 13.

10.6 References

1. G. Krishnamohan, E.M. Kurian and K.R.K. Rao, 8th Int. Pyro. Sem., (1982) 404.
2. T.T.L. Leeuw, Report No. RN 0861/A, AECI Explosives and Chemicals Ltd., 1988.
3. O. Kubaschewski, E.L. Evans and C.B. Alcock, "*Metallurgical Thermochemistry*", 4th Edition, Pergamon Press, 1967.
4. T.T.L. Leeuw, Report No. RN 0839/A, AECI Explosives and Chemicals Ltd., 1988.

11. COMBUSTION OF THE TERNARY PYROTECHNIC SYSTEMS

11.1 Systems with two fuels

11.1.1 *Ferrosilicon*

Mixtures were prepared in which various proportions of silicon were replaced by $FeSi_7$ such that the fuel/oxidant mass ratio was kept constant. The burning rates for the resulting binary and ternary mixtures are shown in Table 11.1.

TABLE 11.1

Burning rates of ternary systems containing various proportions of $FeSi_7$ as replacement fuel

% Si	% $FeSi_7$	Porosity factor ε	Density (g cm^{-3})	v_{exp} (mm s^{-1})	m_{exp} (g s^{-1})	T_{max} (°C)
(a) 40% Si/Sb_2O_3						
40	0	0.39	2.58 ± 0.10	8.77 ± 0.16	0.72 ± 0.03	1329 ± 9
35	5	0.42	2.54 ± 0.04	8.42 ± 0.34	0.70 ± 0.01	1361 ± 16
30	10	0.46	2.49 ± 0.07	7.10 ± 0.25	0.54 ± 0.06	1348 ± 8
20	20	0.47	2.62 ± 0.07	5.98 ± 0.16	0.51 ± 0.03	1381 ± 12
10	30	0.51	2.63 ± 0.02	5.07 ± 0.17	0.43 ± 0.01	1349 ± 13
0	40	0.53	2.69 ± 0.07	4.51 ± 0.07	0.38 ± 0.01	1363 ± 11
(b) 35% Si/Fe_2O_3						
35	0	0.51	1.96 ± 0.01	5.01 ± 0.15	0.30 ± 0.01	1178 ± 16
30	5	0.51	2.03 ± 0.02	5.12 ± 0.13	0.31 ± 0.01	1278 ± 12
25	10	0.53	2.04 ± 0.05	5.17 ± 0.11	0.36 ± 0.01	1288 ± 10
15	20	0.56	2.06 ± 0.04	5.64 ± 0.19	0.40 ± 0.01	1215 ± 20
5	30	0.57	2.17 ± 0.04	5.70 ± 0.10	0.41 ± 0.01	1245 ± 32
0	35	0.58	2.21 ± 0.03	5.91 ± 0.10	0.43 ± 0.01	1241 ± 21

TABLE 11.1 (cont)

% Si	% $FeSi_7$	Porosity factor ε	Density ($g\ cm^{-3}$)	v_{exp} ($mm\ s^{-1}$)	m_{exp} ($g\ s^{-1}$)	T_{max} (°C)
(c) 45% Si/SnO_2						
45	0	0.57	2.14 ± 0.06	16.10 ± 1.25	1.10 ± 0.05	1319 ± 19
40	5	0.58	2.17 ± 0.07	15.41 ± 0.95	1.08 ± 0.07	1314 ± 36
35	10	0.58	2.25 ± 0.04	13.61 ± 0.98	1.04 ± 0.04	1349 ± 7
25	20	0.59	2.38 ± 0.04	13.47 ± 0.25	1.04 ± 0.02	1322 ± 21
15	30	0.62	2.36 ± 0.02	12.59 ± 0.27	1.03 ± 0.02	1347 ± 18
5	40	0.63	2.43 ± 0.06	12.47 ± 0.54	1.00 ± 0.03	1352 ± 12
0	45	0.63	2.46 ± 0.08	12.18 ± 0.63	0.92 ± 0.01	1326 ± 19
(d) 40% Si/KNO_3						
40	0	0.20	1.77 ± 0.04	9.11 ± 0.17	0.72 ± 0.02	tc shorted
30	10	0.19	1.79 ± 0.03	10.84 ± 0.14	0.77 ± 0.02	tc shorted
20	20	0.21	1.75 ± 0.03	12.16 ± 0.21	1.02 ± 0.07	tc shorted
10	30	0.22	1.72 ± 0.04	15.71 ± 0.08	1.09 ± 0.21	tc shorted
0	40	0.23	1.71 ± 0.02	18.66 ± 0.41	1.29 ± 0.07	tc shorted

The burning of mixtures which contained $FeSi_7$ was generally gassy. Temperature profiles were obtained for the Sb_2O_3, SnO_2 and Fe_2O_3 systems but not for the KNO_3 system because of a combination of excessive gassiness and high reaction-temperatures.

The temperature profiles for the 40% Si/Sb_2O_3 with various increments of $FeSi_7$ are shown in Figure 11.1. Temperature profiles showed a decrease in the slope of the rise region and an increase in the induction time with increasing $FeSi_7$. There is an increase in the rise-time to T_{max} with increasing $FeSi_7$ content. Both linear and mass burning rates decreased from 8.77 (Si as fuel only) to 4.51 mm s^{-1} ($FeSi_7$ fuel only) with increasing $FeSi_7$. Maximum temperatures were unchanged.

XRD patterns of the combustion residue of the 40% $FeSi_7/Sb_2O_3$ mixture showed the presence of unreacted $FeSi_7$ and Si. Sb and possibly Fe_2O_3 were also among the combustion products identified.

The temperature profiles for ternary systems with Fe_2O_3 as oxidant (mass percent fuel was 35%) are shown in Figure 11.2. A decrease in the rise-time to T_{max} for each of the mixtures which contained $FeSi_7$ was observed and T_{max} (~1330°C) is approximately 100°C higher than the corresponding binary systems. The temperature profiles still appear to be complex but not to the same degree as when Si alone is the fuel. The burning rates increased only slightly with increasing $FeSi_7$. The XRD pattern for the combustion residue of a 35% $FeSi_7/Fe_2O_3$ mixture was identical to that of the corresponding 35% Si/Fe_2O_3 mixture.

Figure 11.1 Temperature profiles for the $Si/FeSi_7/Sb_2O_3$ system

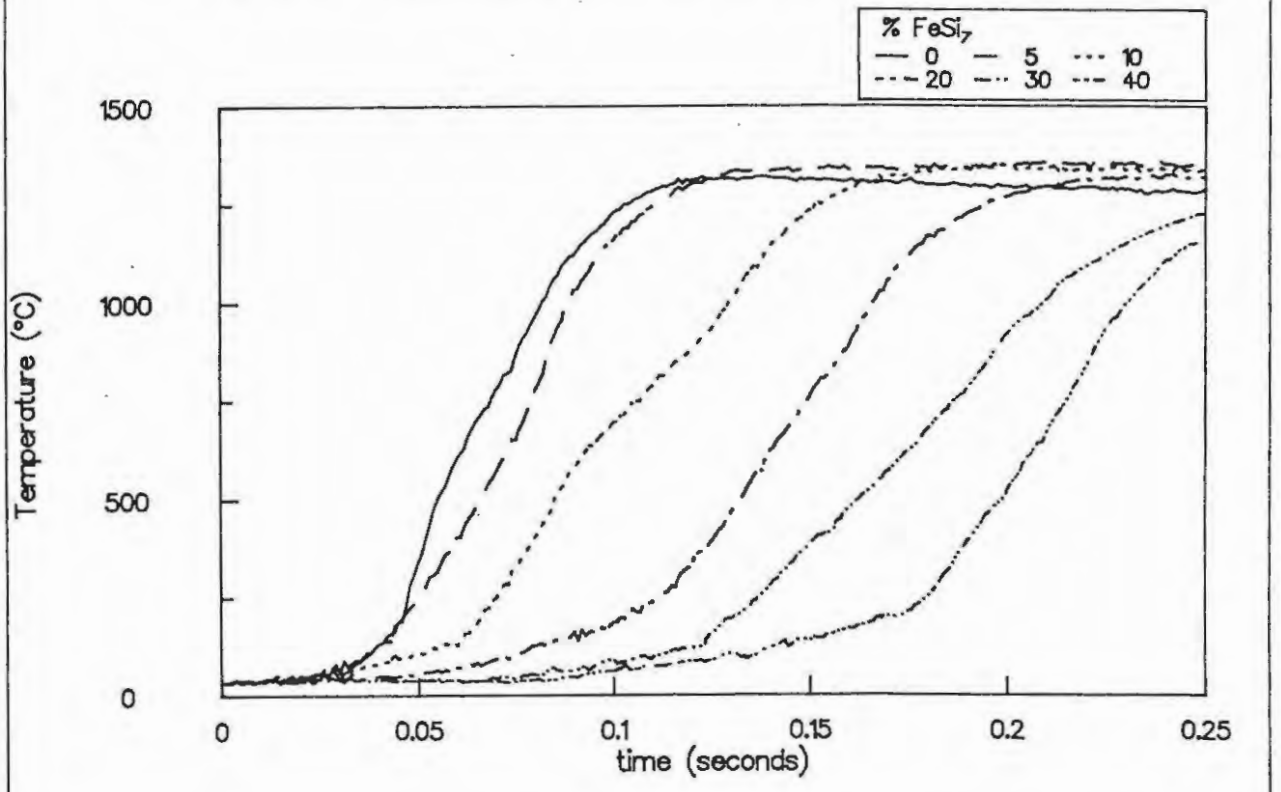

Figure 11.2 Temperature profiles for the $Si/FeSi_7/Fe_2O_3$ system

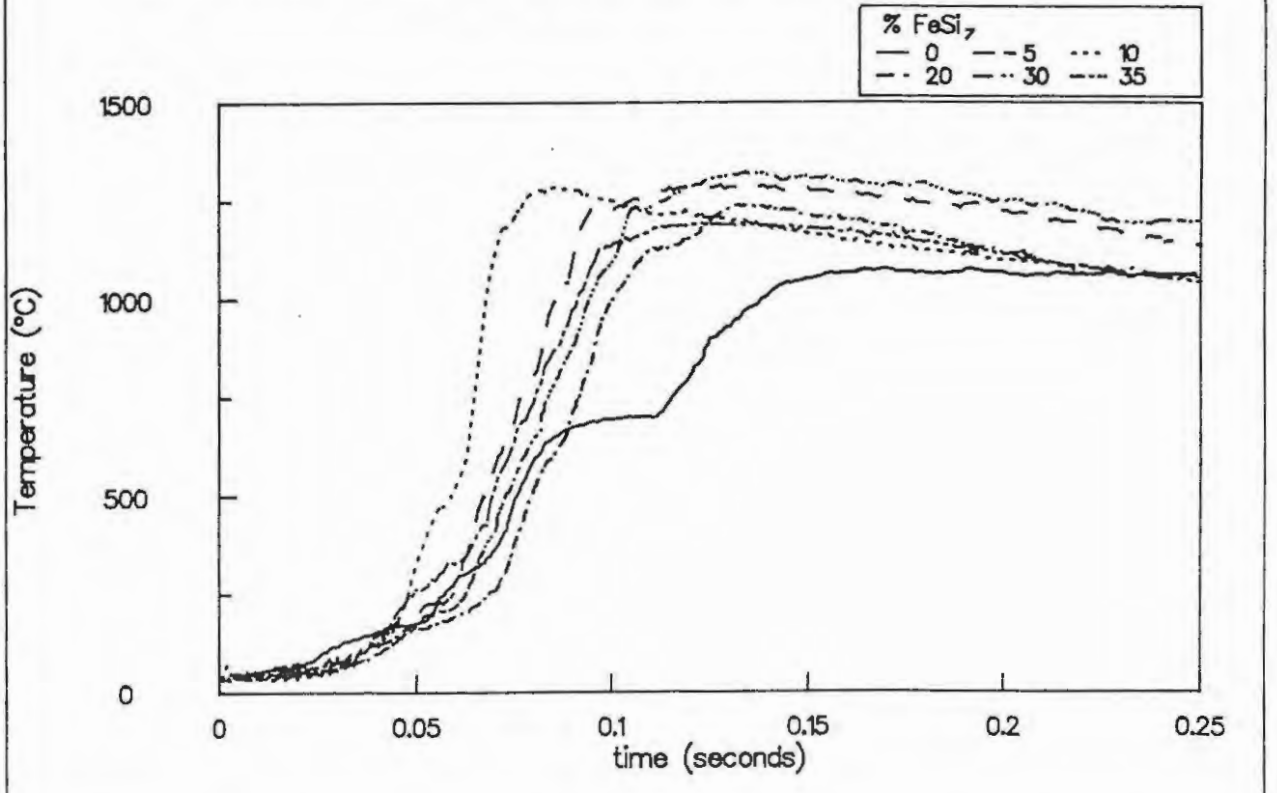

For the Si/$FeSi_7$/SnO_2 system (45% fuel by mass), profiles (see Figure 11.3) were little changed with increasing $FeSi_7$. Burning rates decreased slightly with $FeSi_7$ increasing up to 10%, but thereafter were similar. The XRD pattern for the combustion residue of a 45% $FeSi_7$/SnO_2 mixture showed mainly the presence of unreacted $FeSi_7$, Si and SnO_2.

The burning rates for the KNO_3 system with Si and $FeSi_7$ increased with increasing $FeSi_7$. Burning was gassy and the unburnt mixture was ejected from the channel. Temperature profiles could not be recorded because of excessive gassiness during burning. Infrared spectroscopy and XRD patterns of the combustion residues (40% $FeSi_7$/KNO_3) mixture were similar to those observed with Si as the fuel.

Thus the general tendency, except for the Si/KNO_3 system, is for substitution of $FeSi_7$ for Si to decrease the burning rate. Again the question arises as to whether this is a chemical effect resulting from the presence of Fe in the fuel or, more simply, from the changes in the physical contact arising from different size or shaped particles. Additional experiments on Fe/Si/oxidant systems might provide addtional insights.

11.1.2 *Calcium silicide*

Burning studies were also carried out on systems in which the Si was partially replaced by various proportions of $CaSi_2$. The burning of all mixtures which contained $CaSi_2$ was gassy and thermocouple response was lost for mixtures beyond 10% $CaSi_2$. The burning rates for various mixtures are listed in Table 11.2.

TABLE 11.2

Burning rates of ternary systems containing various proportions of fuels

% $CaSi_2$	Density (g cm^{-3})	ε	v_{exp} (mm s^{-1})	m_{exp} (g s^{-1})	T_{max} (°C)
40% Si/Sb_2O_3					
0	2.25 ± 0.11	0.47	9.11 ± 0.84	0.72 ± 0.06	1329 ± 9
5	2.51 ± 0.01	0.42	10.16 ± 0.96	0.87 ± 0.02	1356 ± 7
10	2.68 ± 0.03	0.40	10.38 ± 1.19	0.89 ± 0.05	1224 ± 15
20	2.74 ± 0.04	0.42	10.63 ± 0.87	0.95 ± 0.04	tc shorted
30	3.03 ± 0.07	0.39	12.40 ± 0.93	1.19 ± 0.04	tc shorted
40	2.95 ± 0.04	0.43	16.85 ± 1.23	1.58 ± 0.06	tc shorted

Figure 11.3 Temperature profiles for the $Si/FeSi_7/SnO_2$ system

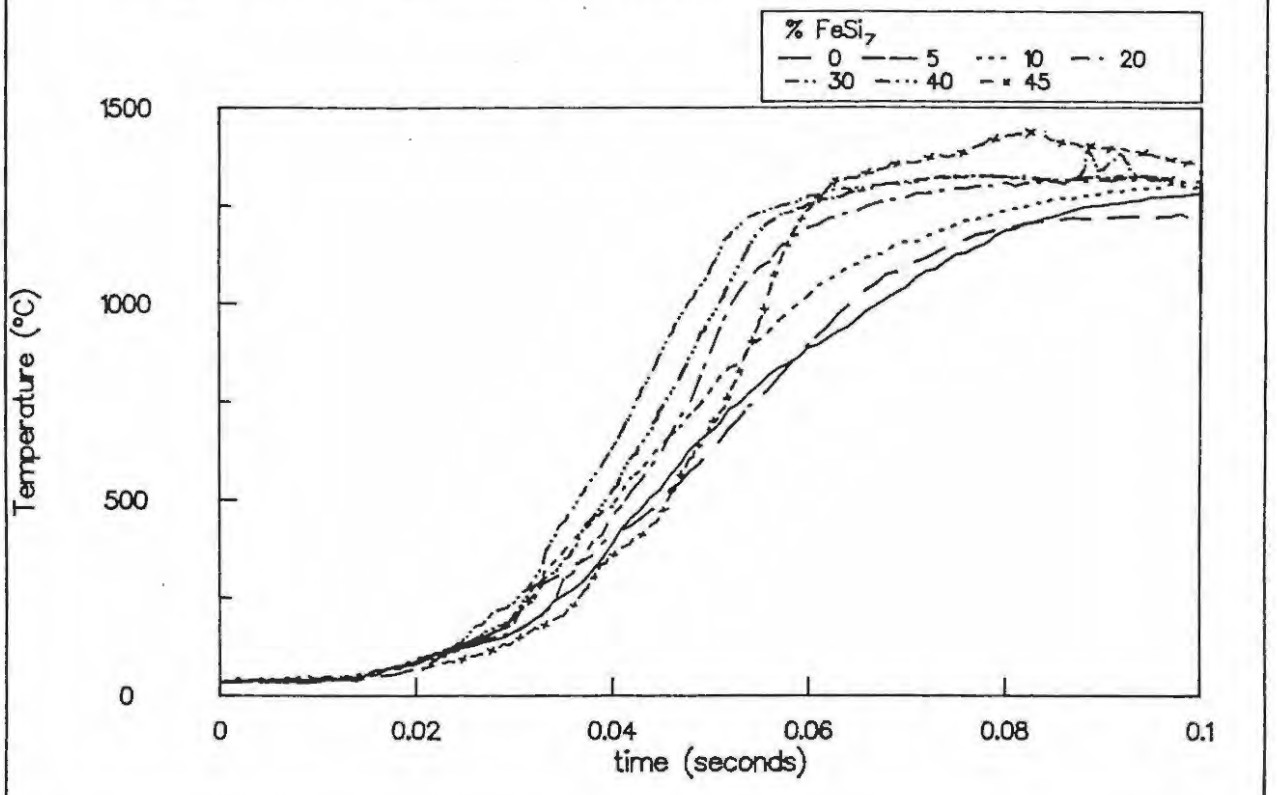

Figure 11.4 Temperature profiles for the $Si/CaSi_2/Sb_2O_3$ system

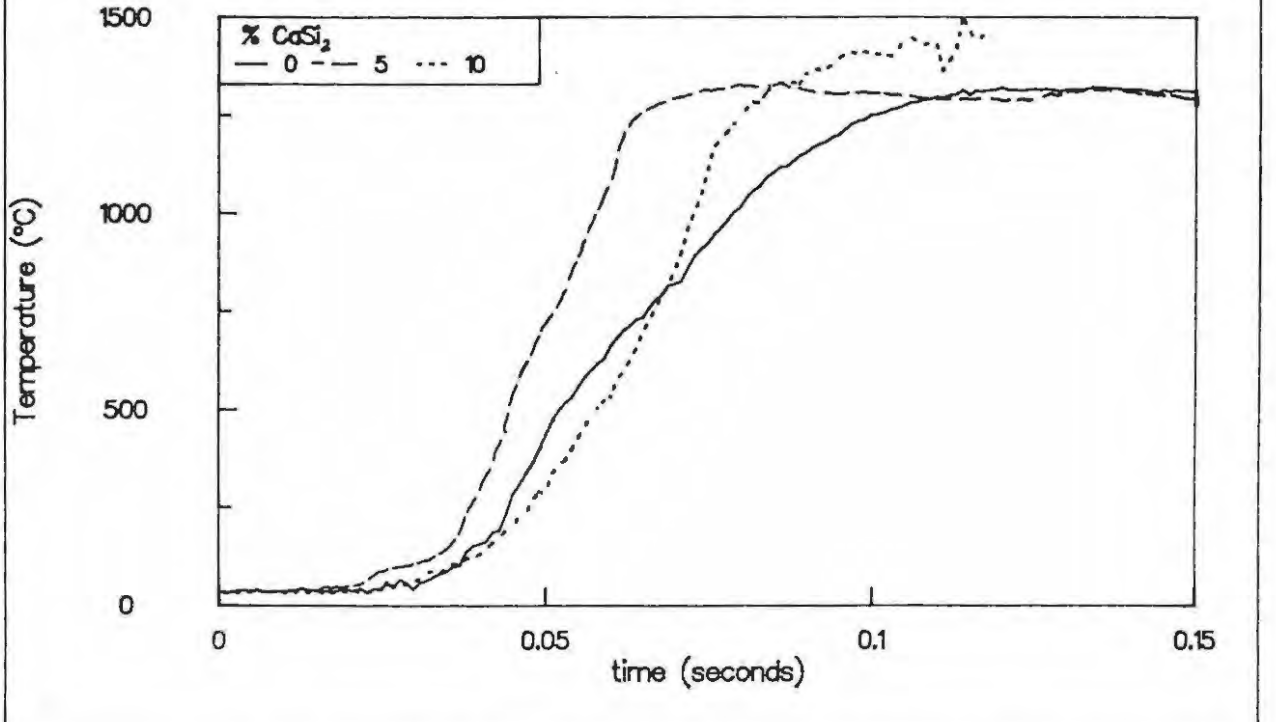

TABLE 11.2 (cont)

% $CaSi_2$	Density (g cm^{-3})	ε	v_{exp} (mm s^{-1})	m_{exp} (g s^{-1})	T_{max} (°C)
35% Si/Fe_2O_3					
0	2.10 ± 0.02	0.52	5.64 ± 0.09	0.30 ± 0.02	1210 ± 16
5	1.85 ± 0.03	0.59	9.23 ± 0.31	0.44 ± 0.02	1309 ± 30
10	1.66 ± 0.01	0.64	8.52 ± 0.15	0.40 ± 0.03	1369 ± 14
30	1.68 ± 0.02	0.67	6.91 ± 0.32	0.38 ± 0.03	TC shorted
35	1.76 ± 0.02	0.66	5.73 ± 0.27	0.32 ± 0.02	TC shorted
45% Si/SnO_2					
0	2.55 ± 0.01	0.48	17.05 ± 0.37	1.39 ± 0.05	1319 ± 19
5	2.46 ± 0.01	0.51	14.59 ± 0.35	1.27 ± 0.05	1363 ± 10
10	2.55 ± 0.09	0.50	13.07 ± 0.07	1.17 ± 0.04	1262 ± 35
30	2.49 ± 0.05	0.56	11.32 ± 0.21	0.79 ± 0.04	tc shorted
45	2.59 ± 0.07	0.57	5.93 ± 0.13	0.50 ± 0.03	tc shorted
40% Si/KNO_3					
0	1.77 ± 0.03	0.20	2.78 ± 0.13	0.17 ± 0.03	tc shorted
10	1.84 ± 0.05	0.25	3.86 ± 0.07	0.22 ± 0.04	tc shorted
20	1.81 ± 0.04	0.33	3.72 ± 0.09	0.24 ± 0.02	tc shorted
30	1.76 ± 0.03	0.40	5.11 ± 0.10	0.27 ± 0.05	tc shorted
40	2.08 ± 0.01	0.35	5.94 ± 0.19	0.28 ± 0.03	tc shorted

The burning rates for Si/Sb_2O_3 mixtures with various proportions of $CaSi_2$ generally increased with increasing proportions of the additive. Mixtures which contained between 5 and 20% $CaSi_2$ had approximately similar burning rates. The temperature profiles (Figure 11.4) were not very reproducible and do not show any clear trends. From the XRD patterns of the combustion residues, the presence of unreacted $CaSi_2$, Sb and traces of Sb_2O_3 amongst other minor unidentified patterns were observed. Only the presence of SiO_2 could be detected in the infrared spectrum of the residues.

For the two-fuel system in which Fe_2O_3 was the oxidant, the burning rates initially increased to a maximum at 10% $CaSi_2$ (25% Si) and then decreased with increasing $CaSi_2$ content. The temperature profiles show a fairly smooth rise to maximum temperature (Figure 11.5). T_{max} generally increased with increasing $CaSi_2$. Temperature profiles could not be recorded for mixtures containing >10% $CaSi_2$. The combustion products identified from the most intense XRD patterns, were Fe, Fe_2O_3, $CaSi_2$ and possibly Si and FeO. Infrared spectra showed the strong presence of SiO_2.

By replacing Si with various quantities of $CaSi_2$ in a 45% Si/SnO_2 mixture, the burning rate decreased from ~17 to ~6 mm s^{-1}. The temperatures profiles (see Figure 11.6) showed an increase in the induction time with increasing $CaSi_2$ and a decrease in T_{max}. The slopes in the rise portion of the temperature profile remained approximately unchanged. The profile of the mixture containing 10% $CaSi_2$ had a lower maximum temperature and also showed exothermic processes beyond T_{max} possibly due to solidification of molten products. The combustion residue was shown to consist of SiO_2, Sn and unreacted SnO_2. Unidentified XRD patterns were probably due to formation of silicates.

The burning rate of a 40% Si/KNO_3 mixture increased on replacing various proportions of Si with $CaSi_2$ while keeping the fuel ratio constant. These mixtures were very gassy and appeared to burn at a higher temperature than the corresponding silicon containing mixtures. The infrared spectrum showed the strong presence of SiO_2 and only the presence of $CaSi_2$ could be deteeted in the XRD patterns. Other relatively minor peaks correspond to K_2CO_3, which was probably formed on exposing the combustion residue to air.

In contrast to the effects of $FeSi_7$, substitution of $CaSi_2$ for Si in all the systems, except the Si/SnO_2 system, tended to increase the burning rate. More information on the reactivity of silicides relative to silicon would be valuable as the apparent sequence would be $CaSi_2$ > Si > $FeSi_7$.

11.2 **Systems with two oxidants**

Various ternary mixtures consisting of silicon and two oxidants were prepared in which a proportion of one oxidant was replaced by increments of a second oxidant while keeping the fuel/oxidant ratio constant. The oxidants used were the four selected for this study, i.e. Sb_2O_3, Fe_2O_3, SnO_2 and KNO_3. The ternary mixtures were burnt in the usual manner and the burning rates obtained are listed in Table 11.3. The temperature profiles for the ternary systems are shown in Figures 11.7 to 11.9.

The addition of Fe_2O_3 to the 40% Si/SnO_2 binary mixture decreased the burning rate of the mixture from approximately 17 mm s^{-1} (at 60% SnO_2) to 4.5 mm s^{-1} (at 0% SnO_2). The maximum temperatures for the various mixtures were similar. Temperature profiles showed a smooth rise to maximum temperature for 0% Fe_2O_3 mixture but became more complex, as expected, on increasing the Fe_2O_3 content to 60% (see Figure 11.7). Fe_2O_3 has been reported (1) to act as a burning rate retardant when added in small amounts to the Si/Pb_3O_4/$KClO_4$ system (Section 2.3).

Figure 11.5 Temperature profiles for the $Si/CaSi_2/Fe_2O_3$ system

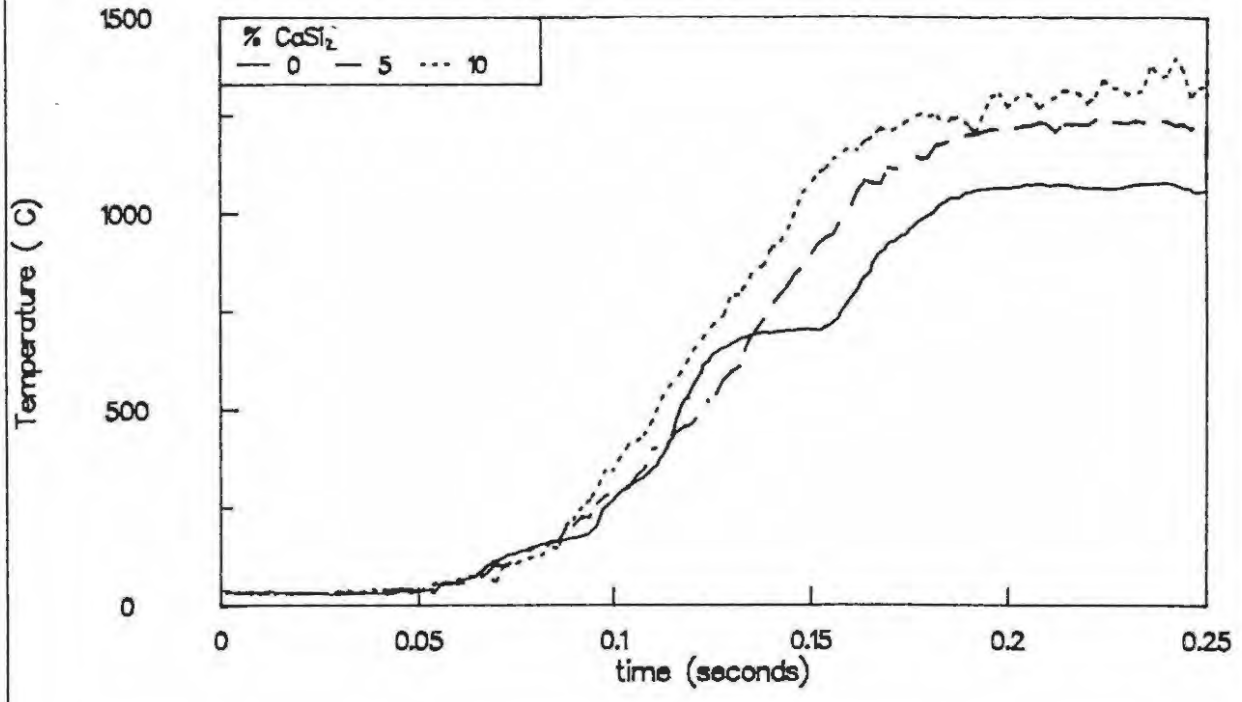

Figure 11.6 Temperature profiles of the $Si/CaSi_2/SnO_2$ system

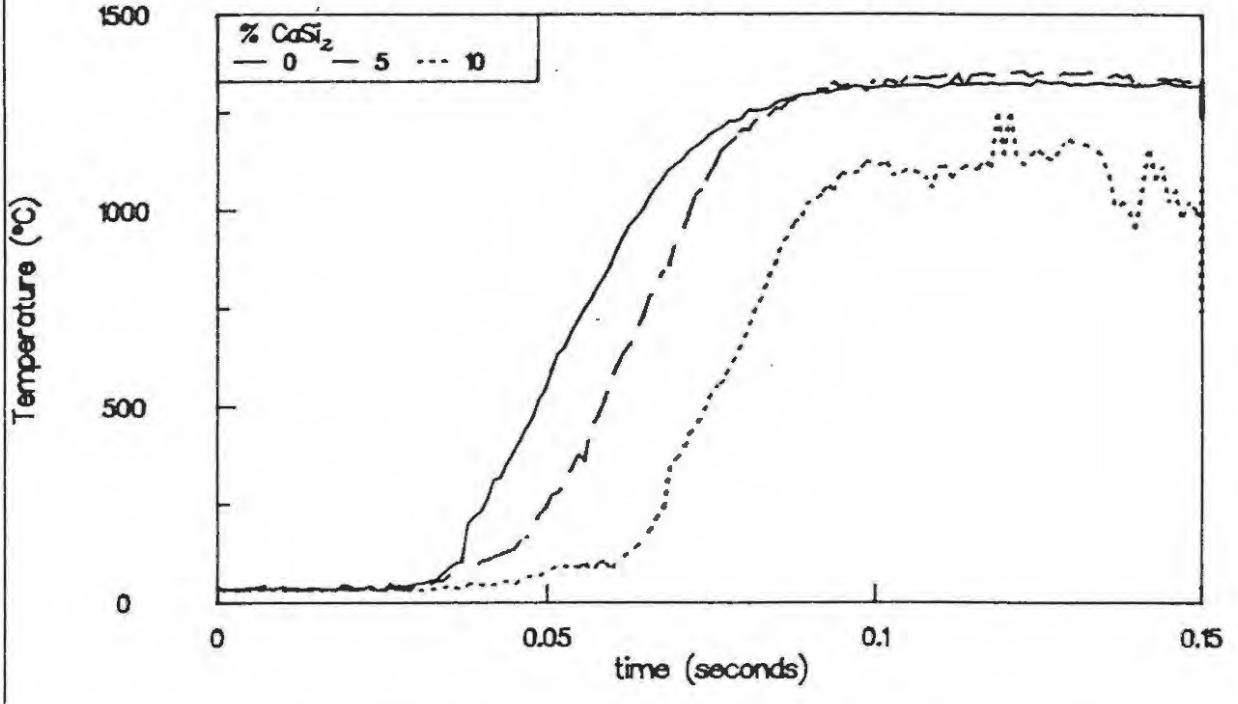

Figure 11.7 Temperature profiles of a 40% Si/SnO_2 mixture with various substitutions of SnO_2 with Fe_2O_3

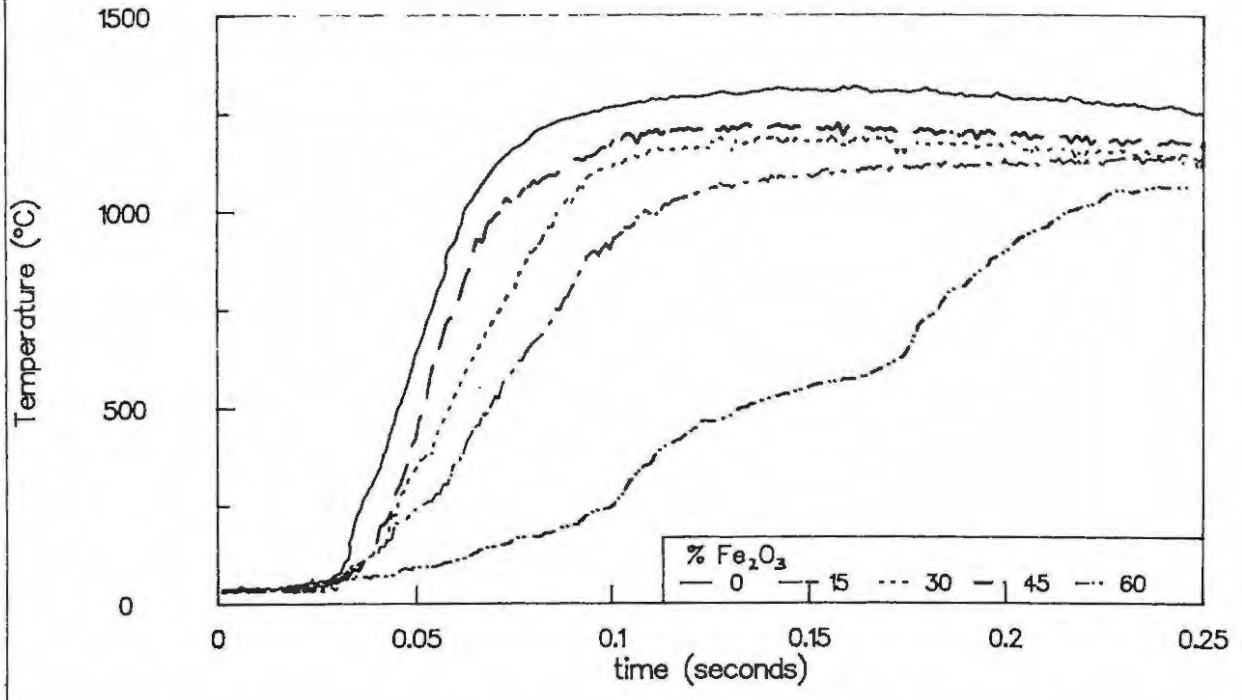

Figure 11.8 Temperature profiles of a 40% Si/Fe_2O_3 mixture with various substitutions of Fe_2O_3 with Sb_2O_3

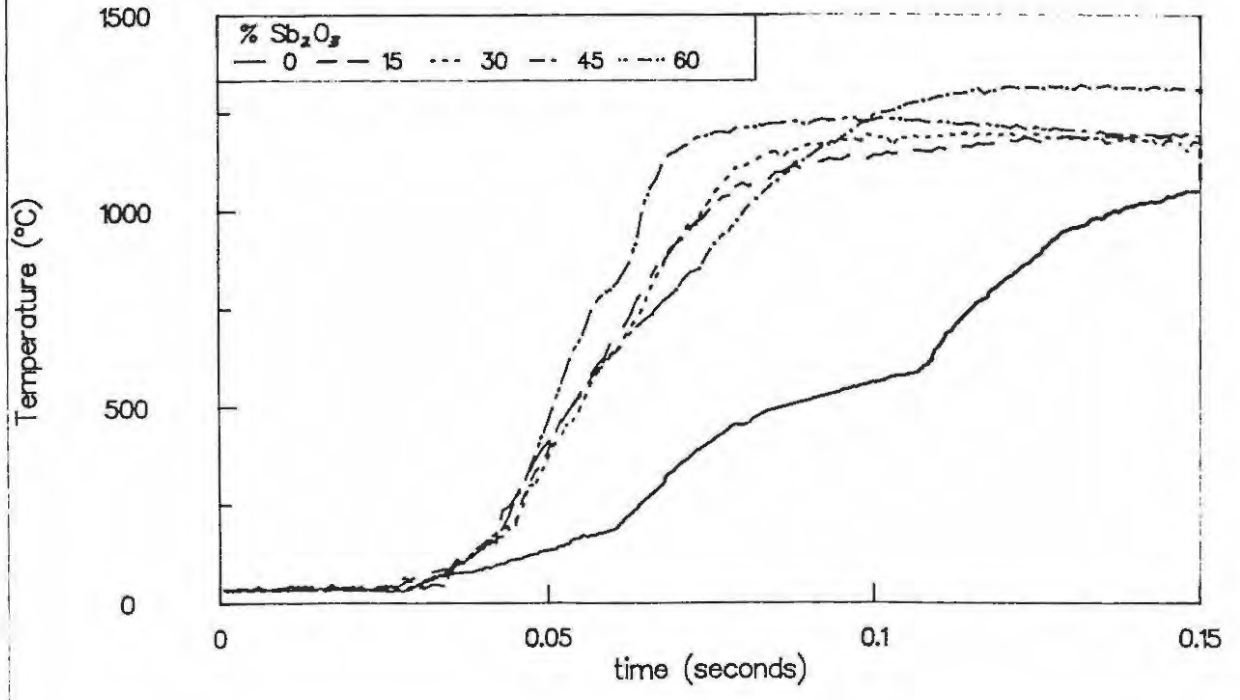

TABLE 11.3

Burning rates of ternary systems containing various binary combinations of oxidants

% composition	ε	Density (g cm^{-3})	Burning rates		T_{max} °C
			v_{exp} (mm s^{-1})	m_{exp} (g s^{-1})	
Si/SnO_2/Fe_2O_3 system					
40/60/ 0	0.48	2.55 ± 0.05	17.05 ± 1.29	1.39 ± 0.06	1348 ± 19
40/45/15	0.53	2.20 ± 0.04	12.15 ± 0.91	0.84 ± 0.03	1242 ± 32
40/30/30	0.55	2.00 ± 0.03	9.61 ± 0.10	0.55 ± 0.02	1223 ± 46
40/15/45	0.59	1.75 ± 0.03	8.77 ± 0.11	0.47 ± 0.02	1208 ± 18
40/ 0/60	0.48	2.10 ± 0.04	4.51 ± 0.24	0.30 ± 0.02	1179 ± 24
Si/SnO_2/Sb_2O_3 system					
40/60/ 0	0.48	2.55 ± 0.05	17.05 ± 1.29	1.39 ± 0.06	1343 ± 17
40/45/15	0.48	2.46 ± 0.04	15.69 ± 0.15	1.18 ± 0.07	1372 ± 20
40/30/30	0.45	2.50 ± 0.02	17.54 ± 1.21	1.27 ± 0.08	1300 ± 22
40/15/45	0.40	2.63 ± 0.03	15.55 ± 0.59	1.19 ± 0.10	1322 ± 14
40/ 0/60	0.46	2.25 ± 0.05	8.52 ± 0.33	0.63 ± 0.02	1329 ± 9
Si/SnO_2/KNO_3 system					
40/60/ 0	0.48	2.55 ± 0.05	17.05 ± 1.29	1.39 ± 0.06	-
40/45/15	0.40	2.51 ± 0.02	6.78 ± 0.15	0.54 ± 0.01	-
40/30/30	0.43	2.03 ± 0.02	5.94 ± 0.10	0.30 ± 0.01	-
40/15/45	0.28	2.08 ± 0.10	2.58 ± 0.07	0.15 ± 0.01	-
40/ 0/60	0.19	1.77 ± 0.03	2.78 ± 0.16	0.17 ± 0.06	-
Si/Fe_2O_3/Sb_2O_3 system					
40/60/ 0	0.48	2.10 ± 0.01	4.51 ± 0.21	0.30 ± 0.02	1329 ± 9
40/45/15	0.55	1.85 ± 0.03	14.16 ± 0.25	0.79 ± 0.06	1201 ± 24
40/30/30	0.51	2.02 ± 0.01	15.86 ± 0.95	0.95 ± 0.05	1254 ± 39
40/15/45	0.44	2.33 ± 0.04	13.06 ± 0.62	0.93 ± 0.05	1253 ± 14
40/ 0/60	0.46	2.25 ± 0.05	8.52 ± 0.33	0.63 ± 0.02	1329 ± 9

TABLE 11.3 (cont)

% composition	ε	Density (g cm^{-3})	Burning rates		T_{max} °C
			v_{exp} (mm s^{-1})	m_{exp} (g s^{-1})	
$Si/Fe_2O_3/KNO_3$ system					
40/60/ 0	0.48	2.10 ± 0.01	4.51 ± 0.21	0.30 ± 0.02	-
40/45/15	0.55	1.63 ± 0.02	9.85 ± 0.07	0.46 ± 0.01	-
40/30/30	0.42	1.80 ± 0.01	8.49 ± 0.12	0.43 ± 0.02	-
40/15/45	0.29	1.89 ± 0.01	4.09 ± 0.08	0.23 ± 0.02	-
40/ 0/60	0.19	1.77 ± 0.03	2.78 ± 0.16	0.17 ± 0.06	-
$Si/Sb_2O_3/KNO_3$ system					
40/60/ 0	0.46	2.25 ± 0.10	8.52 ± 0.33	0.63 ± 0.02	-
40/45/15	0.43	2.34 0.16	14.19 ± 1.01	1.34 ± 0.13	-
40/30/30	0.38	2.08 ± 0.06	10.93 ± 0.68	0.76 ± 0.09	-
40/15/45	0.31	2.03 ± 0.07	2.68 ± 0.17	0.18 ± 0.10	-
40/60/ 0	0.19	1.77 ± 0.04	2.78 ± 0.16	0.17 ± 0.06	-

Since reaction in the Si/SnO_2 and Si/Fe_2O_3 systems occurs predominantly between solids reactants (see Sections 8.2 and 9.2 respectively), various proportions of KNO_3 and Sb_2O_3, which produce molten and gaseous intermediates and products on reacting with Si, were added separately to the SnO_2 and Fe_2O_3 systems. The burning rates for the resulting systems ($Si/SnO_2/Sb_2O_3$, $Si/SnO_2/KNO_3$, $Si/Fe_2O_3/Sb_2O_3$ and $Si/Fe_2O_3/KNO_3$) are given in Table 11.3. Burning rates for the ternary systems Si/Fe_2O_3 with Sb_2O_3 or KNO_3 as the second oxidant showed a maximum at approximately 30% Sb_2O_3 and 40% KNO_3, respectively. The temperature profiles for the $Si/Fe_2O_3/Sb_2O_3$ systems were less complex than those for the binary Si/Fe_2O_3 mixture (Figure 11.8). No marked trends in the maximum temperatures for the ternary systems were observed but the time taken to rise to maximum temperature generally increased with increasing Fe_2O_3 content. The thermocouples melted during the burning of the $Si/Fe_2O_3/KNO_3$ systems.

The burning rates obtained on addition of either Sb_2O_3 or KNO_3 as the third oxidant to the Si/SnO_2 system are listed in Table 11.3. Temperature profiles could only be captured for the $Si/SnO_2/Sb_2O_3$ system (see Figure 11.9). The profiles had similar maximum temperatures and no marked trends were observed. The addition of Sb_2O_3 or KNO_3, generally, decreased the burning rate of the Si/SnO_2 system. The decrease in the burning rate was greater in the presence of KNO_3 than in the presence of a similar proportion of Sb_2O_3.

Figure 11.9 Temperature profiles of 40% Si/SnO_2 with various substitutions of SnO_2 with Sb_2O_3

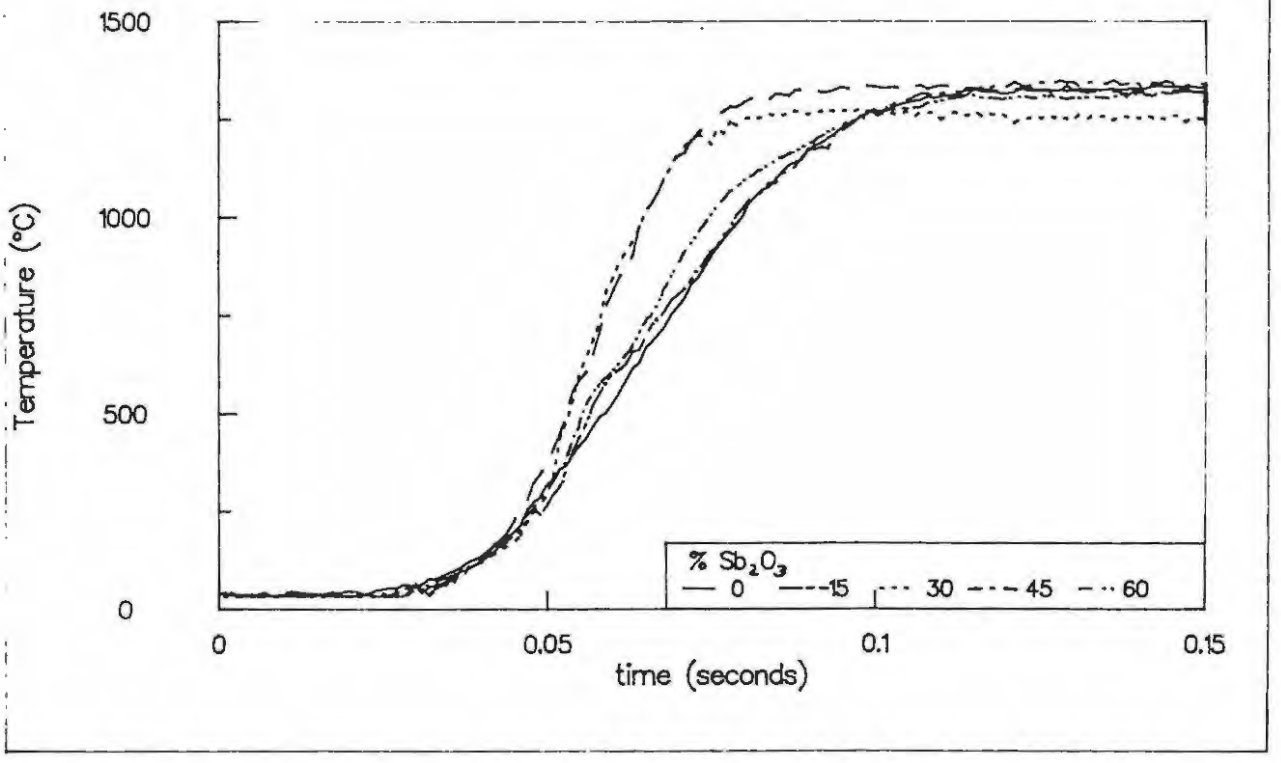

The addition of small proportions of KNO_3 to the 40% Si/Sb_2O_3 system caused the burning rate to speed up. On increasing the KNO_3 content, v_{exp} decreased. Temperature profiles could not be obtained for the $Si/Sb_2O_3/KNO_3$ system.

11.3 Comment

Further discussion of ternary systems is given in Section 14.

11.4 References

1. S.R. Yoganarasimhan, J. Thermal Anal., 34 (1985) 937.

12 THERMAL CONDUCTIVITY

12.1 Introduction

The propagation of the burning of pyrotechnic materials depends strongly on the way in which heat is transferred from the burning front to the adjacent unburnt material (see Section 4.1). The rate at which the temperature increases in the unburnt powder depends on the heat capacity and thermal conductivity of the material. In the study of the combustion processes, values of the thermal conductivity of the pyrotechnic are required to estimate the burning rate from temperature profiles (1-3).

There are several methods described in the literature for determining the thermal conductivity of granular material. A relatively simple technique for use with sand samples (4) has been adapted for use with pyrotechnic material (5) and used in this study. In this method, a suitably-shaped copper probe, consisting of a small resistor as a heat source and a chromel-alumel thermocouple, is embedded in the sample material. The temperature is then measured as a function of time during the application of a potential to the resistor.

The temperature of the probe can be approximated as

$$T = \frac{Q}{4\pi a\lambda}\left(1 - \frac{2}{\pi}\, I(t)\right) \qquad \ldots(12.1)$$

where Q is the rate of supply of heat (power) to the probe, λ is the thermal conductivity, a is the effective radius of the probe and

$$I = \int_0^\infty \frac{\exp\{-(\lambda t u^2/a^2\rho c)\}}{[(u^2/k - 1)]^2 + u^2}\, du = \int_0^\infty f(u,t)\, du$$

where u is the radial distance in the medium from the probe, relative to the effective radius, a, t is the time during which the power is applied and *k* is the probe constant which is characteristic of a particular probe of effective radius a, mass M_p and of specific heat capacity c_p and is defined as

$$k = \frac{4\pi a^3 \rho c}{M_p c_p} = k_p \rho c$$

where ρ is the density and c the speeific heat capacity of the test material. The integral, I, may be rewritten as

$$I = \int_0^\infty \frac{\exp(-yu^2)}{[(u^2/k) - 1]^2 + u^2}\, du$$

and

$$y = \lambda t/a^2 \rho c = Dt/a^2$$

where the thermal diffusivity $D = \lambda/(\rho c)$.

Beck *et al* (5) have noted that for any given value of t, f(u,t) rapidly approaches zero. The integral I, approaches zero as t increases such that at the maximum temperature, T_∞, T is equal to $Q/4\pi a\lambda$. Under ideal circumstances then, λ can be evaluated directly at T_∞, but the approach to T_∞ may take a very long time. The integral may be evaluated by determining the area under the curve of

$$\frac{\exp\{-(\lambda t u^2/a^2\rho c)\}}{[(u^2/k - 1)]^2 + u^2}$$

against u.

An alternative to numerical integration was also suggested (5).

12.2 **Experimental**

The copper probe used in this study is shown in Figure 12.1. The probe was suitably drilled to allow fitting a 10Ω resistor and a thermocouple junction. The resistor provided the heat source when a low-voltage DC source was applied. The potential was adjusted to produce a steady-state temperature of 20°C above ambient. The power output of the resistor was approximately 0.3 W. A chromel/alumel thermocouple (0.25 mm wire diameter), fixed to the probe, was used to monitor the temperature of the probe as a function of time (the reference junction was kept at the ice point). The thermocouple output was amplified (gain 254) and the amplified signal was digitised by a 12-bit A/D converter which was interfaced to a CW-16 Exel (IBM compatible) microcomputer. A BASIC routine was used to capture data at a sampling interval of 1 s and the thermocouple output was converted to temperature values using a polynomial of the form

$$T = a + bV + cV^2 + dV^3$$

where T is the temperature in °C, V is the thermocouple output and the coefficients were $a = 7.1223 \times 10^{-2}$, $b = 25.3591$, $c = 0.283818$ and $d = 3.1733 \times 10^{-3}$. The temperature-time data were stored on diskette for later processing. The raw temperature-time data were smoothed using a digital smoothing routine in BASIC. Further BASIC software was used to reduce the number of raw data points at given time intervals. These data were then imported into a spreadsheet in which menu-driven macros were used to calculate a temperature-time curve according to equation (12.1) (see Scheme 12.1). The spreadsheet allowed the calculated and experimentally determined temperature-time curves to be compared.

Sample preparation involved packing the powdered material into a metal cylinder on a Perspex platform recessed to accommodate the probe (see Figure 12.2). The samples were then gently tamped until firm, after which a metal piston was inserted. Because initial runs showed that the thermocouple response was sensitive to the packing of the mixture, a loading pressure of approximately 15 MPa was

Figures 12.1 and 12.2

Figure 12.1 Thermal conductivity probe

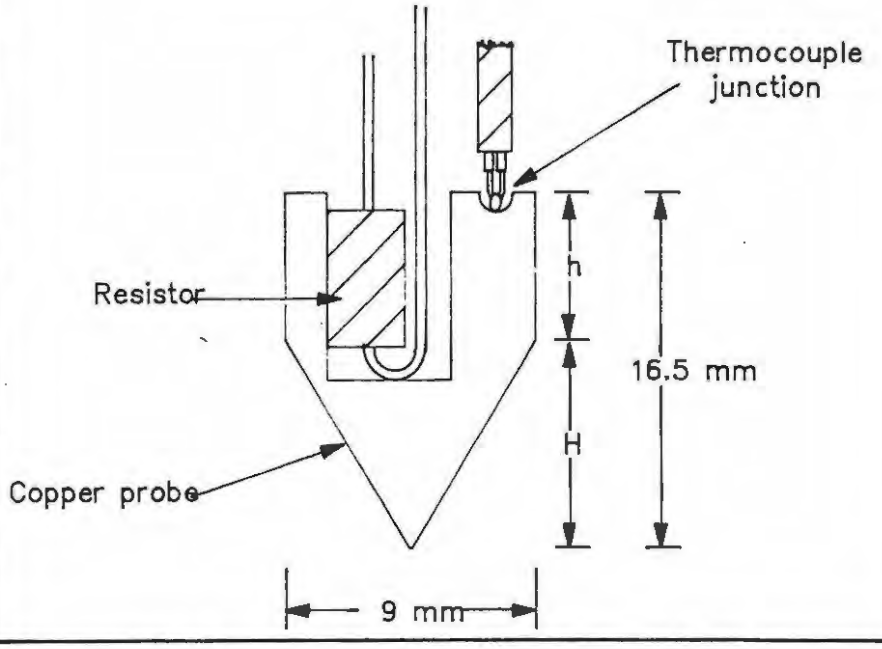

Figure 12.2 Thermal conductivity apparatus for compacting powdered samples

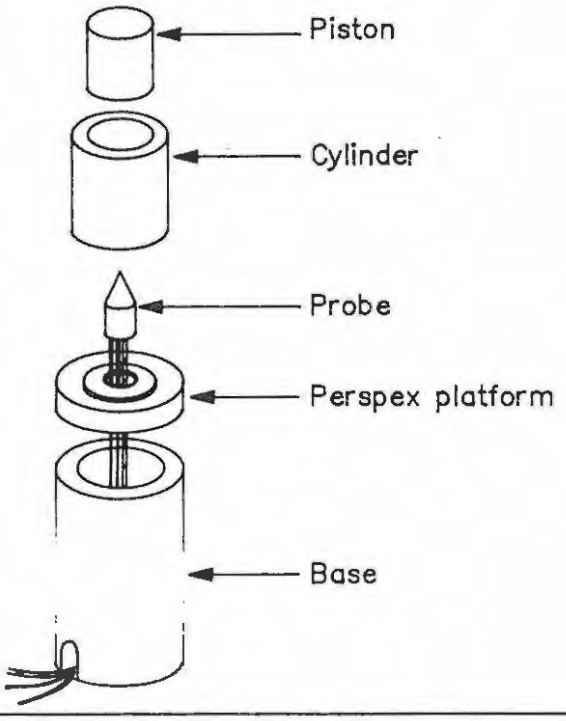

assembly for a dwell period of 1 minute to consolidate the powder. The density of the sample was estimated from the volume and the mass of the sample. The specific heat capacities of the mixtures were calculated from the bulk heat capacities of the constituents and the composition of the mixture. The contribution of trapped air was neglected.

The effective radius, a, of the probe was found by assuming an initial value equal to the actual surface area of the probe, and using the literature value for the thermal conductivity (λ) of Al_2O_3 to calculate expected temperature-time curves for Al_2O_3. These curves were compared with an experimentally determined curve for Al_2O_3 (Merck, particle-size < 38 μm). Both a and λ were adjusted, until a reasonable fit was obtained (see Figure 12.3). Once a value for the effective radius was obtained, only the value of λ needed to be adjusted on subsequent runs for other samples. The characteristics of the probe used in this study are listed in Table 12.1.

TABLE 12.1

Characteristics of the probe used in this study

Characteristic	Probe
Mass of probe (g)	5.50
Effective radius, a (mm)	6.10 ± 0.06
Surface area (mm^3)	268 ± 17
Thermal conductivity of Al_2O_3 ($W\ m^{-1}\ K^{-1}$)	0.22 ± 0.02

Thermal conductivities of the separate constituents and the various binary mixtures used in this study were determined. All the results shown are the mean of three runs and errors were calculated from range estimates of the results.

Figure 12.3 Experimental and calculated thermal conductivity curves for Al_2O_3 powders

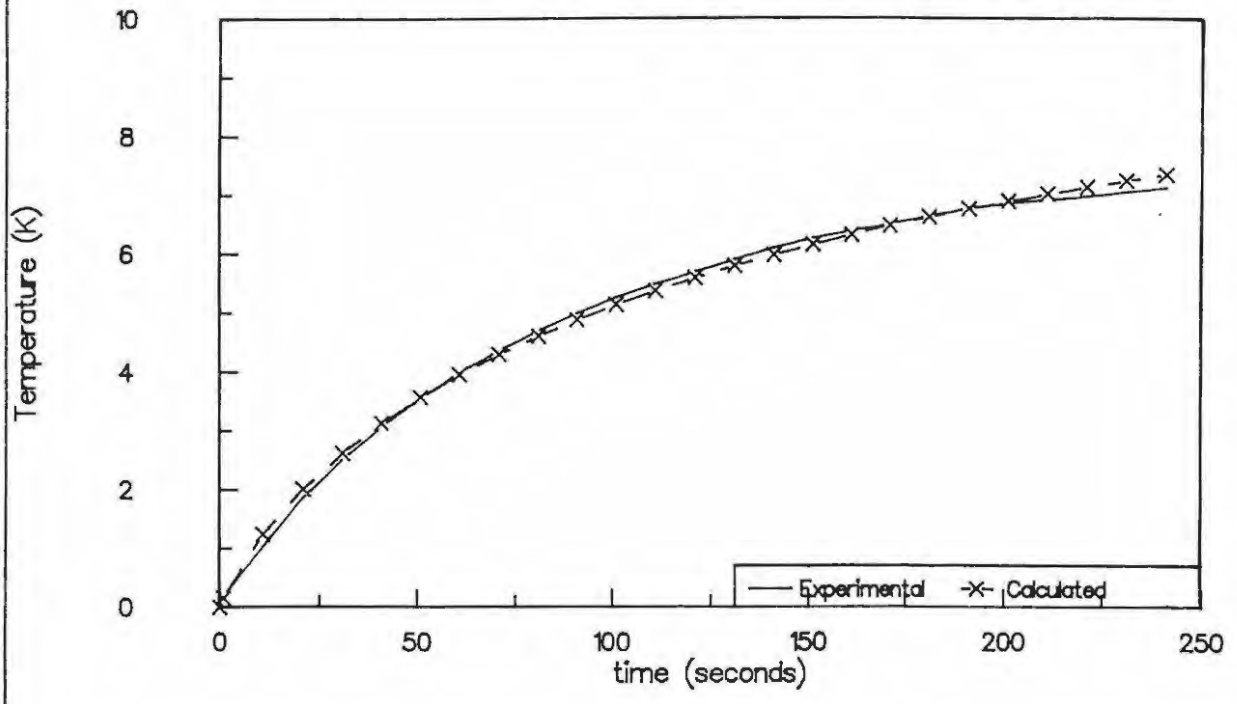

Figure 12.4 Thermal conductivity curves showing various "estimates" for λ for Si powder

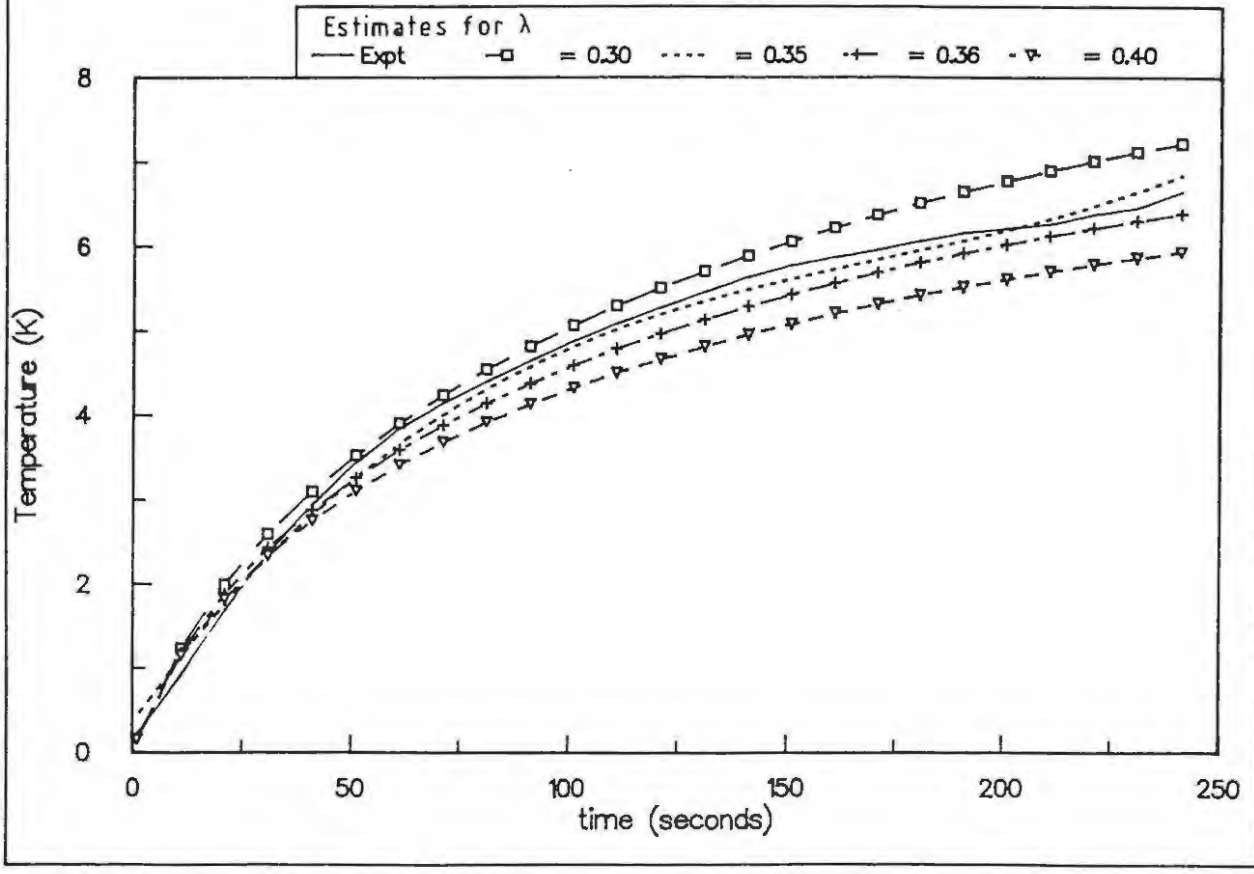

12.3 Results

12.3.1 *Constituents*

The temperature-time curves of Si, showing various initial "estimates" for λ, are shown in figure 12.4. The curves for each of the fuels used are shown in Figure 12.5 and those for the oxidants in Figure 12.6. The thermal properties of the constituents are listed in Table 12.2.

TABLE 12.2

Physical properties of the constituents

Sample	Heat capacity, c x 10^3 (J K^{-1} g^{-1})	Bulk density, ρ_c x 10^3 (kg m^{-3})	Powder density ρ x 10^3 (kg m^{-3})	ε	Thermal conductivity, λ (W m^{-1} K^{-1})	Thermal diffusivity, D (10^{-7} m^2 s^{-1})
Al_2O_3	0.78	3.97	1.83 ± 0.04	0.54	0.22 ± 0.01	1.54 ± 0.21
Si	0.72	2.33	1.42 ± 0.04	0.39	0.35 ± 0.01	3.42 ± 0.20
$FeSi_7$	0.60#	6.10#	2.76 ± 0.09	0.55	0.33 ± 0.06	1.99 ± 0.36
$CaSi_2$	0.96*	2.50	2.14 ± 0.08	0.15	0.42 ± 0.02	2.04 ± 0.20
Sb_2O_3	0.35	5.45	3.36 ± 0.14	0.38	0.24 ± 0.02	2.04 ± 0.17
Fe_2O_3	0.65	5.24	1.71 ± 0.14	0.67	0.29 ± 0.01	2.61 ± 0.09
SnO_2	0.35	6.95	3.23 ± 0.02	0.53	0.40 ± 0.01	3.54 ± 0.17
KNO_3	0.95	2.11	2.16 ± 0.04	0.45	0.34 ± 0.01	1.66 ± 0.10

* Estimated according to Ref. (6)
\# Used the values for $FeSi_2$

The thermal conductivities of the individual powdered constituents are all of the same order of magnitude. SnO_2 has the highest value of the oxidants (0.40 W m^{-1} K^{-1}) and this is slightly higher than that of the main fuel, Si. The thermal conductivity of $CaSi_2$ is higher than that of Si. Most calculations of thermal properties of pyrotechnic systems assume temperature independence of thermal conductivities and there is little experimental information available on values at high temperatures encountered in combustion.

12.3.2 *Binary mixtures with Si as fuel*

The thermal properties of binary silicon/oxidant mixtures used in this study are listed in Table 12.3.

Figure 12.5 Thermal conductivity curves of the fuels

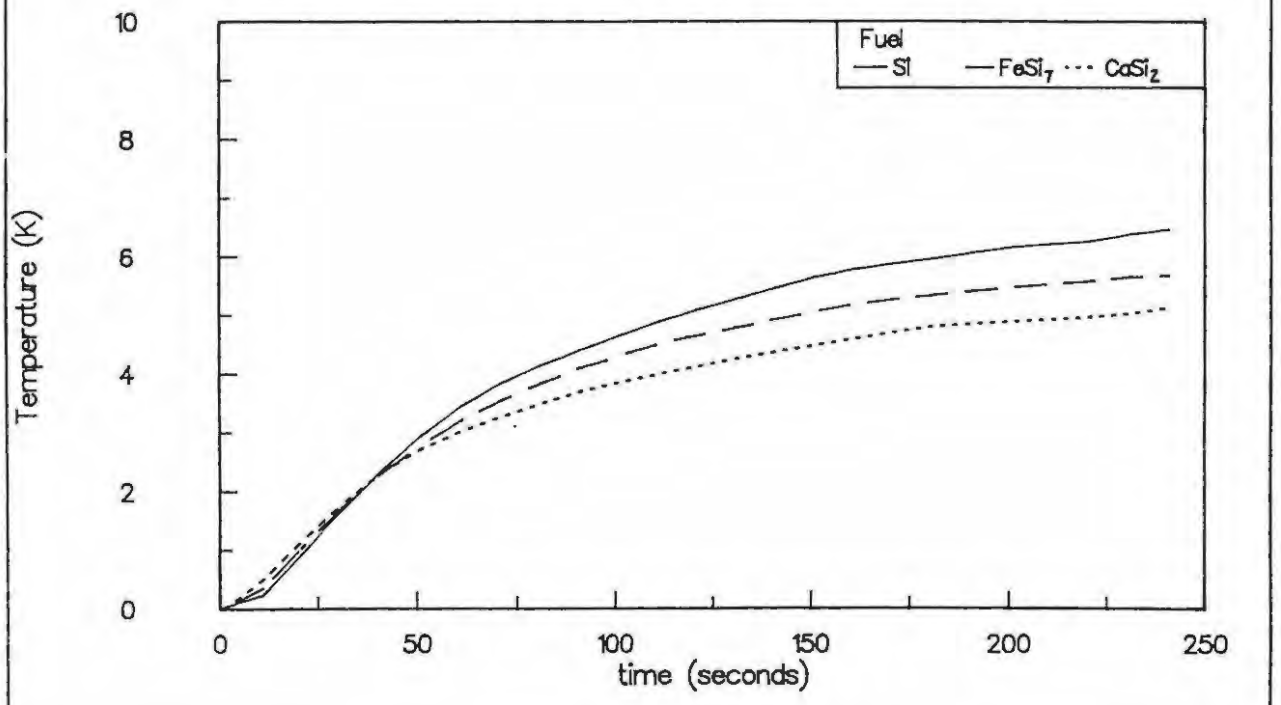

Figure 12.6 Thermal conductivity curves of the oxidants

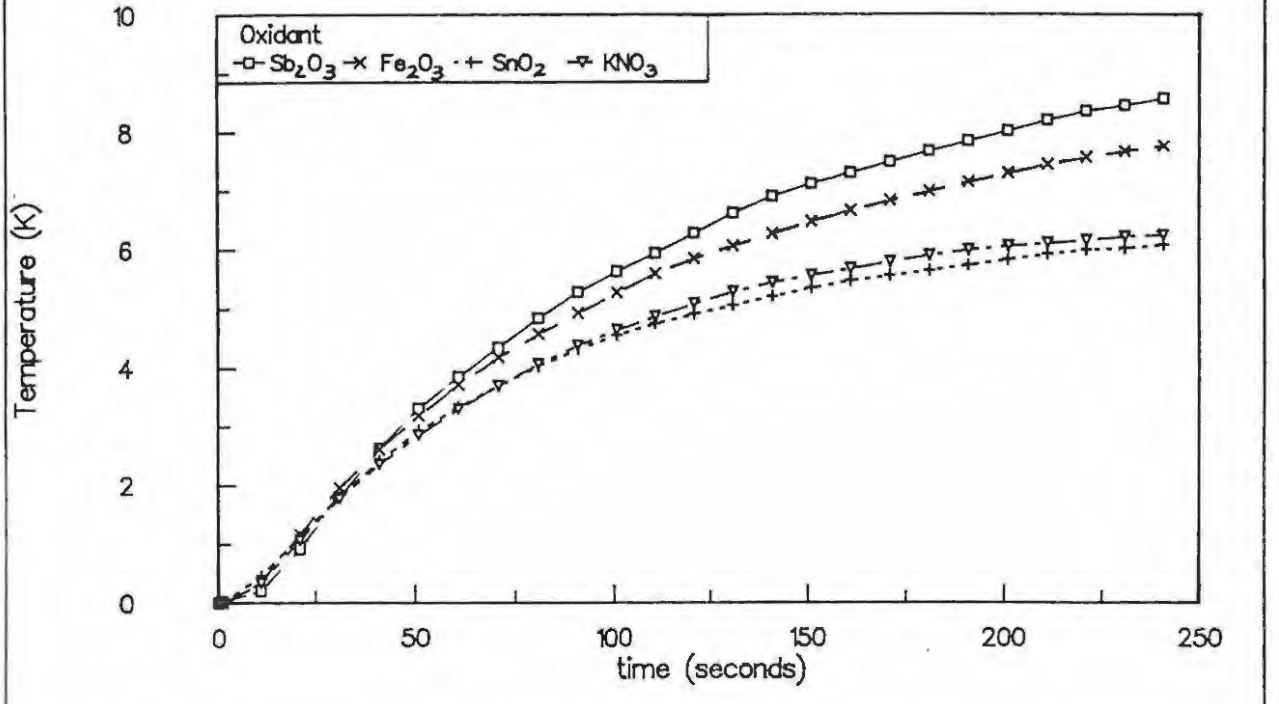

TABLE 12.3

Thermal properties of various binary mixtures with Si as fuel

% fuel	Heat capacity, c x 10^3 (J K^{-1} kg^{-1})	Powder density, ρ x 10^3 (kg m^{-3})	Porosity factor ε	Thermal conductivity, λ (W m^{-1} K^{-1})	Thermal diffusivity, D (10^{-7} m^2 s^{-1})
Si/Sb_2O_3					
0	0.35	3.36 ± 0.14	0.38	0.24 ± 0.02	2.04 ± 0.17
20	0.42	2.67 ± 0.11	0.45	0.26 ± 0.02	2.32 ± 0.18
30	0.46	2.69 ± 0.08	0.41	0.28 ± 0.03	2.26 ± 0.24
40	0.49	2.69 ± 0.10	0.36	0.28 ± 0.01	2.12 ± 0.08
50	0.53	2.50 ± 0.06	0.36	0.31 ± 0.01	2.17 ± 0.14
60	0.57	2.44 ± 0.07	0.32	0.30 ± 0.01	2.15 ± 0.14
100	0.72	1.42 ± 0.04	0.39	0.35 ± 0.01	3.42 ± 0.20
Si/Fe_2O_3					
0	0.65	1.71 ± 0.14	0.67	0.29 ± 0.01	2.61 ± 0.09
20	0.66	1.68 ± 0.06	0.64	0.25 ± 0.01	2.26 ± 0.09
30	0.67	1.66 ± 0.07	0.62	0.26 ± 0.02	2.34 ± 0.18
35	0.67	1.69 ± 0.04	0.60	0.26 ± 0.01	2.30 ± 0.09
40	0.68	1.78 ± 0.04	0.56	0.27 ± 0.05	2.23 ± 0.42
50	0.68	1.79 ± 0.07	0.53	0.27 ± 0.01	2.22 ± 0.08
100	0.72	1.42 ± 0.04	0.39	0.35 ± 0.01	3.42 ± 0.20
Si/SnO_2					
0	0.35	3.23 ± 0.02	0.53	0.40 ± 0.01	3.54 ± 0.17
20	0.42	2.60 ± 0.20	0.57	0.45 ± 0.02	4.12 ± 0.18
30	0.46	2.49 ± 0.09	0.55	0.46 ± 0.02	4.02 ± 0.18
40	0.50	2.65 ± 0.10	0.50	0.44 ± 0.01	3.32 ± 0.08
45	0.51	2.39 ± 0.08	0.51	0.35 ± 0.06	2.87 ± 0.49
50	0.53	2.68 ± 0.10	0.42	0.34 ± 0.01	2.39 ± 0.07
100	0.72	1.42 ± 0.04	0.66	0.35 ± 0.01	3.42 ± 0.20

Table 12.3 (continued)

% fuel	Heat capacity, c x 10^3 (J K^{-1} kg^{-1})	Powder density, ρ x 10^3 (kg m^{-3})	Porosity factor ε	Thermal conductivity, λ (W m^{-1} K^{-1})	Thermal diffusivity, D (10^{-7} m^2 s^{-1})
Si/KNO_3					
0	0.95	1.16 ± 0.04	0.45	0.34 ± 0.01	1.66 ± 0.10
20	0.91	1.19 ± 0.06	0.45	0.38 ± 0.01	2.12 ± 0.06
40	0.93	1.15 ± 0.10	0.48	0.30 ± 0.03	1.53 ± 0.15
60	0.81	1.09 ± 0.11	0.51	0.34 ± 0.02	2.00 ± 0.12
80	0.76	1.14 ± 0.08	0.50	0.35 ± 0.01	2.15 ± 0.06
100	0.72	1.42 ± 0.04	0.39	0.35 ± 0.01	3.42 ± 0.20

Since the thermal conductivities of the individual constituents are so similar, it is not unexpected that the room temperature thermal conductivities and the thermal diffusivities of the above systems showed only small changes (within experimental error) with composition. The changes follow the direction of increased proportion of the constituent with the higher thermal conductivity.

12.3.3 *Binary mixtures with other fuels*

The thermal properties of binary mixtures with either $FeSi_7$ or $CaSi_2$ as fuel are listed in Table 12.4. Also shown are the properties of the corresponding Si/oxidant systems. The thermal conductivities and thermal diffusivities of the Si and the $FeSi_7$ systems are similar. The mixtures $CaSi_2/SnO_2$ and $CaSi_2/KNO_3$ have thermal properties which are considerably greater than those containing either Si or $FeSi_7$.

TABLE 12.4

Thermal properties of the binary mixtures containing $FeSi_7$ and $CaSi_2$ as fuels

Mixture	c x 10^3 (J K^{-1} kg^{-1})	Powder density, ρ x 10^3 (kg m^{-3})	ε	Thermal conductivity, λ (W m^{-1} K^{-1})	Thermal diffusivity, D (10^{-7} m^2 s^{-1})
Si systems					
40% Si/Sb_2O_3	0.49	2.69 ± 0.10	0.36	0.28 ± 0.01	2.12 ± 0.08
35% Si/Fe_2O_3	0.67	1.69 ± 0.04	0.60	0.26 ± 0.01	2.30 ± 0.09
45% Si/SnO_2	0.51	2.39 ± 0.08	0.51	0.35 ± 0.06	2.87 ± 0.49
40% Si/KNO_3	0.93	2.15 ± 0.10	0.48	0.30 ± 0.03	1.53 ± 0.15
$FeSi_7$ systems					
40% $FeSi_7$/Sb_2O_3	0.45	2.59 ± 0.13	0.55	0.24 ± 0.02	2.06 ± 0.17
35% $FeSi_7$/Fe_2O_3	0.63	1.52 ± 0.12	0.55	0.23 ± 0.03	2.40 ± 0.31
45% $FeSi_7$/SnO_2	0.46	2.59 ± 0.12	0.61	0.37 ± 0.02	3.10 ± 0.17
40% $FeSi_7$/KNO_3	0.65	2.57 ± 0.07	0.31	0.38 ± 0.03	2.28 ± 0.18
$CaSi_2$ systems					
40% $CaSi_2$/Sb_2O_3	0.59	1.91 ± 0.14	0.55	0.31 ± 0.01	5.15 ± 0.17
35% $CaSi_2$/Fe_2O_3	0.76	1.84 ± 0.17	0.57	0.38 ± 0.05	2.72 ± 0.36
45% $CaSi_2$/SnO_2	0.63	2.03 ± 0.19	0.59	0.67 ± 0.06	5.24 ± 0.50
40% $CaSi_2$/KNO_3	0.96	2.08 ± 0.10	0.52	0.67 ± 0.03	3.36 ± 0.15

12.4 Calculation of burning rates

As discussed in Sections 7.1.3, 8.1.3 and 9.1.3, burning rates calculated from experimental rise times, t_r, and room temperature thermal conductivities and heat capacities, $v_{calc} = (D/t_r)^{1/2}$, gave values that are usually far from the measured burning rates. The thermal diffusivities, calculated from t_r and the experimentally obtained burning rates, v_{exp}, are listed in Table 12.5

TABLE 12.5

Calculated thermal diffusivities for binary Si/oxidant mixtures

% fuel	Linear burning rate, v_{exp} (mm s^{-1})	Rise time t_r x 10^{-3} (seconds)	Thermal diffusivity, D_{calc} x 10^{-7} (m^2 s^{-1})
	Si/Sb_2O_3		
30	6.30 ± 0.29	22.3 ± 4.1	8.85
35	8.17 ± 0.42	23.3 ± 2.5	15.56
40	8.52 ± 0.33	23.9 ± 1.3	17.34
45	8.73 ± 0.40	30.0 ± 3.5	22.86
50	7.25 ± 0.11	29.0 ± 4.2	15.24
	Si/Fe_2O_3		
25	2.33 ± 0.17	30.2 ± 1.2	1.64
30	3.67 ± 0.08	59.9 ± 0.1	8.07
35	3.82 ± 0.12	58.0 ± 2.7	8.46
40	3.60 ± 0.10	44.7 ± 1.3	5.79
45	4.54 ± 0.21	-	-
	Si/SnO_2		
20	5.25 ± 0.06	-	-
25	7.54 ± 0.39	15.6 ± 0.9	8.86
30	11.60 ± 0.64	13.9 ± 0.2	18.70
35	14.78 ± 0.64	7.6 ± 0.8	16.60
40	17.05 ± 1.29	7.5 ± 0.1	21.80
45	15.68 ± 0.35	3.3 ± 0.4	8.11
50	12.84 ± 0.49	9.4 ± 0.4	15.50
55	9.11 ± 0.39	12.8 ± 0.5	10.62

The calculated thermal diffusivities values, D_{calc} were much greater (by between 160 to 720%) than those obtained from room temperature experiments. The thermal conductivities or the heat capacities of the mixtures, or both, would have to undergo large changes at the temperatures associated with burning to account for the increase in D. Earlier calculations showed that the heat capacities of the reactants at 1600 K were between 40 to 70% greater those at 298 K (for example, see Table 9.5, Section 9.1.2). Hence, the values of the thermal conductivities are expected to inerease as the pyrotechnic mixtures reaches reaction temperatures. Thermal diffusivity data at elevated temperatures is sparse but for Sn, D at 1000 K is 25 m^2 s^{-1} compared to 40.2 m^2 s^{-1} at 300 K (7).

12.5 **References**

1. T. Boddington, P.G. Laye, J.R.G. Pude and J. Tipping, Comb. Flame, **47** (1982) 235.
2. T. Boddington, A. Cottrell and P.G. Laye, Comb. Flame, **76** (1989) 63.
3. T. Boddington, P.G. Laye and J.Tipping, Comb. Flame, **50** (1983) 139.
4. H.J. Goldsmid, E.K. Davies and V. Papazian, J. Phys. E: Sci. Instrum., **14** (1981) 1149.
5. M.W. Beek, M.E. Brown and N.J.H. Heideman, J. Phys. E: Sci. Instrum., **17** (1984) 793.
6. D.K Nordstrom and J.L. Munoz, "*Geophysical Thermodynamics*", Blackwell Scientific Publications, 1986, p. 350.
7. O. Kubachewski, E.Li. Evans and C.B. Alcock, "*Metallurgical Thermochemistry*" 4th Ed., Pergamon Press 1967.

SCHEME 12.1

Schematic layout of the LOTUS 123 spreadsheet for the calculation

of thermal conductivity curves

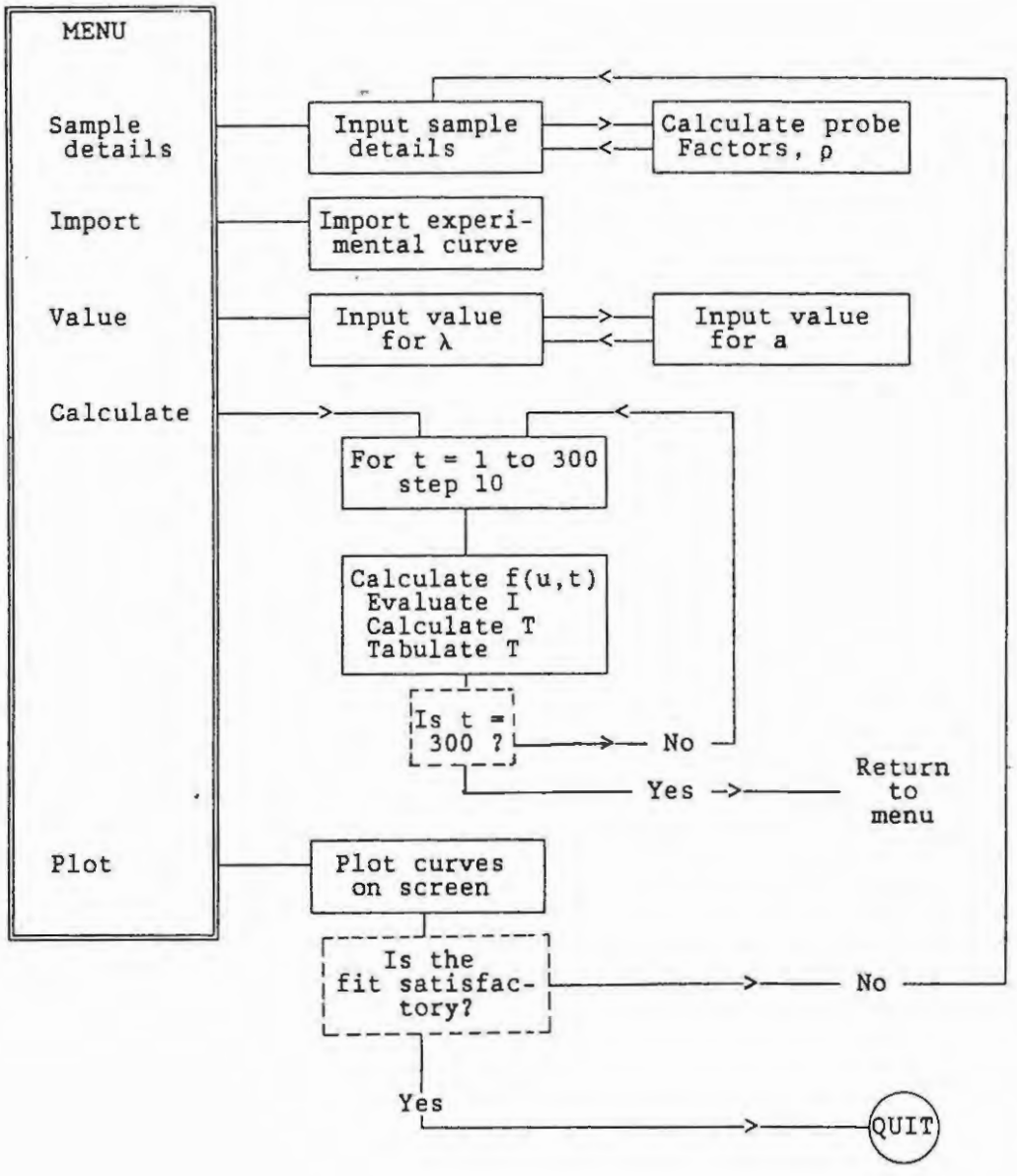

13. DISCUSSION OF BINARY SYSTEMS

13.1 Thermal analysis

Thermal analysis (Section 6) showed that oxidation of silicon (m.pt. 1410°C) powder, heated at 20°C min^{-1} on its own in air or in oxygen became detectable above 700°C and was incomplete at 1000°C. TG curves showed that only small amounts (<1%) of oxide were formed under the conditions of thermal analysis (temperature limit is 1000°C). Oxidation occurred more readily in O_2 than in air. Similar trends were observed for $FeSi_7$ (m. pt. ~1300°C) and for $CaSi_2$ (m. pt. ~980°C).

The individual oxidants behaved very differently on heating. Fe_2O_3 (m. pt. 1565°C) and SnO_2 (m. pt. 1630°C) showed no thermal events on heating on their own in either N_2 or air. KNO_3 melts at relatively low temperatures (325°C) and decomposes in the melt at above 500°C. Sb_2O_3 (m. pt 650°C) sublimes readily and may also melt. Simultaneous oxidation to Sb_2O_4 occurs in air. These differences in behaviour have a marked effect on the binary combinations as discussed below.

All of the binary mixtures have been shown (Sections 7 to 10) to propagate combustion after suitable ignition. However, the reactions which occur during thermal analysis are not always identical to those which occur under the conditions of ignition because of different temperature-time histories. The information obtained from thermal analysis, however, provides some insight into the reaction mechanisms which may occur during the burning of pyrotechnic compositions.

The Si/Fe_2O_3 and the Si/SnO_2 systems, as loose or compacted powders, showed no significant thermal activity in the temperature range studied and at heating rates <150°C min^{-1}. The binary systems with $FeSi_7$ or $CaSi_2$ as fuels and with SnO_2 and Fe_2O_3 as oxidants also showed no significant thermal events under similar conditions.

The thermal analysis curves of binary mixtures of Sb_2O_3 and either Si, $FeSi_7$ or $CaSi_2$ as fuel, were very similar (Section 6). Both the mass loss and the exothermicity of reaction depended on the heating rate and the mass of the sample. The exotherm due to reaction between fuel and Sb_2O_3 occurred at temperatures (590 to 615°C) below the melting point of the oxidant. TG curves showed a significant mass loss between 420 and 630°C due to sublimation of the oxidant, so reaction between solid fuel and Sb_2O_3 vapour is possible. The loss of Sb_2O_3 vapour could be decreased by covering the sample pans with lids, but could not be prevented entirely. The main product formed during reaction is SiO_2. In air, the reaction of silicon with Sb_2O_3 is further complicated by simultaneous oxidation of Sb_2O_3 by gaseous oxygen. If, in the absence of air, any Sb was formed by the reduction of Sb_2O_3, it would be molten above 631°C.

TABLE 13.1

Summary of thermoanalytical data for binary fuel/Sb_2O_3 mixtures in nitrogen

Fuel (40% by mass)	TG		DSC		
	Range (°C)	% mass loss	Range (°C)	$-\Delta H$ (kJ g^{-1})	$-\Delta H$ (kJ (mol Si)$^{-1}$)
Si	420 to 630	48.5 ± 0.4	590 to 615	0.53 ± 0.13	37.2
$FeSi_7$	430 to 620	49.0 ± 2.0	510 to 635	0.34 ± 0.17	30.7
$CaSi_2$	500 to 620	35.3 ± 1.2	570 to 620	0.25 ± 0.14	28.2

The enthalpy of reaction (from DSC curves) decreased as shown in Table 13.1 when $FeSi_7$ or $CaSi_2$ were used as replacement fuels.

A single highly exothermic reaction between decomposing molten KNO_3 and silicon occurred at ~550°C (Section 6.4.4). There was an exothermic contribution to reaction from gaseous oxygen when mixtures were heated in air.

The DSC traces of $FeSi_7/KNO_3$ and $CaSi_2/KNO_3$ mixtures showed two well-defined exotherms due to reaction with molten oxidant. The first exotherm was a low intensity broad exothermic process (onset 460°C) (see Table 13.2). The second was a complex process which, in $CaSi_2/KNO_3$ systems, invariably lead to the ignition at an onset temperature of 590°C. TG curves showed only a single continuous mass loss over the temperature range of these two exotherms.

TABLE 13.2

Summary of thermoanalytical data for binary fuel/KNO_3 systems in nitrogen

Fuel	TG		DSC		
	Range (°C)	% mass loss	Range (°C)	$-\Delta H$ (kJ g^{-1})	$-\Delta H$ (kJ (mol Si)$^{-1}$)
Si (60%)	540 to 720	10.9 ± 0.4	570 to 700	1.64 ± 0.01	76.8
$FeSi_7$ (65%)	370 to 860	7.3 ± 0.1	500 to 580	0.03 ± 0.01	19.3
			585 to 700	0.29 ± 0.07	
$CaSi_2$ (65%)	390 to 795	8.3 ± 2.4	520 to 590	0.16 ± 0.10	12.0
			595 to 690	ignited	

The results of thermal analysis thus show considerably different behaviour for the binary systems. Two of the oxidants, Fe_2O_3 and SnO_2, are thermally inert below 1000°C and do not interact with Si as fuel (or $FeSi_7$ or $CaSi_2$) under the conditions of thermal analysis. Initial fuel/oxidant interactions are thus almost certainly solid-solid reactions in these systems possibly leading to eutectic formation at temperatures at least beyond the limit of the DSC (730°C). The other two oxidants, KNO_3 and Sb_2O_3, both melt and KNO_3 decomposes and Sb_2O_3 vapourises so fuel/oxidant interactions may be solid-liquid reactions and/or solid-gas reactions.

13.2 Combustion of binary systems

13.2.1 *Burning rates*

Effect of composition

The Si/Sb_2O_3, Si/Fe_2O_3 and Si/SnO_2 systems sustained combustion over a narrow range of compositions (20 to 55% Si). Binary systems based on KNO_3 burned over a much wider range of up to 90% Si. The burning of all binary Si/oxidant compositions, except those which contained KNO_3 as oxidant, was essentially gasless. The linear burning rates for the four binary Si/oxidant systems are summarised in Tables 13.3 and 13.4. Plots of the burning rates against % Si for various binary Si/oxidant compositions are shown in Figure 13.1.

TABLE 13.3

Summary of burning rates for binary Si/oxidant systems

Oxidant	% Si	Range of v_{exp} (mm s^{-1})	Proportion of Si at v_{max}
Fe_2O_3	20 to 40	2.3 to 4.5	40%
Sb_2O_3	20 to 50	1.6 to 8.7	35%
SnO_2	20 to 55	5.3 to 17.1	40%
KNO_3	20 to 85	1.7 to 34.5	85%

The fastest maximum burning rate occurred for 85% Si/KNO_3 (34.5 ± 3.3 mm s^{-1}) and the slowest at 30% Si/KNO_3 (1.7 ± 0.2 mm s^{-1}). The shape of this curve is not the more normal concave down type. For a given composition of 40% silicon by mass, the order of decreasing burning rates for the binary Si/oxidant systems decreased in the order

$$Si/SnO_2 > Si/Sb_2O_3 > Si/Fe_2O_3 > Si/KNO_3$$

Figure 13.1 Comparison of burning rate against % silicon

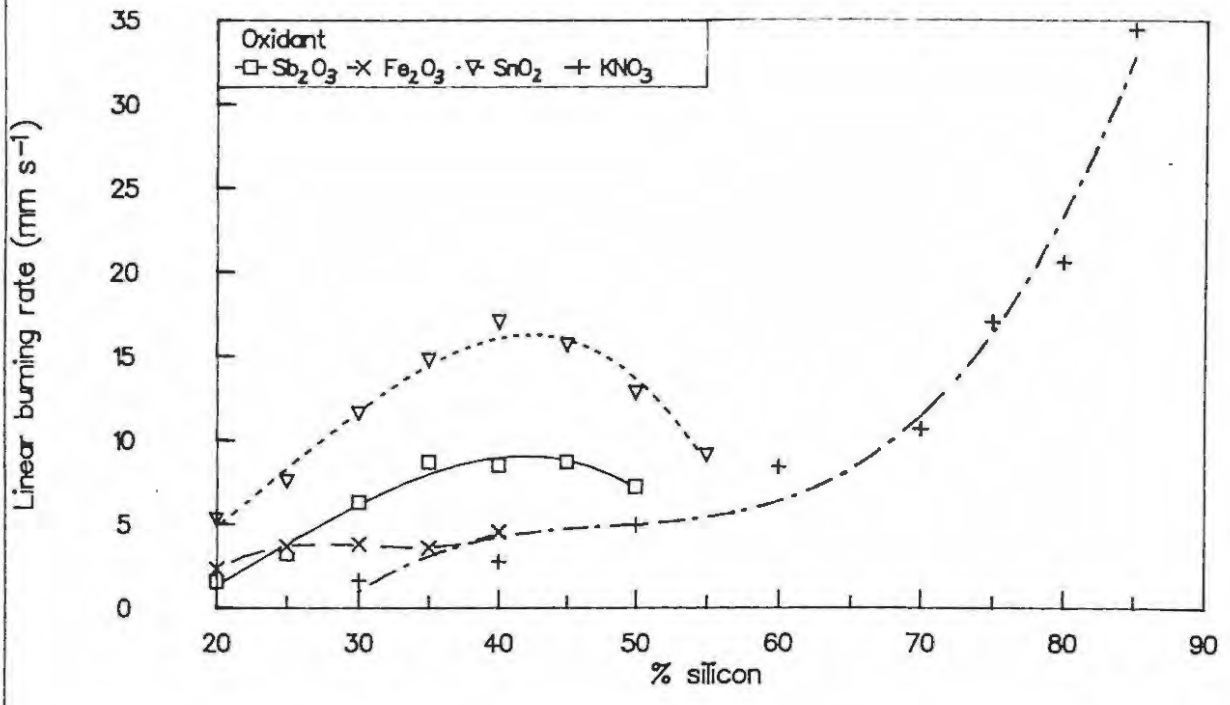

Figure 13.2 Comparing burning rate with SiO_2 as diluent

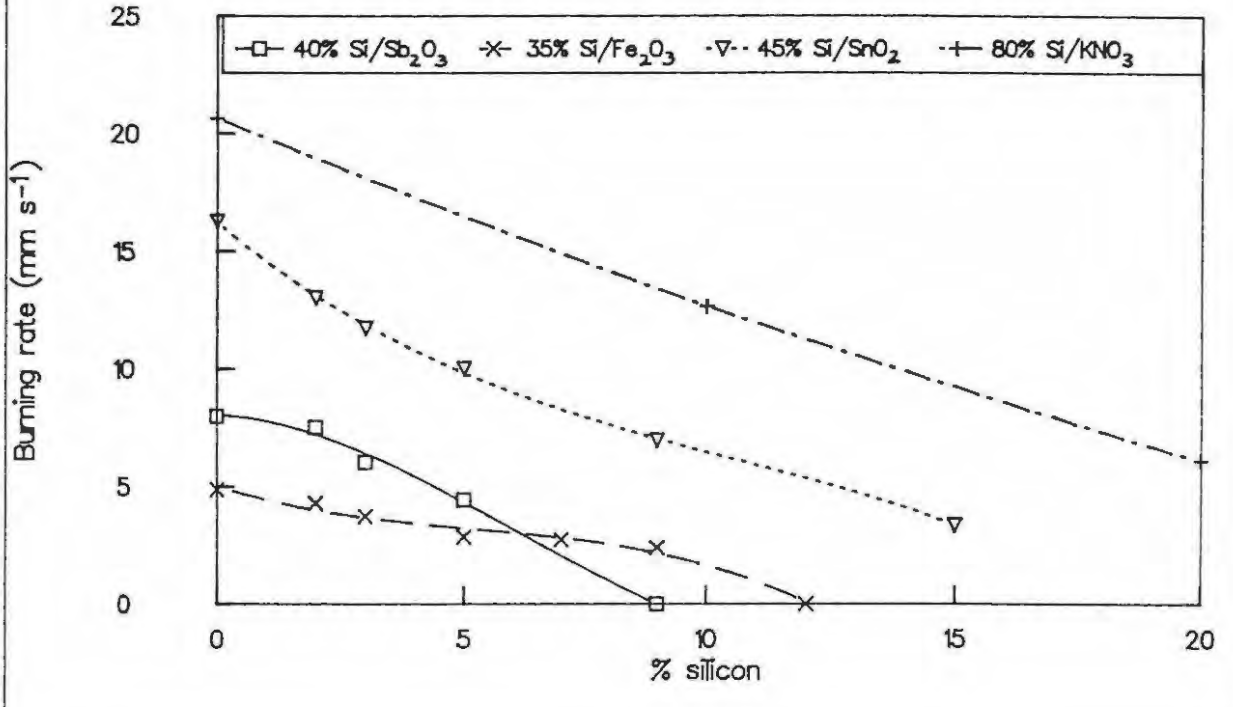

TABLE 13.4

Comparison of burning rates for selected Si/oxidant compositions

Composition	Burning rate (mm s^{-1})			
	Si/Sb_2O_3	Si/Fe_2O_3	Si/SnO_2	Si/KNO_3
40% Si *	8.5 ± 0.3	4.5 ± 0.2	17.1 ± 1.3	2.8 ± 0.2
mol ratio 2:1 (% silicon)	- (16.2)	3.6 ± 0.3 (26.0)	9.8 ± 0.7 (27.2)	3.6 ± 0.5 (35.7)
mol ratio 4:1 (% silicon)	8.2 ± 1.1 (27.8)	- (41.3)	16.4 ± 1.2 (42.7)	5.1 ± 0.7 (52.6)

* mol ratio corresponds to fuel:oxidant ratio

Effect of density

The burning rate against density curves for the four binary Si/oxidant systems showed very different characteristics. From thermal analysis (see Section 13.1) it could be deduced that the reactions between fuel and oxidant for the Si/Fe_2O_3 and Si/SnO_2 systems occurs predominantly between solid fuel and solid oxidant. Scanning electron micrographs showed evidence of solidified melts so the formation of liquid eutectics, or Sn(l) as a product of reduction of SnO_2(s), cannot be ruled out. The reactions in the Si/Sb_2O_3 and Si/KNO_3 systems are expected to involve gaseous or molten intermediates. The burning rates for 40% Si/Sb_2O_3 and 40% Si/KNO_3 compositions decreased and failed, respectively, as the density of the sample was increased, but the burning rates of 35% Si/Fe_2O_3 and 45% Si/SnO_2 compositions increased with compaction.

Effect of specific surface area (SSA)

The burning rate for the systems Si/Sb_2O_3, Si/Fe_2O_3 and Si/SnO_2 increased with increasing SSA of silicon. An increase in burning rate is expected because the larger surface area allows a more intimate mixture of fuel with oxidant and also means that a greater proportion of the silicon should react if formation of a protective oxide layer of uniform thickness limits reaction.

Effect of additives

Additives or diluents are routinely added to pyrotechnic systems to modify the burning rate. These additives may be inert and act by reducing the interparticle contact between fuel and oxidant and/or interfering with the conduction of heat from the reaction front to the adjacent unburnt material. Additives may also participate in the reaction and give rise to side reactions which then influence the heat output of the mixture and its burning rate.

Two supposedly inert diluents SiO_2 and Al_2O_3 were added in various proportions to the four binary Si/oxidant systems. The burning rate for all four systems decreased with increasing proportions of SiO_2 or Al_2O_3. The effect of SiO_2 on the burning rate of the binary systems is shown in Figure 13.2. The Si/KNO_3, Si/SnO_2 and Si/Fe_2O_3 mixtures sustained combustion over a much wider range of SiO_2 content than the Si/Sb_2O_3 mixtures. The similar behaviour of Al_2O_3 and SiO_2 suggests that SiO_2, even though a product of combustion, acts as an inert additive.

Water as an additive, decreased the burning rate more effectively than either of the solid additives and burning failed beyond 3% moisture. This influence of water would be of great practical importance in assessing the binary compositions for actual use as delays.

Summary

The burning rates (in parentheses) of various compositions of the Si/oxidant systems are shown schematically in Figure 13.3. The burning rates for the Si/Fe_2O_3 and Si/Sb_2O_3 systems are "slow" compared to the faster Si/SnO_2 system and the fast Si/KNO_3 system. The variation in v_{exp} for each Si/oxidant system under various conditions, **on the same burning rate scale**, are shown in Figures 13.4 to 13.7. The burning rates for the compositions chosen for detailed study (35% Si/Fe_2O_3, 40% Si/Sb_2O_3, 45% Si/SnO_2 and 80% Si/KNO_3) are represented by the dotted lines and are given in bold and underlined print. The conditions where maximum burning rate occurred for various compositions, densities and specific surface areas are emphasised in bold print. For the additives, the conditions at which burning failed are similarly emphasised.

The variations in the burning rates for the slow burning systems under various conditions were small compared to the faster systems. The burning rates for the systems at various densities and specific surface areas do not exceed by much the compositions at which maximum v_{exp} occurred when the Si content was varied. For all systems, failure occurred at approximately 2.6 mm s^{-1} in the presence of diluents. Water, as a diluent reduced the burning rates more drastically, in small amounts, than did SiO_2 and Al_2O_3 and burning failed beyond 3% moisture. Very large quantities of SiO_2 (60% by mass), compared to the other systems, were required for burning of the 80% Si/KNO_3 mixture to fail.

It is possible that the M-O bonding situation in the oxidants may influence the burning. Beardell and Kirschenbaum (1) have calculated M-O bond energies, B, in metal oxides from the relationship

$$B = (Q_B/2n) + (Q_D/4)$$

where $Q_B = -\Delta H_f$ of the oxide, Q_D is the dissociation energy of the O_2 molecule (489.5 kJ mol^{-1}) and n is the number of O atoms in the oxide. Values of B for the oxidants and related compounds are given In Table 13.5.

Figure 13.3 Comparing burning rates for binary Si/oxidant systems

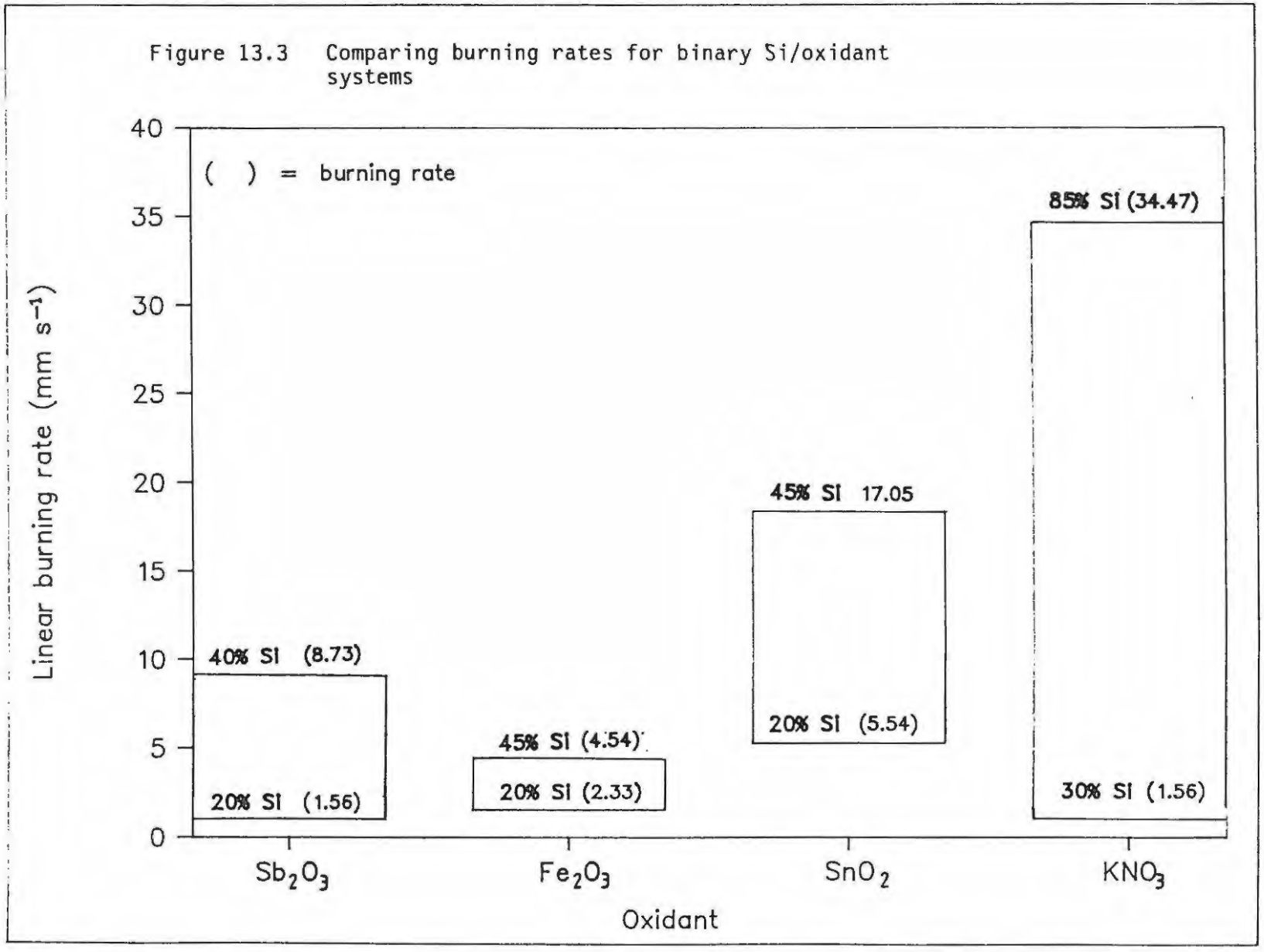

Figure 13.4 Variation in the burning rate of the Si/Fe_2O_3 system

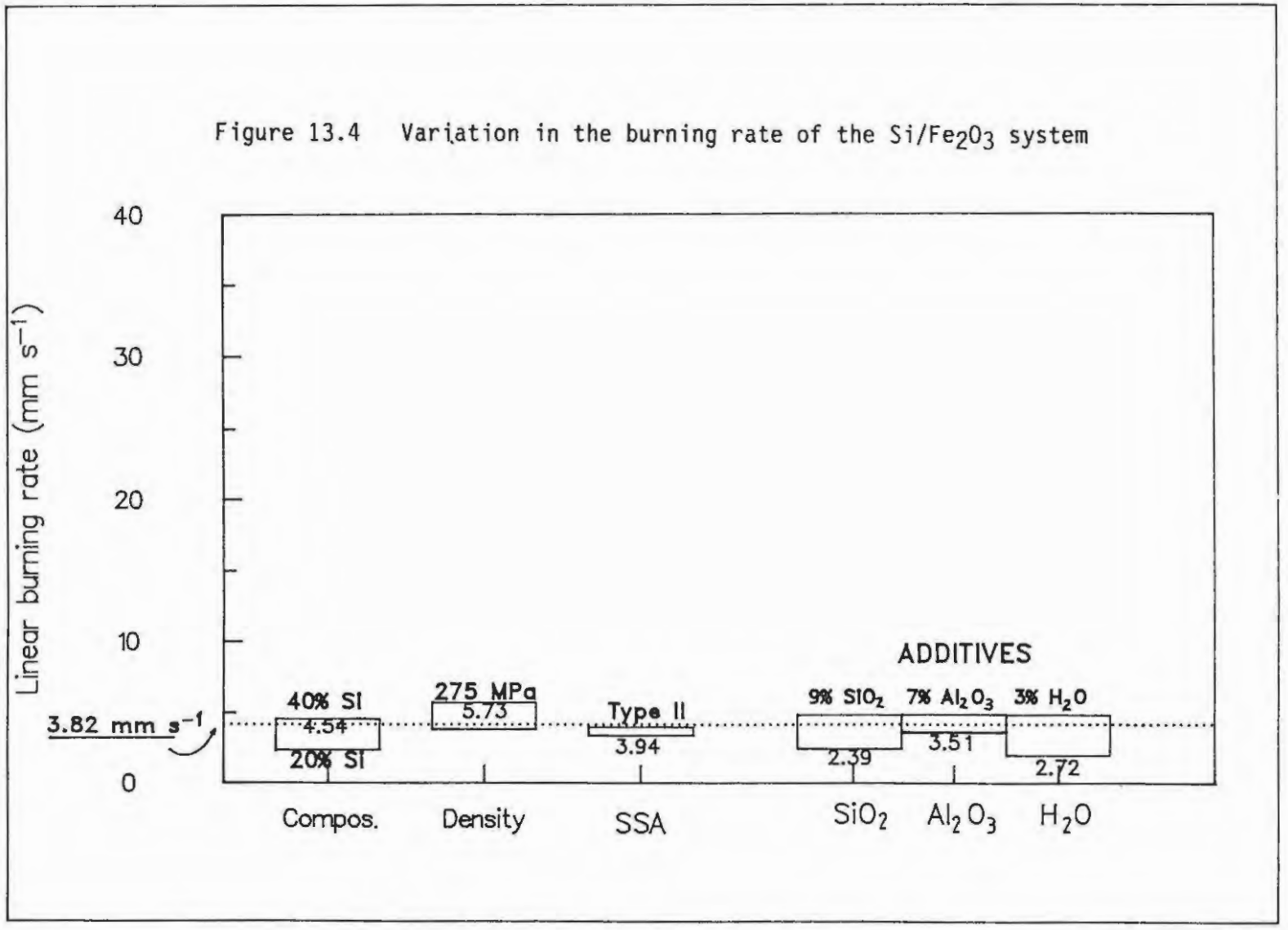

Figure 13.5 Variation in the burning rate of the Si/Sb_2O_3 system

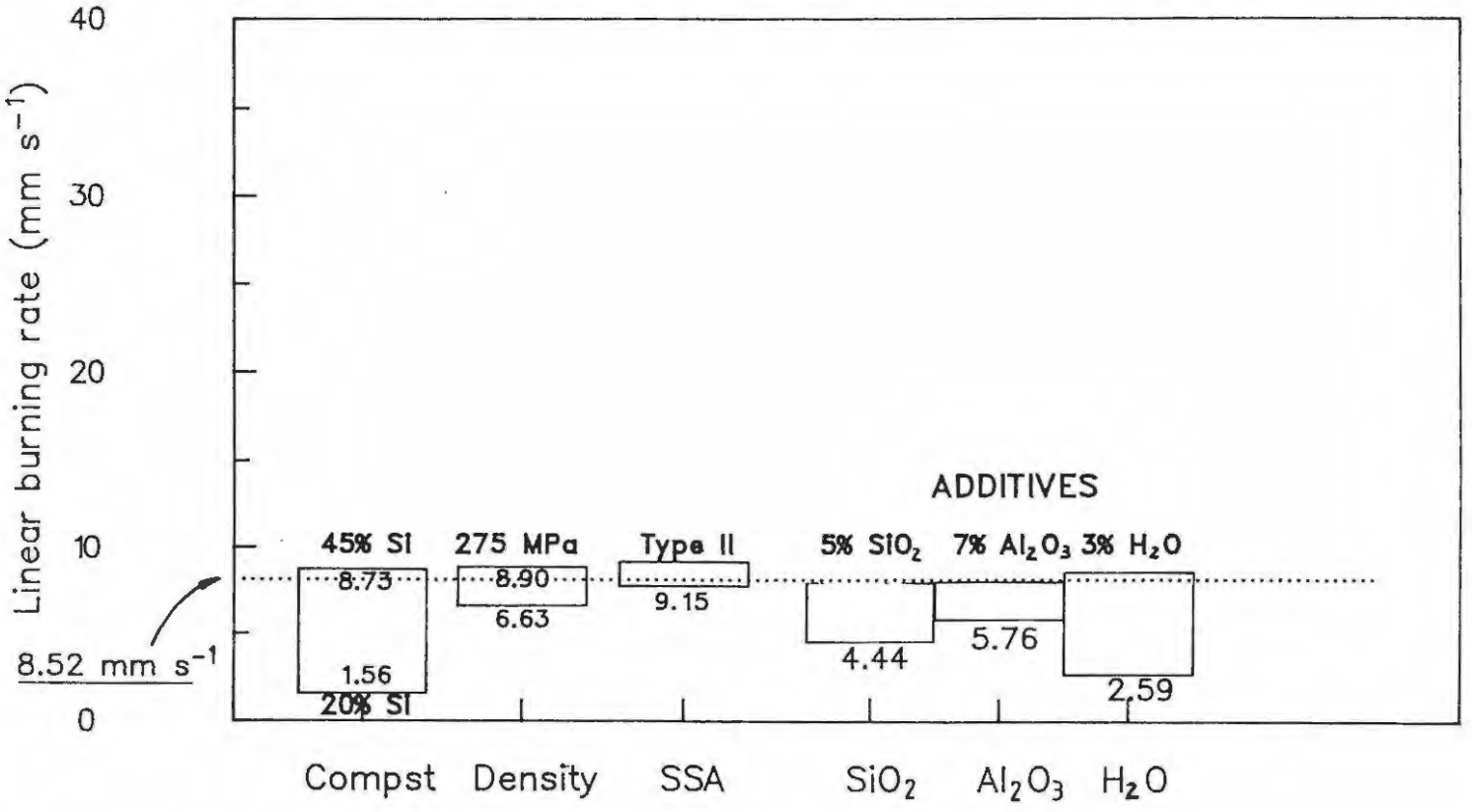

Figure 13.6 Variation in the burning rate of the Si/SnO_2 system

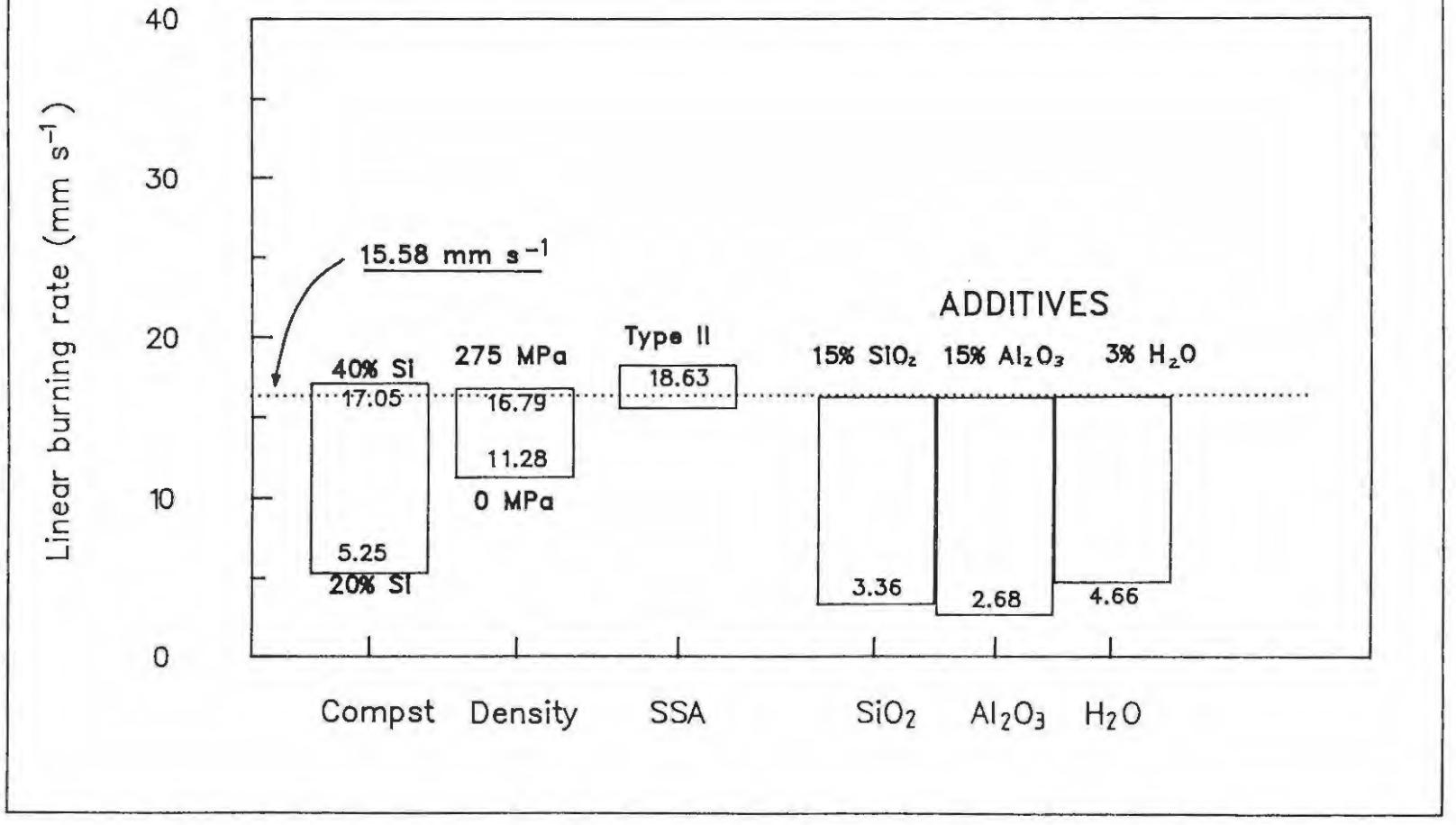

Figure 13.7 Variation in the burning rate of the Si/KNO_3 system

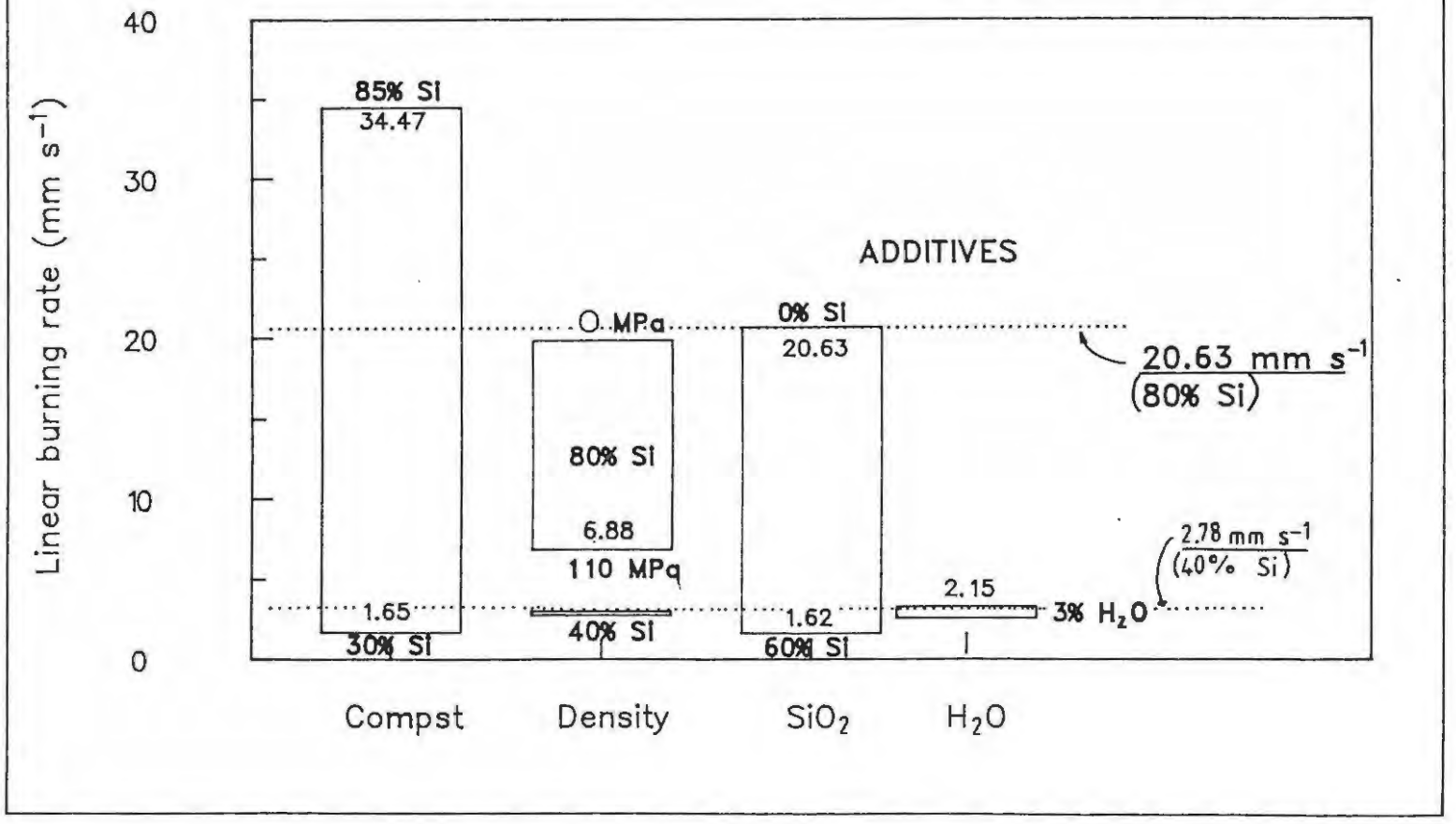

TABLE 13.5

M-O bond energies for some of the oxides encountered in this study

Oxide	Q_B (kJ mol^{-1})	B (kJ)
SiO_2	903.3	350
SnO_2	580.7	268
Sb_2O_3	696.6	238
FeO	266.5	256
Fe_2O_3	822.2	259
KNO_3	492.7	204
Fe_2SiO_4	1448	303

There is not sufficient variation in the value of B to account for the variations in burning rate.

13.2.2 *Temperature profiles*

The shapes of the temperature profiles varied with the composition of a given binary system, but generally the shapes for all the compositions examined for a particular binary mixture were similar. The temperature profiles for systems with different oxidants were very different (see Figure 13.8). Some of the features of the temperature profiles of the different Si/oxidant systems are summarised below.

(i) Si/Sb_2O_3 system

A smooth rise to T_{max} followed by cooling. The rise to T_{max} occurs rapidly initially and slows down before reaching T_{max} Slight, but not very reproducible changes in the slope of the rise region were observed.

(ii) Si/Fe_2O_3 system

First approximately sigmoidal curve followed by a plateau and then a second sigmoidal region.

(iii) Si/SnO_2 system

Smooth rise to T_{max} followed by cooling.

(iv) Si/KNO_3 system

A smooth rise to $\sim 500°C$ followed by a brief plateau and a second steeper rise to T_{max} and cooling (for 90% Si by mass).

Figure 13.8 Comparison of temperature profiles

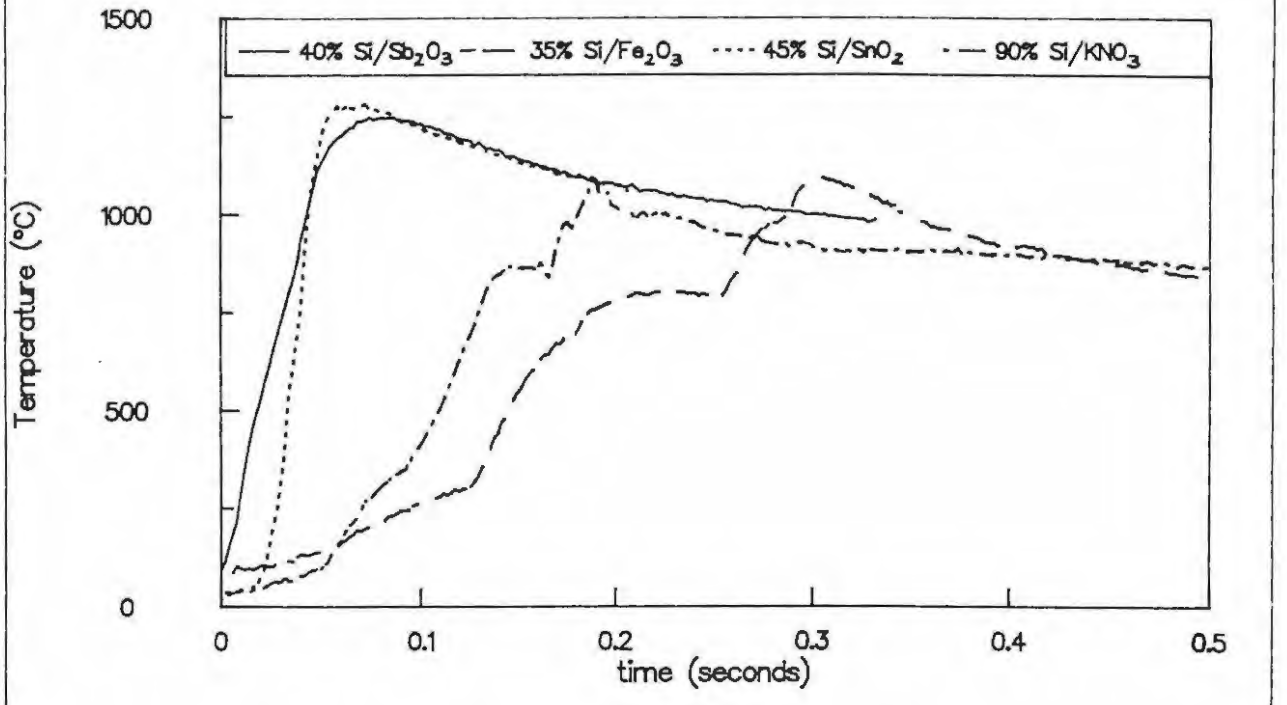

Figure 13.9 Comparison of maximum temperatures

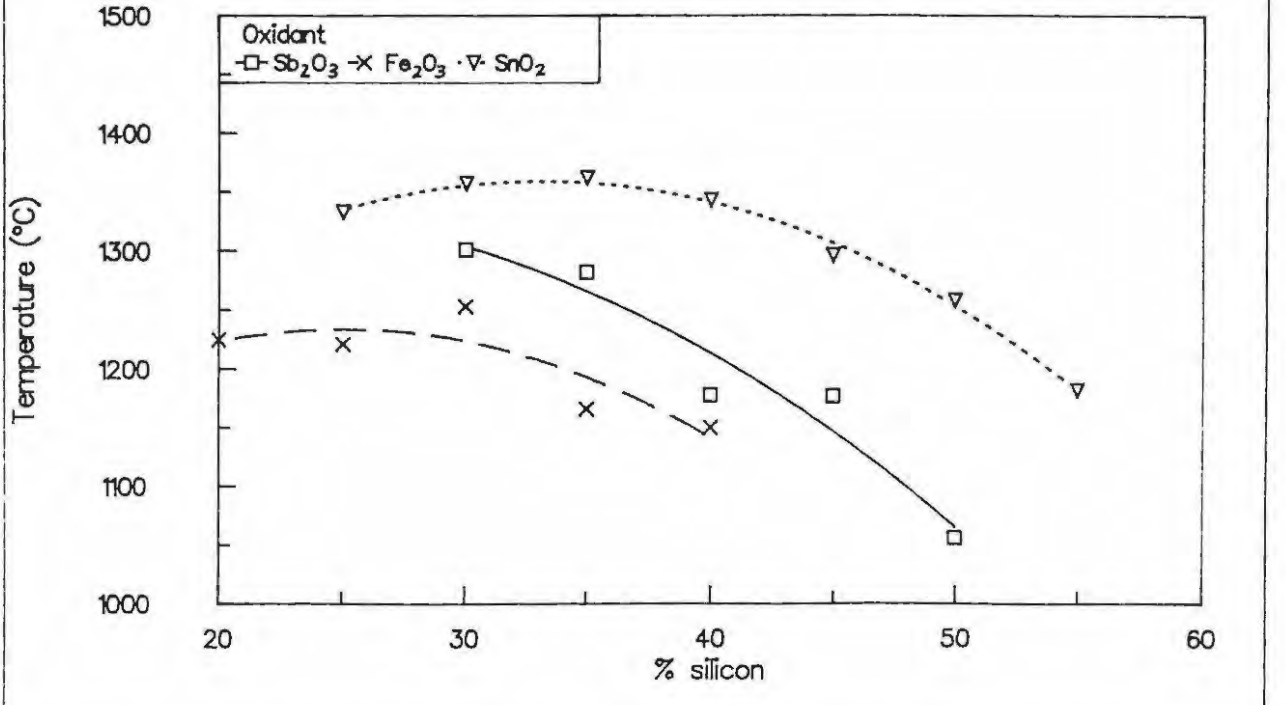

The shape of temperature profiles can often yield important information about the burning front (2,3). The plateau in the rise region of the profiles for the Si/Fe_2O_3 system (and for the 90% Si/KNO_3 mixture), according to Merzhanov (4,5), arises from either a two-stage reaction or from simultaneous phase transition and reaction. Thermodynamic calculations have shown (see Section 8.1.1) that a two stage mechanism, involving the formation of FeO and, subsequently, further reduction to Fe, is a possibility although the predicted maximum temperatures for such a mechanism is considerably higher than those observed. Another possibility is the formation of a eutectic melt between FeO and SiO_2 to form Fe_2SiO_4 which could also account for the plateau observed.

The rise times and maximum temperatures were affected by changing the fuel/oxidant ratio, by the presence of additives, and by changing the density of the samples, but the general shape of the profiles for a given system remained unchanged. The complex shape of the Si/Fe_2O_3 profiles changed to a simple sigmoidal shape with water as the additive or on inclusion of a second oxidant or a second fuel (see Section 14).

13.2.3 *Thermochemistry*

A plot of T_{max} against composition for the various Si/oxidant systems is shown in Figure 13.9. Although the highest maximum burning temperature recorded was for the Si/SnO_2 system, maximum temperatures for the Si/KNO_3 system (see Table 10.2) were generally beyond the thermocouple limits (1760°C).

Figure 13.10 shows that ΔH values from bomb calorimetry per gram of mixture were similar for the Si/Sb_2O_3 and Si/SnO_2 systems, but were lower than those obtained for the Si/Fe_2O_3 system and very much lower than those for the Si/KNO_3 system. The thermochemical information derived from the burning of 40% Si/oxidant systems is summarised in Table 13.6.

The measured heat of reaction (ΔH_{exp} (per g of mixture)) showed the following trends

$$Si/Fe_2O_3 > Si/SnO_2 > Si/Sb_2O_3$$

Maximum reaction temperatures for compositions containing 40% silicon were in order:

$$Si/KNO_3 >> Si/SnO_2 > Si/Sb_2O_3 > Si/Fe_2O_3$$

Figure 13.10 Comparison of reaction enthalpies per g of mixture

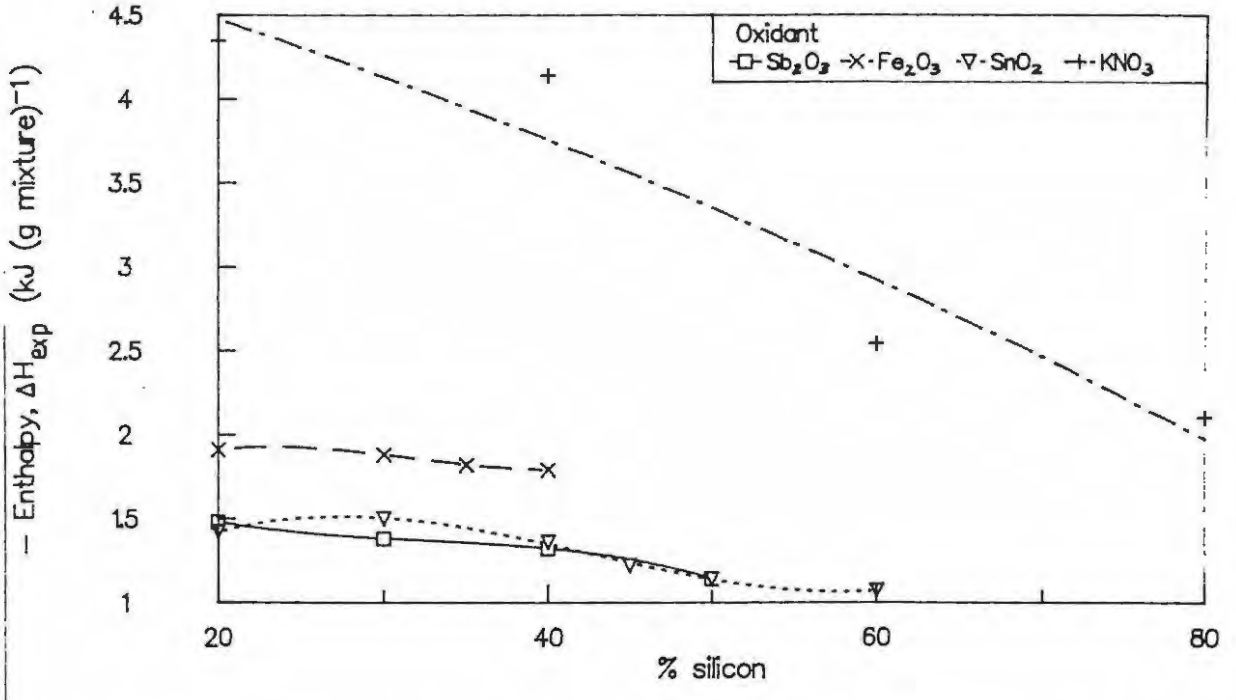

Figure 13.11 Comparison of thermal conductivities (at 298 K)

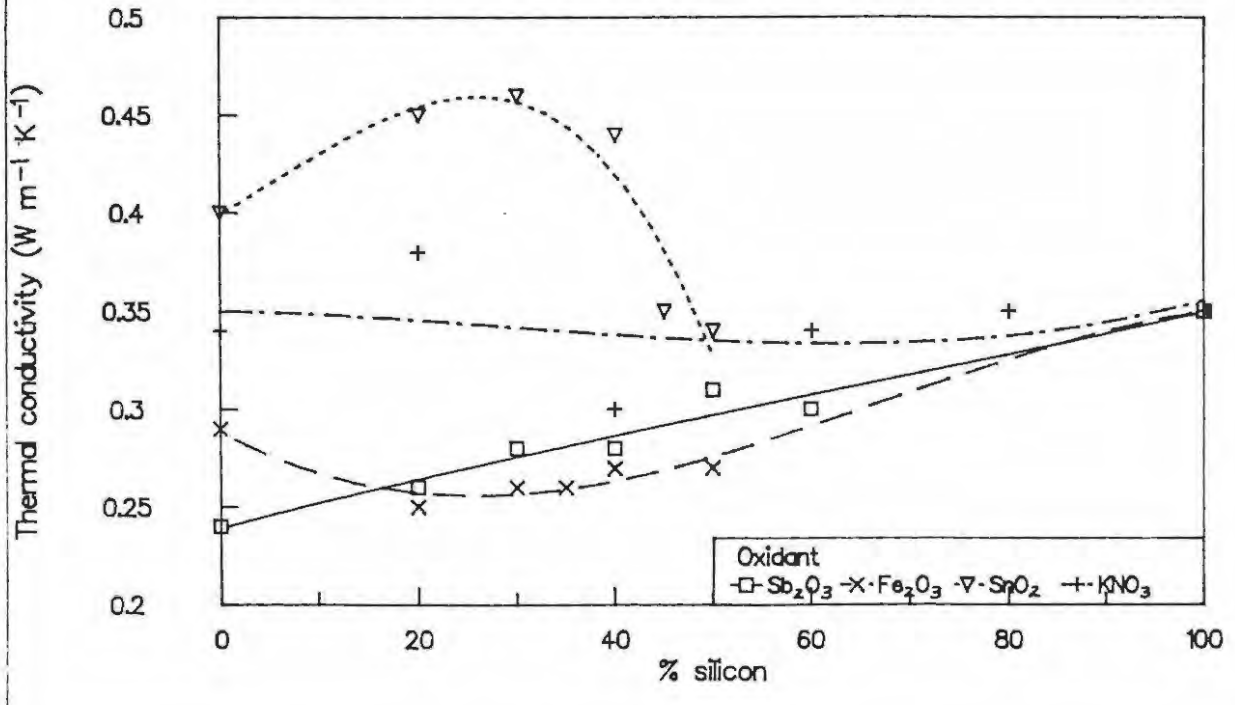

TABLE 13.6

Summary of thermochemical information for binary Si/oxidant mixtures

Proportion of fuel	Si/Sb_2O_3	Si/Fe_2O_3	Si/SnO_2	Si/KNO_3
	$-\Delta H_{exp}$ (kJ (g of mixture)$^{-1}$)			
40% Si	1.3 ± 0.1	1.8 ± 0.1	1.4 ± 0.1	4.1 ± 0.1
Stoichiometric (% silicon)	1.5 ± 0.1 (~20)	1.9 ± 0.1 (~20)	1.5 ± 0.1 (~30)	4.4 ± 0.1 (~20)
Mol ratio 3:1 (% silicon)	- (22.4)	1.8 ± 0.1 (34.6)	1.4 ± 0.1 (35.9)	3.0 ± 0.5 (45.5)
Mol ratio 5:1 (% silicon)	1.4 ± 0.1 (32.5)	- (46.9)	1.2 + 0.1 (48.2)	2.6 ± 0.5 (58.2)
	T_{max} (°C)			
40% Si	1179 ± 12	1150 ± 10	1343 ± 17	-
Mol ratio 3:1 (% silicon)	- (22.4)	1199 ± 38 (34.6)	1359 ± 28 (35.9)	- (45.5)
Mol ratio 5:1 (% silicon)	1291 ± 18 (32.5)	- (46.9)	1272 ± 26 (48.2)	- (58.2)
	U_{ad} (°C)			
40% Si	1231 ± 23	1358 ± 31	1376 ± 17	-
Mol ratio 3:1 (% silicon)	- (22.4)	1373 ± 114 (34.6)	1377 ± 46 (35.9)	- (45.5)
Mol ratio 5:1 (% silicon)	1382 ± 26 (32.5)	- (46.9)	1292 ± 43 (48.2)	- (58.2)

13.2.4 *Thermal conductivity*

The physical properties of the binary systems are listed in Table 13.7. The thermal conductivities, λ (at 298 K), for the Si/SnO_2 systems were most sensitive to composition of the mixture (Figure 13.11). λ for the Si/KNO_3, Si/Sb_2O_3 and the Si/Fe_2O_3 systems increased almost linearly with increasing silicon. The thermal conductivities (at 298 K) of the various systems were in the following order:

$$Si/SnO_2 > Si/KNO_3 > Si/Sb_2O_3 > Si/Fe_2O_3$$

TABLE 13.7

Summary of the physical properties of the binary Si/oxidant systems*

System	Density ($g\ cm^{-3}$)	Specific heat capacity, c ($J\ K^{-1}\ g^{-1}$)		Thermal conductivity λ ($W\ K^{-1}\ m^{-1}$) (298 K)	Thermal diffusivity $D \times 10^{-7}$ ($m^2\ s^{-1}$) (298 K)
		(298 K)	(1600 K)		
Si/Sb_2O_3	2.9 to 2.1	0.42 to 0.53	0.73 to 0.81	0.26 to 0.30	2.32 to 2.15
Si/Fe_2O_3	2.4 to 2.1	0.66 to 0.68	1.29 to 1.21	0.25 to 0.27	2.26 to 2.22
Si/SnO_2	3.1 to 2.0	0.42 to 0.55	0.64 to 0.78	0.45 to 0.34	4.13 to 2.39
Si/KNO_3	1.8 to 1.6	0.91 to 0.76	1.43 to 1.08	0.38 to 0.35	2.12 to 2.15

* Physical properties for the various systems are given in order of increasing silicon content.

The specific heat capacities for the binary systems (estimated at either 298 K or 1600 K (6)) decreased, in the order

$$Si/KNO_3 > Si/Fe_2O_3 > Si/Sb_2O_3 > Si/SnO_2$$

Thermal diffusivities ($D = \lambda/\rho c$) calculated at 298 K, however, showed the following order

$$Si/SnO_2 > Si/Sb_2O_3 > Si/Fe_2O_3 > Si/KNO_3$$

D therefore follows the same order as the burning rates for mass ratios of less than 40% silicon. The high burning rates for the Si/KNO_3 mixtures (above 50% Si) can therefore not be explained by the thermal diffusivity of the mixture.

The values of the thermal diffusivities calculated from the measured rise times and burning rates ($D = v^2/t_r$) were much greater than those determined from room-temperature experiments (see Section 12). Since the thermal diffusivity depends on both λ and c, and c increases substantially with temperature (values at 1600 K are given in Table 13.7), λ for the system would be expected to increase with increasing temperature. Of the little information available, λ for SiO_2 does increase with T, but λ for SnO_2 decreases. In a powder, however, the effects will be further complicated by the occurrence of melting.

13.2.5 *Kinetic information*

Thermal analysis

A summary of the kinetic parameters (derived for n = 1) (see Section 6.8) from thermal analysis experiments and at controlled heating rates is given in Table 13.8. No exotherms were obtained in the traces for Si/Fe_2O_3 and Si/SnO_2 up to the limits of the DSC (720°C).

TABLE 13.8

Comparison of kinetic parameters derived from thermal analysis

System	E_a (kJ mol^{-1})	A (s^{-1})
Si in O_2	85 ± 18	1.10 ± 0.05
40% Si/Sb_2O_3	339 ± 8	$(1.12 \pm 0.04)x10^{20}$
60% Si/KNO_3	813 ± 168	$(1.02 \pm 0.10)x10^{51}$

These kinetic parameters for the Si/oxidant mixtures are considerably greater than the parameters derived from the analysis of temperature profiles (see below).

The activation energies determined from the application of the Borchardt and Daniels method to suitable results of programmed temperature experiments were very different for the Si/Sb_2O_3 and Si/KNO_3 systems and were even different for different compositions of the same system. For some systems, the E_a values varied markedly with the value of the "apparent order-of-reaction", n, chosen. Although there is uncertainty about the validity of applying the Borchardt and Daniels method (7) to such systems, and on the interpretation of the significance of the derived E_a values, the analysis is common to all systems and the results show considerable differences.

The values for the reaction of Si with gaseous oxygen (~85 kJ mol^{-1}) are low compared to the values of 130 kJ mol^{-1} reported (8,9). If the activation energy is interpreted in the simplest terms as the temperature coefficient of the reaction rate, then the Si/KNO_3 system with a definitely molten oxidant has a greater dependence on T than the Si/Sb_2O_3 system, where the oxidant sublimes and melts. Both of these systems have E_a values greater than that for the $Si/O_2(g)$ reaction.

The $Si/O_2(g)$ reaction is known to be hindered by the formation of a protective layer of SiO_2 product (see Section 2.2). In the other systems, there is the possibility of disruption or dissociation of such a layer by the molten oxidant or by formation of eutectic melts.

Analysis of temperature profiles

Kinetic parameters were also determined from the temperature profiles i.e. obtained under ignition conditions, using the Hill and the Leeds approaches (see Section 4).

The Hill activation energies and pre-exponential factors generally increased when the reaction order used in the analysis was increased from 0.50 to 0.67, 1 and 2 for a given profile. E_a values (n = 0.67) for the various compositions were generally low (6.0 to 21.3 kJ mol^{-1}) (see Table 13.9). Leeds E_a values were slightly greater than the corresponding Hill values, while Leeds pre-exponential factors were generally lower than the Hill values. Reaction orders, as determined in the Leeds analysis, and ranged between 0.32 and 0.95. The low activation energies are characteristic of diffusion-controlled reactions.

Plots of the various contributions to the power function showed that lateral thermal losses are small. The contributions to the thermal power (dU/dt) and axial conduction ($t^*(d^2U/dt^2)$) varied depending on the composition of the mixture and also on the oxidant used. No trends were, however, noted.

Slight differences in the Hill and Leeds values for E_a are expected since (i) the Hill approach ignores lateral heat loss, (ii) the extent of reaction α is defined slightly differently, and (iii) the calculations are lengthy.

Plots of the Hill values for E_a, for $n = 0.67$, for various compositions are shown in Figure 13.12. The value of E_a for a given Si/oxidant system did not vary much with composition. The differences in the E_a values for systems with a different oxidants were greater at low % silicon. The activation energies for the second rise region of the Si/Fe_2O_3 profiles (60 to 73 kJ mol^{-1}) were considerably greater than for the first rise region (12.9 to 21.3 kJ mol^{-1}). The activation energies for the Si/Sb_2O_3 system (6 to 14 kJ mol^{-1}) showed a slight maximum at ~37% Si. The plot of E_a against % Si for the Si/SnO_2 system was almost horizontal at~9 kJ mol^{-1}.

Similar trends were observed with the Leeds values of the activation energies (see Figure 13.13 and Table 13.9). Leeds E_a values were generally greater than the corresponding Hill values for the Si/Fe_2O_3 system. Hill and Leeds E_a values were similar for the Si/Sb_2O_3 and the Si/SnO_2 systems.

The activation energies for the Si/oxidant systems were in the order

$$Si/Fe_2O_3 > Si/Sb_2O_3 > Si/SnO_2$$

This could be as a result of the temperature dependence of diffusion in systems where melts are formed being greater than in a probable exclusively solid system (Si/SnO_2).

Other kinetic considerations

The kinetic parameters derived for the 40% Si/Sb_2O_3 composition from thermal analysis and from the analysis of temperature profiles are listed in Table 13.10.

Plots of the rate constant as a function of temperature for the 40% Si/Sb_2O_3 system using Hill and Leeds kinetic parameters derived from temperature profiles and using $n = 1$, are shown in Figures 13.14 and 13.15. The Hill and Leeds parameters for 40% Si/Sb_2O_3 gave very different k values at a common temperature. The Hill kinetic parameters, did not give an acceptable representation of the calculated power functions (G).

The applicability of Arrhenius kinetics to reactions involving solid reactions has been the source of much debate. Boddington *et al* used a modified rate equation (see Section 4.7) which combines the temperature-dependent Arrhenius rate equation with a diffusion dependent kinetic term to describe, more accurately, the kinetic behaviour of pyrotechnic reactions (10)

$$k = k_{AR}^{-1} + (BT^m)^{-1}$$

TABLE 13.9

Kinetic parameters from the analysis of temperature profiles

Proportion of fuel	Hill approach		Leeds approach	
	E_a (kJ mol^{-1})	A (s^{-1})	E_a (kJ mol^{-1})	A (s^{-1})
Si/Sb_2O_3				
40% Si	14.3 ± 1.7	998 ± 27	13.3 ± 4.7	81 ± 16
mol ratio 3:1 (%Si = 22.4)	-	-	-	-
mol ratio 5:1 (%Si = 32.5)	16.0 ± 3.6	3662 ± 295	16.1 ± 8.1	92 ± 21
Si/Fe_2O_3 (1st rise region)				
40% Si	14.5 ± 3.4	$(80.8 \pm_3 5.8) \times 10^{-3}$	29.5 ± 4.8	1978 ± 461
mol ratio 3:1 (%Si = 34.6)	22.0 ± 3.7	$(29.7 \pm_4 1.8) \times 10^{-4}$	33.8 ± 8.0	3295 ± 780
mol ratio 5:1 (%Si = 46.9)	-	-	-	-
Si/SnO_2				
40% Si	11.6 ± 0.5	$(32.7 \pm_4 1.6) \times 10^{-4}$	7.3 ± 1.8	68 ± 3
mol ratio 3:1 (%Si = 35.9)	11.5 ± 1.5	$(24.8 \pm_4 1.1) \times 10^{-4}$	9.3 ± 2.3	137 ± 7
mol ratio 5:1 (%Si = 48.2)	13.0 ± 1.7	$(44.1 \pm_5 3.6) \times 10^{-5}$	10.7 ± 2.7	99 ± 5

TABLE 13.10

Comparison of kinetic parameters for 40% Si/Sb_2O_3 from thermal analysis and temperature profiles

Thermal analysis		Temperature profiles	
E_a (kJ mol^{-1})	A (s^{-1})	E_a (kJ mol^{-1})	A (s^{-1})
338.7 ± 8.3	(1.12 ± 0.04) x 10^{20}	*Hill*: 14.3 ± 1.7	998 ± 27
		Leeds: 13.3 ± 4.7	81 ± 16

Figure 13.12 Comparison of activation energies from the Hill approach

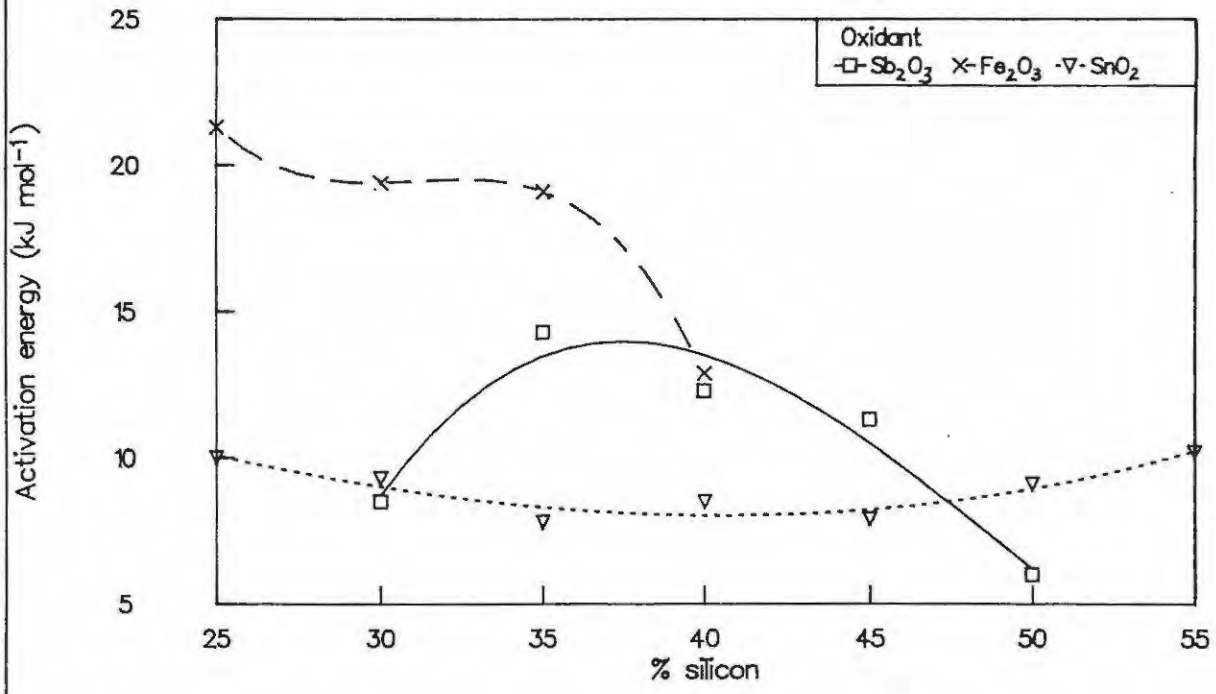

Figure 13.13 Comparison of activation energies from the Leeds approach

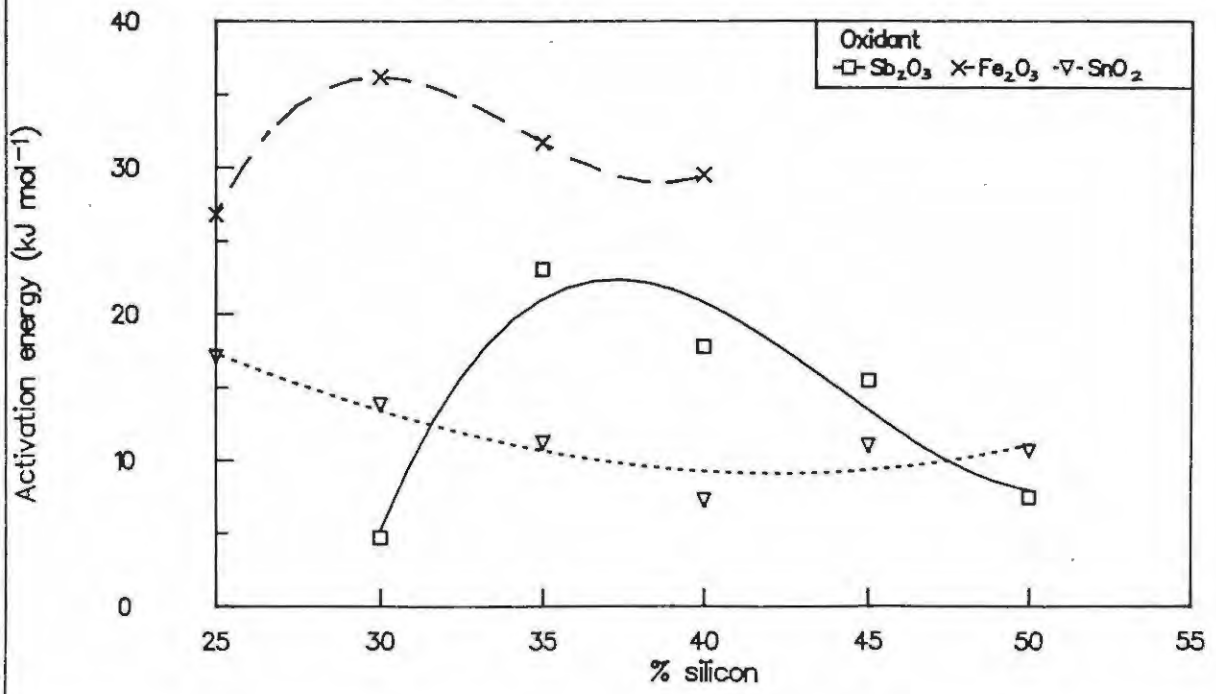

Figure 13.14 Rate constant for a 40% Si/Sb_2O_3 mixture using the Hill kinetic parameters (E_a = 14.3 kJ mol^{-1} and A = 9.9 x 10^4 s^{-1})

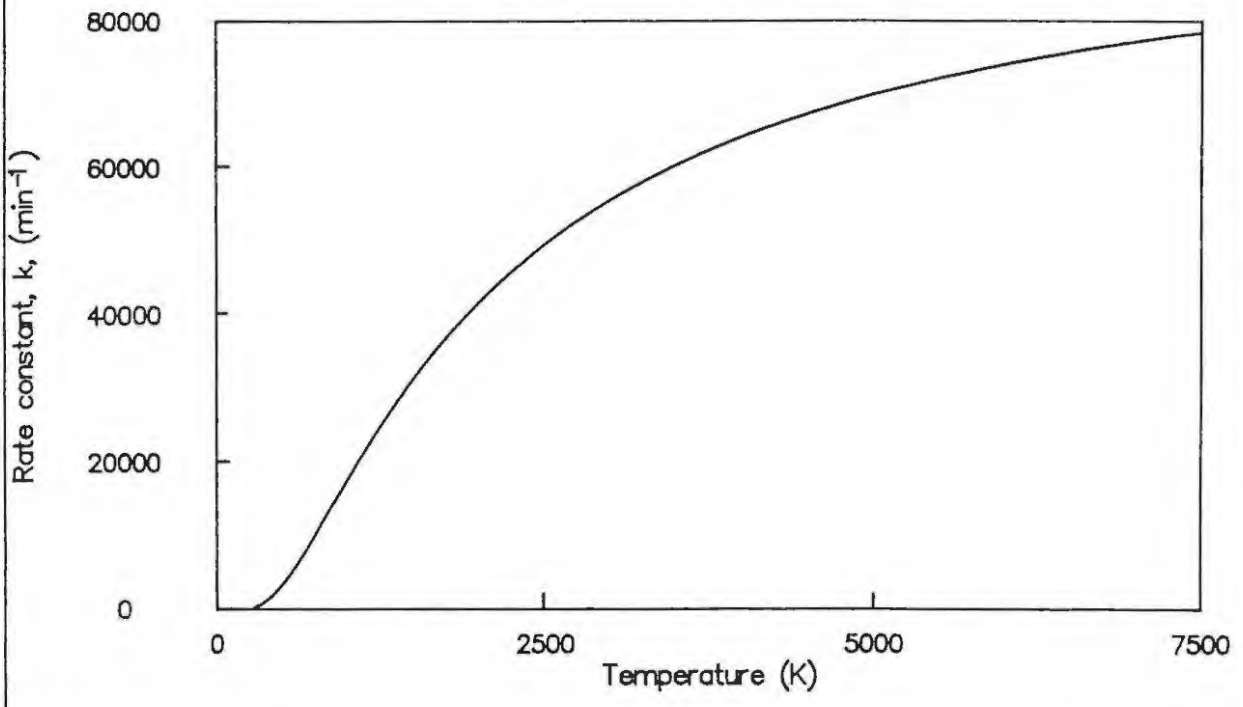

Figure 13.15 Rate constant for a 40% Si/Sb_2O_3 mixture using the Leeds kinetic parameters (E_a = 17.8 kJ mol^{-1} and A = 2.4 x 10^2 s^{-1})

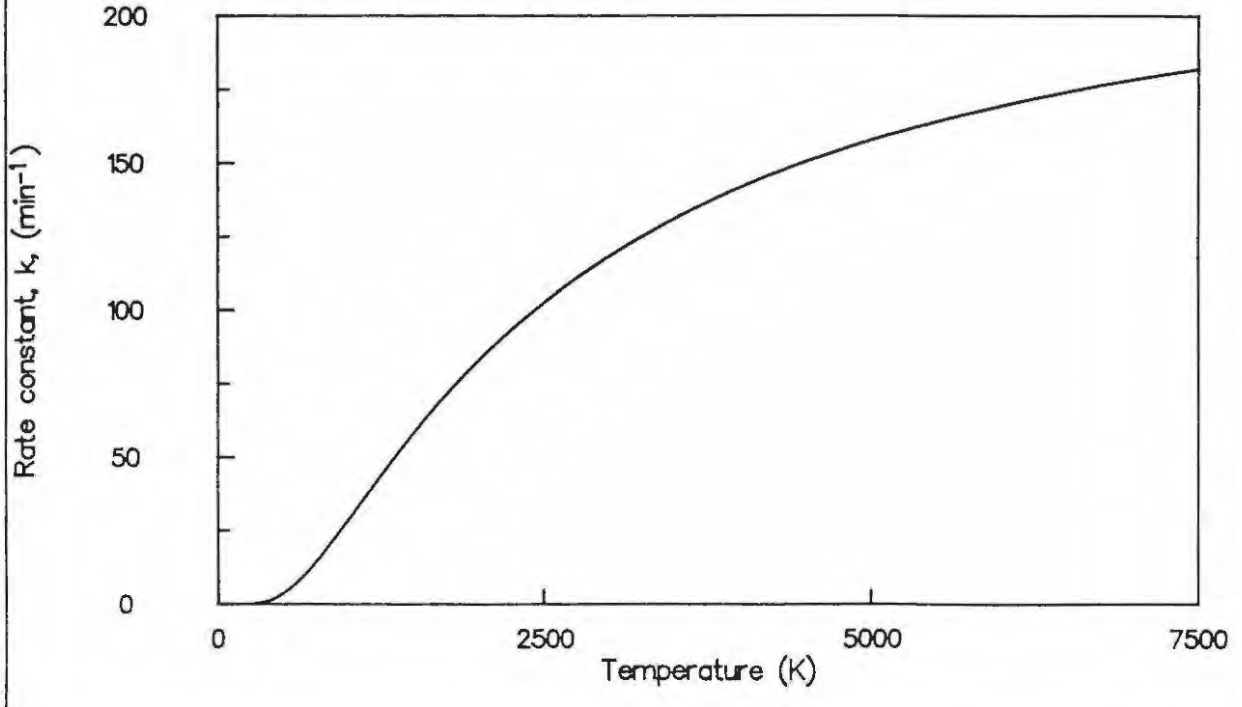

The low-temperature kinetic behaviour

$$k_{AR}^{-1} = k_{AR} \exp(-E_a/RT)$$

is assumed to be adequately described by the kinetic behaviour derived from thermal analysis, and the high-temperature diffusion kinetics by the kinetic behaviour derived from the analysis of temperature profiles. In the temperature range 900 to 950 K, m = 1.61 ± 0.01, B = (4.23 ± 0.03) x 10^{-3} s^{-1} $K^{1.61}$ and r = 0.99 using the Hill kinetic data. When the Leeds kinetic data were used, m = 2.20 ± 0.01, B = (6.15 ± 0.08) x 10^{-8} s^{-1} $K^{2.22}$ and r = 0.99 over the temperature range 800 to 850 K. The rate coefficients derived from classical Arrhenius kinetic data from temperature profiles (k_{TT}) and thermal analysis (k_{TA}) for a 40% Si/Sb_2O_3 mixture and the rate coefficient from the modified equation (k_{comb}), are compared in Figure 13.16 (using Hill parameters) and Figure 13.17 (using Leeds parameters). The Hill parameters gave a much higher rate dependence on temperature than the Leeds parameters did.

At low temperatures, the rate coefficient derived from thermal analysis (where dT/dt is a constant), k_{TA}, is similar to that for the rate coefficient for the combined equation (k_{comb}). At high temperatures, k_{AR} is very large and $k_{comb} \equiv k_{TP} \equiv BT^m$.

13.2.6 *Summary*

A summary of the various trends related to the burning of Si/oxidant compositions is given in Table 13.11.

T_{max} and maximum v_{exp} followed the same trends. The same trends were also noted for ΔH_{exp} and c and for v_{exp} (at 40% Si) and D

Figure 13.16 Comparison of the rate coefficients for 40% Si/Sb_2O_3 using Hill parameters

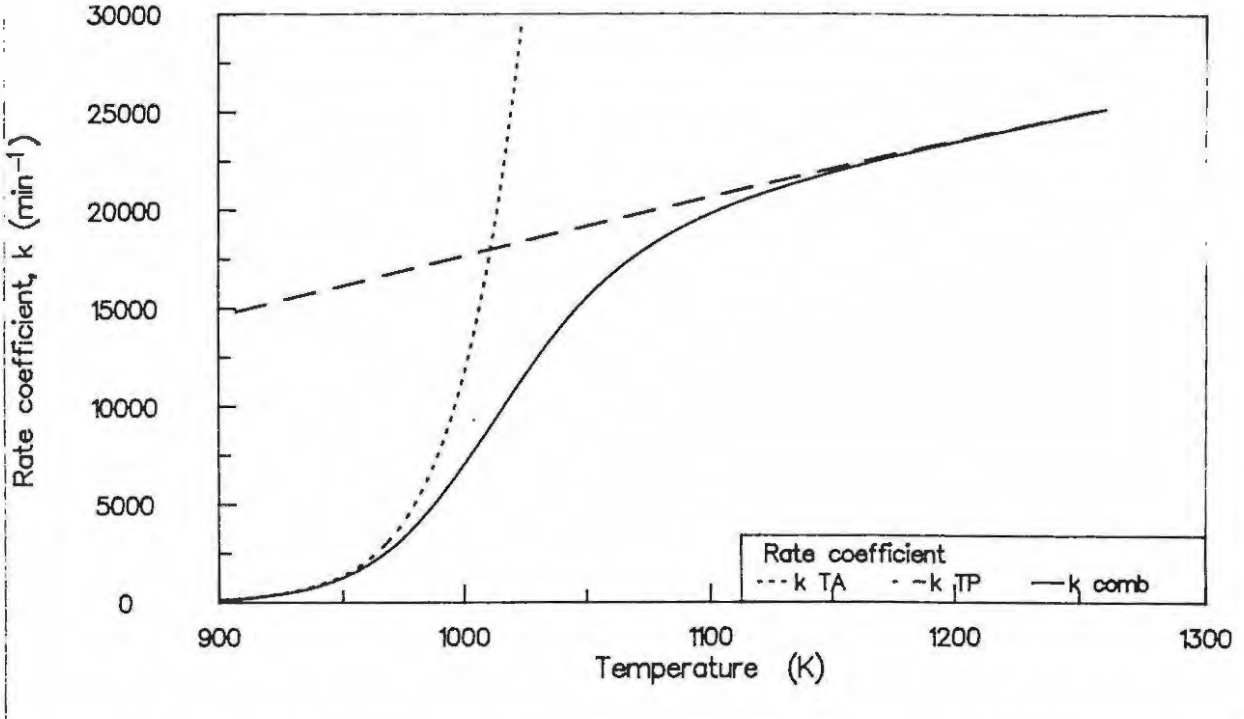

Figure 13.17 Comparison of the rate coefficients for 40% Si/Sb_2O_3 using Leeds non-linear regression parameters

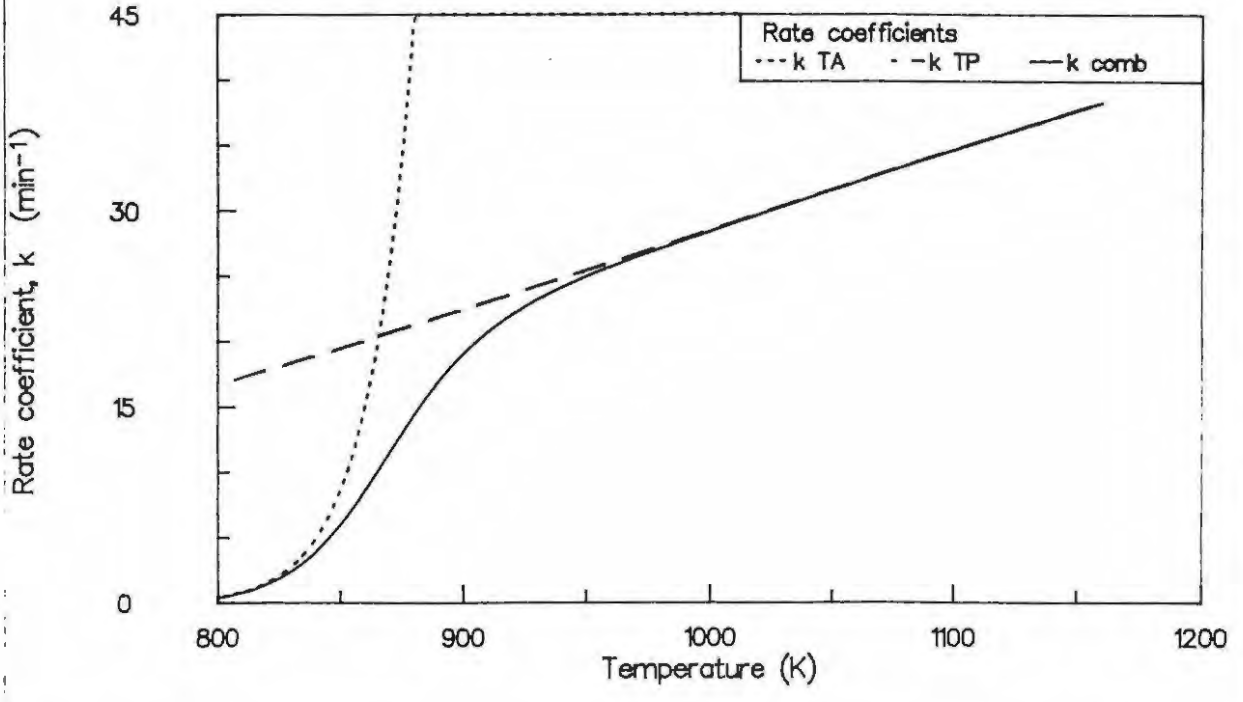

TABLE 13.11

Summary of the burning behaviour of Si/oxidant systems

Property	Order of decrease			
Burning rate,				
v_{exp} (40% Si)	SnO_2	Sb_2O_3	Fe_2O_3	KNO_3
maximum v_{exp}	KNO_3	SnO_2	Sb_2O_3	Fe_2O_3
Maximum temperature,				
T_{max} (°C)	KNO_3	SnO_2	Sb_2O_3	Fe_2O_3
Heat output,				
ΔH_{exp} (kJ (g mixture)$^{-1}$	KNO_3	Fe_2O_3	SnO_2	Sb_2O_3
Specific heat capacity,				
c (J K^{-1} g^{-1})	KNO_3	Fe_2O_3	SnO_2	Sb_2O_3
Thermal conductivity,				
λ (W m^{-1} K^{-1})	SnO_2	KNO_3	Sb_2O_3	Fe_2O_3
Thermal diffusivity,				
D (m^2 s^{-1}) (298 K)	SnO_2	Sb_2O_3	Fe_2O_3	KNO_3
Activation energy,				
E_a (kJ mol^{-1})	Fe_2O_3	Sb_2O_3	SnO_2	

13.3 References

1 A.D. Kirshenbaum and A.J. Beardell, Thermochim. Acta, **8** (1974) 35.

2. Z.A. Munir and J.B. Holt (Eds.), *Combustion and Plasma Synthesis of High Temperature Materials*", VCH Verlag, New York, 1990 p. 7.

3 T. Boddington, P.G. Laye, J.R. Pude and J. Tipping, Comb. Flame, **47** (1982) 254.

4. A.G. Merzhanoz, Ed. Rumanov and B.I. Khaikin, J. App. Mechanics Techn. Phys., **6** (1972) 99.

5. A.G. Merzhanov, Dokl. Acad, Nauk SSSR, **233** (1977) 1130.

6. O. Kubachewski, E. Li. and C.B. Alcock, "*Metallurgical Thermochemistry*", 4th Edition, Pergamon Press, 1967.

7. H.J. Borchardt and F. Daniels, J. Am. Chem. Soc., **79** (1957) 41.

8. B.E. Deal and A.S. Grove, J. App. Phy., **36** (1965) 3770.

9. E.A. Irene and D. Dong, J. Electrochem. Soc., **125** (1978) 1146.

10. T. Boddington, A. Cottrell and P.G. Laye, Comb. Flame, **79** (1990) 234.

14. DISCUSSION OF TERNARY SYSTEMS

14.1 Thermal analysis

14.1.1 *Mixed fuel systems*

No interactions between the fuels Si, $FeSi_7$ and $CaSi_2$ were anticipated on heating in nitrogen to the limits of the thermal analysis equipment.

14.1.2 *Mixed oxidant systems*

Thermal analysis curves in nitrogen of ternary systems with two oxidants generally showed that there was very little interaction between the oxidants. The thermal events observed were similar to those noted for the individual oxidant systems.

TG and DSC traces of the $Si/Fe_2O_3/SnO_2$ mixtures showed that no reaction could be induced in the Si/Fe_2O_3 mixture in the presence of SnO_2. For binary Si/Fe_2O_3 and Si/SnO_2 mixtures with Sb_2O_3 as the second oxidant, only the usual reaction between Si and Sb_2O_3 was noted. There were indications that Sb_2O_3 may have caused ignition in the Si/SnO_2 system but this could not be confirmed due mainly to the loss of Sb_2O_3 as volatiles.

In the $Si/SnO_2/KNO_3$ system, reaction between the three ingredients could only be induced when the KNO_3 content was 15% and the SnO_2 content was 45%. A sharp exotherm was observed in the $Si/Fe_2O_3/KNO_3$ system at approximately 530°C. Ignition occurred at approximately the same temperature as the onset of the reaction between Si and KNO_3.

The DSC traces of the $Si/Sb_2O_3/KNO_3$ system, showed two overlapping but well-defined exotherms. The first exotherm at ~500°C occurred in the same temperature range as the reaction between Si and Sb_2O_3 alone. The size of this exotherm increased with increasing Sb_2O_3. The second exotherm is due to the reaction between silicon and KNO_3. Enthalpy measurements from DSC traces showed that both oxidants contributed to the oxidation of silicon during the first exotherm.

14.2 Combustion of ternary systems

14.2.1 *Mixed fuel systems*

The burning behaviour of systems with $FeSi_7$ or $CaSi_2$ as fuel were very different from those in which Si was used as a fuel. Burning rates for binary compositions containing silicon, $FeSi_7$ and $CaSi_2$ as fuels are summarised in Table 11.3. These results are plotted for comparison in Figure 14.1.

TABLE 14.1

Burning rates for binary systems containing various fuels

Composition	v_{exp} (mm s^{-1})	m_{exp} (g s^{-1})	T_{max} (°C)
Sb_2O_3			
40% Si	8.77 ± 0.16	0.72 ± 0.03	1329 ± 9
40% $FeSi_7$	4.51 ± 0.07	0.38 ± 0.01	1364 ± 11
40% $CaSi_2$	16.85 ± 1.23	1.58 ± 0.06	tc shorted
Fe_2O_3			
35% Si	5.01 ± 0.15	0.30 ± 0.01	1210 ± 16
35% $FeSi_7$	5.91 ± 0.10	0.43 ± 0.02	1241 ± 21
35% $CaSi_2$	5.73 ± 0.27	0.32 ± 0.03	tc shorted
SnO_2			
45% Si	16.10 ± 1.25	1.10 ± 0.05	1319 ± 19
45% $FeSi_7$	12.18 ± 0.63	0.92 ± 0.10	1326 ± 18
45% $CaSi_2$	5.93 ± 0.13	0.50 ± 0.03	tc shorted
KNO_3			
40% Si	9.11 ± 0.17	0.72 ± 0.02	tc shorted
40% $FeSi_7$	18.66 ± 0.41	1.29 ± 0.02	tc shorted
40% $CaSi_2$	5.94 ± 0.13	0.50 ± 0.03	tc shorted

These changes in burning rates could arise from one or more of the following factors. Changing the fuel can:

(i) change the composition in molar terms

(ii) change the chemical reactions occurring

(iii) change the particle-size and fuel/oxidant contact

From Table 3.1, the mean particle diameters of Si, $FeSi_7$ and $CaSi_2$ are 3.4 μm, 6.0 μm and 25.8 μm, respectively. Increasing the particle-size usually decreases the burning rate, so the expected order of burning rate based on factor (iii), would be Si > $FeSi_7$ > $CaSi_2$.

One gram of fuel corresponds to 35.6 mmol Si (Si), 27.7 mmol Si ($FeSi_7$) and 20.8 mmol Si ($CaSi_2$). The proportion of Si thus decreases in the order Si > $FeSi_7$ > $CaSi_2$.

The order of burning rate, Si > $FeSi_7$ > $CaSi_2$ is found (Figure 14.1) only for the fuel/SnO_2 systems.

The opposite trend is observed for the fuel/Fe_2O_3 systems, but the changes are relatively smaller. It appears that the substitution of $FeSi_7$ for Si in a system containing Fe_2O_3 has less of an effect on the burning rate than in the other systems, which supports factor (ii) i.e. the occurrence of different chemical reactions. This is supported by the large and very different variations observed for fuel/Sb_2O_3 and fuel/KNO_3 systems (Figure 14.1).

Figure 14.1 Comparison of burning rates of binary mixtures with Si, $FeSi_7$ and $CaSi_2$ as fuels

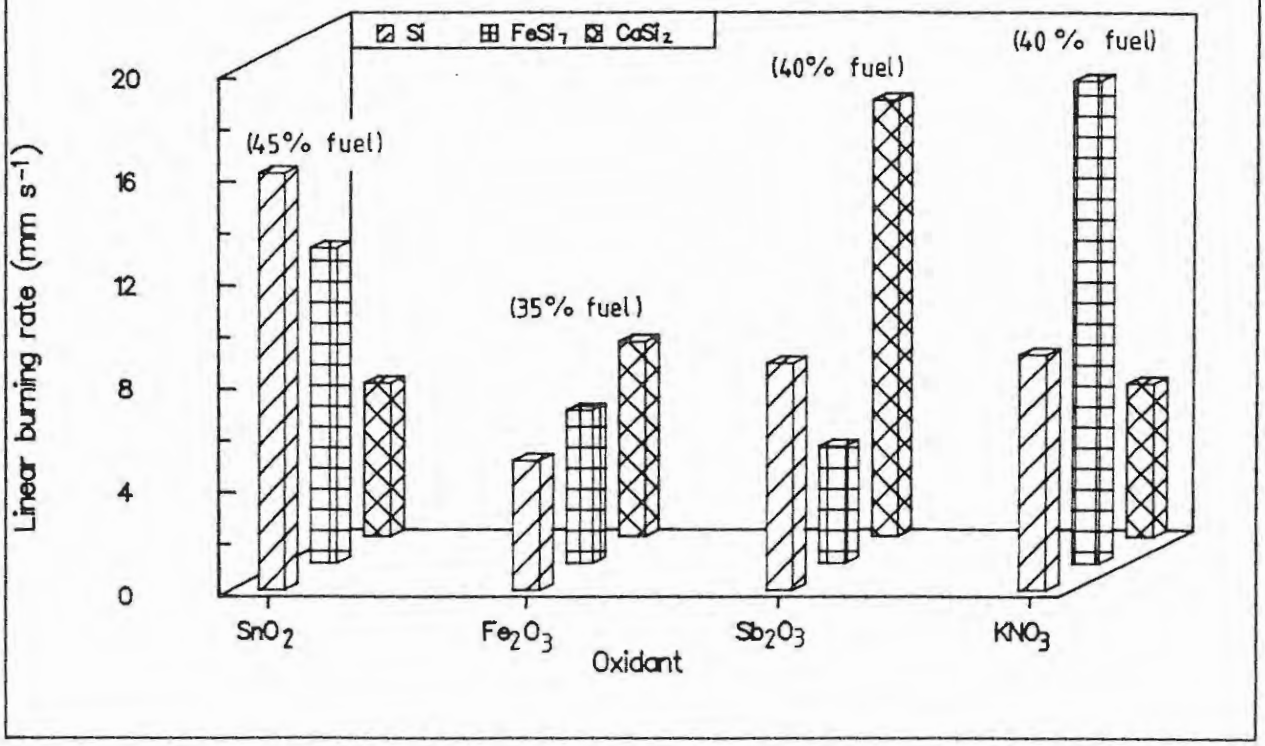

The temperature profiles for 40% $FeSi_7/Sb_2O_3$ were simple and had a longer induction time than that observed for the binary mixture with silicon as fuel. Temperature profiles of a 35% $FeSi_7/Fe_2O_3$ mixture did not show the complexity of those recorded for the 35% Si/Fe_2O_3 mixture. The temperature profiles for 45% $FeSi_7/SnO_2$ mixture showed no significant differences from those captured with Si as fuel. Temperature profiles could not be captured for mixtures with $CaSi_2$ as fuel due to excessive gassiness.

14.2.2 *Systems with two oxidants*

The oxidants used in this study could be regarded as being either "inert" (SnO_2 and Fe_2O_3 with high melting points and no thermal activity under the conditions of thermal analysis) or "active" (KNO_3 melts and decomposes above 330°C and Sb_2O_3 which sublimes or melts and vaporises above 540°C). A summary of the burning rates of ternary compositions with various proportions of active and inert oxidants is given in Table 14.2.

When Fe_2O_3 was added to Si/SnO_2, v_{exp} and T_{max} decreased with increasing Fe_2O_3. Both oxidants when used separately in binary mixtures with silicon react in apparently solid-solid reactions. The temperature profiles of the $Si/SnO_2/Fe_2O_3$ compositions showed a smooth rise to T_{max}. A plot of the burning rates of the ternary systems, compared with the respective binary systems is given in Figure 14.2. There is a smooth decrease in v_{exp} with increasing Fe_2O_3. This suggests that the second oxidant acts virtually as a diluent.

Burning rates for $Si/SnO_2/Sb_2O_3$ and $Si/Fe_2O_3/Sb_2O_3$ compositions (see Figures 14.3 and 14.4, respectively) increased to values higher than those recorded for either the binary systems. This effect is very marked for the $Si/Fe_2O_3/Sb_2O_3$ system and indicates considerable changes in the reactions occurring. The temperature profiles recorded for the $Si/Fe_2O_3/Sb_2O_3$ showed a relatively smooth rise to T_{max} compared to those recorded for the Si/Fe_2O_3 compositions.

The use of KNO_3 as a second oxidant decreased the burning rate of the $Si/SnO_2/KNO_3$ compositions (Figure 14.5), but increased the burning rate of the $Si/Fe_2O_3/KNO_3$ compositions (Figure 14.6) to values above those of either binary systems. Because of the steep slope of the burning rate plot for the binary Si/KNO_3 system, values for the burning rates of more ternary systems would be necessary to define trends more clearly. No temperature profiles could be recorded for the ternary mixtures with KNO_3 as the second oxidant.

The burning rate for the 40% Si/Sb_2O_3 composition increased initially when the oxidant was partially replaced with KNO_3 and then decreased with further increase in KNO_3 (see Figure 14.6). No temperature profiles could be recorded for mixtures which contained KNO_3.

Figure 14.2 Burning rates of the $Si/SnO_2/Fe_2O_3$ system

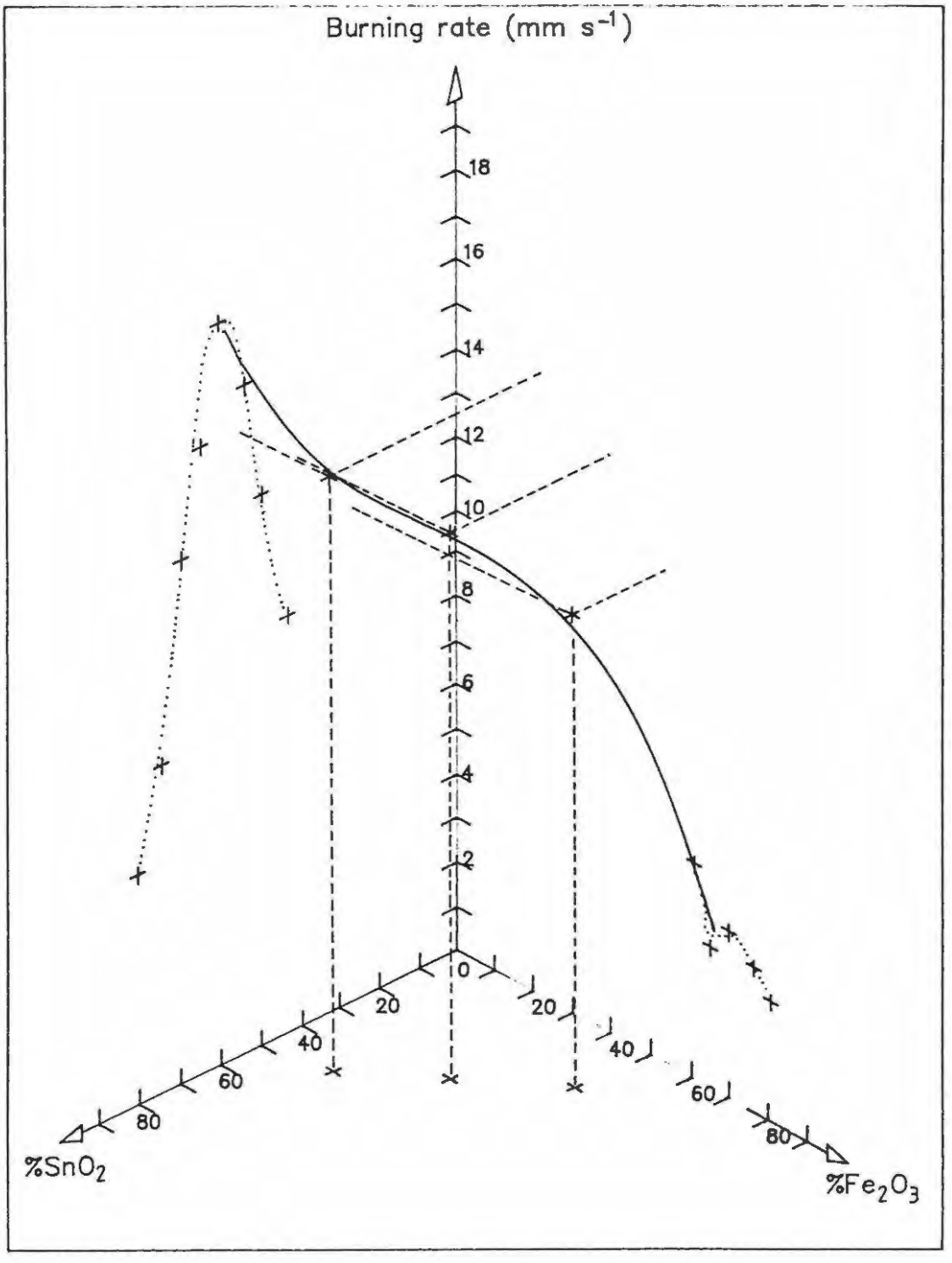

Figure 14.3 Burning rates of the $Si/SnO_2/Sb_2O_3$ system

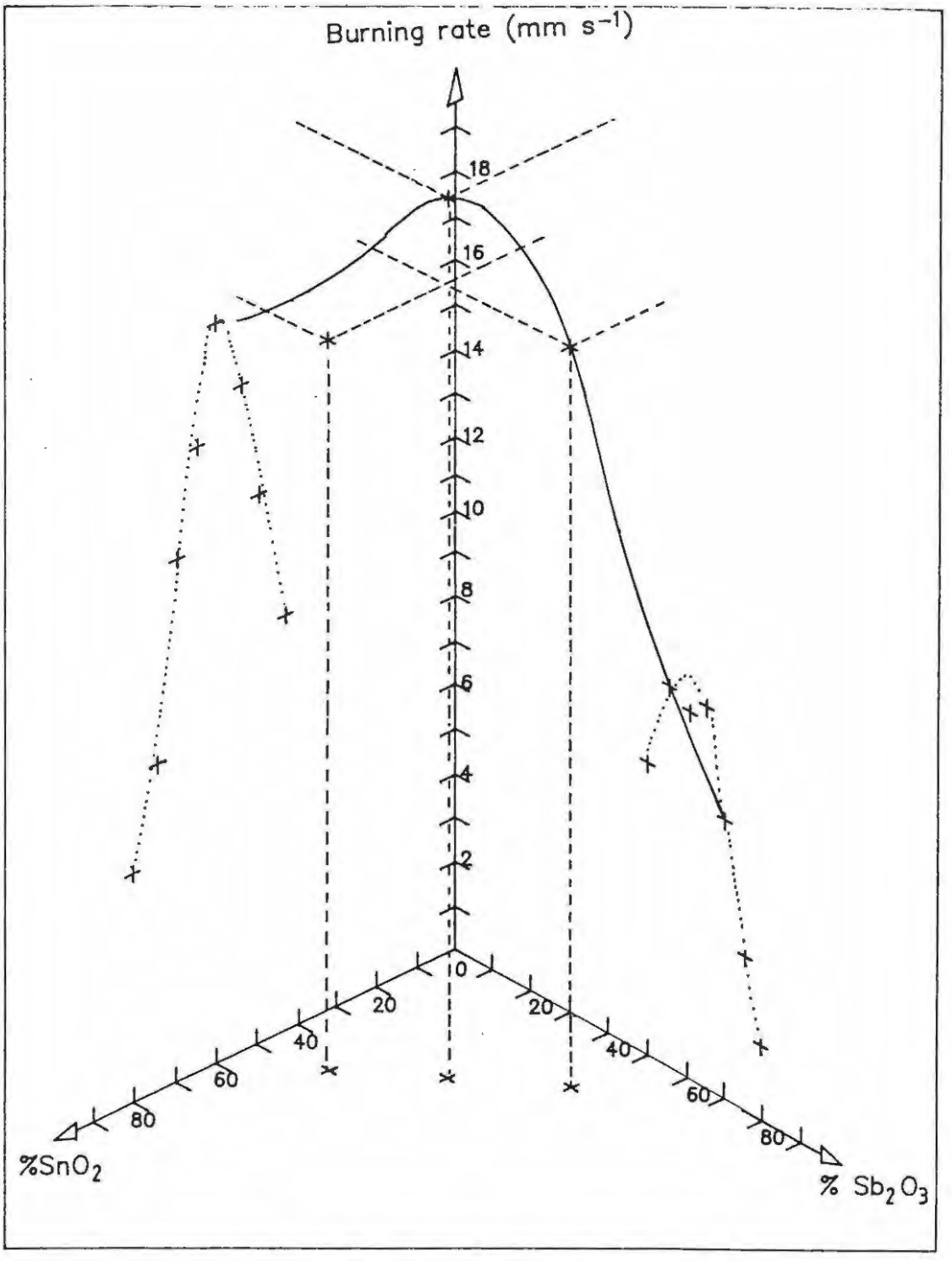

Figure 14.4 Burning rates of the $Si/Fe_2O_3/Sb_2O_3$ system

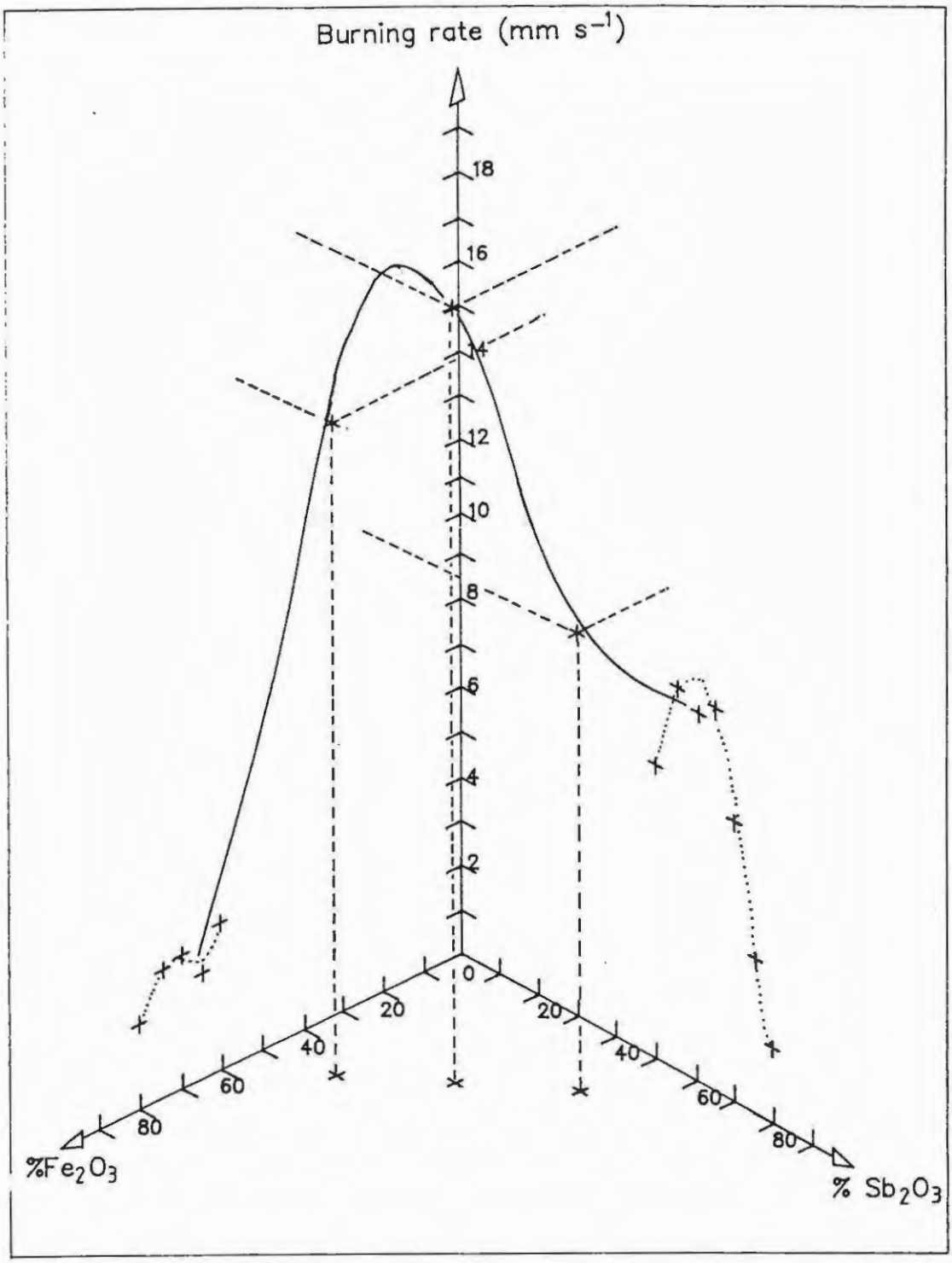

Figure 14.5 Burning rates of the $Si/SnO_2/KNO_3$ system

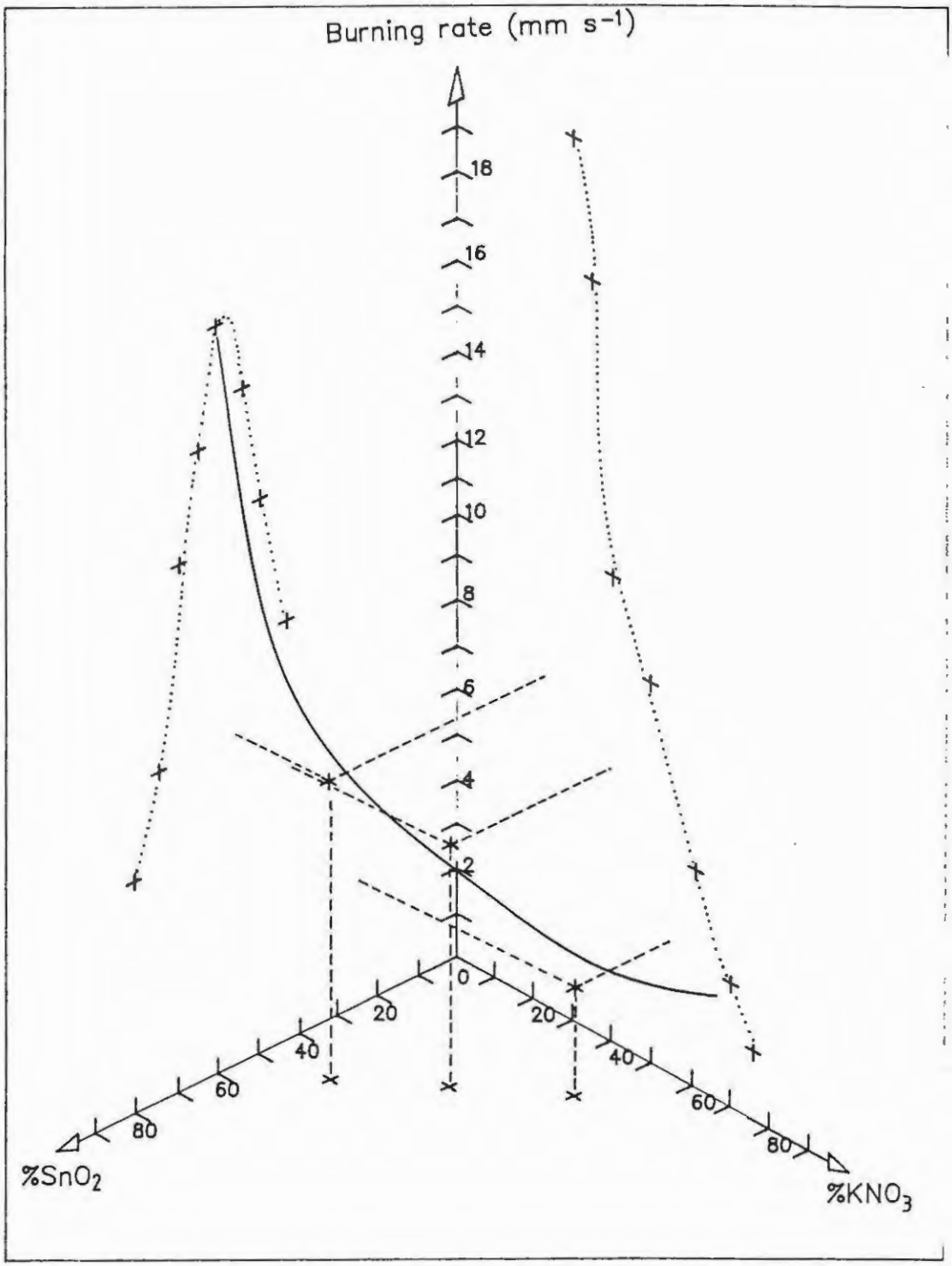

Figure 14.6 Burning rates of the $Si/Fe_2O_3/KNO_3$ system

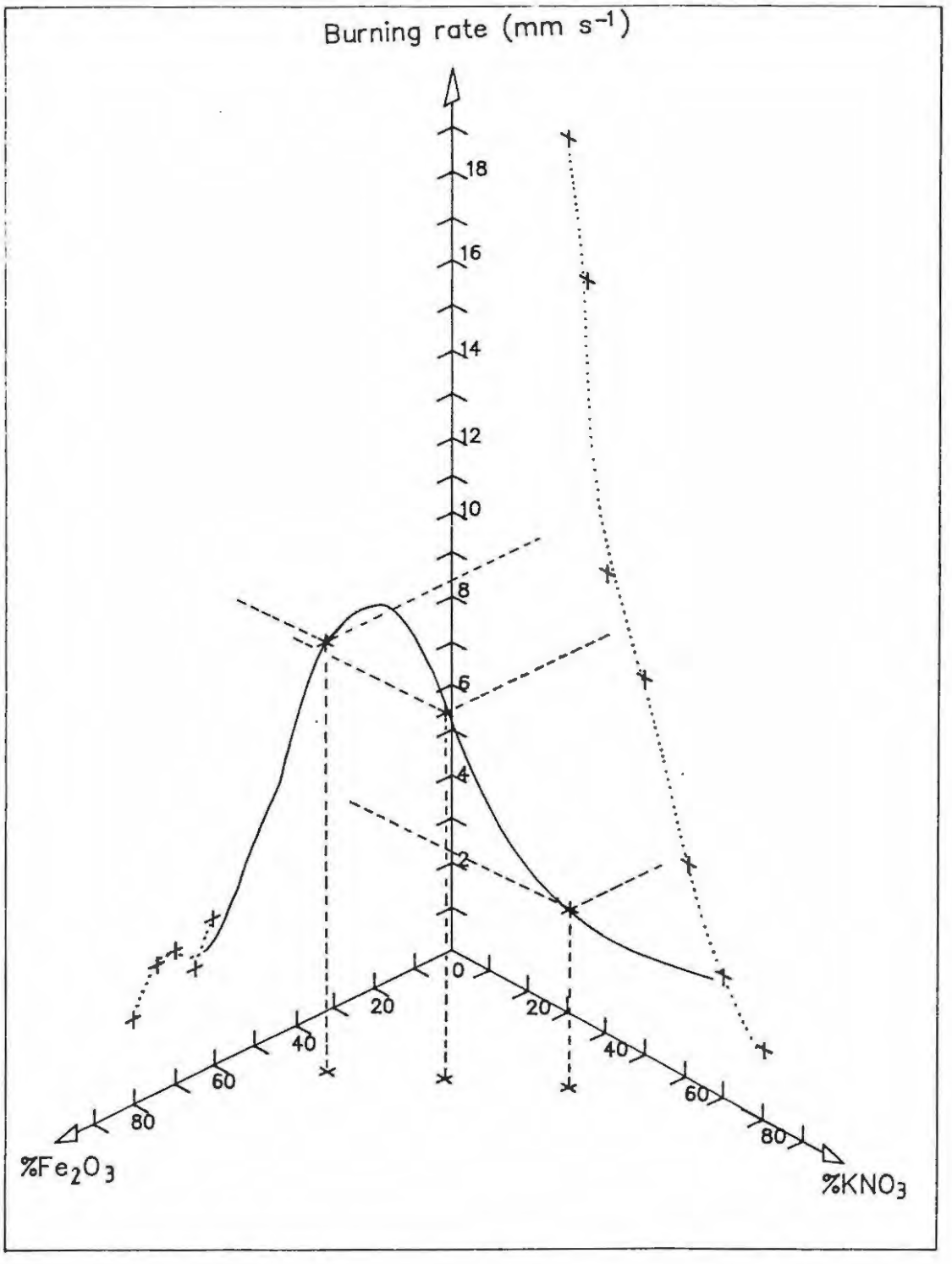

Figure 14.7 Burning rates of the $Si/Sb_2O_3/KNO_3$ system

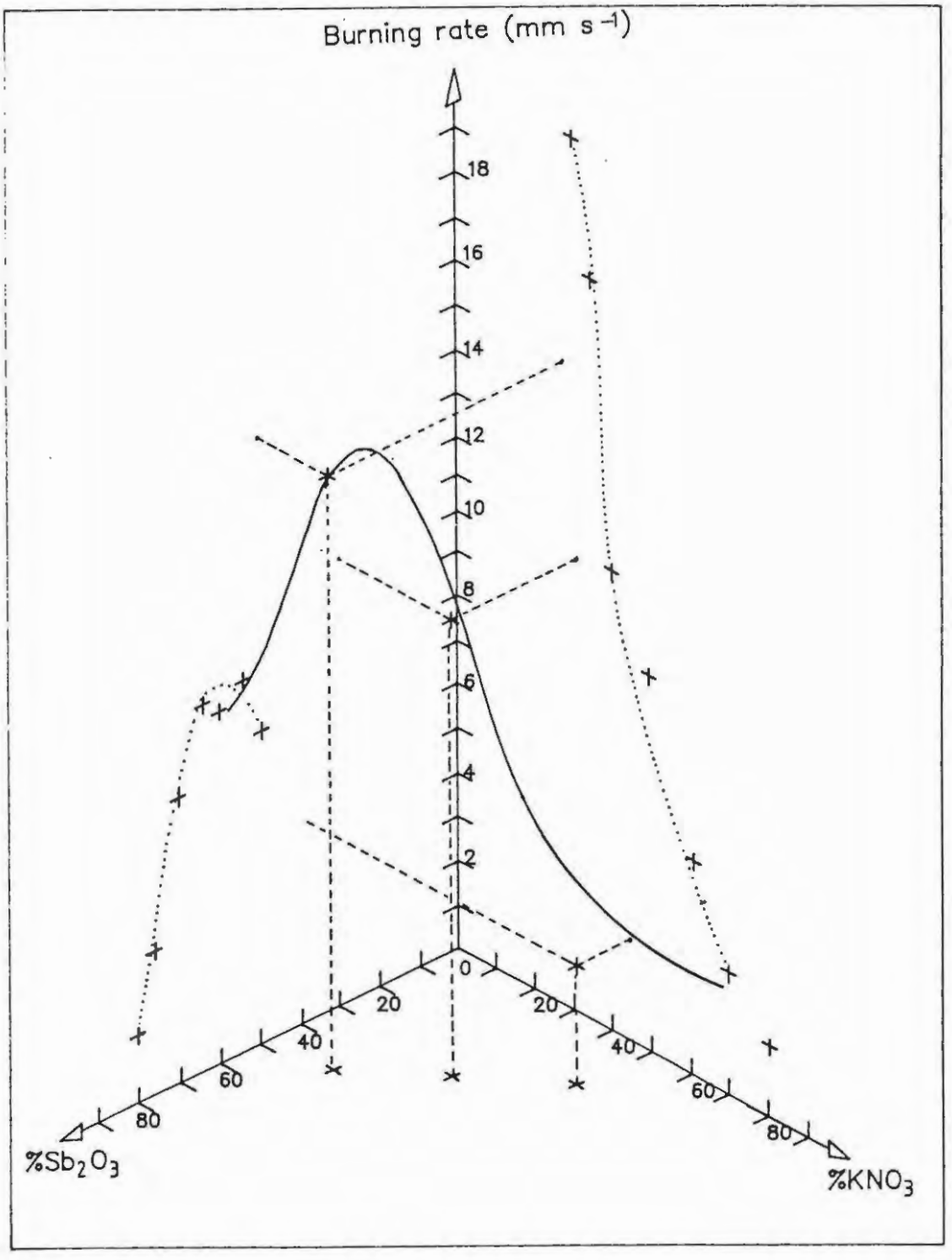

15. CONCLUSIONS

15.1 Thermal analysis

Si powder, alone, oxidises in air or oxygen only above 700°C and oxidation is incomplete at 1000°C.

Fe_2O_3 and SnO_2 when heated alone to 1000°C, did not undergo any significant decomposition and were thermally stable. Sb_2O_3 sublimes (~550°C) and is also oxidised in the presence of oxygen. KNO_3 melts (~325°C) and decomposes beyond 500°C.

Thermal analysis results (1) showed that there were no significant interactions in either the Si/Fe_2O_3 or the Si/SnO_2 system below 730°C on the DSC or 1000°C on the TG. The DSC traces of the Si/Sb_2O_3 and Si/KNO_3 systems showed strong exotherms due to oxidation of the silicon. The Si/Sb_2O_3 exotherm occurs within the same temperature range observed for the sublimation and melting of Sb_2O_3, so reaction between Si and Sb_2O_3 is likely to involve Sb_2O_3 vapour. The reaction is further complicated by the oxidation of Sb_2O_3 in the presence of atmospheric oxygen. Reaction between Si and KNO_3 certainly occurs between molten and decomposing KNO_3.

The thermal analysis curves of binary mixtures with $FeSi_7$ and $CaSi_2$ as fuels were very similar to those with silicon as fuel.

15.2 Burning studies

Some binary compositions of silicon with Sb_2O_3, Fe_2O_3, SnO_2 and KNO_3 as oxidants sustained self-propagating combustion.

For a given mixture, the main controls over burning rate are: (i) the adjustment of the composition of the mixture; and (ii) the addition of suitable quantities of suitable additives. The effects of varying the compaction, or the particle-size of the fuel are usually less significant. These conclusions generally apply to the four binary systems studied (Si/Fe_2O_3, Si/SnO_2, Si/Sb_2O_3 and Si/KNO_3). The effect on the burning rate of changing the oxidant used is by far the most significant.

One of the most important results of this study is the considerable difference observed in the burning rates of mixtures prepared from the common fuel, silicon, and the four different oxidants selected. The mean particle diameters of three of these oxidants were similar (Table 3.1), Sb_2O_3 0.6 μm, Fe_2O_3 0.4 μm and SnO_2 0.4 μm, and smaller than the silicon particles (3.4 μm). Fuel/oxidant contact would thus be similar. The KNO_3 particles were larger (9.7 μm), but KNO_3 melts at relatively low temperatures (and also decomposes giving rise to a very gassy systems), contact between fuel and oxidant is likely to be good.

Si/KNO_3 mixtures burn over a wide range of compositions at rates from 1.7 to 34.5 mm s^{-1}. Oxidation of silicon is normally limited by the formation of a protective layer of SiO_2. In the presence of NO_3^- the reaction may be more complicated.

Mobility of Sb_2O_3 is expected to be relatively high, but the range of burning rates in the Si/Sb_2O_3 system is only 1.6 to 8.7 mm s^{-1} (20 to 45% Si). In the Si/Fe_2O_3 system where complex combustion is indicated and where eutectic formation at relatively high temperatures may occur, the range of burning rates measured is very limited 2.3 to 4.5 mm s^{-1} (20 to 40% Si). In the Si/SnO_2 system, the range of burning rates is larger and shifted towards higher values (5.3 to 17.1 mm s^{-1} for 20 to 40% Si).

These variations in burning rate resulting from changes of the oxidant cannot arise from the properties of the fuel, since these have been kept constant in this study, except where the influence of the particle size has been examined.

The changes with change in oxidant must thus be related to one or more of the following factors:

(i) changes in the fuel/oxidant contact

(ii) changes in the reaction associated with the chemical nature of the oxidant.

Although factor (ii) might seem an easy and obvious answer, it does not account for the fact that the burning rates of most binary pyrotechnic systems depend to a greater or lesser extent on the composition. This variation is sometimes explained by the occurrence of different reactions at different compositions. Such an explanation would be hard to justify at a microscopic level where particles of fuel, A, and oxidant, B, are in limited contact with each other and must undergo some primary interaction which cannot depend on what lies beyond this point of contact. Secondary interactions between this initial product and additional fuel or additional oxidant, or even another unit of primary product, could lead to different "final" products, but prediction of such processes would be difficult.

In the binary systems studied, the mean particle sizes of the oxidants (except KNO_3) are similar and they are all (except KNO_3) smaller than the Si particles, so contact could only be influenced by particle shapes and/or size distributions.

The burning rates of the four oxidant systems changed considerably when silicon was replaced by either $FeSi_7$ or $CaSi_2$. These effects may, again, arise from changes in contact, or changes in chemistry, or both, as discussed in Section 14.

15.3 Temperature profiles

Temperature profiles of the various binary Si/oxidant mixtures were recorded. A smooth rise to maximum temperature was noted for the Si/Sb_2O_3 and Si/SnO_2 mixtures. The temperature profiles of the Si/Fe_2O_3 system showed at least two stages with plateaus of short duration (see Figure 8.1). The temperature profiles of only 90% Si/KNO_3 could be recorded and showed a complex shape with at least one plateau. Possible reasons for the occurrence of stepped profiles have been discussed in Section 8.

15.4 Kinetics

Activation energies of the combustion reactions for all four oxidants are all similarly low values (6 to 37 kJ mol^{-1}). These low values have been associated with (unspecified) diffusion processes. Values of the activation energies derived from thermal analysis were considerably larger (> 251 kJ mol^{-1}).

If diffusion through a protective layer of SiO_2 was the rate-controlling process, then the diffusing species might be expected to be an O atom or an O^{2-} ion. The influence of the oxidant would then be in the way in which such a species would be formed at the SiO_2/oxidant interface. Simple calculations (Section 13.2.1) of metal-oxygen (M-O) bond energies in the oxidants did not provide much further insight into such processes.

15.5 Comments and suggestions for further work

A major objective of this study was to obtain information on the role of different oxidants in reaction with a single, common fuel. Other recent studies (2) have examined the reactions of several different fuels with barium and strontium peroxides as common oxidants.

The range of pyrotechnic compositions which can be studied is restricted by the limits of the experimental techniques available. Thermal analysis provides very reliable information on the thermal behaviour of the constituents of pyrotechnic mixtures. Results obtained on heating the mixtures themselves are less reliable because conditions may either not lead to ignition, and hence show only the slower processes occurring or, when ignition occurs, the response and the design of the thermal analysis equipment may be inadequate.

Thermal analysis equipment designed specifically or modified to cope with rapid ignition processes have been reported (3) but is not generally available.

Measurement of temperature profiles is a relatively simple experimental technique in principle, although requiring great care in practice. The extraction of kinetic information, however, involves many assumptions (see Section 4) which are often not met in practice.

Much consideration has been given to the possibility of extending the range of measurable temperatures by use of infrared pyrometry (4,5,6). There is concern that by restricting the systems to those which burn at maximum temperatures below 1700°C and with relatively slow burning rates (< 50 mm s^{-1}), we may have pre-determined the range of thermal and kinetic parameters which are likely to be derived.

At present, commercially available pyrometers do not have fast enough response and a fine enough resolution to allow for accurate measurement of temperature profiles. There is also the problem of surface emissivity changes. Such profiles, even if accurately measured, would still refer to surface temperatures rather than core temperatures and further assumptions on the temperature distributions within the burning compositions would have to be made.

Much experimental work could benefit from comparison with computer simulations of combustion (7).

15.6 References

1. R.A. Rugunanan and M.E. Brown, J. Thermal Anal., in press.
2. R.L. Drennan, PhD Thesis, Rhodes University, 1991.
3. T. Boddington, F. Hongtu, P.G. Laye, M. Nawaz and D.C. Nelson, Thermochim. Acta, 170 (1990) 81.
4. R.A. Rugunanan and M.E. Brown, Journal of Thermal Analysis, 37 (1991) 2125.
5. G. Hussain and G.J. Rees, 15th Int. Pyro. Sem., ITT Res. Inst., (1990) 469.
6. T. Boddington, A. Cottrell and P.G. Laye, Combust. Flame, 70 (1990) 234.
7. M.W. Beck and M.E. Brown, J.Chem. Soc. Faraday Trans., 87 (1991) 711.

16. APPENDIX

16.1. Program for capturing temperature profiles

PROFILE.PAS (see below) was used to record the output of the thermocouples during the burning of pyrotechnic compositions. Only the main program is shown below. Details of the software may be obtained from Professor M.E. Brown, Chemistry Department, Rhodes University, Grahamstown, 6140.

```
(* {$C-}                {Disable Ctrl-Break}  query - how in tp4*)

PROGRAM PROFILE;

uses dos,crt,general,inter,turbo3,graph, ghutils,
     globals,plot_graph,collect_,file_, init_sys;

{  ************************************************************** }
{  *                                                            * }
{  *   Temperature Profile software written in TURBO PASCAL V3.1  * }
{  *   for the PC-26 A/D card for the IBM-PC and Compatibles.     * }
{  *                                                            * }
{  *   The PC-26 card must be set to 0v to +10v mono-polar,       * }
{  *   with a base-address of $700 (Hex) !                      * }
{  *                                                            * }
{  *   Created by Barry Guthrie, RHODES UNIVERSITY, January 1988. * }
{  *   Some original code by Mattias H. Popp, April 1986.       * }
{  *                                                            * }
{  *   Modified by David Williams RHODES UNIVERSITY December 1989 * }
{  *        - proposed modification = accept the first 256      * }
{  *            points prior to the burn                        * }
{  *                                                            * }
{  *                                                            * }
{  *                                                            * }
{  ************************************************************** }


BEGIN
  for count := 0 to 30720 do
    values[count] := 0;

  GetDir(0,Help_drive);  (* drive containing program disk *)

  key := '0';
  Sample_No := 0;

  Text_Normal;
  Define_System;
  WHILE NOT (key = 'E') DO
  BEGIN
     MARK (heap_top);
```

```
      Process_Data;
      RELEASE (heap_top);
   END;
   CLRSCR;
   ChDir(Help_drive);  (* drive containing program disk *)
END.
```

16.2. Software for smoothing

Raw data was smoothed by using the BASIC routine called MSPLINE.BAS (1) (see below).

```
0  REM "REGSPL1 "          EBERT/EDERER           881207
1 REM ************************************************
2 REM *** A regression - spline function is         ***
3 REM *** calculated. Equidistant grid points      ***
4 REM *** are needed.                              ***
5 REM *** The algorithm is taken from:             ***
6 REM *** Lawson/Hanson: Solving Least Squares     ***
7 REM *** Problems. Prentice Hall 1974.            ***
9 REM ************************************************
10 REM ***********************************************
11 REM ***                                           ***
12 REM ***      Version as at 25 October 1990        ***
13 REM ***                                           ***
14 REM ***      by  Anil Rugunanan                   ***
15 REM ***                                           ***
16 REM ***********************************************
17 KEY 6,"SYSTEM "
18 CLS
19 SCREEN 9: COLOR 7,1,4
20 PRINT "*****************************************
21 PRINT "*                                        *
22 PRINT "*    MSPLINE - a data smoothing routine  *
23 PRINT "*                                        *
24 PRINT "*****************************************
25 PRINT: PRINT: PRINT:
100   DIM X(500),Y(500),Z(500)
110   DIM A(552,5),D(552,7)
120   DIM B(500),C(500)
130 DIM YS(500)
200   DEF FNP(T)=.25*T*T*T
210   DEF FNQ(T)=1-.75*(1+T)*(1-T)*(1-T)
300   INPUT "How many grid points ";N
310   IF N<2 THEN N=2
320   GOSUB 10000 : REM Reading data in X() and Y()
330   GOSUB 11000 : REM Sorting data ascending in X()
360   IF N>=M-2 THEN N=M-2
400   B(1)=X(1) : B(N)=X(M)
410   H=(B(N)-B(1))/(N-1)
420   FOR I=2 TO N-1
430     B(I)=B(1)+H*(I-1)
```

```
440   NEXT I
460   GOSUB 12000 : REM Filling of matrix A
480   GOSUB 13000 : REM Filling of band matrices
481                 REM D=At*A und Z=At*Y
500   GOSUB 14000 : REM Solving equation D*C=Z
550   GOSUB 20000 : REM Calculating spline
560 GOSUB 24000
9900 PRINT:PRINT"run ended - data in file:";FOUT$
9999 END
10000 REM ******************************************
10001 REM *** Reading data in X() and Y()          ***
10002 REM ******************************************
10004 INPUT"Enter drive:filename ",FILE$
10006 OPEN"I",#1,FILE$
10008 FOR I=1 TO 500
10010 IF EOF(1) THEN 10026
10012 INPUT#1,X(I),Y(I)
10014 PRINT X(I),Y(I)
10020 NEXT I
10026 CLOSE#1
10028 M=I-2
10030 RETURN
11000 REM ******************************************
11001 REM ***  Data are sorted ascending in x.     ***
11002 REM ***  The minima and maxima in x and y    ***
11003 REM ***  are determined.                     ***
11005 REM ******************************************
11020 X0=X(1) : Y0=Y(1) : XM=X0 : YM=Y0
11040 FOR I=2 TO M
11060   IF X0>X(I) THEN X0=X(I)
11080   IF XM<X(I) THEN XM=X(I)
11100   IF Y0>Y(I) THEN Y0=Y(I)
11120   IF YM<Y(I) THEN YM=Y(I)
11140 NEXT I
11200 D=INT(LOG(M)/LOG(2)):D=2^D-1
11220 FOR I=1 TO M-D
11240   FOR J=I TO 1 STEP -D
11260     IF X(J)<=X(J+D) THEN 11300
11270     HY=Y(J) : Y(J)=Y(J+D) : Y(J+D)=HY
11280     HX=X(J) : X(J)=X(J+D) : X(J+D)=HX
11290   NEXT J
11300 NEXT I
11320 D=INT(D/2) : IF D>0 THEN GOTO 11220
11900 RETURN
12000 REM ******************************************
12001 REM ***  Filling of the matrix A            ***
12002 REM ******************************************
12010 IB=1 : REM Index for grid points
12020 IX=1 : REM Index for data points
12050 IF X(IX)>B(IB+1) THEN GOTO 12150
12060 T=(X(IX)-B(IB))/H
12070 A(IX,1)=FNP(1-T)
12080 A(IX,2)=FNQ(1-T)
12090 A(IX,3)=FNQ(T)
12100 A(IX,4)=FNP(T)
12110 A(IX,5)=IB
12120 IF IX=M THEN GOTO 12200
```

```
12130 IX=IX+1 : GOTO 12050
12150 IB=IB+1 : GOTO 12050
12200 RETURN
13000 REM ******************************************
13001 REM *** Filling of the band matrices        ***
13002 REM *** D=At*A and Z=At*Y                   ***
13003 REM ******************************************
13060 FOR I=1 TO N+2
13080   FOR J=1 TO 7 : D(I,J)=0
13100   NEXT J : Z(I)=0 : NEXT I
13140 FOR K=1 TO M
13160   FOR I=1 TO 4 : FOR J=1 TO I
13200       I0=I+A(K,5)-1 : J0=J+A(K,5)-1
13220       D(I0,J0-I0+4)=D(I0,J0-I0+4)+A(K,I)*A(K,J)
13240       NEXT J : Z(I0)=Z(I0)+A(K,I)*Y(K)
13260   NEXT I : NEXT K
13300 FOR I=1 TO N+2 : FOR J=1 TO 3
13320     IF D(I,J)=0 THEN GOTO 13400
13340     D(J+I-4,8-J)=D(I,J)
13400 NEXT J : NEXT I
13900 RETURN
14000 REM ******************************************
14001 REM *** Solving equation system D*C=Z       ***
14002 REM ******************************************
14040 FOR I=1 TO N+2 : D4=D(I,4) : FOR J=1 TO 7
14060     D(I,J)=D(I,J)/D4 : NEXT J : Z(I)=Z(I)/D4
14080   J=I+3 : IF J>(N+2) THEN J=N+2
14100   IF I=N+2 THEN GOTO 14400
14140   FOR K=I+1 TO J
14150     L3=D(K,4 -(K-I))
14160     FOR L=1 TO 4
14180       L1=L+3 : L2=L+3-(K-I)
14200       D(K,L2)=D(K,L2)-L3*D(I,L1)
14220     NEXT L : Z(K)=Z(K)-L3*Z(I)
14240   NEXT K
14400 NEXT I
14500 FOR I=1 TO N+5 : C(I)= 0 : NEXT I
14520 FOR I=N+2 TO 1 STEP -1
14540 C(I)=Z(I)-D(I,5)*C(I+1)-D(I,6)*C(I+2)-D(I,7)*C(I+3)
14560 NEXT I
14900 RETURN
20000 REM ******************************************
20001 REM *** Calculating the spline function     ***
20002 REM ******************************************
20020 FOR I=1 TO M
20030   X=X(I)
20040   GOSUB 21000 : REM determining spline interval j
20060   T=(X-B(J))/H
20080   Y=C(J)*FNP(1-T)+C(J+1)*FNQ(1-T)+C(J+2)*FNQ(T)
20090   Y=Y+C(J+3)*FNP(T)
20100   PRINT I,X(I),Y(I),Y
20110 YS(I)=Y
20200 NEXT I
20990 RETURN
21000 REM ******************************************
21001 REM *** Determining spline interval j       ***
21002 REM ******************************************
```

```
21010 J=0
21020 IF X<=B(1) THEN : J=1 : RETURN
21040 IF X>=B(N) THEN : J=N-1 : RETURN
21060 J=J+1
21080 IF X>B(J) THEN GOTO 21060
21100 J=J-1
21200 RETURN
22000 REM ****************************************
22001 REM ***  Evaluating the spline function      ***
22002 REM ****************************************
22040 GOSUB 21000 : REM determining spline interval j
22060 T=(X-B(J))/H
22070 Y=C(J)*FNP(1-T)+C(J+1)*FNQ(1-T)+C(J+2)*FNQ(T)
22080 Y=Y+C(J+3)*FNP(T)
22900 RETURN
24000 REM ***************************************
24010 REM     OUTPUT TO FILE
24020 REM ***************************************
24025 PRINT:INPUT"Enter output filname ";FOUT$
24030 OPEN"O",#2,FOUT$
24040 FOR J=1 TO M
24050 WRITE#2,X(J),YS(J)
24060 NEXT J
24100 CLOSE#2
24200 RETURN
63999 END
```

16.3 Software to reduce the number of points in a file

A BASIC routine called FILERED.BAS was used to reduce the number of data points in a file. The routine prompts the user for a step value, Z, for file reduction. Every Z data point is then saved into a second file.

16.4 Software for temperature profile analysis

The analysis of temperature profiles, based on the Hill and Leeds approach, was carried out on four LOTUS 123 spreadsheets:

1. TEMP.WK1 Converts raw data into temperature-time values, plots the profile and saves the T,t data into a file TEMP.PRN.
2. EXCESS.WK1 Imports TEMP.PRN and calculates U_{ad}, t_r and t_d. The data required for Hill kinetic analysis are saved into file KINET.PRN.
3. KINET.WK1 Calculates α and plots $h(\alpha)$ at various n values. E_a is obtained by linear regression analysis.

4. LEEDS.WK1 T,t data is converted into G, (1-α) and 1/T data for further analysis on BMDP routines (2).

Each of the data manipulation steps are performed using macros. The calculated parameters are dumped onto a printer.

The following algorithms (3) were used for data processing:

Differentiation

The Savitsky-Golay relationship was used to determine the derivatives of data.

$$\frac{dy}{dt} = \frac{(-4y_o - 3y_1 - 2y_2 - y_3 + y_5 + 2y_6 + 3y_7 + 4y_8)}{\Delta t * 60}$$

Savitsky-Golay Convolution integers

N	Integer set								Normalisation factors
5		-2	-1	0	1	2			10
7	-3	-2	-1	0	1	2	3		28
9	-4	-3	-2	-1	0	1	2	3	4	60

The convolution integers may be changed to 7 or 9 points if the data in the file before differentiating is very noisy. Usually, peak sensitivity is is sacrificed for large values of N.

Integration

Integration was carried out using the Trapezoidal Rule.

The cumulative area is

$$Area_{cumulative} = Area_1 + Area_0$$

where

$$Area_0 = (x_1 - x_0) * (y_1 - y_0)/2$$

and

$$Area_1 = (x_2 - x_1) * \{(y_1 - y_0) + (y_2 - y_1)/2\}$$

The determination of the above variables on a curve is shown in the diagram below.

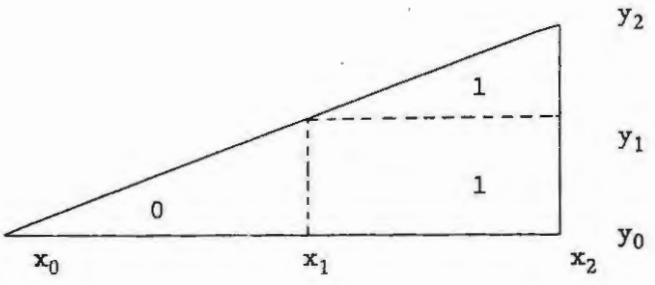

16.5 References

1. K. Ebert, H Ederer and T.L. Isenhour, "*Computer Applications in Chemistry*", VCH Publishers, Weinheim, 1989, p. 494

2. W.J. Dixon (Ed.), "*BMDP Statistical Software Manual*", University of California Press, 1985.

3. S. Leharne and E. Metcalfe, Education in Chemistry, (1989), 143.